Analysis of the Function of TLS/FUS in DNA Repair and Genome Maintenance

by

Kendra Laurie Cann

A Thesis submitted to the Faculty of Graduate Studies of
The University of Manitoba
in partial fulfilment of the requirements of the degree of

Doctor of Philosophy

Department of Biochemistry and Medical Genetics
Faculty of Medicine
University of Manitoba
Winnipeg, Manitoba
Canada

THE UNIVERSITY OF MANITOBA

FACULTY OF GRADUATE STUDIES

*****

COPYRIGHT PERMISSION

Analysis of the Function of TLS/FUS in DNA Repair and Genome Maintenance

by

Kendra Laurie Cann

A Thesis/Practicum submitted to the Faculty of Graduate Studies of The University of Manitoba in partial fulfillment of the requirement of the degree of

Doctor of Philosophy

In loving memory of my grandparents,

Enid Adelung, Carman Cann, and Maybelle Cann

Abstract

TLS$^{-/-}$ mice exhibit characteristics consistently found in mice models of the human genomic instability syndromes AT and NBS, specifically genomic instability, and immune system defects. The causative genes of these syndromes are involved in the DNA damage response pathways (DNA repair, cell cycle checkpoints, and/or apoptosis). We hypothesized that TLS maintains genomic stability through a role in DNA repair, and we now show that TLS is a multifunctional protein required for a proper biological response to both γ-irradiation and mitomycin C in mouse embryonic fibroblasts (MEFs). Therefore, we have identified TLS as a novel member of a group of proteins required for the repair of both DNA double-strand breaks (DSBs) and interstrand cross-links (ICLs). The sensitivity of *TLS*$^{-/-}$ MEFs to DSBs is not due checkpoint failure, and instead represents an inherent susceptibility to DNA damage and/or an error-prone repair. Furthermore, TLS exhibits a duality of function reminiscent of ATM, as it is also required for induction of apoptosis following DNA damage in the form of DSBs, and ICLs in pre-B cells. We have also identified two regulatory regions in TLS (amino acids 1-73 and 93-193) that can mediate its association with the nucleolus, a nuclear suborganelle associated with cell cycle regulation and the maturation of ribonucleoprotein complexes. These observations provide novel insights into the wild-type function of TLS and how TLS-dependent genomic stability may contribute to the TLS-associated cancers.

During this thesis work, I developed a novel strategy for assessing the immediate induction of the DNA damage-induced G1/S checkpoint. The development of this new

assay led to the unexpected result that the majority of late-G1, low-passage, primary MEFs do not halt progression into S phase following γ-irradiation, a finding that contradicts the current model of the G1/S checkpoint. The observed absence of an immediate G1/S checkpoint in primary cells identifies a novel cell cycle switch in late-G1 at which cells are no longer responsive to a global G1/S checkpoint and switch to using origin-specific regulation. This model provides a significant contribution to our general understanding of the regulation of the mammalian cell cycle.

Acknowledgements

I shall begin this thesis with some words from one of my favourite authors:

> It was the best of times, it was the worst of times, it was the age of wisdom, it was the age of foolishness, it was the epoch of belief, it was the epoch of incredulity, it was the season of Light, it was the season of Darkness, it was the spring of hope, it was the winter of despair, we had everything before us, we had nothing before us, we were all going direct to Heaven, we were all going direct the other way... (Dickens 35; bk.1, ch. 1)

With this introduction into what, in my opinion, is not one of his better books, I think he has unintentionally managed to capture the essence of both graduate studies and scientific investigation. It has been an amazing and exhausting journey, and one that has been aided, and been made far richer, by the people I have met along the way. Therefore, I have a very long list of people and organizations that all deserve thanks.

I would first like to thank my supervisor Dr. Geoff Hicks for letting me work in his laboratory, and introducing me to the world of genomic stability, DNA repair, and the cell cycle. I have been interested in DNA ever since the day I learned about genes and inheritance in Grade 6 (and not because I am still trying to find my family castle, which, I am sure, is mouldering away in my absence). I believe that DNA is the key to everything, well at least life, which is obviously the most amazing thing that has been created in this universe of ours. Other people are free to pursue the meaning of existence in the stars, both figuratively and literally; I will pursue it down a microscope. To that end, Geoff has allowed me to follow my "spidey-sense" to both great success, and also failure. But what are graduate studies without a few roadblocks? (Okay, I can hear all the graduate students snickering at my use of "few".) So, thank you, Geoff, for all your support during the years I have spent in your laboratory. I have learned a lot.

Next, I would like to thank my graduate committee, Dr. Jane Evans, Dr. Sabine Mai, and Dr. Dan Gietz, for all their help over the years. It was nice to know that I always had a guaranteed cheering squad in my corner. I would also like to thank them and my external examiner Dr. Stéphane Richard for reading the tome that is my thesis. (And, no, I was not trying to compete with Charles Dickens with respect to length of my writing. He still wins hands-down even in that category.)

During my tenure as a graduate student, I was extremely fortunate in the personnel funding that I was able to obtain, including a Canada Graduate Scholarship-Doctoral Award from the Canadian Institutes of Health Research, a Manitoba Health Research Council Studentship Award, a Natural Sciences and Engineering Research Council of Canada graduate studentship, and a Mona and David Copp Studentship from CancerCare Manitoba. Thank you to all these agencies for keeping me at my laboratory bench. The TLS project is funded by the National Cancer Institute of Canada.

Next, I would like to thank all the past and present members of the Hicks laboratory. Dr. Ludger Klewes was my main partner in crime on the TLS project, and he carried out all the pre-B cell experiments presented in this thesis. Dr. Denis Bosc taught me how to do science, and his "Just do it!" attitude would put Nike to shame. My awesome project student Margot Arntfield created several complicated deletion constructs with virtually no help from me, and was a very efficient second pair of hands for the time she was in the lab. Dr. Luke DeLange contributed numerous deletion constructs to this project, without which a big chunk of Chapter 4 could not have been possible. Djula Arapovic taught be everything I know about genomic DNA preparations and Southern blotting, not a small feat considering I was terrified of ^{32}P at the beginning.

Nichola Wigle provided a sympathetic ear for my frequent rants, and she volunteered to do Southern blots for me numerous times. Warren Law also provided a deletion construct for the work in this thesis. While other past and present members of the lab may not have contributed directly to the work presented in this thesis, they deserve my thanks for, if nothing else, listening to me drone on in lab meetings. The list includes, but is not limited to, Yanglong Mou, Songyan Liu, Debbie Tsuyuki, Yali Xie, and Jessica Gietz.

During my thesis work, I also relied upon the technical expertise of numerous people at the Manitoba Institute of Cell Biology, including Marsha Leith, who taught me how to do MTT assays. Because it occurred so frequently, I will not attempt to list all the other amazing people at MICB who answered questions for me, as this thesis is already long enough. Therefore, I will send out a general thank-you to everybody at MICB. I would also like to thank Dr. Jim Davie and Dr. Mike Mowat for always taking an interest in my work.

Graduate studies would be far less enjoyable and survivable without other graduate students to share the pain. I have been very lucky with the students that have shared my incarceration at MICB, and many have become good friends. I would especially like to thank Paula Espino, Kofi Chapman, Kathy Dunn, and Trung Le for all their support and friendship. For those of you who are already out, I am coming! For those of you still in, keep your chins up. I will see everybody at the next meeting/reunion of the GSSG (Graduate Student Support Group).

Keeping sane while in graduate studies can be a constant battle, and anything that can help you keep everything in perspective is a good thing. Therefore, I would also like

to thank all my furry, feathery, and leafy friends. Thankfully, I was also never more than a paddle, ski, hike, or book away from paradise, so thank-you to the universe!

Next, I would like to thank my brother, Stephen Cann, and his wife, Véronic Bézaire, for reminding me that there is life outside science. While I will never even attempt, let alone complete, an Ironman Triathlon, you guys continually inspire me. I also know that wherever you guys roam, there will always be a bed (or a least a corner of carpet) for me. À bientôt.

Last, but certainly not least, are the two people without whom I would definitely not have completed my PhD. Therefore, my most profound thanks go to my parents, Shirley and Dennis Cann. Without your incredibly broad shoulders to cry upon, I do not know what I would have done. Your support and love have meant the world to me. You guys have always borne the brunt of my somewhat volatile moods with equanimity, and I just want you to know that all the positive things that I have been able to accomplish in my life, and all the things I will accomplish have been made possible by you. All my love, and thank you, thank you, thank you, thank you, thank you.

Works Cited

Dickens, Charles. A Tale of Two Cities. 1859. London: Peguin Classics, 1985.

Contents

List of Figures

Chapter 4: Characterization of the dynamic localization of TLS in response to DNA damage and transcriptional inhibition.

List of Tables

Chapter 1

Introduction

1.1 TLS and cancer

1.1.1 Rearrangements of TLS, EWS, and TAF15 (the TET family) in human cancer

The TET family of proto-oncogenes is made up of the related genes *TLS*, *EWS*, and *TAF15*, and all three family members are translocated in a number of human cancers. *TLS* (*T*ranslocated in *L*ipo*S*arcoma; *FUS*; heteronuclear ribonucleoprotein P2 [*hnRNP P2*]; *pigpen*) was initially identified as the fusion partner of *CHOP* in a t(12;16) translocation found in human myxoid liposarcoma[1-3], and of *ERG* in a t(16;21) translocation found in human myeloid leukemia[4, 5]. In a similar manner, *EWS* (*EWSR1*, Ewing sarcoma breakpoint region 1) was initially identified as the fusion partner of *FLI-1* in the Ewing sarcoma family of tumors (ESFTs)[6]. A complete list of the TET fusion genes and their associated cancers is shown in Table 1.1. The oncogenic fusion genes are usually generated through reciprocal translocations[7-9], and the translocation breakpoints occur such that the TET family member is fused in-frame with a transcription factor[10-14] (see Figure 1.1). The resulting fusion oncoproteins all share a common structure: the N-terminal transcriptional activation domain of TLS, EWS, or TAF15 is fused to the DNA-binding domain of a transcription factor. For example, the N-terminal region of TLS is fused to the ETS DNA-binding domain of ERG[4]; to full-length CHOP, containing its DNA-binding domain and leucine zipper dimerization domain[2, 3]; to the bZIP (basic DNA binding and leucine zipper dimerization) DNA-binding domain of ATF-1[15, 16]; or to the bZIP DNA-binding domain of CREB3L2[17].

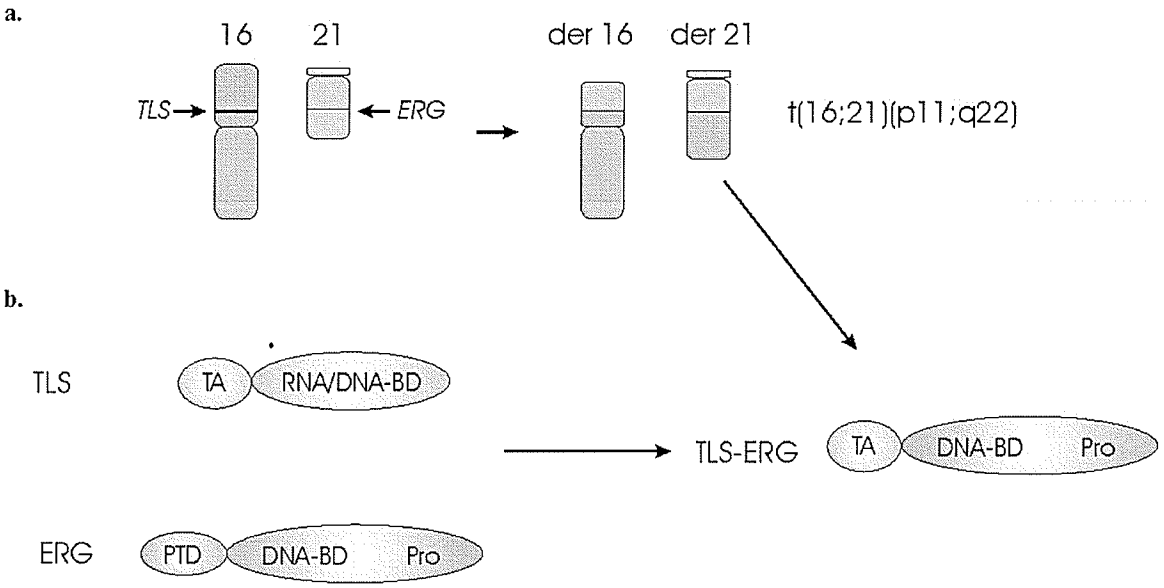

Figure 1.1: Formation of the TLS-ERG oncoprotein. a. A reciprocal t(16;21)(p11;q22) translocation resulting from breakpoints within the *TLS* and *ERG* genes fuses the 5' end of *TLS* in-frame to the 3' end of *ERG*, and vice versa. **b.** Translation of the *TLS-ERG* fusion gene, expressed from the der(21)t(16;21) derivative[18, 19], results in a fusion oncoprotein containing of the transcriptional activation domain of TLS and the DNA-binding domain of ERG. This example is indicative of the TET-family translocations, although more complex chromosomal rearrangements do occur. TA, transcriptional activation domain; BD, binding domain; PTD, pointed domain; and Pro, proline-rich activation domain.

The formations of these fusion genes are thought to be the primary causes of their associated cancers, because of the high frequency and specificity with which some of these fusions are found within their cancers. For example, over 90% of myxoid liposarcomas contain the TLS-CHOP fusion[20], with the rest harbouring a EWS-CHOP fusion[21]. Approximately 85% of Ewing sarcoma family of tumours carry the EWS-FLI-1 fusion[22], and in most of the remaining tumours, EWS is translocated with other members of the ETS transcription factor family (ERG, ETV 1, ETV4, or FEV) (see Table 1.1). In fact, the presence of these translocations and/or the expression of the fusion genes are

used for diagnosis of both myxoid liposarcoma and the Ewing sarcoma family of tumours[21, 23]. In some cancers, more than one TET family member fused to the same partner can initiate the oncogenesis. For example, TLS-CHOP and EWS-CHOP can each initiate myxoid liposarcoma, indicating that there is a functional relationship between the paralogues (see Table 1.1). However, the biology of these cancers becomes more complex when we look at the TLS-ERG and EWS-ERG fusions. The EWS-ERG fusion is found in Ewing sarcoma[9], while the TLS-ERG fusion is found in both myeloid leukemia[4, 5, 24, 25] and Ewing sarcoma[18]. This indicates that the same, or similar fusions can induce oncogenic pathways in different cell types, and that distinct cellular functions of the TET family members may have evolved.

Of note, no loss of heterozygosity of either the TET family members or their associated fusion partners has been reported in the literature as secondary mutations in these cancers, suggesting that the fusions are functioning dominantly in the development of the cancers. It is generally well-accepted that the fusion oncoproteins function as aberrant transcription factors, potentially interfering with the normal transcriptional regulation of the TET fusion partner target genes and/or recognizing new transcriptional targets[26, 27]. However, there is also evidence to suggest that the oncoproteins may interfere with the normal function of the TET family member in a dominant negative manner, and/or function as a dysregulated TET family member[28]. The function of TLS fusion oncoproteins will be described in more detail following a section on TLS-associated cancers.

Table 1.1: TLS/FUS, EWS, and TAF15 translocations in human cancer

	DNA-binding Domain	Cancer	Translocation	References
TLS/FUS	*CHOP*	Myxoid liposarcoma	t(12;16)(q13;p11)	1-3
	ERG	Acute myeloid leukemia Blast crisis of chronic myeloid leukemia Acute lymphoblastic leukemia Ewing sarcoma family of tumours	t(16;21)(p11;q22)	4, 5 24 25 18
	ATF-1	Angiomatoid fibrous hystiocytoma	t(12;16)(q13;p11)	15
	CREB3L2/ BBF2H7	Low-grade fibromyxoid sarcoma	t(7;16)(q33;p11)	17
EWS	*FLI-1*	Ewing sarcoma family of tumours	t(11;22)(q24;q12)	6
	ERG	Ewing sarcoma family of tumours	t(21;22)(q22;q12)	9
	ETV1	Ewing sarcoma family of tumours	t(7;22)(p22;q12)	29
	ETV4/E1AF	Ewing sarcoma family of tumours	t(17;22)(q12;q12)	30, 31
	FEV	Ewing sarcoma family of tumours	t(2;22)(q33;q12)	32
	CHOP	Myxoid liposarcoma	t(12;22)(q13;q12)	33
	ATF-1	Malignant melanoma of soft parts/soft tissue clear cell sarcoma Angiomatoid fibrous hystiocytoma	t(12;22)(q13;q12)	34 35
	WT1	Desmoplastic small round cell tumour	t(11;22)(p13;q12)	36, 37
	ZSG	Small round cell sarcoma	(t(1;22)(p36.1;q12)	38
	POU5F1 (OCT3/4)	Undifferentiated bone sarcoma	t(6;22)(p21;q12)	39
	NR4A3	Extraskeletal myxoid chondrosarcoma	t(9;22) (q22;q12)	40
	CIZ/NMP4	Acute leukemia	t(12;22)(p13;q12)	41
TAF15	*NR4A3*	Extraskeletal myxoid chondrosarcoma	t(9;17)(q22;q11.2)	42, 43
	CIZ/NMP4	Acute leukemia	t(12;17)(p13;q11)	41

1.1.2 Clinical features of TLS-associated cancers

1.1.2a Myxoid and round-cell liposarcoma

Myxoid liposarcoma represents about 10% of adult soft tissue sarcomas, and tends to develop in the deep soft tissue of the extremities, such as the musculature of the thigh. These tumours generally occur between the third and fifth decades of life, and they have no gender preference[21]. The 5-year survival rate is 70%, but this reduces to 20% when there is an extensive round-cell component associated with the tumour[21]. Myxoid and round-cell liposarcomas represent opposing ends of a continuum of myxoid adipocytic tumours, and the entire spectrum of tumours harbours the TLS-CHOP or

EWS-CHOP fusion[21]. The myxoid tumour is characterized by a hypocellular region of spindle cell proliferation in a myxoid background, often with mucin pooling. Another attribute of the tumour is a plexiform, or web like, pattern of capillaries. Small, and often monovacuolated, lipoblasts tend to cluster near these vessels or at the periphery of the tumour[21]. In round-cell liposarcoma, over 80% of the tumour is hypercellular and/or contains undifferentiated round cells. Tumours with between 5-80% hypercellularity and/or undifferentiated round cells represent mixed myxoid/round-cell tumours[21]. Because the presence of the TLS-CHOP or EWS-CHOP fusion can induce liposarcomas with varying degrees of aggressiveness, a better understanding of these fusions and the wild-type function of TLS and EWS may identify methods to convert an aggressive tumour to a non-aggressive tumour less likely to metastasize, reducing the mortality rate associated with the undifferentiated tumours. Myxoid liposarcoma is typically treated with surgery, radiation therapy, and in some cases chemotherapy[44]. Therefore, an adjuvant therapy that causes the cancer to be less aggressive would also reduce the amount of radiation therapy and/or chemotherapy required to effectively treat the cancer.

1.1.2b TLS and Leukemia

Leukemias are haematological cancers that proliferate as single cells, and they can develop in both myeloid and lymphoid lineages[45]. The myeloid stem cell generates progenitors for red blood cells, various white blood cells (eosinophils, basophils, neutrophils, monocytes, and mast cells), and platelets. The lymphoid stem cell generates progenitors for T and B lymphocytes[45]. Acute myeloid leukemia (AML) and acute lymphocytic leukemia (ALL) are rapid-onset leukemias that arise in less mature myeloid and lymphoid cells. These cancers can occur at any age. Chronic myeloid leukemia

(CML) and chronic lymphocytic leukemia (CLL) develop slowly and are seen in adults. When a chronic leukemia progresses to a more aggressive stage, this is termed blast crisis[45]. The presence of the TLS-ERG fusion correlates with a poor prognosis in AML, and patient survival does not normally exceed three years[46].

1.1.2c Ewing sarcoma family of tumours

The Ewing sarcoma family of tumours is made up of classic Ewing sarcoma, primitive neuroectodermal tumour (PNET), and malignant small cell tumour of the thoracopulmonary region (Askin tumour), with these tumours mainly differing on the differentiation state of the tumour[23]. Ewing sarcoma primarily affects children and adolescents, and more commonly affects boys[23]. It is the second most common malignant tumour of the bone within this age group, but can also occur at extraosseous sites, including soft tissue, visceral organs, and skin[23]. Ewing tumours are thought to derive from pluripotent neural crest cells, and manifest as small round cell tumours. However, their defining feature is the presence of a fusion between EWS (or TLS) and a member of the ETS family of transcription factors[23].

Each year, approximately twenty-six Canadian children/youth will be diagnosed with Ewing sarcoma, representing 2% of the new cancer cases within this age group[47]. Unfortunately, almost one-third of the Ewing Sarcoma patients will die from their disease[47], with individual patient prognosis depending on the presence and location of metastases[23]. The current treatment of Ewing sarcoma is chemotherapy followed by local control with surgery and/or radiation therapy[23]. Research into EWS, and by corollary TLS, and their associated fusions will hopefully reduce the high mortality rate associated with this childhood cancer through the development of better tumour-targeted therapies.

1.1.3 The TLS oncoproteins and cell transformation

The three most common TLS breakpoint regions result in the inclusion of exons 1-5 (coding for aa 1-174), exons 1-7 (coding for aa 1-265), or exons 1-8 (coding for aa 1-275) in the oncogenic fusions[48], although other minor variants have been shown to occur[12]. These breakpoints are constrained by the requirement for in-frame translation with its fusion partner, and by the requirement for specific functional domains within TLS, as all fusions encompass the entire SYGQQS transcriptional activation domain[48]. (Undoubtedly the translocation events are also constrained by the existence of binding sites for Translin and topoisomerase II, which have both been implicated in the TLS translocations[49]. However, the formation of a functional oncoprotein is the event that allows for oncogenic transformation and cancer development.) The TLS-ERG fusions found in myeloid leukemia never contain fewer than the first seven exons of TLS (corresponding to aa 1-265)[48]. While this may indicate that an additional region of TLS is required for oncogenic transformation of myeloid precursors, it may also provide a flexible hinge region between the required TET and partner domains[50].

TLS-CHOP and TLS-ERG have both been shown to be able to induce cellular transformation in vitro[51-53]. For example, expression of TLS-CHOP in cell-lines resulted in anchorage-independent growth in soft agar and tumor formation in nude mice[51, 53], and retroviral transduction of TLS-ERG into human cord blood cells caused altered myeloid differentiation, arrested erythroid differentiation, and an increased proliferative capacity of myeloid progenitors[52]. Transformation assays have also supported the earlier finding that the TLS-ERG fusions causing myeloid leukemia require a larger TLS fragment, as TLS amino acids 175-265 (encoded in exons 6 and 7) were also necessary for the

transformation of a mouse myeloid precursor cell line but not a mouse fibroblast cell line[48]. Amino acids 175-265 contain part of the first RGG-repeat region (see section **1.2**). These data indicate that distinct regions of TLS are required for specific transformation events[48].

As mentioned previously, the TLS fusion proteins may function as aberrant transcription factors, and several studies have attempted to identify potential targets genes of the oncoproteins. For example, TLS-CHOP has been found to help promote transcription of C/EBPβ and NF-κB target genes[54]. TLS-CHOP has also recently been found to up-regulate *SERPINB2*, whose protein product functions in cell cycle regulation through an interaction with pRB[55]. The target genes of the oncoproteins are also cell-type specific, as a recent study has also shown that TLS-ERG induces different genes in fibroblasts and hematopoietic cells[56]. The ability of the oncoproteins to induce transcription of target genes in a cell-type specific manner may explain why the TLS-ERG fusion can induce at least two types of cancer[4, 5, 18, 24, 25], and why, as detailed below, TLS-CHOP only induces liposarcoma even when it is expressed in every cell type[57, 58].

1.1.4 TLS-CHOP mouse models

Transgenic mouse models of TLS-CHOP have shown that the presence of this fusion protein is enough to initiate its associated cancer. Mice ubiquitously expressing a TLS-CHOP construct or a reversed order CHOP-TLS construct specifically develop tumours that almost completely recapitulate the phenotype of human myxoid liposarcoma, including the presence of lipoblasts with round nuclei, and the accumulation of intracellular lipid[57, 58]. The presence of the N-terminus of TLS is required for

oncogenesis, as mice only overexpressing CHOP do not develop liposarcoma[58]. The N-terminus of TLS can still promote liposarcoma development in mice when it and CHOP are overexpressed as physically separate domains[59], suggesting that the N-terminus of TLS has a function separate from that of the fusion protein, and may function in a dominant-negative manner against the wild-type function of TLS or as a dysregulated version of TLS. This observation emphasizes the need for a better understanding of the normal function of TLS, and by corollary, EWS and TAF15.

1.1.5 A role for wild-type TLS in oncogenesis, cell proliferation and an undifferentiated state

Wild-type TLS itself has been linked to oncogenesis, as TLS might function as a regulator of BCR-ABL-mediated leukemogenesis[60-62]. BCR-ABL stabilized TLS via a PKCβII-mediated phosphorylation event on serine 256, and knocking down TLS in BCR-ABL-expressing cells increased differentiation and decreased proliferation[60-62]. An association of TLS with proliferation has also been shown in bovine endothelial cells[63] and human fibroblasts[64], and the association of TLS with an undifferentiated state has also been shown in a mouse teratocarcinoma cell line[64] and a myeloid cell line[65]. Therefore, exclusive of its role in the aberrant transcription factors, the N-terminal portion of TLS may also be functioning as a dominant positive, promoting oncogenesis by inducing increased proliferation and preventing cellular differentiation.

1.2 TLS protein structure and function

The mammalian TET family (TLS, EWS, and TAF15) are paralogues, and as such share a similar domain structure. Each protein has the family-defining N-terminal SYGQQS repeat region, RGG repeats, an RNA recognition motif, and a zinc finger[66].

(These regions will be discussed below in detail with reference to TLS). Of note, there is also a *Drosophila homologue* of the TET family, SARFH [sarcoma-associated RNA-binding fly homolog, Cabeza][67].

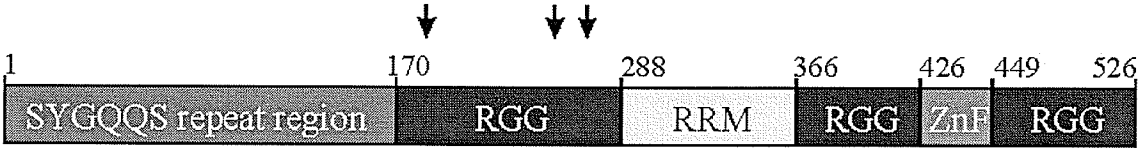

Figure 1.2: Protein structure of TLS. TLS has an N-terminal SYGQQS-repeat region, three RGG repeat regions, an RNA recognition motif (RRM), and a zinc-finger motif. Arrows represent translocation break points. All numbers refer to human TLS[68].

Human TLS is a ubiquitously-expressed heteronuclear ribonucleoprotein that is encoded in 15 exons with two known alternative splicing isoforms[69]. Exon 4 has two possible splice sites, generating a predominant 526-aa form with a TG at amino acids 64-65, and a minor 525-aa variant with an S at amino acid 64. The highly homologous mouse TLS is a 518 aa protein. TLS is typically thought to have two main functional domains: an N-terminal transcriptional activation domain and a C-terminal polynucleotide-binding domain. The N-terminal region of TLS is rich with serines (S), tyrosines (Y), glycines (G), and glutamines (Q), and it is this region that is part of the fusion oncoproteins. The fusions involve exons 1-5 (aa 1-174), exons 1-7 (aa 1-265), or exons 1-8 (aa 1-275), encompassing the entire SYGQQS-repeat region[48]. This region can function as a transcriptional activation domain[70, 71], and it can also interact with RNA polymerase II[72, 73]. The C-terminus of TLS is comprised of an RNA recognition motif (RRM), three RGG-repeat regions, and a zinc-finger motif. Given that TLS has these three different types of nucleotide binding domains, it is not surprising that TLS binds

RNA[1, 2, 70, 74]. However, it can also bind both single-stranded and double-stranded DNA[60, 70]. The RRM is made up of an RNP1 (ribonucleoprotein 1) domain and an RNP2 domain, and this region of TLS has been shown to preferentially recognize a GGUG motif[74]. In the RGG-repeat regions, glycine residues provide flexibility while arginines provide a positive charge[75]. The RGG-repeats of TLS do bind RNA, and, again, appear to favour a GGUG motif[70, 74]. The RGG-repeat regions of both EWS[76] and TLS[77] can be extensively methylated, identifying a potential point of regulation. Furthermore, the RGG-repeats of EWS can also repress transcriptional activity[78]. By corollary, we can hypothesize that the RGG-repeat regions of TLS would share this characteristic. The presence of a zinc finger in heteronuclear proteins is unexpected, and fairly unique to the TET family. This single C4 zinc-finger motif may be responsible for the ability of TLS to bind dsDNA containing a zinc-finger consensus sequence, and even ssDNA containing the complementary zinc-finger consensus sequence[60]. Recent structural analysis of TLS has shown that while the RRM motif and Zn-finger motif are structured, the N-terminus and RGG-repeats are flexible and disordered[68]. Furthermore, the study also found that the Zn-finger binds with high-affinity to the GGUG motif previously identified as the preferential binding substrate for TLS[68].

1.3 TLS is a ribonucleoprotein involved in transcription and RNA processing.

Most of the data to date suggests that TLS functions in transcription, RNA processing, and RNA transport. As described above, TLS binds RNA[1, 2, 70, 74] and both ssDNA and dsDNA[60, 70]. In fact, TLS was also identified as heteronuclear ribonucleoprotein P2 (hnRNP P2) because of its inclusion in hnRNP mega-complexes[1]. It is interesting to note that while the C-terminus of TLS has clear ribonucleoprotein

domains, the N-terminus is completely unique to the TET family, and identifies the family as a unique subset of the hnRNP superfamily. The N-terminal domain region of TLS can function as a transcriptional activation domain[70, 71], and can interact with RNA polymerase II[72, 73]. Furthermore, TLS interacts with the general transcription factor TFIID, which is comprised of TATA-binding protein (TBP) and several TBP-associated factors[79]. TLS can also interact with gene-specific transcription factors, including NF-κB[80] and the steroid, thyroid hormone, and retinoid receptors[81]. NF-κB is an important regulator of apoptosis[82], and also responds to intracellular signals generated by DNA damage, although these pathways are not as well understood as the NF-κB apoptotic pathways[83]. In addition, the Hicks lab has shown that TLS can co-activate NF-κB-directed transcription in vivo (Law and Hicks, unpublished data).

TLS also has mutually antagonistic relationships with transcription factors, specifically Spi-1/PU.1[84, 85], and β-catenin[86]. In its relationships with these two transcription factors, TLS inhibits the transcriptional activity of Spi-1 or β-catenin, and each transcription factor can inhibit the TLS-directed splice-site selection in E1A pre-mRNA splicing. TLS can also interact with the multifunctional, DNA-damage response protein YB-1 (Y-box DNA/RNA-binding factor-1), which itself can affect transcription and splicing[73, 87]. Of note, TLS-ERG and TLS-CHOP can interfere with YB-1-mediated splicing even though they do not directly interact with YB-1[73, 87], again suggesting that TLS-ERG and TLS-CHOP may function in a dominant-negative fashion with respect to wild-type TLS function.

The association with both splicing and transcription is supported by the finding that TLS has been found in joint transcription and splicing machinery complexes that

bind preferentially to 5' splice sites[88]. In these joint complexes, TLS was bound to PSF (PTB [polypyrimidine tract-binding protein]-associated splicing factor), p54[nrb], U1-70K (a component of the U1 snRNP), RNA polymerase II, TFIIF, and TFIIH[88]. Complexes such as these are believed to couple the processes of transcription and splicing together[88]. Furthermore, TLS has also been shown to affect alternative splicing through interactions with other splicing factors, including SC35, TASR (TLS-associated serine-arginine protein)-1[89], TASR-2[72], PTB (hnRNP I)[90], and the splicing coactivator SRm160[90], with one model of TLS function suggesting that TLS mediates spliceosome assembly[90]. Together, these data suggest that TLS functions in conjunction with other factors to modulate transcription and splicing in a concerted response following specific stimuli.

TLS has also been shown to be involved in RNA transport. TLS functions in the nucleo-cytoplasmic shuttling of RNA[91], and can bind the ribonucleoproteins hnRNPA1 and hnRNPC1/C2, proteins involved in RNA maturation and export[53]. Work done in collaboration with the Hicks lab showed that TLS helps direct transport of mRNAs to postsynaptic dendritic spines in mature hippocampal pyramidal neurons for site-specific translation, and that this function was required for proper dendritic spine development[92]. The association of TLS with dendritic RNA was subsequently reported by another group[93]. Finally, a role for TLS and other hnRNPs in general cell spreading and attachment has been established[94]. Therefore, these data support a functional role for TLS in the targeting of specific mRNAs to subcellular locations for site-specific translation.

By being able to regulate gene expression at each step from the level of transcription through to the site-specific localization and translation of transcripts, TLS,

in conjunction with other factors, may be able to orchestrate an integrated, but multi-faceted response to cellular signals (Figure 1.3). Identifying these signals and the methods of TLS regulation will allow a better understanding of TLS function, as both the wild-type protein and within the oncoproteins.

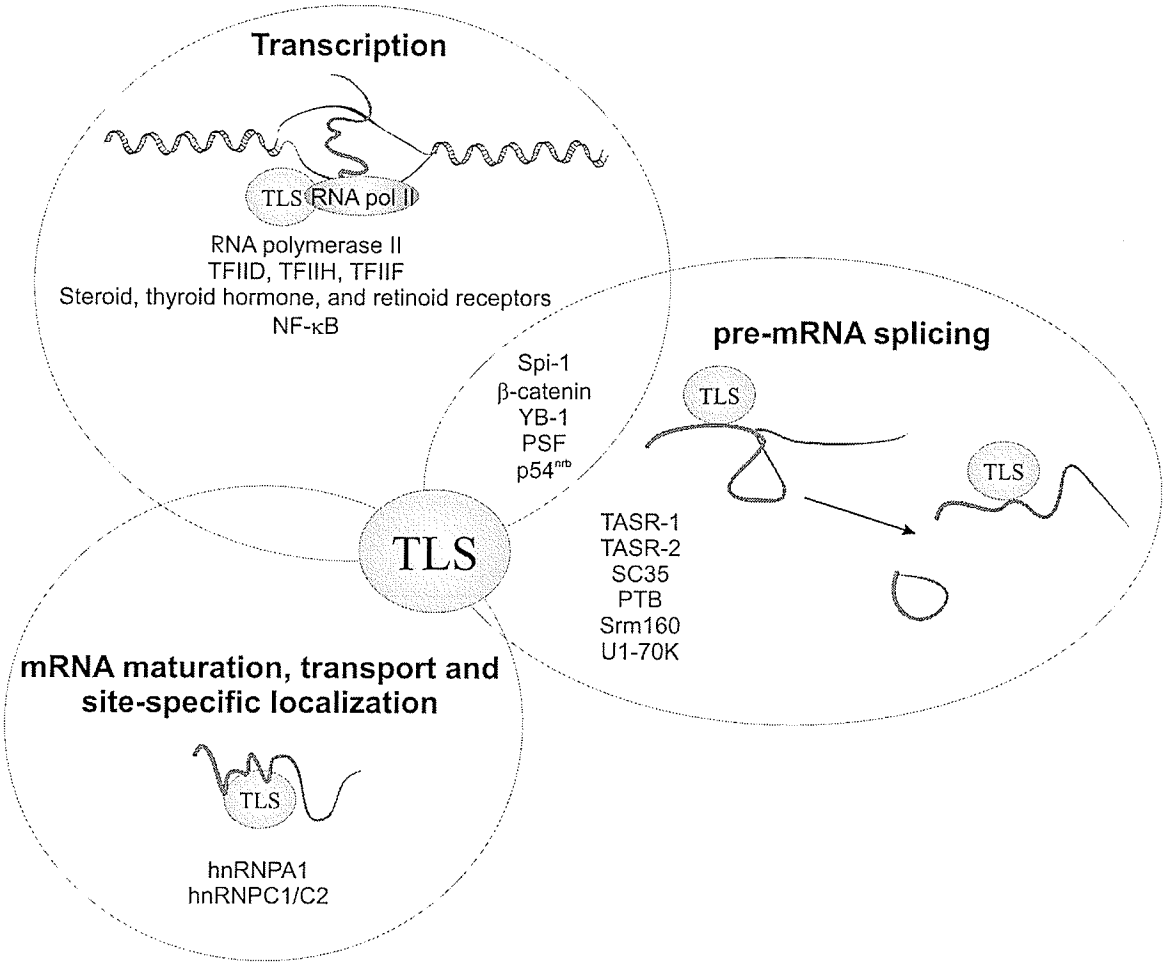

Figure 1.3: TLS is a multifunctional protein regulating several levels of gene expression. TLS can affect gene expression from the initiation of transcription, through mRNA splicing, to mRNA maturation, transport and site-specific localization. The identification of the cellular signals that activate TLS and its multifaceted response is an area of current research. Proteins known to interact with, or are found in the same complexes as TLS are listed within the circle surrounding the specific step in which they function.

1.4 TLS cellular localization and its association with the nucleolus

TLS is found predominantly in the nucleus (our data and [91, 95, 96]), and is generally excluded from the nucleoli. Following transcriptional inhibition by actinomycin D, TLS relocalizes from the nucleoplasm to the nucleoli (our data and [91, 95, 96]) into structures that have been identified as dark nucleolar caps (DNCs)[95]. DRB (5,6-dichloro-benzimidazole riboside) and α-amanitin, other inhibitors of transcription, also induce a relocalization of TLS to the nucleolus[53, 96]. These observations demonstrate that TLS dynamically relocalizes to signals within the cell.

Actinomycin D is a DNA intercalator, and inhibits all three RNA polymerases (I, II, and III)[97]. Following actinomycin D treatment, the nucleoli segregate, and proteins such as nucleolin and nucleophosmin, which are normally found in the granular component (GC) of the nucleolus, disperse into the nucleoplasm[95]. Other proteins segregate into distinct, but juxtaposed nucleolar caps and a central body[95]. Besides TLS, the dark nucleolar caps also contained PSF, EWS, Cdk2 (see section **1.9**), $p54^{nrb}$, the p68 helicase, hnRNP F, and U1-70K[95]. As mentioned above, TLS, PSF, $p54^{nrb}$ and U1-70K were previously found bound, in addition to RNA polymerase II, TFIIF, and TFIIH, in joint transcription and splicing machinery complexes[88]. RNA polymerase II, TFIIF, and TFIIH were not found in the DNCs, suggesting that this relocalization is not a general trait of all RNA transcription and processing machinery, and that it may be part of a regulated stress response to transcriptional inhibition[95]. While these studies have identified many potential interaction partners for TLS, the exact domain in TLS that is responsible for this relocalization has only been narrowed to the N-terminus[53, 96].

The function of TLS's association with the nucleolus is unknown, but it is intriguing given the multifunctional nature of this structure, the most prominent suborganelle in the nucleus. The nucleolus has three morphologically distinct components: fibrillar centres (FCs) are surrounded first by dense fibrillar components (DFCs), and then by the granular component (GC) [98]. The FCs contain tandemly repeated ribosomal (rDNA) genes, genomic segments that also contain the nucleolar-organizing regions. RNA polymerase I transcribes these genes, and newly minted pre-rRNAs radiate out into the DFCs[98]. The nucleolus is also the site of post-transcriptional modification of the pre-rRNAs, and assembly of the pre-ribosomal subunits[98]. The role of the nucleolus in ribosome biogenesis is well known; however, more recently, the nucleolus has been found to be critical for other cellular processes. It is associated with the assembly of ribonucleoprotein complexes, including telomerase[99], and both spliceosomal snRNA (small nuclear RNA) and tRNA maturation[98]. Perhaps most relevant with respect to the role of TLS as a proto-oncoprotein, the nucleolus is also associated with the regulation of the cell cycle. The nucleolus itself is cell cycle regulated, as Cdk1-cyclin B represses RNA polymerase I function from the beginning of prophase to the end of anaphase, causing the nucleolus to disintegrate[100]. Also, ARF can sequester MDM2 in the nucleolus, activating p53 and potentially the cell cycle checkpoints it regulates[101]. Other proteins that have been found associated with the nucleolus include ATR (ATM- and Rad3-related, see section **1.6**), TASR-1, RAD50 (see section **1.6**), and p80-coilin[102].

Other associations between TLS and specific nuclear suborganelles have also been found. For example, both TLS and the protein SMN (survival motor neuron) have

been found to interact with nuclear factor associated with dsRNA (NFAR)-2[103]. SMN is a protein that is involved in snRNP biogenesis[104]; it localizes to Cajal (coiled) bodies in some cell types, but in other cell types, forms distinct SMN-containing gems that localize adjacent to Cajal bodies[105-107]. Finally, TLS itself has also been localized to Cajal bodies[108]. Cajal bodies are dynamic structures that can move in and out of the nucleoli, and they are typically present as 1-5 structures per cell in a perinucleolar location[98]. p80-coilin, a protein involved in nucleo-cytoplasmic shuttling, is the marker for Cajal bodies[98]. Cajal bodies are thought to function in the transport and maturation of snRNPs and snoRNPs, and as an assembly site for RNA polymerase I, RNA polymerase II, and RNA polymerase III transcriptosomes[98]. Furthermore, they have been found preferentially localized to tandemly repeated genes, including those for histones and snRNAs[98]. Besides the association with histone gene expression, Cajal bodies have another association with the cell cycle, as CDK2-cyclin E is localized to Cajal bodies in a cell-cycle-dependent manner[109].

1.5 TLS and genomic stability

Despite its well-documented association with transcription, splicing, and RNA transport, the exact function of TLS and the processes it helps regulate are unknown. To better understand the wild-type function of TLS, the Hicks laboratory generated TLS-deficient mice. In these mice, TLS is disrupted in exon 12 by the U3NeoSV1 gene trap provirus[110, 111]. While the insert was in the 3' end of the gene, the gene trap resulted in a null mutation as assessed by northern, western, and RT-PCR analysis[111], probably because of instability in any fusion mRNA, and truncated TLS protein expressed. Mice homozygous for the mutation ($TLS^{-/-}$) exhibit perinatal lethality, with no mice surviving

longer than 16 h following birth[111]. The mice had undersized thymus glands and decreased white blood cell counts, but otherwise were morphologically and histologically normal[111]. The observed lymphopenia was due to a defect in B cell development, specifically the transition between the pre-B cells and IgM^+ B cells[111]. This defect was not cell intrinsic, as *TLS* $^{-/-}$ IgM^+ B cells developed following transfer of *TLS* $^{-/-}$ fetal liver cells to lethally-irradiated congenic mice. However, these *TLS* $^{-/-}$ B cells exhibited a defective proliferation response to specific mitogenic stimuli, and they also failed to produce as many antigen-specific IgM, but not IgG_1, antibodies following immunization with ovalbumin, indicating that the mature *TLS* $^{-/-}$ B cells are defective in specific B cell activation pathways[111]. Intriguingly, the unpassaged (P0) mouse embryonic fibroblasts (MEFs) from the *TLS* $^{-/-}$ embryos exhibited a high degree of genomic instability, with over 67% of cells exhibiting abnormal karyotypes[111]. The observed instability included aneuploidy, extrachromosomal elements, chromosome breakage, centromere loss, chromosome fusion, and defects in chromosome segregation[111]. This phenotype is consistent with mouse models involving genes responsible for human DNA breakage syndromes, such as the *ATM*-deficient mouse[112-114], and the *NBS1*-mutant mouse[115], both of which are described in section **1.6**, and suggests that TLS is an essential genomic caretaker. The involvement of a ribonucleoprotein in genome maintenance is a novel finding, and indicates that there are unknown mechanisms by which cells maintain genomic stability.

Consistent with the Hicks data, another mouse model of *TLS* disruption showed that *TLS* mutation does lead to radiation sensitivity in the whole mouse and mouse embryonic fibroblasts (MEFs), to synaptic aberrations in premeiotic spermatocytes, and

male infertility[116]. In this mouse model, outbred *TLS* $^{-/-}$ mice survived post-natally, but, as in the Hicks mouse model, their inbred mice failed to survive post-natally, suggesting that there are modifier genes affecting the severity of the *TLS* $^{-/-}$ phenotype. TLS can also mediate homologous pairing[64] and D-loop formation[117], properties that suggest that TLS functions in the homologous recombinational repair of DNA damage (see section **1.8d**). Furthermore, EWS has been found to interact with BARD1 (BRCA1 associated RING domain protein), a protein that, as its name suggests, interacts with BRCA1 (Breast cancer susceptibility 1)[118]. BRCA1 is an important mediator protein in the ATM DNA double-strand break (DSB) signalling cascades initiating both repair and cell-cycle checkpoints[119], providing further evidence for an association of the TET proteins with genome maintenance.

1.6 Human genomic instability syndromes

1.6.1 Genetic determinants of genomic instability syndromes

Human genomic instability syndromes are characterized by genomic instability (point mutations or chromosome aberrations) and cancer predisposition[120-122]. Mapping of their causative genes has identified many of the proteins involved in DNA repair, including *ATM*. *ATM* is the gene mutated in the recessive disorder ataxia telangiectasia (AT)[123], and its protein product is now believed to be the pinnacle kinase of the DNA double-strand break (DSB) cascade, regulating repair, cell cycle checkpoints, and even apoptosis[124-126]. AT patients are sensitive to γ-irradiation, which causes DSBs as its most lethal form of DNA damage, and exhibit a predisposition to cancer[124-126]. AT carriers are also at an increased risk for cancer[123]. ATM is a member of the phosphatidylinositol 3-kinase-like family of serine/threonine protein kinases, which also includes ATR (ATM-

and Rad3-related), and DNA-PKcs (DNA-dependent protein kinase catalytic subunit), a protein that will be described in section **1.8d**. These kinases phosphorylate SQ or TQ motifs[127]. Like ATM, ATR has also been found to be a critical kinase responding to DNA damage, although in the case of ATR the activating signal is a stalled replication fork due to damage induced by ultraviolet (UV)-irradiation, hydroxyurea, or replication inhibitors such as aphidicolin[128]. Hypomorphic mutations in *ATR* cause ATR-Seckel syndrome[129].

Other syndromes that are caused by a defective DSB-response include AT-like Disorder (ATLD), Nijmegen Breakage Syndrome (NBS), LIG4 syndrome, and RS-SCID (severe combined immunodeficiency with sensitivity to ionizing radiation)[129]. ATLD, and NBS are caused by mutations in *Mre11*, and *NBS1*, respectively[129]. Mre11, Nbs1, and Rad50 form the MRN complex, and this complex has roles in DNA damage recognition, DNA processing and repair, and cell cycle checkpoints[130]. The clinical features of AT, ATLD, and NBS are described in more detail in Table 1.2. LIG4 syndrome is caused by hypomorphic mutations in the gene for DNA ligase IV, an important component of the non-homologous end-joining (NHEJ) pathway (see section **1.8d**) while RS-SCID is caused by null or hypomorphic mutations in *Artemis*, another component of the NHEJ pathway[129].

Xeroderma pigmentosum (XP), Cockayne's syndrome, and Trichothiodystrophy (TTD) are all caused by mutations in genes involved in global nucleotide excision repair (NER) or the NER subpathway of transcription-coupled repair. Affected individuals are all photosensitive, but only XP patients exhibit a predisposition to UV-induced skin cancer[120, 122]. Bloom's syndrome, Werner's syndrome, and Rothmund-Thompson

syndrome are all caused by mutations in DNA helicases of the reqQ-like family, specifically *BLM*, *WRN*, and *RECQL4*, respectively, and all feature chromosomal instability and cancer predisposition[122].

Fanconi Anemia patients exhibit sensitivity to cross-linking agents, specifically mitomycin C, and can be caused by mutations in *BRCA2* (*FANCD1*), or any of the other FANC genes (*FANCA, B, C, D2, E, F, G, I, J, L, or M*)[121, 131, 132]. In addition, mutations in *BRCA2* (breast-cancer susceptibility gene 2) or *BRCA1* can also predispose individuals to breast and ovarian cancers[119]. Another cancer predisposition syndrome is Li-Fraumeni syndrome, which can be caused by mutations in *TP53*, the gene for p53, or *CHK2*[133], which are both important proteins for initiating DNA damage-induced cell-cycle checkpoints. Mice deficient for p53 exhibit genomic instability, and cancer susceptibility[134, 135].

1.6.2 Mouse models of human genomic instability syndromes

A comparison of the clinical features of AT, ATLD, NBS, and FANCD2 and the phenotypes of their mouse models is shown in Table 1.2. Mouse knock-outs of *Mre11* or *Nbs1* are embryonic lethal; therefore, the ATLD and NBS mouse models only have truncated *Mre11*[136] or *Nbs1*[115, 137], respectively. This also better models the clinical disease, as patients only exhibit hypomorphic mutations of these genes[121].

Patients with ataxia telangiectasia exhibit multi-system defects, including a predisposition to cancer, sensitivity to γ-irradiation, and immune system defects. The mouse models of AT recapitulates this phenotype, with these mice exhibiting radiation hypersensitivity, chromosome instability, cancer predisposition, abnormal immune system development, DNA damage-induced apoptotic defects, and checkpoint failure[112-

[114]. In fact, genomic instability, IR-sensitivity, immune-system defects, and cancer predisposition are common elements in patients and mice models for both AT and NBS[112-115, 137-139]. ATLD patients and mice also exhibit genomic instability and IR-sensitivity, and the patients also exhibit immune-system defects[136, 140, 141]. Fanconi anemia subtypes and their mouse models also exhibit genomic instability and cancer predisposition, but they are sensitive to DNA cross-linking agents such as mitomycin C instead of IR[122].

The *TLS*$^{-/-}$ mice exhibit characteristics consistently found in mouse models of human genomic instability syndromes, specifically genomic instability[111], immune system defects[111], and sensitivity to ionizing irradiation[116]. Because the causative genes of these syndromes are all involved in the DNA damage response pathways (repair, cell cycle checkpoints, and/or apoptosis), this suggests that TLS also plays a role in these pathways.

Table 1.2: Features of human genomic instability syndromes and their mouse models

Syndrome	*Gene*	*Clinical Features*	*Mouse Features*
Ataxia telangiectasia (AT)	*ATM* (hypomorphic and null mutations[121])	Genomic instability, cancer predisposition, IR sensitivity, immune system defects, ataxia and other neurological defects, telangiectasias (chronic dilation of capillaries leading to red blotches), cellular radioresistant DNA synthesis[112-114]	Genomic instability, cancer predisposition, IR sensitivity, abnormal immune system development, cellular DNA damage-induced apoptotic defects, and checkpoint failure[112-114]
AT-like Disorder (ATLD)	*MRE11* (hypomorphic[121])	Genomic instability, IR sensitivity, may have reduced levels of specific functional antibodies, ataxia and other neurological defects (which have a later onset, and slower progression than that observed in AT patients), cellular radioresistant DNA synthesis[140, 141]	Mice homozygous for a truncated Mre11 exhibit genomic instability, IR sensitivity, checkpoint defects, reduced latency of lymphomagenesis in a *p53* +/– background[136]
Nijmegen Breakage Syndrome (NBS)	*NBS1* (hypomorphic[121])	Genomic instability, cancer predisposition, cellular IR sensitivity, immune system defects, microcephaly and other congenital malformations, cellular radioresistant DNA synthesis[138, 139], cellular sensitivity to mitomycin C[142]	Knock-out mice exhibit early embryonic lethality[143]. Mice homozygous for a truncated Nbs1 exhibit genomic instability after IR, cancer predisposition, and IR sensitivity[115, 137]. Knock-out B cells exhibit a class-switch recombination defect and genomic instability[144]
Fanconi Anemia D2	*FANCD2* (hypomorphic[121])	Genomic instability, cancer predisposition, cellular sensitivity to cross-linking agents such as mitomycin C, bone-marrow depletion leading to aplastic anemia, congenital malformations[145]; cellular sensitivity to IR in an immortalized cell-line from a patient with a null genotype[146]	Knock-out mice exhibit chromosomal mispairing in male meiosis, cancer predisposition, cellular sensitivity to mitomycin C, increased perinatal lethality in a C57BL/6J strain, germ cell loss, eye abnormalities[145]

1.7 DNA damage and repair mechanisms

The human genome is made up of approximately 3.3 x 10^9 base pairs organized into 46 chromosomes[147]. This is over 2 m of DNA that needs to be accurately replicated in each of the cell divisions required to produce the approximately 1x 10^{14} cells in a human body[148]. Furthermore, this blueprint of life exists in a hostile environment, being constantly damaged by both endogenous and exogenous sources[120]. To maintain the integrity of the genome, cells have developed complex pathways to minimize the acquisition of mutations, including both genomic caretakers that repair DNA, and cell gatekeepers that control the cell cycle and/or apoptosis[120, 149-155]. On the most basic level, genomic integrity is required for maintaining critical cellular genes whose products allow life to exist at both the cellular and organism level. Genomic stability is also required for fidelity in inheritance, between mother and daughter cells at a single-cell level, and between parents and offspring at an organism level. In metazoans, genomic integrity is also critical for ensuring proper development, and for the prevention of cancer development. Ironically, most cancer treatments kill cells by further damaging their DNA, resulting in either mitotic catastrophe or programmed cell death. As such, we need to know how these pathways function in order to better understand how to design treatments with respect to the gene mutations that led to the cancer in the first place, and to minimize secondary cancers induced by the therapies themselves[120, 149-155].

The DNA repair mechanisms in mammalian cells can be broadly considered in seven categories: mismatch repair, direct repair, base excision repair, nucleotide excision repair, translesion synthesis, interstrand cross-link repair, and double-strand break repair. These pathways are summarized in Table 1.3 and described in detail in the text.

Table 1.3: Mammalian DNA repair mechanisms

Specific type of error/damage	*Source of errors/damage*	*Most common repair mechanism*
Base mismatches	DNA polymerase errors	Mismatch repair (MMR)
O6-methylguanine	Methylating agents	Direct repair via methylguanine methyltransferase
Chemically modified bases, base mismatches	Spontaneous chemical reactions, endogenous and exogenous chemicals, DNA polymerase errors	Base excision repair (BER)
Pyrimidine dimers, and pyrimidine (6-4) pyrimidone photoproducts	UV-irradiation	Nucleotide excision repair (NER)
DNA damage blocking DNA polymerase progression	Endogenous and exogenous chemicals	Translesion synthesis
Interstrand cross-links	Interstrand cross-linking agents, including mitomycin C	Interstrand cross-link repair incorporating NER, translesion synthesis and homologous recombination
DNA double-strand breaks	Ionizing radiation (X-ray, γ irradiation), radiomimetic drugs, reactive oxygen species, other endogenous sources	Homologous recombination (HR) or non-homologous end-joining (NHEJ)

1.7a Mismatch Repair (MMR)

MMR increases the fidelity of DNA replication by correcting base mismatches that have escaped the proofreading capabilities of the polymerases during synthesis[156]. MSH2/MSH6 and MLH1/PMS2 heterodimers initially recognize the mismatch via a

scanning mechanism[156]. As both bases in a mismatch can be normal, undamaged nucleotides, the next critical step is identifying which is the incorrect base. The only way of correcting the error is to identify and remove the base on the newly synthesized strand. The new strand is identified by the presence of gaps between Okazaki fragments on the lagging strand or the free 3' end on the leading strand. Therefore, the MMR can only function if the mismatch occurs near a strand discontinuity[156]. Exonucleases will remove the bases beginning at the discontinuity all the way to the base mismatch, at which point a DNA polymerase fills the gap correcting the mismatch[156]. The MMR system has also been implicated in homologous recombination by preventing strand exchange between nonhomologous sequences[156].

1.7b Direct repair

Direct repair in mammals specifically removes the O^6-methyl group from O^6-methylguanine, a modified base formed by methylating reactions. This repair is mediated by methylguanine DNA methyltransferase in a simple enzymatic reaction[153]. If the methyl group is not removed, O^6-methylguanine can lead to a vicious cycle of removal/attempted repair by the mismatch repair system. The MMR will see the paired thymine as a mismatch, and will remove it. Unfortunately, the thymine will be replaced during the repair, only to be removed again by the MMR. As the mismatch is never repaired, and the process repeats itself in a futile cycle, it ultimately leads to cell death[153].

1.7c Base excision repair (BER)

BER repairs alkylated bases (generally methylated bases), oxidized or reduced bases, deaminated bases, base mismatches, and apurinic or apyrimidinic (AP) sites. Cells have a whole array of glycosylases that recognize specific damaged bases, and these

enzymes remove the damaged bases to create apurinic or apyrimidinic sites[153]. Lyase and endonuclease activities remove the single abasic sugar (short patch repair) or multiple nucleotides (long patch repair), and then polymerases and ligases fill and seal the gap[153].

1.7d Nucleotide excision repair (NER)

NER removes bulky DNA adducts, including intrastrand cross-links, formed by exposure to radiation or chemicals, or aberrant protein-DNA bonds[153]. For example, NER is responsible for repairing damage caused by UV-irradiation, specifically cyclobutane pyrimidine dimers and pyrimidine (6-4) pyrimidone photoproducts[157]. First, the lesion is recognized by the presence of an abnormal conformation of phosphodiester backbone, and then enzymes cut incisions flanking the damage. The detached oligomer is removed, and the resulting gap is filled in by polymerases and ligated shut. TFIIH, which contains XPB (Xeroderma pigmentosum B) and XPD, is an important NER factor. Furthermore, when lesions such as cyclobutane pyrimidine dimers and pyrimidine (6-4) pyrimidone photoproducts block a replication fork, ATR becomes activated[128]. Actively transcribed DNA is also repaired faster by NER than nontranscribed DNA, but the precise mechanisms of this transcription-coupled NER have not been clarified in eukaryotes yet[153].

1.7e Translesion synthesis

When a replication fork encounters a lesion in the DNA, DNA polymerase δ (or ε) is replaced by one of the translesion DNA polymerases. These polymerases are able to replicate through the DNA damage, preventing the replication fork from stalling and potentially collapsing. Translesion synthesis also plays a role in homologous recombination, especially in the repair of lesions such as interstrand cross-links, which have repair intermediates that could stall replication forks[158] (also see section **1.7f**).

1.7f Interstrand cross-link (ICL) repair

ICLs are covalent links that occur between the two strands of DNA, rather than intrastrand cross-links that occur on the same strand of DNA. Because ICLs affect both strands of DNA, they are among the most lethal and mutagenic types of DNA damage[159]. Furthermore, they can adversely affect both transcription and replication, which require the two strands of DNA to be separated[159]. Although some endogenous agents formed during lipid peroxidation have the potential to form ICLs, they do not seem to cause ICLs under physiological conditions. Therefore, exogenous agents cause most ICLs, especially chemotherapeutic drugs such as mitomycin C, cisplatin, and nitrogen mustards[159]. Other ICL agents include furocoumarins, which are found in plants and cosmetics[159]. The drug mitomycin C (MMC), the ICL agent used in this thesis, binds in the minor groove[159] to the N^2 amino groups of the two guanines in a 5'-GC-3' or 5'-CG-3' sequence, creating an interstrand cross-link[160, 161] (see Figure 1.4). (MMC causes monoadducts and intrastrand cross-links as well[159].)

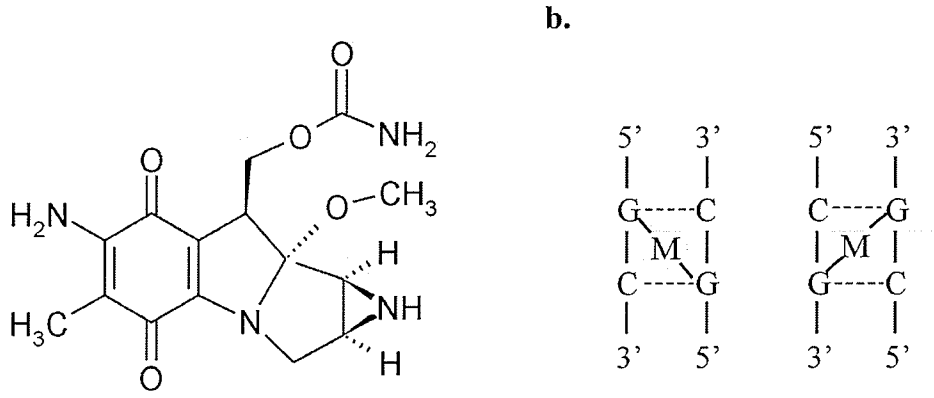

Figure 1.4: Mitomycin C and interstrand cross-links a. Structure of mitomycin C. Yellow circles identify the carbons involved in the interstrand cross-link across two guanine bases. **b.** The two types of interstrand cross-links caused by mitomycin C in DNA.

The mammalian ICL repair pathway(s) have not been completely elucidated yet, but it is known that multiple pathways are involved to some extent, specifically NER, translesion synthesis, and homologous recombination[162]. In mammalian cells, ICLs seem to be repaired predominantly during S phase[162]. The first step in repair is a replication-independent incision by ERCC1/XPF, and when a replication fork encounters this ICL/incision, it first stalls and then collapses, generating a DSB[163] (Figure 1.5). The stalled replication fork will result in the activation of ATR, which initiates the ICL repair pathways. The importance of ATR to the ICL-repair pathways is demonstrated by the fact that ATR-Seckel cells are hypersensitive to MMC and are prone to MMC-induced genomic instability[164, 165]. Furthermore, ATR directly phosphorylates FANCD2[166], and is required for efficient FANCD2 monoubiquitination following MMC[165]. As mentioned earlier, Fanconi Anemia patients have a pronounced sensitivity to interstrand cross-linking agents[121, 131, 132]. While the exact functions of all the FANC proteins have not been identified yet, one of the main purposes of the FA complex, specifically FANCL,

appears to be as a putative E3 ligase for the monoubiquitination of FANCD2, although only the BRCA1/BARD1 complex has been shown to ubiquitinate FANCD2 in vitro[132]. Once FANCD2 is activated, it binds chromatin[167], and can interact with DNA repair proteins such as BRCA1[168], NBS1[142, 169], BRCA2[168], and the recombination protein RAD51[168]. The next step is that of "unhooking" the interstrand cross-link by an incision on the other side of the lesion. A translesion polymerase then synthesizes a complementary strand to the unhooked cross-link, after which the NER system cleaves out the unhooked lesion (Figure 1.5). The homologous recombination repair machinery, potentially including the recombinases Rad51, XRCC2 and/or XRCC3, then repairs the induced DSB, and the replication fork is restarted[132, 159, 162, 166]. Because a translesion polymerase is used in the repair of ICLs, point mutations are frequently incorporated[166]. There is also some evidence that ICLs can be repaired via a transcription-coupled NER repair, and translesion synthesis, although this is probably a minor pathway compared to the homologous recombination-mediated repair pathway outlined above and shown in Figure 1.5[170, 171].

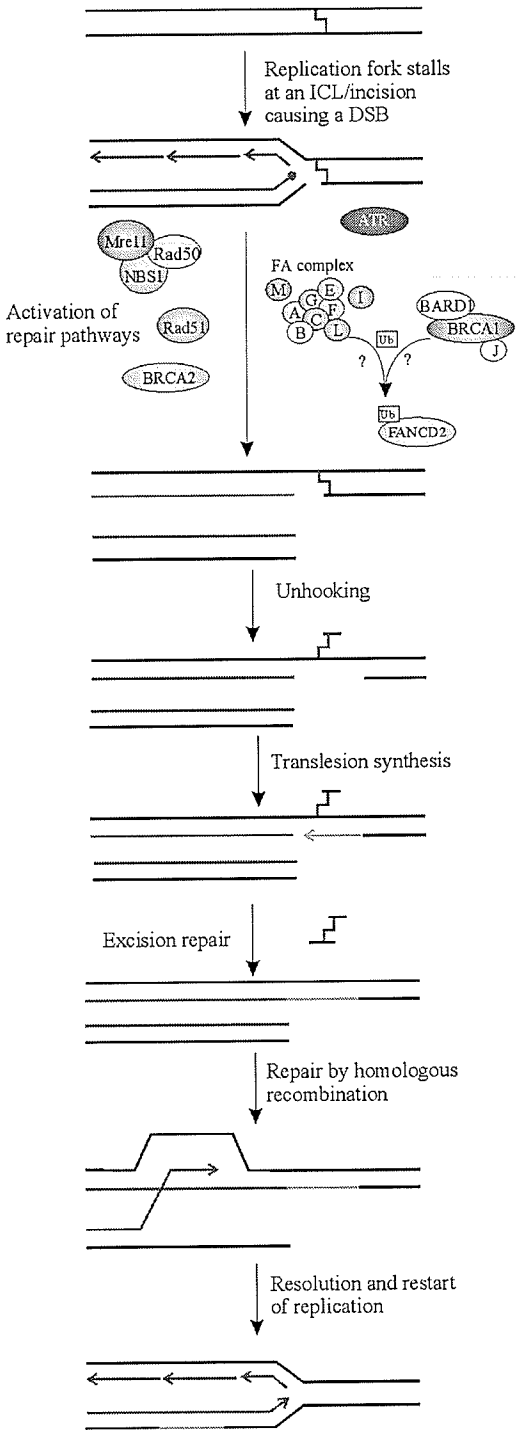

Figure 1.5: The mammalian interstrand cross-link (ICL) repair pathway. ATR is the pinnacle kinase in the interstrand cross-link repair pathway, and it becomes activated during S phase when a replication fork stalls and collapses at the site of the ICL. The cross-link is first "unhooked" from one strand, and then excised from the other strand. Both translesion synthesis and homologous recombination is required for this type of repair. Further details of this pathway can be found in the text.

1.8 DNA double-strand break (DSB) repair

1.8a Endogenous and exogenous sources of DSBs

Every cell cycle approximately 50 DNA double-strand breaks (DSBs) occur in a human cell, or one DSB per 10^8 base pair[172]. This is equivalent to the number of DSBs approximately produced by 1.5 Gy of ionizing irradiation in the form of γ-irradiation or X-rays[172]. Endogenous DSBs are produced when a single-strand lesion is not repaired and encounters a replication fork in S phase. The single-strand lesion can be a single-strand break (SSB), an apurinic/apyrimidinic (AP) site, an oxidized base, such as 8-oxoguanine or thymine glycol, or by endogenous alkylation products, including 3-methyl adenine. When a replication fork encounters one of these single-strand lesions, it may either collapse in the case of an SSB, or stall in the case of base damage, potentially resulting in a DSB[172]. Almost all of the endogenously produced DSBs are generated during S phase; therefore, nondividing cells are predicted to produce endogenous DSBs at a very low rate, and they do in fact exhibit a very low background level of DSBs[173]. Reactive oxygen species (ROS) do not directly produce endogenous DSBs at a biologically relevant rate, but do so indirectly through single-strand lesion formation. Another source of endogenously produced DSBs is the rearrangement of immunoglobin, and T-cell-receptors in B- and T-cells, respectively, and meiotic recombination in germ cells[120, 126].

Given that cells can normally repair these endogenously produced DSBs[172], why is a dose of 1.5 Gy of ionizing irradiation, which produces the same number of DSBs as a normal S phase, toxic to mammalian cells? Experimentally administered ionizing irradiation is usually given at a dose rate of greater than 1 Gy/min, but if this dose rate is

lowered to generate DSBs at a similar rate to that occurring during S phase, these lesions are then repaired with a low error rate by non-homologous end-joining (NHEJ)[174]. Therefore, it is the rate of DSB formation, and not the overall number of DSBs, that is responsible for the toxicity caused by 1.5 Gy of experimentally delivered ionizing irradiation: the cellular DNA damage response pathways become overwhelmed by the sudden occurrence of a large number of DNA double-strand breaks[172]. Besides ionizing radiation (X-rays and γ-irradiation), other exogenous sources of DSBs include radiomimetic drugs, such as bleomycin[175].

1.8b Activation of ATM, the pinnacle kinase of the DSB signalling cascade

Like interstrand cross-links, DSBs are a highly lethal form of DNA damage because they affect both strands of DNA. Failure to repair or incorrect repair of a DSB could result in deletions, inversions, and/or translocations[176]. While interstrand cross-links, especially those induced by MMC, can have little affect on DNA structure[159-161], DSBs remove topological constraints on DNA loops[177-179], potentially causing drastic changes in chromatin structure[180]. Chromatin changes such as this might be enough to activate ATM, the pinnacle kinase in the DSB signalling cascade[180], but there is also evidence that suggests that the MRN (Mre11/Rad50/Nbs1) complex first detects the DSB, then interacts with ATM, and is required for efficient ATM kinase activity following IR[181-187]. The MRN complex binds DNA, and has nuclease activity via Mre11; therefore this complex may be required for the initial processing of the DSB[130, 188].

ATM is normally present in cells as an inactive dimer or multimer, with each internal domain containing serine 1981 being blocked by another ATM molecule. Following ionizing radiation, the kinase domain of one ATM molecule phosphorylates

the 1981 serine residue of another ATM molecule, breaking up the dimer/multimer and freeing ATM to phosphorylate other targets[180]. These targets include Nbs1[189, 190], suggesting that there is mutual promotion of activity between the MRN complex and ATM. Furthermore, Nbs1 contains a BRCT (BRCA1 carboxy-terminal) domain, and a FHA (fork-head associated) domain, and both domain-types have been shown to bind phosphorylated proteins, suggesting that Nbs1 could bind other ATM targets post-phosphorylation[130, 191-195].

1.8c Activation and recruitment of DSB response proteins by ATM

Once ATM is activated, it initiates the DSB signalling cascades, directly activating proteins required for repair, cell-cycle checkpoints (G1/S, intra-S-phase, and G2/M) and apoptosis[122, 124-127, 176]. The DSB-induced cell-cycle checkpoints and apoptotic pathway will be discussed in more detail in later sections. While it is convenient to discuss the cellular DSB response in the context of the ATM-dependent signalling cascade, an important caveat to this simplification is the fact there are AT patients with null mutations in ATM, and ATM knock-out mice are viable[112-114, 121]. On the other hand, completely knocking-out Nbs1[143], Mre11[196], Rad50[197], ATR[198, 199], or the recombinase Rad51[200, 201] results in early embryonic lethality in the mouse models. These observations suggest that the MRN complex and Rad51 have additional functions exclusive of the ATM pathway and/or can function to some extent without the presence of ATM.

Within minutes following IR, ATM phosphorylates H2AX in the C-terminal tail at serine 139 over a region of megabases surrounding a DSB[202-204]. (DNA-PK has also been shown to phosphorylate H2AX after IR[205], and ATR can phosphorylate H2AX after

replicational stress[206], indicating that there is some potential functional redundancy in the DNA damage response pathways.) Recruitment of DNA damage response proteins to sites of γH2AX (H2AX phosphorylated on serine 139) and DSBs appears to be in two phases: an initial recruitment of factors that is visible when using a laser beam to induce DSBs, and a later build-up of factors into ionizing radiation-induced foci (IRIF)[207, 208]. While IRIF foci formation of γH2AX[202], 53BP1 (p53 binding protein 1) [209, 210], and MDC1 (mediator of mammalian DNA damage checkpoint 1)[211] occurs within minutes following IR, other factors, such as Rad51, MRN complex, ATM, BRCA1, and Rad52 do not form IRIF until over 30 min post-IR[207, 208, 212, 213]. Yet, damaging cells with laser scissors has shown that BRCA1, ATM, and the MRN complex are recruited within minutes to sites of DSBs, and that while this initial recruitment is not dependent on γH2AX, the later formation of IRIF is[207, 208].

Interestingly, like $ATM^{-/-}$ mice, $H2AX^{-/-}$ mice are viable, suggesting that the absence of H2AX phosphorylation can be circumvented to some extent[207]. ($H2AX^{-/-}$ mice exhibit genomic instability, IR-sensitivity, male infertility, and immune system defects[207]. At low IR doses, $H2AX^{-/-}$ MEFs also exhibit a G2/M checkpoint failure[214].) Recently, Protein Phosphatase 2A has been identified as the phosphatase that removes the phosphate from γH2AX, and this enzyme is required for efficient DNA repair[215].

Following IR, ATM also directly phosphorylates 53BP1[210], MDC1[216], BRCA1[217, 218], and c-Abl[219]. ATM also indirectly activates BRCA1 via Chk2[220], and Rad51 via c-Abl[221-223] (see Figure 1.6). The BRCT-containing proteins Nbs1, MDC1, 53BP1, and BRCA1 are all thought to function as mediators, helping to bring together various repair and checkpoint proteins[150, 152]. MDC1 has been shown to be critical for recognizing

γH2AX, and amplifying the DSB signal through interaction with ATM for a more effective and maintained response[224]. MDC1 also interacts with the recombinase Rad51[225], and functions in checkpoint control[216, 226, 227]. BRCA1 can interact with both Rad51 and BRCA2[119, 168, 228], is required for some ATM-dependent phosphorylation events[229], and functions in checkpoint control[217, 218, 230]. As described in section **1.8b**, Nbs1 functions directly in sensing damage and activating ATM via the MRN complex[181-187]. The MRN complex is also directly involved in repair via the nuclease activity of Mre11[130], and Nbs1 also functions in the intra-S-phase checkpoint[190] and helps promote ATM-dependent phosphorylation events required for the G1/S checkpoint[185]. Finally, 53BP1 also appears to help promote ATM activation following DSBs[231], and functions in activating the G2/M checkpoint[214].

1.8d DNA double-strand break repair pathways

Once the DSB response pathways have been initiated, DSBs can be repaired by two main pathways: non-homologous end-joining (NHEJ) or homologous recombination (HR)[126, 176, 232-234] (Figure 1.6). NHEJ is the predominant pathway in mammalian cells, and during G1 and early S-phase is used almost exclusively. In this pathway, the regulatory subunits of DNA-PK, Ku70 and Ku80, first bind the broken ends of the DNA, recruiting the catalytic subunit of DNA-PK (DNA-PKcs). After end processing by the MRN complex (or Artemis), the Ligase IV/XRCC4 complex can ligate the strands together, usually with incurred deletions of nucleotides. Therefore, this pathway is an error-prone pathway[126, 176, 232-234]. During late S phase and G2, there are elevated levels of Rad52, a protein thought to compete with Ku70/Ku80 for binding to the broken DNA ends, and to initiate repair through the homologous recombination pathway instead of the

NHEJ pathway[235]. The sister chromatid is the preferred substrate for homologous recombination in mammalian cells, which is why HR appears to be only used in late S phase and G2.[235]. The MRN complex also functions in processing the broken ends for HR. Following end-processing, the recombinase Rad51 and RPA (replication protein A) bind the DNA, and promote strand invasion, forming a D-loop[126, 176, 232-234]. Other proteins are also involved in the repair, including Rad54. Rad54 is a SWI2/SNF2 family member, and can unwind DNA, suggesting that it functions in chromatin remodelling during repair[176, 236]. DNA polymerases prime off the free 3' ends in the D-loop structure, filling in the missing nucleotides. The Holliday junctions are then resolved, producing two error-free strands[126, 176, 232-234].

There is also another, error-prone type of homologous repair: single-strand annealing (SSA). SSA can be used when there are direct repeats on either side of the break. The ends of the break are resected until the repeats are reached, and the complementary single-stranded regions can then be annealed together, but this leads to deletion of the intervening sequence[176].

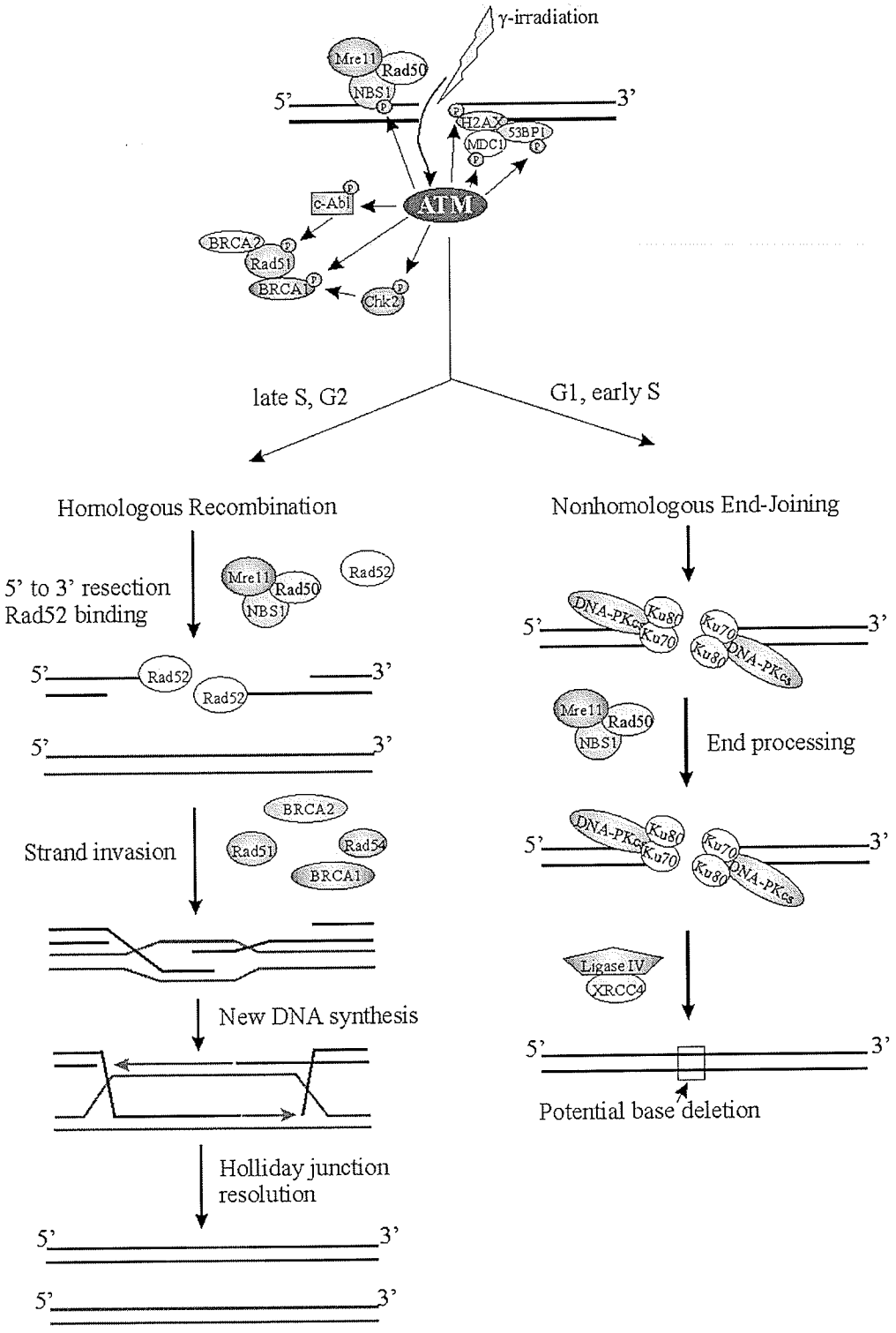

Figure 1.6: Mammalian DNA double-strand break (DSB) repair pathways. Following DSBs, ATM initiates repair via either homologous recombination or nonhomologous end-joining (NHEJ) depending on the stage of the cell cycle. Details of these pathways are given in the text. Phosphate groups are denoted by Ⓟ. The purple and black DNA strands represent sister chromatids.

1.9 The DSB-induced cell cycle checkpoints

There are three main cell cycle checkpoints responding to DNA double-strand breaks (DSBs): the G1/S, the intra-S-phase, and the G2/M checkpoints[153]. The immediate induction of these checkpoints after DNA damage provides time for repair before the damage is exacerbated through DNA replication or mitosis[153].

1.9a The G1/S checkpoint

The G1/S checkpoint is induced to prevent cells that were in G1 from progressing into S phase with DNA damage[153]. The current model of the G1/S checkpoint is that of a two-wave response: p53-independent pathways initiating an immediate G1 block, and a delayed p53-dependent arrest[237] (Figure 1.7).

The immediate G1/S checkpoint is thought to stop progression of cells into S phase after IR even if they have passed the restriction point, the point at which cells no longer require growth factors to enter S phase. This model has been developed in part based on studies with a Chinese hamster ovary (CHO) cell line. Propidium iodide staining and subsequent flow cytometric analysis showed that at 2-3 h post-γ-irradiation, CHO cells developed a shoulder peak off the larger G1 peak, and this minor peak of apparently irradiation-synchronized cells was then seen to progress through S-phase. The CHO cell line used had mutant p53, but when wild-type p53 was exogenously expressed in these cells, they still exhibited this synchronization peak[238]. However, a more complete analysis of the immediate G1/S checkpoint in asynchronous cultures has been hampered by the inability to distinguish cells that were replicating DNA prior to the DNA damage from cells that had entered S phase following DNA damage.

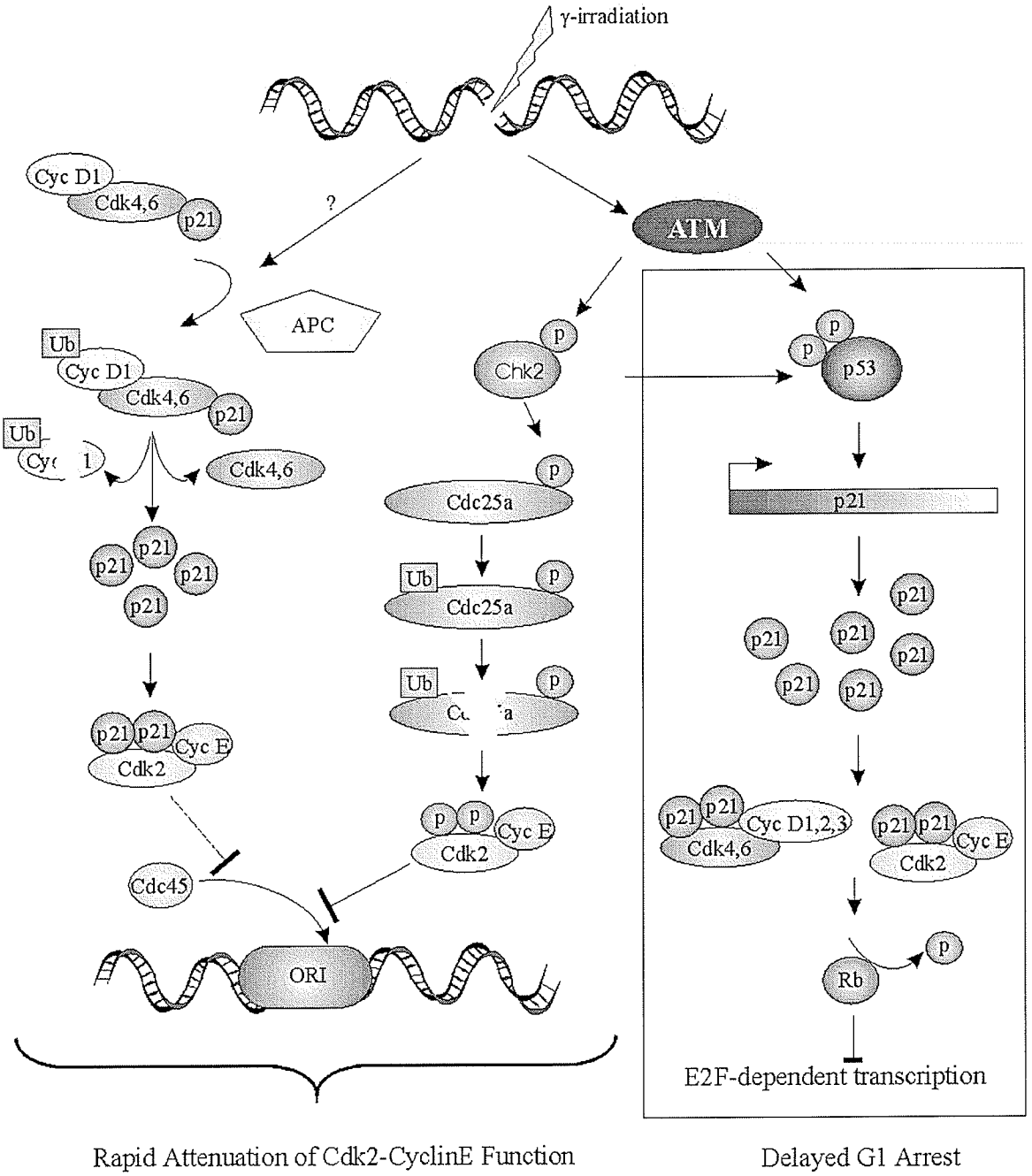

Figure 1.7: The DSB G1/S checkpoint pathways. The current model of the G1/S checkpoint is that of a two-wave response: p53-independent pathways initiating an immediate G1/S checkpoint, and a delayed p53-dependent arrest. Details of these pathways are given in the text. Phosphate groups are denoted by Ⓟ. Degraded Cdc25a protein is represented by ⊂⊃. Degraded cyclin D1 is represented by ⊂⊃.

Two pathways with the potential to initiate this immediate G1/S checkpoint have been identified, and both function to inhibit Cdk2. The first pathway targets Cdc25a, the phosphatase responsible for removing inhibitory phosphates on Cdk2. Following IR, ATM phosphorylates Chk2, which then phosphorylates Cdc25a on serine 123, leading to its ubiquitination and proteasomal degradation[239, 240]. While this pathway has been shown to be critical for preventing radioresistant DNA synthesis[240], it is also assumed to function at the G1/S transition[237]. The second pathway targets cyclin D1. The D-type cyclins function in mid-G1 in conjunction with Cdk4(6), and they at least partially function to inhibit pRB. Following IR, cyclin D1, but not cyclin D2 or cyclin D3, is degraded. The p21 that was bound to Cdk4(6)/cyclin D1 complexes is then free to bind and inhibit Cdk2/cyclin E complexes[241]. By targeting Cdk2, both of these pathways have the potential to affect origin licensing[242, 243] and origin firing[244].

The classical p53-dependent delayed G1/S checkpoint manifests itself as an overall decrease in S-phase cells observable 13-24 h post-ionizing-irradiation[245, 246]. This delayed G1/S checkpoint functions through an ATM-p53-p21-Cdk2 pathway[122, 237, 247, 248]. Following IR, ATM directly phosphorylates the critical tumour suppressor p53 on serine 15, and also activates Chk2, which further phosphorylates p53 on serine 20. These phosphorylation events stabilize p53 by interrupting its association with its negative regulator MDM2[122, 237, 247, 248]. ATM also directly phosphorylates MDM2, which also interferes with its ability to export p53 to the cytoplasm for proteasomal degradation[122, 249, 250]. Following activation, p53 can then induce the transcription of its target genes, including the critical G1/S regulator p21. p21 inhibits the Cdk2/cyclin E, Cdk2/cyclin A, and Cdk4(6)/cyclin D complexes[125]. This ATM-p53-p21-Cdk2 pathway has been

implicated in regulating both origin licensing[242, 243] and firing[244]. Inhibiting the Cdk2 and Cdk4(6) complexes also prevents them from phosphorylating pRB, allowing pRB to inhibit E2F-dependent transcription[237]. E2F targets include the genes for the origin licensing factors Cdc6, Orc1, and Mcm(2-7), Dbf4 (the regulatory subunit of the critical S-phase promoting kinase Cdc7), DNA polymerases, and the G1/S regulators cyclin A, cyclin E, Cdk2, and Cdc25a[251]. p21 can also directly prevent replication through an interaction with PCNA[252, 253] that prevents the loading of DNA polymerase δ.[254] Because these pathways require both the transcription and translation of p21, they are not thought to induce an immediate block to S phase entry[237].

1.9b The intra-S-phase checkpoint

The intra-S-phase checkpoint manifests as a decrease in DNA synthesis, as measured by ^{3}H-thymidine incorporation post-IR[255]. This decrease in DNA synthesis is primarily caused by a down-regulation of unfired origins until the DNA damage has been repaired[256]. A phenomenon known as radioresistant DNA synthesis (RDS) occurs when cells fail to initiate this checkpoint following IR, and cells with defective ATM[257], Nbs1[190], MDC1[211], or BRCA1[218] all exhibit this defect. The ATM-Chk2-Cdc25a-Cdk2 pathway that shuts down replication origins, and therefore initiates the intra-S-phase checkpoint, is shown in Figure 1.8 and described in section **1.9a**. The DNA damage-response kinases ATM and/or ATR are active throughout S phase[258, 259], and control both the timing and spacing of origin firing via feedback from active replicons even in the absence of DNA damage[260, 261]. Therefore, ATM and ATR are poised to quickly down-regulate unfired origins in the event of DNA damage. While ATM and ATR have long been assumed to respond to non-overlapping damage signals (DNA double-strand breaks

in the case of ATM, and UV-induced base damage and stalled replication forks in the case of ATR), recent data suggests that ATM, in conjunction with the Mre11-Rad50-Nbs1 (MRN) complex, can activate ATR after DSBs in S phase and G2 phase. Importantly, both ATM and ATR are required for Chk1 phosphorylation following ionizing irradiation. Once ATM activates the MRN complex, the nuclease activity of Mre11 processes the DSB to produce RPA-coated ssDNA, which in turn leads to the recruitment of ATR[262]. Chk1 is then phosphorylated and activated[262], and this leads to degradation of Cdc25a[263]. It is worth noting that stalled replication forks also lead to Cdc25a degradation through ATR and Chk1[239, 264], and ATR can also prevent Cdc7 from binding Dbf4 and Cdc45 from loading onto the DNA[265] (see section **1.9d**).

There is at least one other ATM-dependent pathway that can induce the intra-S-phase checkpoint (Figure 1.8). Following IR, ATM phosphorylates SMC1 (structural maintenance of chromosomes-1), a component of Cohesin, and this is required for the proper down-regulation of DNA replication. Furthermore, efficient phosphorylation of SMC1 also requires the presence of Nbs1 and BRCA1[266, 267]. MDC1, 53BP1, and FANCD2 also seem to be involved in this pathway[266, 267]. Exactly how SMC1 functions to down-regulate DNA replication is unknown[267], although it is not through Cdc45 loading[268]. One hypothesis is that repair by homologous recombination requires and results in the slowing of replication forks, as ATM, Nbs1, and BRCA1 are all involved in HR, and Cohesin adheres sister chromatids together following replication[158].

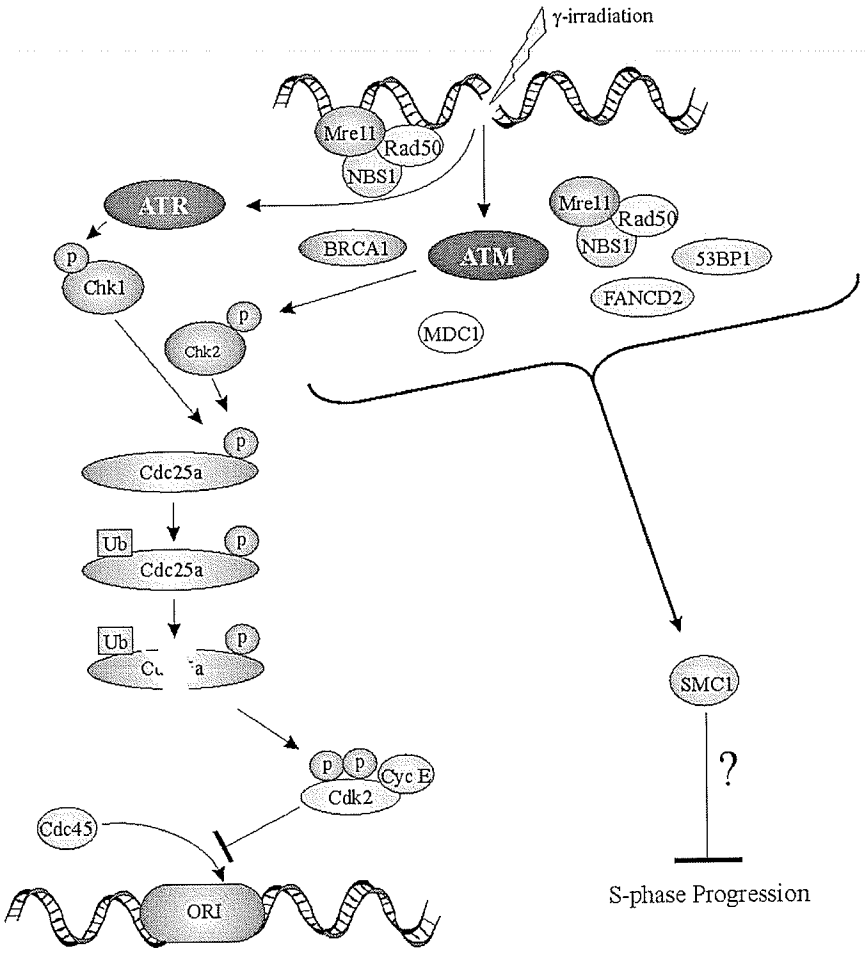

Figure 1.8: The DSB intra-S-phase checkpoint pathways. Both ATM and ATR are required for an efficient intra-S-phase checkpoint following DSBs. This pathway functions as a replication slow-down in which unfired replication origins adjacent to DNA damage are downregulated until the lesions have been repaired. Details of these pathways are given in the text. Phosphate groups are denoted by Ⓟ. Cdc25a protein degradation is represented by ⊂⊃.

1.9c The G2/M checkpoint

The G2/M checkpoint manifests itself initially as a rapid reduction in mitotic cells, which is then followed by a build-up of cells with a 4N, or G2/M, content of DNA[214, 230]. There are multiple pathways that can initiate a G2 arrest. This is shown by the observation that *ATM*$^{-/-}$ cells, which are defective in the intra-S-phase checkpoint and the immediate G2/M checkpoint, exhibit a later build-up of cells with a 4N DNA content that is maintained for days after IR. This maintained G2 arrest is not observed in wild-type cells, and is thought to be due to cells that were irradiated in S phase but failed to induce the intra-S-phase checkpoint[230].

Like in the G1/S checkpoint, ATM becomes activated following ionizing irradiation, and phosphorylates Chk2 and p53[125] (Figure 1.9). It also inactivates MDM2, the negative regulator of p53[122, 249, 250]. p53 can then upregulate transcription of p21 and 14-3-3σ, which can both help initiate the G2/M checkpoint[152, 269]. 14-3-3σ binds to Cdk1/cyclin B1 and sequesters it to the cytoplasm[270], while p21 inhibits Cdk2/cyclin A, and Cdk4(6)/cyclin D complexes, which will result in the inhibition of E2F-dependent transcription via Rb[269]. Important G2/M regulators that are target genes of E2F include Cdk1 (Cdc2), Cyclin A, Cyclin B1, and Cyclin B2[251]. p21 can also directly inhibit the required mitotic kinase Cdk1/cyclin B1, which targets both structural proteins (nuclear lamins, for example) and proteins that regulate processes such as transcription and replication[271, 272].

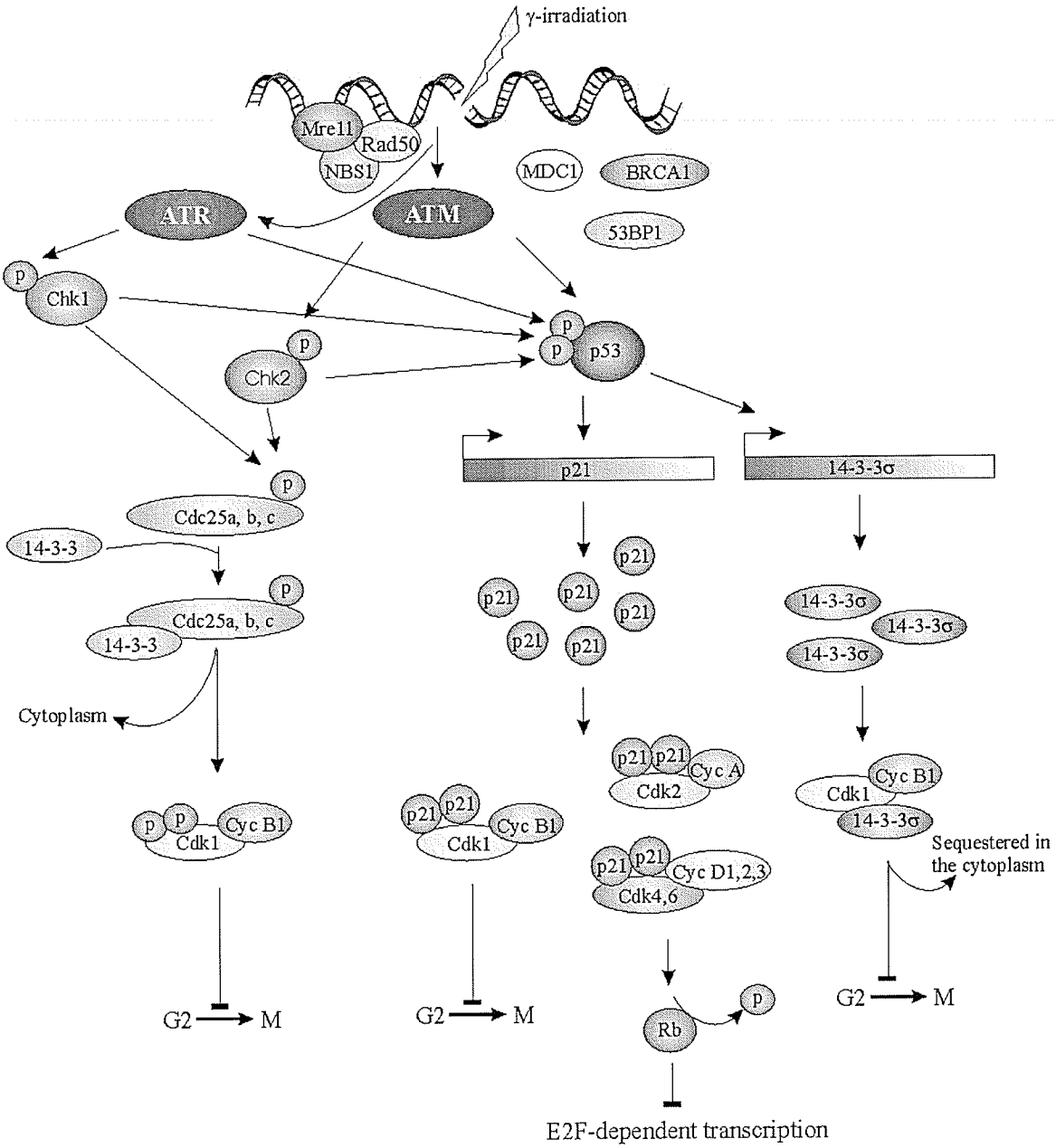

Figure 1.9: The DSB G2/M checkpoint pathways. Following DSBs, ATM and ATR initiate signalling cascades that ultimately block progression into mitosis by inactivating Cdk1/cyclinB complexes. Details of these pathways are given in the text. Phosphate groups are denoted by Ⓟ.

Besides further stabilizing p53[125], Chk2 also phosphorylates Cdc25 family members. The Cdc25 family of phosphatases (Cdc25A, Cdc25B, and Cdc25C) remove inhibitory phosphates on the Cdks (Cdk1 and Cdk2). The phosphorylation of Cdc25 by Chk2 is thought to lead to its ubiquitination and proteasomal degradation[239, 240] or to Cdc25 binding to 14-3-3 proteins, leading to cytoplasmic export and sequestration[152, 273]. Because both result in inactive Cdc25, Cdk1/cyclin B1 remains inactive[152, 269, 272]. Therefore, all of these pathways result in the inactivation of Cdk1/cyclin B1.

ATM can also help activate ATR following IR, which then leads to Chk1 activation[262]. In fact, Chk1 appears to be the critical checkpoint kinase after IR, as Chk2 is not actually required for the G2/M checkpoint[214, 274]. Furthermore, Chk1, but not Chk2, can directly inhibit Cdc25 phosphatases through phosphorylation[275]. Mediator proteins carrying BRCA1 C-terminal repeat (BRCT) domains, including 53BP1[214], MDC1[211], and BRCA1[218], have also been implicated in the G2/M checkpoint, possibly functioning as general docking sites to localize proteins in sites of DNA damage and instigate other protein-protein interactions[150].

1.9d Regulation of replication origin licensing, maturation, and firing

One under-investigated field of research is how the regulation of replication origin maturation and activation is linked to the DNA damage-induced G1/S and intra-S-phase checkpoints. To properly understand the G1/S transition, and therefore the G1/S checkpoint, we need to have an understanding of replication origins, their licensing, and their individual activation. The regulation of origin firing is also important for understanding the intra-S-phase checkpoint, as origin firing is staggered throughout S phase[276].

The initiation of DNA replication during S phase occurs at many sites, or origins of replication, throughout the genome. *Saccharomyces cereviseae* has well-defined cis-acting origins of replication, known as autonomously replicating sequences (ARSs). In metazoans, replication initiation is far more complex, as no cis-acting elements have been identified in higher eukaryotes. Instead, higher-order chromatin structure and epigenetic signals, as well as the presence of initiator molecules are thought to define the replication origins[277-279].

Mammalian cells initiate replication from origins in a staggered, but well-defined, manner throughout S-phase. Distinct replication patterns for early, mid-, and late S phase can be visualized by pulse-labelling synchronized cells with BrdU[276]. Replication timing is correlated to both transcriptional activity, as highly transcribed genes are replicated early, and chromosomal context, as sequences near telomeres are replicated late[280]. The temporal order of replication is established 1-2 hr after mitosis, and appears to occur after the completion of chromosomal domain positioning within the nucleus. This cell cycle point has been designated the replication timing decision point, or TDP[280].

The origin licensing proteins are conserved from yeast to mammals, and consist of the ORC (Origin Recognition Complex), Cdc6/18, Cdt1, and the MCM (mini-chromosome maintenance complex). The ORC complex is composed of six subunits (Orc1-Orc6), all of which are essential[281]. The ORC complex remains bound to DNA throughout the cell cycle, except for Orc1, which is cell-cycle regulated[282]. Origin licensing begins in telophase and continues into the G1 phase[283]. First, Cdc6 and Cdt1 are recruited to the ORC, and then they act as a loading factor for the MCM complex, forming the pre-replicative complex (pre-RC) in a process called licensing[281]. The MCM

complex is a hexameric complex of MCM2 through MCM7 and is a putative replication helicase[281].

Cdc6 is a target gene for E2F[251], but it is also regulated at the protein level through APC (anaphase-promoting complex)-targeted degradation by the proteasome[284]. Recently, phosphorylation of Cdc6 by Cdk2/cyclin E has been shown to protect Cdc6 from this APC-directed degradation[242, 243, 285]. Following γ-irradiation, p53 activation and the subsequent p21 accumulation inhibit Cdk2/cyclin E. The unphosphorylated Cdc6 can then be degraded by the APC; therefore, activation of p53 following DNA damage can prevent origin licensing by inducing the degradation of Cdc6[243].

In metazoans, a protein called geminin inhibits Cdt1, preventing origin licensing[281]. The APC targets geminin for degradation; therefore, the APC ubiquitinates both the licensing factor Cdc6 and the licensing inhibitor geminin[284]. The model that can be constructed from this apparently contradictory system is that during mitosis and G1 when the APC is active, both geminin and Cdc6 are targeted for degradation. As the level of Cdk2-cyclin E increases during G1, Cdc6 is phosphorylated and protected from degradation, allowing both Cdc6 and Cdt1 to be present for origin licensing in G1[243].

Cells have a certain amount of flexibility as to which origins are actually fired, as many more origins are licensed than are actually fired. The point at which this is decided is termed the origin decision point (ODP). The ODP is after the timing decision point (TDP) and after the formation of the pre-RCs, but before the restriction point[280]. Once initiated, DNA replication *must* be completed. Therefore, external growth factors do not and should not control S-phase progression. The point at which a cell no longer requires growth factors to complete the cell cycle is defined as the restriction point[286].

A pre-RC matures into a pre-initiation complex (pre-IC) with the recruitment of Cdc45 and potentially other replication factors[287]. When and how Cdc45 is loaded onto the pre-RC, especially in mammalian cells, remains poorly understood. Yeast and in vitro Xenopus egg extract studies have shown that Cdc45 loading may require Cdk activity, but this has yet to be shown in mammalian cells[288]. Another model developed after the recent data on Cdc6 stabilization by Cdk2/cyclin E is that the MCM complex recruits Cdc45 independent of further Cdk activity[288]. The MCM complex and Cdc45 unwind the replication origin and recruit replication proteins such as RPA, and DNA polymerases α and ε. The MCM complex and Cdc45 progress along with the replication enzymes, leaving the origin and converting it to a post-replicative complex (post-RC)[281]. Targeting of Cdc45 to specific chromosomal sites in mammalian cells results in a Cdk2-dependent chromatin decondensation that correlates with histone H1 phosphorylation. Therefore, Cdc45 is thought to facilitate replication fork progression throughout S phase by decondensing the surrounding chromatin[289].

The observation that origins are fired in a staggered fashion throughout S-phase suggests that origins are individually activated for replication. In this model, the G1/S transition is necessarily separate from the activation of individual replication origins, or at most is defined as the activation of the "first" replication origin. The event at each origin that actually induces the change from a pre-IC to a "fired" or post-RC is unknown, but the Cdk2 and the Cdc7 kinases are both potential candidates. Cdc7-Dbf4 selectively phosphorylates the MCM2 subunit in mammalian cells, but a phosphorylation site that appears to initiate replication has yet to be identified[290, 291]. Furthermore, as mentioned in section **1.9b**, ATM and/or ATR are active throughout S phase[258, 259], and can control both

the timing and spacing of origin firing via feedback from active replicons even in the absence of DNA damage[260, 261], indicating that the DNA damage response pathways, and the normal regulation of origin firing are interconnected.

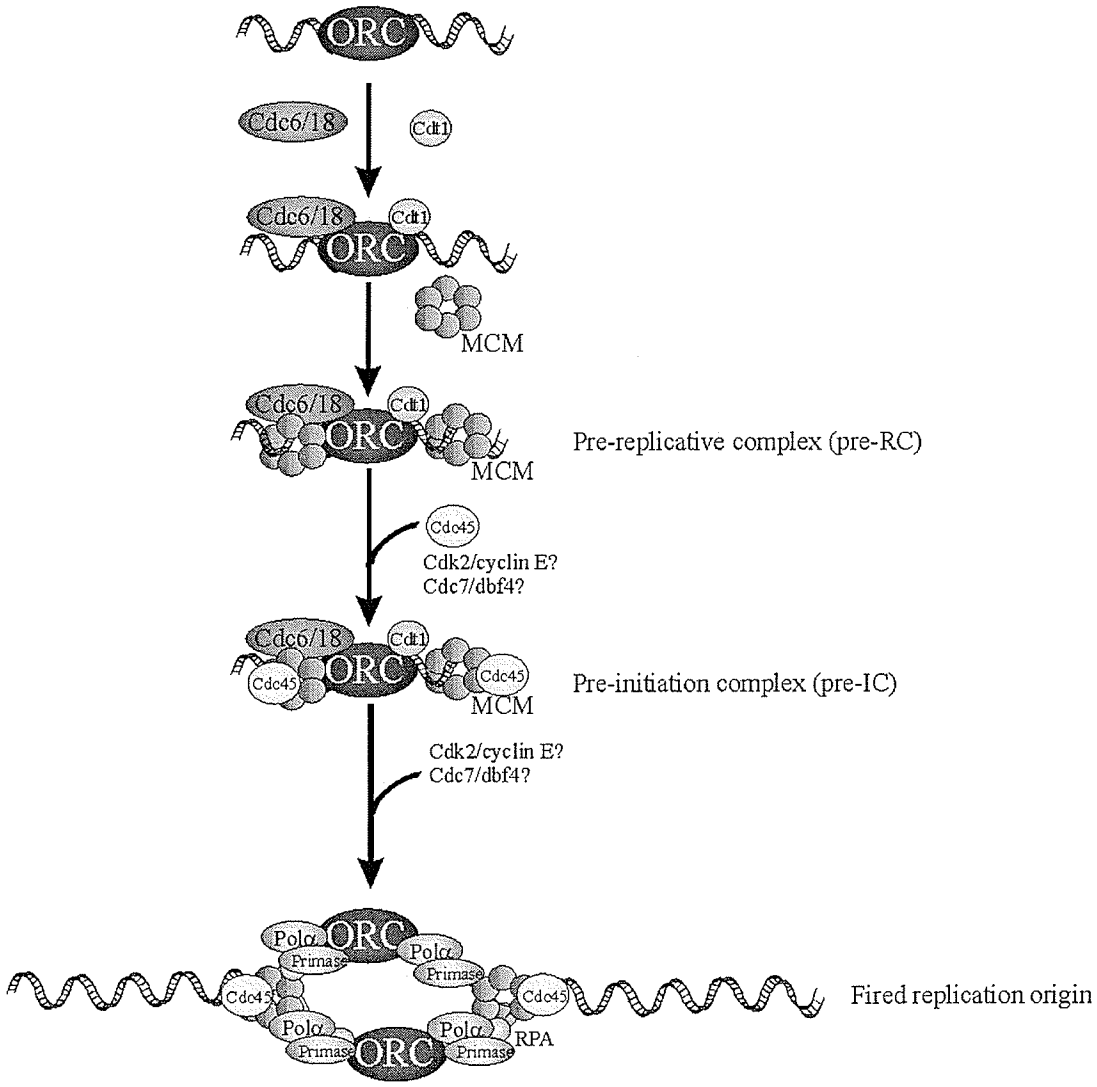

Figure 1.10: Mammalian replication origin licensing and activation. Replication origin licensing begins in telophase with the binding of the ORC complex. Subsequent binding of Cdc6/18, Cdt1, and the MCM hexamer results in the formation of the pre-replicative complex. Cdc45 binding then completes the pre-initiation complex. The signal that initiates origin firing is unknown, but Cdk2/cyclin E and Cdc7/dbf4 are both potential candidates as the critical kinase. Further details of origin licensing and activation are described in the text.

1.10 DSBs and apoptosis

Depending on the severity of the DNA damage, or the cell type involved, cells may undergo apoptosis (programmed cell death) instead of attempting to repair the damage[292]. For example, lymphocytes are particularly sensitive to apoptosis, due in part to the fact that they induce Bax expression in response to IR, which fibroblast cell lines do not[292]. Mouse embryonic stem (ES) cells also respond to IR by undergoing apoptosis, and do not initiate G1/S checkpoint following DSB. However, if the G1S checkpoint is reinstated with exogenous expression of Chk2, the cells are then protected from apoptosis[293].

As in the rest of the DSB-signalling cascades, ATM can initiate a pathway to induce apoptosis (see Figure 1.11). ATM activates p53 directly, and indirectly via Chk2[274, 294-297]. Again, ATM also inactivates MDM2, the negative regulator of p53[122, 249, 250]. p53 then upregulates transcription of NOXA, PUMA, and Bid[298]. All three are BH3-only proteins that function by inhibiting anti-apoptotic BCL-2- and BCL-XL-like proteins[295, 299]. The proteins of the Bcl-2 family are important regulators of apoptosis, and include both anti-apoptotic members (such as Bcl-2 and Bcl-XL) and pro-apoptotic members (such as Bax, Bak, NOXA, PUMA, Bad, Bid, and Bik). The family is defined by the presence of at least one Bcl homology (BH) domain (BH1-BH4). These domains regulate the homo- and heterotypic interactions of the family members, interactions that are thought to be critical for the regulation of apoptosis[299]. p53 also upregulates the transcription of Bax, a BH123 protein that forms channels in mitochondria, resulting in the loss of mitochondrial membrane potential, and the release of cytochrome c and Smac/DIABLO[298]. Cytochrome c activates the Apaf-1/Caspase-9 apoptosome, initiating

the caspase cascade and apoptosis, and Smac/DIABLO inhibits IAPs (inhibitor of apoptosis proteins), which would otherwise inactivate caspases[299].

Recently, p53 has been shown to have transcription-independent activity in apoptosis. Following IR, p53 translocates to the mitochondria, and inhibits Bcl-2/Bcl-XL and/or helps activate Bak, another BH123 pro-apoptotic protein[295, 298, 300]. The linker histone subtype H1.2 also translocates to the mitochondria after IR in a p53-dependent and Chk2-dependent manner, and also appears to help activate Bak, resulting in cytochrome C and Smac/DIABLO release[295, 300]. Finally, the DNA repair proteins Rad51 and DNA-PK are both subject to proteolytic cleavage following caspase activation[301], shutting down what would be futile DNA repair.

The dual functions of ATM and p53 in promoting cell cycle arrest and apoptosis lead to some seemingly contradictory phenotypes. While $ATM^{-/-}$ cells are generally associated with radiation hypersensitivity[112, 296], $ATM^{-/-}$ thymocytes are actually resistant to radiation-induced apoptosis[296, 297]. This duality of function also exists in other DNA damage response proteins, including p53[302-305] and DNA-PKcs[303].

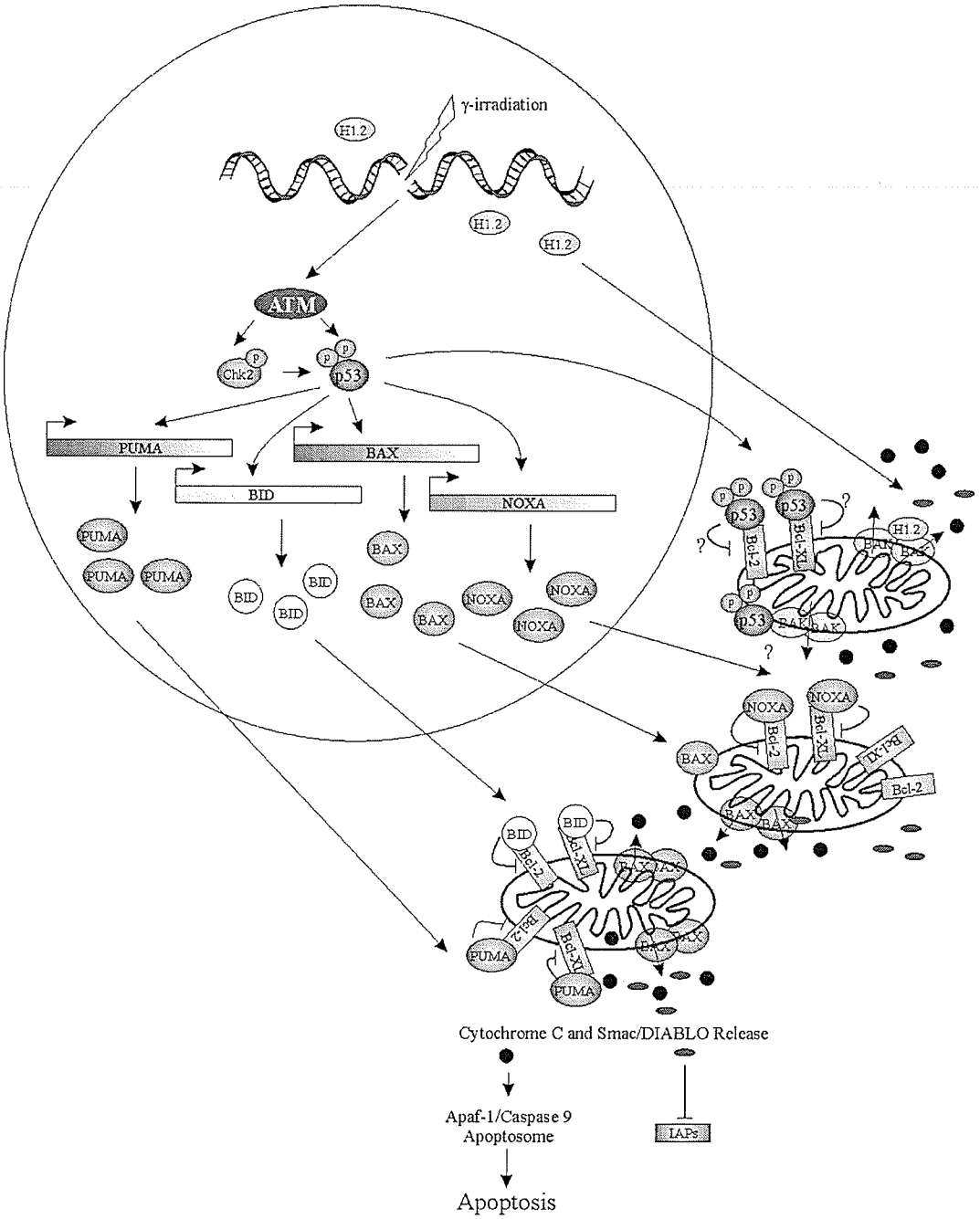

Figure 1.11: The DSB-initiated apoptotic pathways. Following DSBs, depending on the extent of damage and the cell type involved, the cells may undergo programmed cell death. ATM activates p53, leading to p53-dependent transcription of Bid, Bax, NOXA, and PUMA. This ultimately results in the release of Cytochrome C and Smac/DIABLO from the mitochondria, initiating the caspase cascade and apoptosis. Further details of these pathways are described in the text. Phosphate groups are denoted by Ⓟ. Cytochrome C is represented by ●, and Smac/DIABLO by ⬬.

1.11 Thesis Rationale and Objectives.

TLS is associated with the development of certain cancers, including myxoid liposarcoma and myeloid leukemia, through its presence in several fusion oncoproteins[1-5, 15, 17, 18, 24, 25]. However, the exact mechanisms regulating the oncogenesis of these cancers remain ill-defined. Elucidating the wild-type function of TLS will provide a greater understanding of these mechanisms. To that end, the Hicks lab has been investigating the normal, wild-type function of TLS through the use of *TLS*$^{-/-}$ mice and cells. *TLS*$^{-/-}$ mice exhibit characteristics consistently found in mouse models of the human genomic instability syndromes AT[112-114] and NBS[115], specifically genomic instability[111], immune system defects[111], and sensitivity to ionizing irradiation[116]. The causative genes of these syndromes are involved in the DNA damage response pathways (repair, cell cycle checkpoints, and/or apoptosis), and this suggests that TLS also plays a role in these pathways.

Thesis Hypothesis: TLS maintains genome stability through a role in DNA repair.

Thesis Aims: The aims of this thesis work were to identify a role for TLS in the cellular response to DNA damage, and to evaluate its function within the ATM-activated signalling pathways responding to DNA double-strand breaks. The specific research objectives of this thesis are as follows:

1. Identify TLS as a DNA-damage response protein.

2. Characterize the dynamic localization of TLS to better understand the wild-type function of TLS and how it may contribute to the DNA damage response.

3. Characterize the ability of *TLS* $^{-/-}$ MEFs to recognize DNA double-strand breaks, and to subsequently activate the cell cycle checkpoints that provide time for DNA repair.

These objectives are presented in three separate chapters. During the course of this thesis work, I developed a novel method for analyzing the immediate G1/S checkpoint using a staggered CldU/IdU-labelling strategy. This assay led to the unexpected finding that the majority of late-G1 primary MEFs do not initiate an immediate G1/S checkpoint following γ-irradiation, indicating that the current model of the G1/S checkpoint needs to be re-evaluated. This work was recently published[306], and is presented in Chapter 6. Each of the chapters presents the rationale of the specific experiments contained within the chapter and the results obtained. Each chapter then concludes with a summary of the results, and the overall conclusions that could be reached. Finally, a more comprehensive discussion of all the results can be found in Chapter 7.

Chapter 2

Materials and Methods

2.1 Materials

For the experiments presented in this thesis, materials and equipment were purchased from the following companies:

Abcam, Cambridge, UK

Amersham Biosciences, Baie d'Urfé, PQ, Canada

Atomic Energy of Canada Limited (AECL), Mississauga, ON, Canada

BD (Becton, Dickinson, and Company) Biosciences, Mississauga, ON, Canada

Beckman Instruments Canada Inc., Mississauga, ON, Canada

Bio-Rad Laboratories Inc., Mississauga, ON, Canada

Calbiochem, San Diego, CA, USA

Cansera International, Etobicoke, Ontario, Canada

Clontech, Palo Alto, CA, USA

Carl Zeiss Canada Ltd., Toronto, ON, Canada

Corning Life Sciences Inc., Acton, Ma, USA

Fisher Scientific, Nepean, ON, Canada

GIBCO [Grand Island Biological Co.]-Invitrogen Inc., Bulington, ON, Canada

Hyclone, Logan, UT, USA

Improvision Ltd, Coventry, England

Invitrogen, Bulington, ON, Canada

Jackson ImmunoResearch Laboratories, Inc, West Grove, PA, USA

Leica Microsystems (Canada) Inc., Richmond Hill, ON, Canada

Manitoba Liquor Control Commission, Winnipeg, MB, Canada

Nalge Nunc International, Rochester, NY, USA

New England Biolabs (NEB) Ltd., Pickering, Ontario, Canada

Olympus, Melville, NY, USA

QIAGEN, Mississauga, ON, Canada

Qimaging, Burnaby, BC, Canada

Santa Cruz Biotechnology Inc., Santa Cruz, CA, USA

Sigma-aldrich Canada Ltd., Oakville, ON, Canada

Stratagene, La Jolla, CA, USA

Syngene USA, Frederick, MD, USA

Upstate Biotechnology, Lake Placid, NY, USA

Vector Laboratories, Burlingame, CA

VWR International, Mississauga, Ontario, Canada.

2.1.1 Antibodies

2.1.1a Primary antibodies

Actin. An affinity isolated rabbit antibody that recognizes Actin was purchased from Sigma (Catalogue #A2066).

BrdU. An anti-BrdU-FITC conjugated antibody was purchased from BD Biosciences (Catalogue #556028). This antibody works very well for both immunocytochemistry and flow cytometric analysis.

Cdc25a. A mouse monoclonal antibody that recognizes Cdc25a (F-6 monoclonal) was purchased from Santa Cruz Biotechnology, Inc.

CldU. Anti-BrdU clone BU1/75[ICR1] rat monoclonal was purchased from Abcam. This antibody will recognize CldU but not IdU[307].

Cyclin D1. A mouse monoclonal antibody that recognizes cyclin D1 (72-13G monoclonal) was purchased from Santa Cruz Biotechnology, Inc.

FLAG Epitope. An Anti-Flag® M2 monoclonal antibody was purchased from Sigma.

IdU. Anti-BrdU clone B44 mouse monoclonal was purchased from BD Biosciences. This antibody recognizes both IdU, and CldU, but when washed with a high salt buffer, it releases from CldU[307]. The high salt buffer used in this thesis was 100 mM Tris, 0.5 M NaCl, 0.5% Tween 20, pH 8.0.

γH2AX. A mouse monoclonal phosphospecific antibody that recognizes histone H2AX phosphorylated on serine 139 [clone JBW301] was purchased from Upstate. This antibody was used for both immunoblotting and immunocytochemistry.

Histone H3, phosphorylated on serine 28. A rat monoclonal phosphospecific antibody that recognizes histone H3 phosphorylated on serine 28 (clone HTA28) was purchased from Sigma. Several different antibodies to phosphorylated H3 on serine 10 and 28 were tested, and this antibody was found to be the most specific for use in immunocytochemistry and flow cytometry.

p21. A mouse monoclonal antibody that recognizes p21 (F-5 monoclonal) was purchased from Santa Cruz Biotechnology, Inc.

p53. A pantropic mouse monoclonal antibody that recognizes p53 (Pab421 monoclonal) was purchased from Calbiochem.

p80 Coilin. A mouse monoclonal antibody that recognizes coilin (monoclonal clone 56) was purchased from BD Biosciences. This antibody was only tested for use in immunocytochemistry.

Phosphatidylserine. Annexin V is a phosphatidylserine-binding protein[308-310]. An Annexin V-FITC conjugate was purchased from Sigma.

TLS. A mouse monoclonal antibody (10F7) to TLS had been previously developed in the Hicks laboratory by immunizing BALB/c mice with GST (glutathione-s-transferase)-TLS fusion protein. Various clones were screened using western blotting, immunocytochemistry, and flow cytometry, and the 10F7 antibody was found to work for all three methods. This antibody recognizes amino acids 34-51 of TLS.

2.1.1b Secondary/tertiary antibodies

Fluorescein (FITC)-conjugated AffiniPure Donkey Anti-Mouse IgG (H+L) (minimal cross-reaction to bovine, chicken, goat, guinea pig, Syrian hamster, horse, human, rabbit, rat, and sheep serum proteins), and Texas Red® dye-conjugated AffiniPure Donkey Anti-Rat IgG (H+L) (minimal cross-reaction to bovine, chicken, goat, guinea pig, Syrian hamster, horse, human, mouse, rabbit, and sheep serum proteins) were purchased from Jackson ImmunoResearch Laboratories. Anti-rat IgG (whole molecule) FITC conjugate, anti-mouse IgG (whole molecule) peroxidase conjugate, anti-rabbit IgG (whole molecule) peroxidase conjugate, and an anti-mouse IgG biotin conjugate were all purchased from Sigma. Streptavidin-Fluorescein and Streptavidin-Texas Red were purchased from Vector Laboratories.

2.1.2 Oligonucleotides

All primers used in this thesis were purchased from Invitrogen.

2.1.3 Transcriptional inhibitors and DNA-damaging agents

All of the following chemicals were purchased from Sigma.

Mitomycin C. 2 mg of Mitomycin C (catalogue # M4287) was resuspended to a concentration of 2 mM in DMSO and stored at –20°C.

Actinomycin D. 2 mg of actinomycin D (catalogue # A9415) was first resuspended in 100 µL DMSO, and then diluted to a concentration of 1 mg/mL in ddH_2O. The resulting solution was stored at 4°C.

DRB (5,6-dichlorobenzimidazole riboside). DRB (catalogue # D1916) was resuspended to a concentration of 5 mM in 100% ethanol and stored at –20°C.

Camptothecin. Camptothecin (catalogue # C9911) was resuspended to a concentration of 10 mM in DMSO and stored at 4°C.

2.1.4 γ-Irradiation Source

Cells were γ-irradiated at room temperature using a cesium 137 source (Gammacell 1000, Atomic Energy of Canada Limited, dose rate of 2.4 Gray/minute). For most experiments, MEF and HeLa cells were γ-irradiated while on 60 mm cell culture dishes. In the experiments requiring histone preparations or for experiments with the pre-B cells, the cells were γ-irradiated while in suspension in complete medium in 15 mL or 50 mL tubes.

2.1.5 UV (ultraviolet)-irradiation

A Stratagene UV Stratalinker 1800, which has an internal UV dose sensor, was used to expose cells to different doses of 254 nm irradiation, a short UV wavelength in the UVC range. To ensure the cells were given an accurate dose, the cells were washed

twice with PBS, and a minimal amount of PBS (0.5 mL for a 60 mm dish) was used to cover the cells (MEFs), or resuspended in a minimal amount of PBS (pre-B cells). Cells were UV-irradiated without the lids of their plates.

2.1.6 Mammalian cells

Most experiments carried out in this thesis were done on low passage, primary mouse embryonic fibroblasts (MEFs) (see section **2.4**). While *TLS* $^{+/-}$ MEFs were included in pilot experiments, no phenotype was ever observed in heterozygous animals or in the heterozygous cells. Therefore, the experiments presented in this thesis only show data for *TLS* $^{-/-}$ and *TLS* $^{+/+}$ cells. *TLS* $^{-/-}$ (cell line 6-4) and *TLS* $^{+/+}$ (cell line 10-4) pre-B cells had been derived previously in the Hicks lab by transforming fetal liver cells of TLS $^{-/-}$ and *TLS* $^{+/+}$ mice[111] with v-abl[311, 312]. The other cell types used in this thesis were HeLa cells (American Type Culture Collection), a human cervical cancer cell line, and 293T cells, a human embryonic kidney cell line.

2.2 General maintenance of mammalian cells

All adherent cells, MEFs (mouse embryonic fibroblasts), HeLa cells, and 293T cells, were cultured in Dulbecco's Modified Eagle Medium (DMEM) (GIBCO-Invitrogen Inc., catalogue # 11960-044) supplemented with 10% fetal bovine serum (FBS) (Cansera) or 10% Bovine Growth Serum (BGS) (Hyclone, catalogue # SH30541.03), 2 mM L-alanyl-L-glutamine (GIBCO, catalogue # 35050-061), 100 units/mL penicillin G sodium and 100 μg/mL streptomycin sulfate (100x stock Penicillin-Streptomycin [GIBCO, catalogue #15140-122]), and 1 mM sodium pyruvate (GIBCO, catalogue #11360-070). Cells were cultured on treated, non-pyrogenic polystyrene tissue culture plates (Corning Inc.). Mouse pre-B cells were cultured in suspension in RPMI (Roswell Park Memorial

Institute)-1640 media (GIBCO, catalogue #22400-089) supplemented with 10% FBS/BGS, 50 μM 2-Mercaptoethanol, 2 mM L-alanyl-L-glutamine (GIBCO), 100 units/mL penicillin G sodium and 100 μg/mL streptomycin sulfate (100x stock Penicillin-Streptomycin [GIBCO]), and 1 mM sodium pyruvate (GIBCO). All references to media within this thesis refer to complete media prepared as described above unless otherwise indicated. All cells were maintained at 37°C in 6.0% CO_2 and 100% humidity.

Cultured cells were monitored daily by visual inspection using a microscope, and once they reached ~70% confluency (adherent cells) or became dense (pre-B cells), they were passaged. Typically, the cells were passaged every three days. For adherent cells, the cells were washed with filter sterilized (with a 0.2 μm filter) Dulbecco's Phosphate Buffered Saline (PBS) (GIBCO, catalogue # 21600-069), and then detached from the plates using 0.05% Trypsin-EDTA (GIBCO, catalogue # 25300-054) (2 mL for a 15 cm dish, 0.5 mL for a 60 mm dish). The cells were incubated with the trypsin at room temperature for 30 s to 2 min, and monitored under the microscope to prevent over trypsinization. The trypsin was then neutralized with medium (10 mL complete DMEM for a 15 cm dish or 4 mL for a 60 mm dish), and the cells were transferred to a 15 mL screw-cap tube, and collected by tabletop centrifugation at 1200 rpm (290x g) at 4°C for 5 min. The cells were then resuspended in fresh medium, and split into fresh complete media accordingly (typically 1/3 for MEF cells and 1/10 for other cell types including pre-B cells).

2.3 Cryopreservation of mammalian cells

Cells were cryopreserved in freezing medium made up of 48% complete medium (DMEM or RPMI depending on the cell type), 40% additional FBS/BGS, and 12% sterile

DMSO. Typically, 10^6 cells were resuspended in 1 mL of freezing medium and transferred to a CryoTube vial (NUNC). (For MEFs, four tubes of 1 mL each would be prepared per 15 cm dish. For other cell types, this number would be 10 tubes of 1 mL each per 15 cm dish.) The CryoTube vials were then cooled at a rate of 1°C/min, and stored for short term at –80°C or long term in liquid nitrogen. To reanimate cryopreserved cells, a tube would be rapidly warmed to 37°C, and added to 10 mL of complete medium. The cells would then be pelleted and gently resuspended in fresh medium to remove the DMSO. One tube of cells would be plated on one 15 cm dish.

2.4 Preparation of Mouse Embryonic Fibroblasts (MEFs) from day E14.5 embryos

MEFs were prepared as described[313]. A pregnant mouse on day 14.5 dpc (days post coitum) was sacrificed using cervical dislocation or CO_2 asphyxiation. The abdomen was washed with 70% ethanol, and the abdominal cavity was dissected to expose the uterine horns. The uterine horns were removed and washed in sterile PBS. All steps from now on were preformed in a biosafety cabinet. Each embryo was dissected away from the uterine wall and the placenta using watchmaker forceps, and washed with sterile PBS. The head and dark coloured tissues (heart and fetal liver) were removed. At this point, a portion of the embryo was also removed for genomic DNA extraction and genotyping. The remainder of the embryo was dissected apart in a fresh culture dish using a razor blade. 2 ml of 0.05% Trypsin-EDTA (GIBCO) was added to each embryo and the mixture was transferred to a 15 mL screw-cap tube. The mixture was agitated until a cell suspension was visible (typically 1 to 2 min), but before lysed cells became visible. 10 mL of complete DMEM was then added to each embryo to stop

the digestion. This mixture, excluding any lysed material, was transferred to a 15 cm tissue culture dish and mixed with an additional 10 ml of media. The cells were grown until the plates were just sub-confluent (~3 days), at which point the cells were cryopreserved in 4 vials per plate.

2.5 Genotyping

2.5a Genomic DNA preparation

Genomic DNA was prepared as described[313, 314]. Tissue samples from the embryo or mouse (generally 3 mm tail tissue) were digested with 400 μL Lysis Buffer (100 mM Tris pH 8.5, 5 mM EDTA, 0.2% SDS (sodium dodecyl sulfate), 200 mM NaCl, and 100 μg Proteinase K/mL) overnight at 65°C with rotation. The next day, the samples were monitored for complete digestion. If the samples did not appear to be completely digested, more Proteinase K was added at this point, and the samples incubated further. After digestion was complete, mouse samples were spun down and the supernatants placed in fresh tubes to remove any debris. Embryonic tissue samples were processed directly without centrifugation. 1 mL of 100% ethanol was added to each lysate, and mixed by inversion. A flame-sealed glass Pasteur pipette was used to remove the DNA from the tube by spooling, and the DNA was then washed in fresh 70% ethanol. The DNA was then air-dried on the end of the sealed pipette. Finally, the DNA was resuspended in 100 μL 1x TE buffer (10mM Tris, 0.1 mM EDTA, pH 7.5). Complete dissolution typically required agitation and incubation at 56°C for several hours, followed by an overnight incubation at room temperature. The DNA preparations can then be stored indefinitely at 4°C.

2.5b PCR genotyping and general DNA TAE gel electrophoresis

To genotype for the *TLS* knockout allele, two PCR reactions were used as previously described[111]. One, for the mutant allele, creates an amplification product (~450 bp) only if the U3NeoSV1 gene trap provirus is present. The other only creates an amplification product for the wild-type allele (1.2 kb).

Each PCR reaction contained 0.5 μL 5' primer (100 μM stock), 0.5 μL 3' primer (100 μM stock), 5 μL 10x PCR buffer, 4 μL 5 mM dNTPs, 2 μL (~1 μg) genomic DNA, 0.25 μL (1.25 U) *Taq* DNA polymerse (NEB), 37.75 μL ddH_2O (deionized, distilled water). See Table 2.1 for the 5' and 3' primers for each reaction.

Table 2.1: Primers for TLS genotyping

Reaction	Primer Name	Direction	Primer Sequence
Mutant	NeoF	Reverse (3')	5'-aat cat gcg aaa cga tcc tc-3'
	EX11F	Forward (5')	5'-aag ttt cat ttg cta ccc gca-3'
Wild-type	IN11F	Forward (5')	5'-tgg aag agg tag gct aac caa a-3'
	EX13B	Reverse (3')	5'-agg tgc ctt aca ctg gtt gc-3'

The PCR reactions were all carried out in a MJ Research DNA Engine Thermal Cycler or MJ Research DNA Engine Dyad® Thermal Cycler using the following PCR conditions: 3 min at 94°C; 40 cycles of 15 s at 94°C, 15 s at 60°C, and 2 min at 72°C; followed by a final 10 min elongation step at 72°C.

The PCR products with Orange G Loading Buffer (6x Orange G Loading Buffer: 30% glycerol, 2 mg/mL Orange G), along with an aliquot of a control 1kb ladder standard (NEB), were then separated on a 1% agarose gel made up in 1x TAE running buffer (50x TAE is 2 M Tris base, 5.71% v/v glacial acetic acid, and 50 mM EDTA) with 0.1 μl/mL of ethidium bromide stock solution (10 mg/mL) by electrophoresis in a Bio-

Rad Sub Cell or Bio-Rad Mini-Sub Cell at approximately 10 V/cm for 30-60 min. The bands were then visualized using a Gene Genius Bioimaging System (see Figure 3.1a). The PCR reaction for the mutant allele gives a product of around 450 bp, while the PCR reaction for the wild-type allele gives a product of around 1200 bp.

2.5c Genotyping by Southern analysis

Southern analysis was performed on all MEF cell preparations used in the experiments presented in this thesis. To prepare samples for Southern analysis, 20 μL (~10 μg) of each genomic DNA sample was digested with 5 μL 10x buffer 2, 0.5 μL high-concentration Stu I (50 U) (NEB), 0.5 μL 100x BSA (Bovine Serum Albumin), and 24 μL ddH_2O (deionized, distilled water) for 6 h at 37°C. The digests were then separated in a 0.8% agarose TAE gel by electrophoresis using a Bio-Rad Sub Cell at ~1 V/cm overnight. The gel was then soaked in 0.1 M HCl for 10-15 min with shaking, incubated in Soak 1 (1.5 M NaCl, 0.5 M NaOH) with shaking for 30 min, and then incubated in Soak II (1.5 M NaCl, 1 M Tris pH 7.4) with shaking for 30 min. The DNA was then transferred overnight to a Hybond XL nylon membrane (previously activated in ddH_2O) using capillary action with 10x SSC (For stock 20x SSC, 3 M NaCl, 0.3 M Na-Citrate, pH 7.0). Following transfer, the membrane was marked for orientation, and auto cross-linked using a Stratagene UV Stratalinker 1800. At this point, the membrane was processed immediately or stored at 4°C. Next, the membrane was incubated with rotation in a hybridization oven at 42°C with 2x SSC in a hybridization tube for 10 min. The 2x SSC was then replaced with prehybridization buffer pre-warmed to 65°C, and with SDS to a concentration of 0.5% added after the buffer had been pre-warmed. (For 1 L of prehybridization buffer, 500 mL formamide, 250 mL SSCPE [For 1 L: 140 g NaCl, 88 g

Na-Citrate, 35 g KH_2PO_4, and 40 mL 0.5 M EDTA], 100 mL 50x Denhart's [For 500 mL, 5 g Ficol, 5 g polyvinylpyrrolidone, 5 g BSA, and up to a total volume of 500 mL with ddH_2O], 10 mL prepared salmon testes ssDNA [10mg/mL] [Sigma, catalogue # D7656], and ddH_2O up to 1 L. 15 mL aliquots were stored at –20°C.) The membrane was then incubated in prehybridization solution for at least 4 h at 42°C with rotation in a hybridization oven.

A TLS DNA probe was prepared by digesting the pTLS vector with NheI and EcoRI, separating the fragments on a 1% agarose 1x TAE gel, and extracting the 375 bp band (see section **2.8b** for the gel extraction protocol). The pTLS vector was the plasmid rescue vector made during the initial characterization of the embryonic stem cell clone in which TLS was disrupted by the U3NeoSV1 gene trap provirus[110, 111]. The 375 bp fragment contains *TLS*-specific genomic sequences spanning the intron 11 to exon 12 junction[110, 111]. 25 ng of the TLS probe was radiolabelled using [α-P^{32}]-dCTP and a Random Primers DNA Labeling System (Invitrogen) as per the manufacturer's instructions. Prior to use, the probe was re-denatured by boiling and placed on ice.

After 4 h, SDS to a concentration of 0.5% and the radiolabelled probed was added to hybridization buffer pre-warmed to 65°C. The prehybridization solution was replaced with this mixture. (For 1 L of hybridization buffer, 100 g dextran sulfate, 500 mL formamide, 250 mL SSCPE, 20 mL 50x Denhart's, 2 mL prepared salmon testes ssDNA [10mg/mL] [Sigma, catalogue # D-7656], and ddH_2O to 1 L. 15 mL aliquots were stored at –20°C.) The membrane was incubated with this hybridization mixture overnight at 42°C. The following day, the membrane was washed sequentially with pre-warmed 2x SSC with 0.1% SDS at 42°C for 30 min, pre-warmed 1x SSC with 0.1% SDS at 65°C for

30 min, and then pre-warmed 0.2x SSC with 0.1% SDS at 65°C for 30 min. The blot was then exposed to Molecular Dynamics Storage Phosphor Screen (Amersham) for several hours to overnight, or to Hyperfilm™ MP film (Amersham) for 1-3 days at –80°C. If the Phosphor Screen was used, the screen was then read using a Molecular Dynamics Storm 860 (Amersham). An example blot is shown in Figure 3.1b. The expected band size for wild-type allele is 8.2 kb, while the expected band size for the mutant allele is 13.8 kb, as it also includes the provirus.

2.6 Mouse Embryonic Fibroblast (MEF) cell doubling time assay

Ten thousand (10^5) passage 3 MEFs were plated in triplicate on 10 cm dishes for each experimental day 1, 3, 5, 7, 9, and 11. (Cell concentration was determined using a Coulter Counter Z_{B1} [amp=4, aperture=2]). Triple aliquots of each cell type were also counted at day 0. Cells were then incubated under normal culture conditions. On each of day 1, 3, 5, 7, 9, and 11, three plates of each genotype were harvested. (Cell counts were taken at the same time each day.) The cells were resuspended in DMEM, and an aliquot was counted, with three counts taken for each sample. A total cell count per plate was then calculated. A graph of Days After Plating (arithmetic scale) versus Plate Count (natural log scale) was plotted, and a slope was calculated for the best-fit line of the linear portion of the graph. Doubling time in hours was then calculated from the equation:

Doubling time = $\ln(2)/k \cdot 24\text{h/day}$, where k is the slope.

2.7 MTT (3-[4,5-dimethylthiazol-2-yl]-2,5-diphenyl-tetra-zolium bromide) assay

The MTT assay is a standard cytotoxicity assay used to analyze the sensitivity of cells to pharmacological agents[315]. Cells at 50-70% confluency in 60 mm plates were

either treated with increasing concentrations of MMC for 1 h at 37°C, exposed to increasing doses of γ-irradiation and then incubated for 1 h at 37°C, or exposed to increasing doses of UV-irradiation and then incubated for 1 h at 37°C. For all assays, the cells were then harvested, and counted using a Coulter Counter Z_{B1} or a Coulter Z2 Particle Count and Size Analyzer (using a range of 10-30 μm). Serial dilutions of each dose, based on the cell count from the untreated, control plate, were made. Briefly, 48,000 cells were resuspended in 6 mL for 8000 cells/mL, and serially diluted for 6400 cells/mL, 4800 cells/mL, 3200 cells/mL, and 1600 cells/mL. For each dose, 0.25 mL in quadruplet of each dilution (for cell numbers of 2000, 1600, 1200, 800, and 400, respectively) were plated on a 96-well plate. The cells were incubated for four doubling times, and then MTT (Sigma), at a concentration of 0.2 mg/mL in DMEM (stock of 5 mg/mL MTT in PBS), was added. The plates were incubated for a further 6 h, and the medium was then removed. The formazan crystals were resuspended in 150 μL DMSO, and the absorbance of each well was measured at 540 nm using either a Titertek Multiscan MCC/340 or SPECTRAmax 190 with SOFTmax PRO (version 3.1.2). The slope of increasing cell number versus absorbance for each dose was calculated, and the surviving cell fraction is the ratio of each dose slope to the control slope.

2.8 Cloning of *TLS*, *SMN* and *Cdc25a*, and plasmid construction

2.8a Cloning of *TLS*, *SMN*, and *Cdc25a* cDNAs from cDNA libraries

To clone specific cDNAs from a cDNA library, 5' and 3' gene-specific primers with added restriction enzyme (RE) sites were generated to allow for direct cloning in-frame into a specific mammalian expression plasmid. The 5' primer included the sequence coding for the translation start site of the gene, and the 3' primer included the

translation stop sequence. The primers for each cloned gene (TLS, SMN, and Cdc25a) are all shown in Table 2.2. The incorporated RE site is also indicated, as is the source cDNA library for each reaction, and the mammalian expression plasmid that the cDNAs were directly cloned into.

Table 2.2: Primers, source cDNA library, restriction sites (RE) used in cloning, and target plasmid.

cDNA		Primer	RE Site	cDNA library	Plasmid
TLS	**5'**	5'-gca gat ctc cat ggc ctc aaa cga tta tac c-3'	BglII	Human fetal liver pAct2 cDNA Library (Clontech)	**pCMV-Tag1** (Clontech)
	3'	5'-gcg gta cct taa tac ggc ctc tcc ctg-3'	KpnI		
SMN	**5'**	5'-gga att ccg cga tgg gca gtg gcg gag-3'	EcoRI	Mouse 11-day fetal pAct2 cDNA library (Clontech)	**pDsRED-C1** (Clontech)
	3'	5'-gct cta gag ctt aat ttg tat gtg agc act ttc ct-3'	XbaI		
Cdc25a	**5'**	5'-gcg gat cct gat gga act ggg ccc gga g-3'	BamHI	Mouse 11-day fetal pAct2 cDNA library (Clontech)	**pCMV-Tag1** (Clontech)
	3'	5'-gcg gta ccg atc aga gct tct tca ggc gac-3'	KpnI		

All PCR reactions for cloning from a cDNA library or making deletion constructs were carried out using a proofreading Platinum *Pfx*® DNA Polymerase (Invitrogen). A typical PCR reaction contained 0.25 μL 5' primer (100 μM stock), 0.25 μL 3' primer (100 μM stock), 5 μL 10x *Pfx* Amplification Buffer, 3 μL 5 mM dNTPs, 1 μL 50 mM $MgSO_4$, 1 μL pACT2 cDNA library (~350 ng), 0.5 μL (1.25 U) Platinum Pfx® DNA polymerse, and 39 μL ddH_2O (deionized, distilled water).

The PCR reactions were all carried out in a MJ Research DNA Engine Thermal Cycler or MJ Research DNA Engine Dyad® Thermal Cycler using the following PCR conditions: 2 min at 94°C; and 35 cycles of 30 s at 94°C, 30 s at 58°C, and 1 min 30 s at

68°C; followed by 10 min at 68°C. If these conditions did not work, a gradient of annealing temperatures was set up between 54°C and 60°C to identify a more optimal annealing temperature.

The PCR products were separated on a 1% agarose TAE gel with 0.1 µl/mL of ethidium bromide, and visualized using a Gene Genius Bioimaging System in comparison with a control 1 kb ladder standard (NEB). Once a PCR band at the expected size was identified, PCR product from the original amplification reaction was separated on a new 1% agarose 1x TAE gel, and the band was gel extracted (see section **2.8b**). The resulting DNA and the target vector were then digested with the restriction enzymes using the restriction sites that were incorporated into the PCR primers. All restriction enzymes were purchased from NEB, and digestions were processed according to recommended conditions and 1x BSA (bovine serum albumin).

2.8b Gel Extraction

PCR or restriction digestion products were separated on a 1% agarose 1x TAE gel, and visualized with long-wavelength UV (365 nm) light to minimize UV-induced mutation using a Spectroline hand-held UV light. The band of interest was excised from the gel, and the DNA was isolated using QIAEX II Gel Extraction Kit (QIAGEN) following the manufacturer's recommended protocol. The DNA was eluted from the QIAEX II beads using 20 µL ddH_2O.

2.8c Restriction endonuclease digestion

Restriction of the *TLS* band was carried out as follows: 15 µL DNA, 2 µL NEB 10x Buffer 2, 1 µL BSA (20x), 1 µL (10 U) *KpnI*, and 1 µL (10 U) *BglII*. Restriction digest for pCMV-Tag1 was carried out with 2 µL plasmid DNA (generally from a

plasmid maxi-prep and representing approximately 3 μg of DNA), 2 μL Buffer 2, 1 μL BSA (20x), 1 μL *KpnI*, 1 μL *BglII*, and 13 μL ddH_2O. These reactions were incubated for 2-4 h at 37°C. Similar reactions were carried out for the other cDNAs/vectors using the recommended RE buffer for the specific double digest. The products were separated on a 1% agarose TAE gel, and the bands corresponding to the PCR product and the digested vector were gel extracted.

2.8d Ligation

To ligate a DNA fragment into a vector, T4 DNA Ligase (NEB) was used. A typical reaction would be 5 μL digested cDNA (~20 ng), 1 μL digested plasmid (~10 ng), 2 μL 10x T4 DNA Ligase Buffer, 1 μL T4 DNA Ligase (NEB), and 11 μL ddH_2O. This reaction was incubated overnight at 14°C.

2.8e pEGFP-FLAG-TLS

FLAG-TLS cDNA was excised from the pCMV-Tag1 vector using *BamH1* and *KpnI*. This fragment was then cloned into the BglII and KpnI sites of the pEGFP-C1 vector (Clontech), creating the pEGFP-FLAG-TLS construct.

2.9 Bacterial strains and maintenance

Escherichia coli strains used were DH5α, DH10B, or a dam (DNA adenine methylase) negative version of HB101 (for use when a methylase sensitive restriction enzyme was used, for example *XbaI*). All strains were grown on/in Luria-Bertani (LB) media. For LB agar plates, a mixture of 10 g Tryptone, 5 g yeast extract, 5 g NaCl, 1 ml 1 M NaOH, and 15 g agar per litre of ddH_2O was made and autoclaved. For LB broth, the same mixture was prepared without the agar. All plates and liquid cultures were grown at 37°C. Liquid cultures were agitated in an orbital shaker at 250 rpm.

2.9a Bacterial transformation

Bacterial transformation was carried out using the calcium chloride method. A single colony of bacteria was picked using a sterile toothpick and used to inoculate 50 mL of LB medium and grown overnight. 4 mL of this culture was used to inoculate 400 mL of LB medium in a 4 L flask. This was grown until the OD_{590} reached 0.375. Optical density was measured using an UltroSpec2000 UV/visible spectrophotometer (Amersham Pharmacia Biotech). The culture was then divided into eight pre-chilled 50-mL sterile tubes and left on ice for 10 min. The cells were then centrifuged at 1600x g at 4°C for 7 min. The medium was removed by aspiration, and then pellets were resuspended and washed twice with 10 mL cold $CaCl_2$ solution (60 mM $CaCl_2$, 15% glycerol, 10 mM PIPES, pH 7.0, filter-sterilized), with cells being centrifuged at 1100x g at 4°C for 5 min after each wash. The cells were then resuspended in 2 mL of $CaCl_2$ solution, and aliquoted 100μL per microfuge tube. These were frozen immediately at –80°C.

For each bacterial transformation, one of these pre-prepared tubes of 100 μL competent bacteria was used. Briefly, 10 μL of a ligation reaction or 10 ng of plasmid DNA was added to rapidly thawed competent cells, gently mixed and incubated on ice for 10 min. The cells were then heat-shocked at 42°C for 2 min in a water bath, and then placed back on ice. The cells were then added to 0.5-1 mL LB broth in a 15 mL culture tube and incubated at 37°C for 1 h.

The culture was then plated at a couple of dilutions of LB agar plates containing the appropriate antibiotic. All vectors besides the pTLS plasmid provided bacterial cells with resistance to the antibiotic kanamycin. Stock kanamycin was prepared at a concentration of 50 mg/mL in ddH_2O. A final concentration of 30 μg/mL kanamycin

was used in both LB agar plates and LB broth. The pTLS plasmid provided bacterial cells with a resistance to the antibiotic ampicillin. Stock ampicillin was prepared at a concentration of 10 mg/mL in ddH_2O. A final concentration of 50 μg/mL ampicillin was used in both LB agar plates and LB broth. The stock antibiotics were filter sterilized with a 0.2 μm filter, and stored at –20°C.

2.10 Isolation, preparation, and quantification of plasmid DNA

2.10a Plasmid DNA preparation

Plasmid DNA was always prepared from a single *E. coli* colony, with 6-8 colonies tested for each plasmid construction to increase the likelihood of obtaining a plasmid with the correct insert. To verify correct cDNA insertion, each colony was used to inoculate 2 mL of LB broth/kanamycin, and grown overnight. Plasmid minipreps from these cultures were then prepared using a GenElute™ Plasmid Miniprep Kit (Sigma) as per manufacturer's protocol. The DNA was eluted into 100 μL ddH_2O. When maxipreps were prepared, a single colony was used to inoculate a 4 mL starter culture in the morning. This starter culture was added to 400 mL of LB broth at the end of the day and allowed to grow overnight. The maxipreps were then prepared using a QIAGEN Plasmid Maxi Kit (Qiagen) as per manufacturer's instructions. The DNA from maxipreps was resuspended in 0.25x TE buffer.

2.10b DNA quantification

The DNA concentration of each plasmid preparation was determined using the absorbance at 260 nm. Briefly, 1/70 dilution of plasmid DNA in ddH_2O was prepared, and the A_{260} was measured using an UltraSpec 2000 UV/visible spectrophotometer (Amersham Pharmacia). DNA concentrations in μg/μL (C μg/μL) were calculated using

the following equation: C μg/μL = (A_{260} / 0.02) x dilution factor / 1000, or specifically for a 1/70 dilution, C μg/μL = (A_{260} / 0.02) x 70 / 1000.

2.10c Analysis of plasmid DNA

Restriction endonuclease analysis was carried out on each plasmid preparation to ensure that it carried the correct insert. A double digest was done with the same enzymes used to originally cut both the cDNA and the vector. If the restriction site was destroyed at ligation (for example, when FLAG-TLS, excised using *BamHI* and *KpnI*, was subcloned into the BglII/KpnI sites of pEGFP-C1, destroying the BglII site of pEGFP-C1) another enzyme with a known cut site in either the insert or the vector was chosen. All digests were carried out with the manufacturer's (NEB) recommended buffer for that double digest or single digest. Reactions were carried out with approximately 10 μL miniprep DNA or 1 μL maxiprep DNA. The DNA fragments were separated on a 1% agarose TAE gel with 0.1 μl/mL of ethidium bromide, and visualized using a Gene Genius Bioimaging System in comparison with a control 1 kb ladder marker standard (NEB).

2.11 Sequencing of plasmid DNA

All DNA sequencing was done at the MICB DNA Sequencing Facility using recommended conditions. Each sequencing reaction was carried out with ~200 ng plasmid DNA and 5 pmoles of primer.

Table 2.3: Vector-specific sequencing primers

Primer Name	Vector	Sequence	Direction*
EGFP-C	pEGFP-C1	5'-cat ggt cct gct gga gtt cgt g-3'	Forward
EGFP-R	pEGFP-C1	5'-tta tgt ttc agg ttc agg gg-3'	Reverse
T3	pCMV-Tag1	5'-aat taa ccc tca cta aag gg-3'	Forward
T7	pCMV-Tag1	5'-taa tac gac tca cta tag gg-3'	Reverse

*Direction with respect to the reading frame orientation of the insert.

Table 2.4: TLS cDNA-specific sequencing primers

Primer Name	Location*	Sequence	Direction
TLS-NREV	~120 nt	5'-cta taa cca ctg taa ctc tg-3'	Reverse
Ex4	~320 nt	5'-cgg cta tgg cag tag c-3'	Forward
Ex5 Antisense	~500 nt	5'-cac tgc tgc tgt tgt act gg-3'	Reverse
Ex6	~600 nt	5'-ggc aat caa gac cag agt gg-3'	Forward
Ex9	~950 nt	5'-atc tgc ttg aag taa tca gcc a-3'	Reverse
Ex10	~950 nt	5'-aca aga aaa cgg gac agc c-3'	Forward
TLS 1331	~1300 nt	5'-gag gac agc agc gag ctg-3'	Forward
Ex13	~1400 nt	5'-agg ggc ctt aca ctg gtt gc-3'	Reverse
Ex14	~1400 nt	5'-ggt aac tac ggg gat gat cg-3'	Forward

*Approximate location from the ATG of the TLS cDNA.

2.12 Construction of the TLS deletion constructs

2.12a Construction of pEGFP-TLS(1-216)

pEGFP-FLAG-TLS was digested with Sac II, removing the sequence for amino acids 217 to 526, gel purified, and ligated. This construct was made by D. Bosc.

2.12b Construction of pEGFP-TLS(1-265)

A 5' primer to the BamHI/FLAG junction (5'-gcg gat cca cca tgg att ac-3') and a 3' primer corresponding to sequence including that for amino acid 265, an added TAA stop codon, and an EcoRI site (5'-gga att ctt aaa att tat tga agc cac cac g-3') were used to PCR the N-terminal fragment from pEGFP-FLAG-TLS. This was then cut with *BamHI* and *EcoRI* and cloned into the BglII and EcoRI sites of pEGFP-C1.

2.12c Construction of pEGFP-TLS(292-526)

FLAG-TLS cDNA was cut from pCMV-FLAG-TLS using a *BamHI* and *EcoRI* partial digest (because TLS has an internal EcoRI site) and cloned into the BamHI and EcoRI sites of pGEX-2T. This plasmid was cut then with *BamHI* and *StuI*, removing the sequence for FLAG and amino acids 1-291. To blunt the BamHI end, 2 μL of EcoPol Buffer, 1 μL of Klenow, and 1 μL of dNTPs were added to the 20 μL digest, and the mixture was incubated at 30°C for 15 min. The modified vector/insert was gel purified, and then re-circularized by ligation. The final pEGFP-TLS(292-526) plasmid was created by isolating the TLS(292-526) fragment using *BamHI* and *SacI*, and ligating it into the BamHI and SacI sites of pEGFP-C1. This construct was made by W. Law and D. Bosc.

2.12d Construction of the sequential deletions of the N-terminus of TLS

The strategy for making the sequential deletions of TLS utilized an internal EcoRI site in the TLS cDNA at ~1070 nt from the ATG sequence, and a common reverse primer that corresponds to the sequence surrounding this site. A different 5' primer was used for each deletion, and the primer added a BglII site to the 5' end of the sequence. The PCR product was then digested with *BglII* and *EcoRI*, as was pEGFP-FLAG-TLS. The vector band containing the 3' end of TLS was then ligated to the digested PCR product, restoring the junction in TLS and resulting in the fusion of the FLAG tag to a sequentially more deleted 5' end of TLS. The PCR primers used to create the sequential deletions are shown in Table 2.5. Deletions 1-6 were made by Dr. L. de Lange. Deletion 7 was made by M. Arntfield.

Table 2.5: Primers for the sequential deletions of the N-terminus of TLS

	Deletion	Primer Sequence	RE Site
1	TLS[δ1-21]	5'-gaa aga tct atg ggc agg gct att cc-3'	BglII
2	TLS[δ1-34]	5'-gaa aga tct atg gac agc aga gtt aca gtg g-3'	BglII
3	TLS[δ1-51]	5'-caa aga tct gcc aga gca gct att ctt c-3'	BglII
4	TLS[δ1-73]	5'-gaa aga tct tgg gat atg gct cga ctg-3'	BglII
5	TLS[δ1-92]	5'-gga aga tct atc agc agt cct cct acc ct-3'	BglII
6	TLS[δ 1-138]	5'-gga aga tct tac agc agc aaa gct atg g-3'	BglII
7	TLS[δ 1-193])	5'-gaa aga tct atg gca atc aag acc aga-3'	BglII
R	Common Reverse	5'-cgg aga att ctt tac cat caa acc agt c-3'	EcoRI

2.12e Construction of the internal deletions of TLS

A strategy of overlap extension PCR was used to generate the internal deletions of TLS. This strategy required three separate PCR reactions. The first reaction resulted in the amplification of the region 5' of the deleted sequence, but the reverse primer in this reactions also included nucleotides homologous to those 3' of the deleted sequence (just as you would add a restriction enzyme site). The second reaction resulted in the amplification of the sequence 3' of the deleted sequence, but the forward primer included nucleotides homologous to those 5' of the deleted sequence. The third reaction used as its template the products from the first two PCR reactions, and used the most 5' forward primer and the most 3' reverse primer. This strategy also used the internal EcoRI site of TLS as the site of the common 3' reverse primer (Primer #4) for all three internal deletions. The same common 5' forward primer (Primer #1) was used for all internal deletions as well. Primer #2 and Primer #3 were specific for each internal deletion. The sequences of all the primers are shown Table 2.6, and are labelled as 1, 2, 3, or 4, with the internal deletion-specific primers 2 and 3 as indicated.

Table 2.6: PCR primers for the production of the internal TLS deletions

Deletion	#	Primer Sequence	Direction
Common 5' Primer (adds a BglII site)	1	5'-gga aga tct ata tgg cct caa acg att ata c-3'	Forward
TLS(δ74-93)	2	5'-gac tgc tgc tgg gga gtt gac tga g-3'	Reverse
	3	5'ctc ccc agc agc agt cct cct acc c-3'	Forward
TLS(δ74-139)	2	5'-tgc tgc tgc tgg gga gtt gac tga g-3'	Reverse
	3	5'-ctc ccc agc agc agc aaa gct atg gac-3'	Forward
TLS(δ74-193)	2	5'-ttg cca tac tgg gga gtt gac tga g-3'	Reverse
	3	5'-ctc ccc agt atg gca atc aag acc aga g-3'	Forward
Common 3' Primer (adds a EcoRI site)	4	5'-cgg aga att ctt tac cat caa acc agt c-3'	Reverse

For reaction one: 1.5 μL Primer #1 (10 μM stock), 1.5 μL internal deletion-specific Primer #2 (10 μM stock), 10 μL 10x *Pfx* Amplification Buffer, 3 μL 5 mM dNTPs, 1 μL 50 mM $MgSO_4$, 100 pg pEGFP-FLAG-TLS, 0.5 μL (1.25 U) Platinum Pfx® DNA polymerse, and 32.5 μL ddH_2O. The PCR program was 5 min at 94°C; 2 cycles of 15 s at 94°C, 30 s at 50°C, and 1 min at 68°C; 25 cycles of 15 s at 94°C, 30 s at 65°C, and 1 min at 68°C; followed by 10 min at 68°C.

For reaction two: 1.5 μL internal deletion-specific Primer #3 (10 μM stock), 1.5 μL Primer #4 (10 μM stock), 10 μL 10x *Pfx* Amplification Buffer, 25 μL 10x PCR Enhancer Solution, 3 μL 5 mM dNTPs, 1 μL 50 mM $MgSO_4$, 100 pg pEGFP-FLAG-TLS, 0.5 μL (1.25 U) Platinum Pfx® DNA polymerse, and 7.5 μL ddH_2O. The PCR program was 5 min at 94°C; 25 cycles of 15 s at 94°C, 30 s at 55°C, and 1 min at 68°C; and 10 min at 68°C.

For reaction three: 1.5 μL Primer #1 (10 μM stock), 1.5 μL Primer #4 (10 μM stock), 10 μL 10x *Pfx* Amplification Buffer, 10 μL 10x PCR Enhancer Solution, 3 μL 5 mM dNTPs, 1 μL 50 mM $MgSO_4$, 10 ng Rxn 1 PCR Product, 10 ng Rxn 2 PCR

Product, 0.5 μL (1.25 U) Platinum Pfx® DNA polymerse, and up to 50 μL with ddH_2O. The PCR program was the same as for reaction two.

The products from reaction number three were then digested with *BglII* and *EcoRI* and ligated into pEGFP-FLAG-TLS that had also been digested with *BglII* and *EcoRI* in a similar fashion to that of the sequential deletions of TLS. All constructs were validated by sequencing.

2.13 Construction of pEGFP-TLS-ERG and pEGFP-ERG2

pEGFP-FLAG-TLS-ERG was made cutting TLS-ERG cDNA out of pMSCV-TLS-ERG[52] with *BglII* and ligating this into the BglII site of pDsRed1-C1. TLS-ERG was then cut out of this vector using a *XmaI/BglII* double digest, and this was ligated into an pEGFP-FLAG-TLS plasmid digested with *XmaI/BamHI*, creating pEGFP-FLAG-TLS-ERG. pEGFP-FLAG-ERG2 was made by cutting ERG2 cDNA out of pLNCX-ERG2[48] with *HindIII*, and ligating this into the HindIII site of pBluescript SK+. A BglII site was then added to the 5' end of ERG2 by a PCR reaction with 5'-gga aga tct tca tgg cca gca cta tta agg aa-3', and the T7 primer. This fragment was digested with *BglII* and *HindIII*, and then ligated into the BglII/HindIII sites of pCMV-Tag1. The FLAG-ERG2 fragment from a partial digest with *BamHI* and *HindIII* was then ligated into the BglII/HindIII sites of pEGFP-C1. (Constructs made by D. Bosc. pMSCV-TLS-ERG and pLNCX-ERG2 were kind gifts of John Dick.)

2.14 Transient Transfections

Cells (MEFs, 293T cells or HeLa cells) were transiently transfected using the calcium phosphate method[316]. For fluorescence microscopy, MEFs or HeLa cells were

plated onto cover slips (sterilized with 70% ethanol) in the wells of a 6-well plate so that they would be 50-70% confluent the following day. For protein preparations, 293T cells were plated onto 6-well plates pre-coated with gelatin so that they would be 50% confluent the following day. (Wells were pre-coated with gelatin by adding 2 mL of 0.1% w/v gelatin in PBS to each well of a 6-well plate, and incubating the plate at room temperature for 15 min. The plate was then washed with PBS, and treated as normal.) 2 μg of plasmid DNA was mixed with 200 μL HEBS (HEPES buffered saline: 275 mM NaCl, 42 mM HEPES, 9.6 mM KCl, 1.5 mM Na_2HPO_4), and then 200 μL of 250 mM $CaCl_2$ was added with vigorous shaking. This was then added to one well of a 6-well plate containing 2 mL of DMEM, and mixed well by swirling. The mixture was removed 6 h later, and the cells were washed twice with PBS. Fresh DMEM was then added back to the cells. One to two days later, the transfected cells were used for the production of cell lysates (293T), or were processed for fluorescence microscopy with or without immunocytochemistry (MEFs or HeLa cells).

2.15 Protein extracts, SDS-PAGE, and immunoblotting

2.15a Whole-cell lysate preparation using modified RIPA buffer

For the Cdc25a, cyclin D1, p53, and p21 immunoblots, primary MEFs were seeded (60-70% confluency) at least 16 h prior to the start of the experiment. Cells were mock-irradiated or γ-irradiated, and incubated for the indicated times (1, 3, and 6 h, or 1, 3, 6, and 16 h), at which time they were harvested while on ice using cold PBS and a cell scraper. The cell pellets for each time point represent a pooling of nine 60 mm plates. For 293T extracts, the cells of one well of a 6-well plate were collected by washing cells off of the plate using cold PBS. Cells were pelleted by centrifugation at 1200 rpm

(290x g) at 4°C for 5 min. Pelleted cells were then resuspended in 200 μL-400 μL of cold modified RIPA buffer (50 mM Tris-Cl pH 7.4, 1% NP-40, 0.25% Na-deoxycholate, 150 mM NaCl, and 1 mM EDTA) with 2 mM NaF, 1 mM activated Na-orthovanadate, 0.84 μg/mL Pepstatin A, 10 μg/mL trypsin inhibitor, 16 μg/mL benzamidine, 16 μg/mL aprotonin, and 1 mM PMSF) by vortexing. The cells were then incubated at 4°C, with rotation, for 1-2 h. The mixture was vortexed again, and centrifuged at 10,000x g at 4°C for 15 min. The supernatant was then transferred to a new tube, and represented the whole cell lysate.

2.15b Total histone preparations

TLS $^{-/-}$ and *TLS* $^{+/+}$ MEFs were plated in 15 cm dishes and grown to approximately 60% confluency. The cells were harvested with 2 mL of trypsin. Trypsinization was stopped using 10 mL DMEM. The cells were then γ-irradiated in suspension with 0, 0.5, 1.0, 2.5 or 5.0 Gy γ-irradiation, and allowed to recover for 1 h at 37°C in suspension. The cells were then pelleted at 1200 rpm (290x g) at 4°C for 5 min, washed in 5 mL PBS, and repelleted. The cell pellets were then resuspended in 400 μL acid extraction buffer (10 mM HEPES pH 7.9, 1.5 mM $MgCl_2$, 10 mM KCl, 0.5 mM DTT, 1.5 mM PMSF, 1 mM NaF, and 1 mM Na orthovanadate). Sulfuric acid was then added to a final concentration of 0.2 M. The lysates were incubated at 4°C with rotation for 1 h, and then centrifuged for 10 min at 20,000x g at 4°C. The supernatant was transferred to a dialysis tube (Spectrum Spectra/Por molecularporous membrane tubing 132645 MWCO (molecular weight cut-off): 6-8,000) and dialyzed against two changes of 1 M acetic acid for 2 h each time at 4°C. The supernatant was then dialyzed against distilled water overnight at

4°C. The samples were frozen at –80°C, and then lyophilized using a Savant ModulyoD Freeze Dryer. The protein was then resuspended in ddH_2O (40 μL).

2.15c Protein quantification

Histone preparations were quantified using the Bio-Rad Protein Assay (595 nm absorbance) with BSA (bovine serum albumin) as a standard. Whole cell extracts were quantified using the Bio-Rad DC Protein Assay with Bio-Rad Protein Assay Standard 1 (Bovine Plasma Gamma Globulin) as a standard (750 nm absorbance). Absorbances were read using a SPECTRAmax 190 96-well plate reader with SOFTmax PRO version 3.1.2.

2.15d SDS-PAGE (SDS-polyacrylamide gel electrophoresis) and electroblotting of proteins.

Aliquots of the protein preparations were mixed in a 5 to 1 ratio with 6x SDS-PAGE loading buffer (300 mM Tris pH6.8, 0.1 mg/mL bromophenol blue, 15% v/v glycerol, 6% w/v SDS, and 5% w/v DTT) and denatured for 5 min at 100°C. For 293T extracts, 20 μL of the whole cell lysate was used in the sample preparations. For the Cdc25a, cyclin D1, p53, and p21 gels, 100 μg of whole cell lysate was used per sample. For the γH2AX gels, 15 μg of total histone preparations were used per sample. A denatured sample of Prestained Protein Marker, Broad Range, 6-175 kDa (NEB) was used as a molecular mass standard.

All SDS-PAGE electrophoresis was performed using a Mini-PROTEAN II as per manufacturer's instructions. For one 7.5 mL 10% SDS-PAGE separating gel: 2.5 mL 30% acrylamide/0.8% bisacrylamide, 1.875 mL 4x Tris/SDS pH 8.8 (1.5 M Tris pH 8.8, 0.4% w/v SDS), 3.125 mL ddH_2O, 25 μL 10% w/v ammonium persulfate, and 5 μL TEMED. The histone preparations and were separated using a 15% SDS-PAGE gel. For

one 7.5 mL 15% SDS-PAGE separating gel: 3.75 mL acrylamide/0.8% bisacrylamide, 1.875 mL 4x Tris/SDS pH 8.8, 1.875 mL ddH_2O, 25 µL 10% w/v ammonium persulfate, 5 µL TEMED. A 15% SDS-PAGE gel was also used for analysis of p21 protein. A stacking gel (0.325 mL 30% acrylamide/0.8% bisacrylamide, 0.625 mL 4x Tris/SDS pH 6.8 [0.5 M Tris pH 6.8, 0.4% w/v SDS], 12.5 µL 10% w/v ammonium persulfate, 2.5 µL TEMED) was layered on top of each separating gel as per manufacturer's instructions. SDS-PAGE was carried out using 1x SDS-PAGE running buffer (10x SDS-PAGE running buffer: 250 mM Tris, 2.5 M glycine, 1% w/v SDS) at approximately 150 V for 1.5 h. The protein was then transferred to a nitrocellulose membrane using a Mini Trans-Blot Module (Bio-Rad) with a blotting buffer of 25 mM Tris, pH 8.3, 192 mM glycine, and 20% methanol (and with 0.025% SDS for the Cdc25a and cyclin D1 blots). Electroblotting was carried out at 150 mA overnight or at 350 mA for 2 h. The blot was then washed with distilled water, and stained with Ponceau S (0.1% w/v Ponceau S and 5% acetic acid) to verify equal protein loading. The blot was then washed three times in TTBS (1x Tris-buffered saline [100 mM Tris, pH 7.5, 0.9% w/v NaCl] with 0.1% Tween 20) for 10 min each time with shaking, and then processed for immunoblot analysis.

2.15e Immunoblot analysis using antibodies to FLAG epitope, TLS, and γH2AX

Blots were blocked in 1% w/v gelatin in TTBS for 2 h (at room temperature with shaking) or overnight at 4°C, washed three times with TTBS for 10 min each time with shaking, and then incubated with a 1/5 dilution of the TLS 10F7 antibody, a 1/2000 dilution of the anti-FLAG antibody, or a 1/1000 dilution of the anti-γH2AX in TTBS with 0.5% w/v gelatin for 2 h with shaking. The blot was then washed as before, and incubated with a 1/5000 dilution of anti-mouse IgG (whole molecule) peroxidase

conjugate in TTBS with 0.5% w/v gelatin for 2 h with shaking. The blot was then washed twice for 10 min each time with TTBS with shaking, and once with TBS (1x Tris-buffered saline [100 mM Tris, pH 7.5, 0.9% w/v NaCl]).

2.15f Immunoblot analysis using the antibody to Cdc25a

The blot was blocked with 2.5% w/v milk powder in TTBS for 30 min, washed as above, and then incubated overnight at 4°C with a 1/50 dilution of the anti-Cdc25a antibody in TBS. The blot was then washed as above, and incubated for 2 h with 1/2000 dilution of anti-mouse IgG (whole molecule) peroxidase conjugate in TTBS with 2.5% w/v milk powder. The blot was then washed as above.

2.15g Immunoblot analysis using antibodies to cyclin D1, p53, p21, and Actin.

The blots were blocked with 2.5% w/v milk powder in TTBS for 1h, washed as above, and then incubated overnight at 4°C with a 1/200 dilution of the anti-cyclin D1, a 1/2000 dilution of anti-p53 antibody, or a 1/2000 dilution of anti-p21 in TTBS with 2.5% w/v milk powder, or incubated for 1 h at room temperature with a 1/10000 dilution of anti-Actin in TTBS with 2.5% w/v milk powder (following previous detection for p53 or p21). The blots were then washed as above, and incubated for 2 h with a 1/5000 dilution of anti-mouse IgG (whole molecule) peroxidase conjugate or a 1/10000 dilution of anti-rabbit IgG (whole molecule) (for the Actin antibody) in TTBS with 2.5% w/v milk powder. The blots were then washed as above.

2.15h Detection of antibody-antigen complexes

Antibody-antigen complexes were detected using ECL™ Western Blotting Detection Reagents (Amersham) according to the manufacturer's instructions. Complexes were visualized on Hyperfilm™ ECL (Amersham).

2.16 Flow cytometry

Common reagents used in all flow cytometric analysis were PBS (137 mM NaCl, 2.7 mM KCl, 10 mM Na_2HPO_4, and 2 mM KH_2PO_4), and 7AAD (7-aminoactinomycin D) (Sigma, catalogue #A9400, resuspended first to 5 mg/mL in acetone, and then diluted to 1 mg/mL in PBS, stored at –20°C in the dark.).

2.16a Apoptosis assay

TLS $^{+/+}$ and *TLS* $^{-/-}$ pre-B cells were treated with increasing concentrations of mitomycin C, exposed to increasing doses of γ-irradiation, exposed to increasing doses of UV-irradiation, or treated with increasing concentrations of staurosporine (stock solution in DMSO). Six hours post each exposure, the cells were resuspended in 200 μL binding buffer (10 mM HEPES, pH 7.4, 140 mM NaCl, 2.5 mM $CaCl_2$) containing 2.5 μL Annexin V-FITC (BD Biosciences), and 2 μg/mL 7AAD. Samples were analyzed on a FACSCalibur (BD) after a 15-min incubation for 7AAD and FITC. Region statistics were done using BD CellQuest Pro Version 3.5.

2.16b BrdU Labelling

Cells were plated in 60 mm dishes so that they would be 60-70% confluent in 2 days. After 2 days, the cells were γ-irradiated (5 Gy) or mock-irradiated and incubated for 1, 6, or 24 h, at which time the medium was replaced with medium containing 10 μM BrdU (5-Bromo-2'-deoxyuridine, Sigma, catalogue #5002, stock 33.33 mM in PBS) and incubated for a further 1 h. The cells from each plate were then harvested to create a single-cell suspension, washed with PBS, and resuspended in 300 μL cold PBS. The cells were then fixed by adding 700 μL of –20°C 100% ethanol while vortexing lightly to

mix, and incubated for at least 1 h or up to several days at 4°C in the dark. After collection by centrifugation at 1200 rpm (290x g) at 4°C, the cells were then resuspended in 500 µL 2 N HCl (1 part concentrated HCl to 4 parts ddH_2O), and incubated for 30 min at room temperature in the dark. Next, 1 mL of PBS was added to the tube, and the cells were collected again by centrifugation. The cells were washed a further two times with 1 mL PBS each time, and then washed once with 1 mL PBS-TB (PBS with 0.1% BSA and 0.2% Tween 20). Finally, the cell pellet was incubated with 5 µL anti-BrdU-FITC (BD Biosciences) for 2 h at room temperature in the dark with occasional mixing. The cells were then washed once with 1 mL PBS-TB, resuspended in 200 µL PBS with 2 µg/mL 7AAD, and incubated at room temperature for 15 min. The cells were then analyzed using a FACSCalibur (BD) for 7AAD and FITC. Region statistics were done using BD CellQuest Pro Version 3.5.

For the experiments with nocodazole (Sigma, catalogue # M1404, Stock: 1000 µg/mL in DMSO, dissolved with heating at 56°C for 10 min), it was added to a concentration of 1 µg/mL just before γ-irradiation. Nocodazole was maintained in the medium on these plates for the remainder of the experiment. When the cells were labelled with 10 µM BrdU for 1 h, 1 µg/mL nocodazole was also present. The cells were then harvested, fixed, and processed for flow cytometry as above.

2.16c Histone H3 serine 28 phosphorylation

Cells were plated in 60 mm dishes so that they would be 60-70% confluent in 1-2 days. One to two days later, the cells were γ-irradiated as indicated in the experiment or mock-irradiated and incubated for 1, 3, 6, or 24 h. The cells from each plate were then harvested to create a single-cell suspension, washed with PBS, and resuspended in 300

μL cold PBS. The cells were then fixed by adding 700 μL of –20°C 100% ethanol while vortexing lightly to mix, and incubated for at least 1 h or up to several days at 4°C. After collection by centrifugation at 1200 rpm (290x g) at 4°C, the cells were washed with cold PBS, and washed again with PBS and 0.05% Triton X-100, and finally washed with PBS and 1% BSA (PBS-B). The cells were then resuspended in 200 μL PBS-B with 1/100 anti-phospho-histone H3 serine 28, clone HTA28 (Sigma) and incubated on ice for 2 h. The cells were washed in PBS-B, and then resuspended in 200 μL PBS-B with a 1/1000 dilution of anti-rat IgG (whole molecule) FITC conjugate (Sigma) and incubated on ice for 2 h. The cells were washed in PBS-B, resuspended in 200 μL PBS with 2 μg/mL 7AAD, and incubated at room temperature for 15 min. The cells were then analyzed using a FACSCalibur (BD) for 7AAD and FITC. Region statistics were done using BD CellQuest Pro Version 3.5.

2.17 Immunocytochemistry

Common reagents used in all of the immunocytochemistry analysis included PBS (137 mM NaCl, 2.7 mM KCl, 10 mM Na_2HPO_4, and 2 mM KH_2PO_4), PBST (PBS with 0.05% Triton X-100), and a blocking buffer consisting of 1x PBS, 5% FBS, 0.2% Triton X-100, 0.1% BSA.

2.17a Detection of TLS and p80 coilin

Untransfected or transfected cells on cover slips were fixed in 4% paraformaldehyde in PBS for 30 min at room temperature. (4% paraformaldehyde was solubilized in PBS by incubation at 70°C for 1 h.) Next, the cells were permeabilized by washing three times with PBST for 10 min each time, blocked for 2 h with blocking buffer, and incubated overnight with a 1/2 dilution of the 10F7 antibody in blocking

buffer at 4°C in a humidity chamber. The 10F7 antibody was used to detect both endogenous TLS and exogenous TLS. The cells were then washed three times 10 min with PBST with shaking, and then incubated for 2 h with a 1/200 Antimouse IgG Biotin Conjugate (Sigma) in blocking buffer with shaking. The cells were then washed again as before, and then incubated with 1/200 Streptavidin-Texas Red (Vector Laboratories Inc.) in blocking buffer for 2 h. The cells were then washed as before. The cover slips were then mounted onto slides using Vectashield Mounting Medium for Fluorescence with DAPI (4',6'-diamidino-2-phenylindole) (Vector Laboratories Inc.) p80 coilin was detected as described above using a 1/200 dilution of the p80 coilin antibody (BD Biosciences) during the incubation period for the primary antibody.

2.17b Detection of γH2AX

MEFs or HeLa cells were plated so that the following day they would be 50-70% confluent. The next day the cells were mock-irradiated or γ-irradiated, and incubated for the times indicated in the experiments. The cells were then washed with PBS, and fixed in 4% paraformaldehyde in PBS for 30 min at room temperature. The cells were then washed with PBS, and permeabilized and blocked as above. The cells were then incubated overnight at 4°C with a 1/500 dilution of anti-phospho histone H2AX [Ser139] (Upstate) in blocking buffer, and the following day the cells were washed as above. For the data in Figures 5.2, 6.8 and 6.15, the cells were then incubated with a 1/1000 dilution of Fluorescein (FITC)-conjugated AffiniPure Donkey Anti-Mouse IgG (H+L) in blocking buffer for 2 h at room temperature with shaking. For the data in Figure 5.1, the cells incubated with antimouse IgG biotin conjugate (Sigma) diluted 1/1000 in blocking buffer for 1 h at room temperature with shaking The cells were then washed again, and for

those experiments that used the antimouse IgG biotin conjugate, the cells were then incubated with streptavidin-Fluorescein (Vector Laboratories) diluted 1/1000 in blocking solution for 1 h at room temperature with shaking. The cells were washed again as above. All the cover slips were then mounted as above.

2.17c BrdU immunocytochemistry

Cells grown on cover slips were incubated with 10 μM BrdU in DMEM for 1 h. The cells were then washed with PBS, rinsed with Carnoy's Fixative (3 parts methanol: 1 part glacial acetic acid, stored at –20°C), and then fixed for 30 min in Carnoy's Fixative at –20°C. The cells were then rinsed twice with PBS, and the cover slips were transferred to a 24-well plate for further processing. The cells were then incubated for 30 min in 2 N HCl (1 part concentrated HCL to 4 parts ddH_2O) on a platform shaker. The cells were then rinsed three times with 1 mL PBS per well each time, and then washed three times 10 min with PBST. The cells were then incubated for 1 h in blocking solution, and then for another 2 h with 1/200 anti-BrdU-FITC (BD Biosciences). The cells were then washed three times 10 min with PBST, and the cover slips were then mounted onto slides as above.

2.18 Fluorescence Microscopy

For analysis of pEGFP-transfected cells without immunocytochemistry, the cells were fixed in 4% paraformaldehyde, and washed in PBS. The cover slips were then mounted onto slides with Vectashield Mounting Medium for Fluorescence with DAPI (Vector Laboratories Inc.).

Images in Figures 4.2, 4.3, 4.4, 4.5, 4.6, and 5.1 were acquired using an Olympus BX51 microscope (equipped with a mercury lamp), a Spot mono 12-bit digital camera

and associated software (Version 2.1.2) from Diagnostic Instruments, and an Olympus PlanApo 60x oil immersion objective (60x/1.40 Oil; ∞/0.17) or an Olympus UplanFl 40x objective (40x/0.75). The DAPI image was acquired using the U-MNU2 BX2 Narrow UV cube (Dichroic Mirror DM400, Excitation Filter BP360-370, Barrier Filter BA420), the GFP and fluorescein images were acquired using the U-MNIBA2 BX2 Narrow Interference Blue cube (Dichroic Mirror DM505, Excitation Filter BP470-490, Barrier Filter BA510-550), and the Texas Red image was acquired using the U-MNG2 BX2 Narrow Green cube (Dichroic Mirror DM570, Excitation Filter BP530-550, Barrier Filter BA590).

All other images were acquired using Improvision Openlab 3.5 software and a Leica DMRXA fluorescence microscope (equipped with a mercury lamp) attached to a Qimaging RETIGA EXI Cooled Mono 12-bit digital camera. Objectives used included a HCX pL FLUOTAR 40x/0.75 objective, a HC pL FLUOTAR 10x/0.3 objective, a HCX pL APO 63x/1.32-0.6 Oil CS, a HCX pL FLUOTAR 100x/1.30 Oil, and a HC pL FLUOTAR 20x/0.5. FITC images were acquired using a Leica L5 filter (Dichroic Mirror 505, Excitation Filter BP480/40, Suppression Filter BP527/30). DAPI images were acquired using a Leica A4 filter (Dichroic Mirror 400, Excitation Filter BP360/40, Suppression Filter BP470/40). Texas Red images were acquired using a Leica TX2 filter (Dichroic Mirror 595, Excitation Filter BP560/40, Suppression Filter BP645/75).

2.19 G1/S assay

Cells were plated so that they were 60-70% confluent the next day in 60 mm dishes with 4 sterilized cover slips (12mm circle, thickness 1, Fisher Scientific). All subsequent steps were preformed with pre-warmed medium and PBS. At time 0 h, the

medium was changed with medium containing 10 μM CldU (5-Chloro-2'-deoxyuridine, Sigma, catalogue # C6891, stock 10 mM in 1 M ammonium hydroxide). The cells were then immediately taken to the Gammacell for γ-irradiation (5 or 10 Gy) or mock-irradiation. The cells were then incubated for 1 h at 37°C. The cells were then washed twice with PBS, and then incubated in fresh medium for 1 h at 37°C. At time 2 h, the media was replaced with medium containing 10 μM IdU (5-Iodo-2'-deoxyuridine, Sigma, catalogue # I7125, stock 10 mM in 1 M ammonium hydroxide), and incubated for 1 h at 37°C. The cells were then rinsed two times with PBS, rinsed once with Carnoy's Fixative (3 parts methanol: 1 part glacial acetic acid, stored at –20°C), and then fixed for 30 min in Carnoy's Fixative at –20°C. The cells were then rinsed twice with PBS, and the cover slips were transferred to a 24-well plate for further processing. The cells were then incubated for 30 min in 2 N HCl (1 part concentrated HCL to 4 parts ddH_2O) on a platform shaker. The cells were then rinsed three times with PBS, and then washed 3 x 10 min with PBST. The cells were then incubated overnight at 4°C in blocking solution in a humidity chamber.

Antibodies that can distinguish CldU have been described previously[307]. Briefly, the cells were incubated for 2 h with shaking with 1/100 anti-BrdU clone BU1/75[ICR1] rat monoclonal (Abcam), which will recognize CldU but not IdU[307], and 1/50 anti-BrdU clone B44 mouse monoclonal (BD Pharmingen), which will recognize IdU but not CldU when washed with high salt buffer[307], in blocking solution. The cells were then rinsed with high salt buffer (100 mM Tris, 0.5 M NaCl, 0.5% Tween 20, pH 8.0), and then washed two times 15 min with high salt buffer with shaking. The cells were then washed 10 min in PBST with shaking, and then incubated for 2 h with a 1/500 dilution of

Fluorescein (FITC)-conjugated AffiniPure Donkey Anti-Mouse IgG (H+L) (Jackson ImmunoResearch Laboratories) and a 1/500 dilution of Texas Red® dye-conjugated AffiniPure Donkey Anti-Rat IgG (H+L) (Jackson ImmunoResearch Laboratories) in blocking solution. The cells were then washed three times for 10 min each time with PBST, and mounted onto slides using Vectashield Mounting Medium for Fluorescence with DAPI (Vector Laboratories Inc).

Images for G1/S analysis were acquired with the Leica microscrope using the 10x objective. Image intensity was enhanced consistently across each experiment using Corel Photo-Paint 9 to identify cells with even low IdU or CldU incorporation. Total cell numbers (DAPI) were counted with the aid of ImageJ software. Single IdU-labelled and single CldU-labelled cells were counted manually. Total S-phase cells were counted manually or with the aid of ImageJ software.

2.20 RNA preparation and reverse transcription PCR

Primary MEFs were plated onto 60 mm plates so that they would be 50-70% confluent the following day. The cells were mock-irradiated or γ-irradiated with 5 Gy and incubated for the indicated times in the experiment. The cells were then harvested, washed in PBS. For each time point, the cells from six 60 mm plates were used. Total RNA was then prepared using a Mini RNeasy RNA isolation kit (QIAGEN) as per manufacturer's instructions. The RNA concentration was then quantified in triplicate using the absorbance at 260 nm. Briefly, 1/70 dilution of RNA in ddH_2O was prepared, and the A_{260} was measured using an UltraSpec 2000 UV/visible spectrophotometer (Amersham). RNA concentrations in μg/μL (C μg/μL) were calculated using the

following equation: C μg/μL = (A_{260} / 0.025) x dilution factor / 1000, or specifically for a 1/70 dilution C μg/μL = (A_{260} / 0.025) x 70 / 1000.

First-strand cDNA synthesis was done using M-MLV (Moloney Murine Leukemia Virus) reverse transcriptase (Invitrogen) as per manufacturer's instructions using 500 ng of starting RNA template and gene specific primers for p21 and Actin B (see Table 2.7). The 5' and 3' primers for p21 have been described previously[317], as have the 5' and 3' primers for Actin B[318]. The RT primers of both p21 and Actin B were designed by W. Law.

Table 2.7: Primers for reverse transcription PCR

Transcript	Primer	Sequence	Location
p21	RT	5'-gac caa tct gcg ctt gga gt-3'	Exon 3
	5'	5'-agt gtg ccg ttg tct ctt cg-3'	Exon 2
	3'	5'-aca cca gag tgc aag aca gc-3'	Exon 2
Actin B	RT	5'-ggt acc acc aga cag cac tg-3'	Exon 5
	5'	5'-tac aat gag ctg cgt gtg gc-3'	Exon 3
	3'	5'-ata gct ctt ctc cag gga gg-3'	Exon 4

Next, p21 and Actin B fragments were amplified using the following reaction mixture: 2 μL first-strand cDNA, 1 μL 5' primer (10 μM), 1 μL 3' primer (10 μM), 5 μL 10x PCR buffer, 4 μL 5mM dNTPs, 0.5 μL (2.5 U) *Taq*, and 36.5 μL ddH_2O. The PCR conditions were 2 min at 94°C; and 22 cycles (p21) or 18 cycles (Actin B) of 20 s at 94°C, 30 s at 57°C, and 1 min 72°C; and 8 min at 72°C. A negative control with RNA as the template was amplified to verify that the PCR products were not due to genomic DNA contamination. Furthermore, a concentration gradient of mock-irradiated cDNA was used to verify that the amplification had not plateaued in each PCR reaction.

20 μL of each PCR reaction was separated on a 1% agarose 1x TAE gel. Gel images were captured using a Syngene GeneGenius and GeneSnap 6.02 software (Syngene). Band intensities were quantified using GeneTools analysis software (Syngene). The p21 band intensities were first normalized to the corresponding actin B band intensities, and then to the relative p21 band intensity of the mock-irradiated control.

2.21 Statistics

For statistical comparisons between *TLS* $^{-/-}$ MEFs and *TLS* $^{+/+}$ MEFs, the data represent at least three independent experiments. For statistical comparisons between mock-treated and treated cells, the data represent at least three independent values for each group. For normal data with equal variance, a t-test was used to assess differences between groups. For data where the normality test failed, or data without equal variance, a Mann-Whitney Rank Sum Test was used to assess differences. A p value of <0.05 was considered statistically significant. For the statistical testing for the MTT assays, individual dose versus surviving cell fraction slopes for each independent experiment were used in the t-tests. (The graphs shown represent the average data surviving cell fraction for each dose.) For data with multiple groups, one way ANOVA (Analysis of Variance) was used for identifying differences between treatment groups. The Holm-Sidak method was then used for the pairwise comparisons, with the null hypothesis only being rejected if the unadjusted p value for that comparison was less than the determined critical p value. (An overall significance level of $p<0.05$ was used.) All statistical analysis was carried out using SigmaStat Version 2.5 (Systat Software, Inc.).

Chapter 3

Identification of TLS as a DNA damage response protein

Rationale: *TLS* $^{-/-}$ mice exhibit characteristics consistently found in mouse models of the human genomic instability syndromes AT[112-114] and NBS[115], specifically genomic instability[111], immune system defects[111], and sensitivity to ionizing irradiation[116]. Because the causative genes of these syndromes are involved in the DNA damage response pathways (repair, cell cycle checkpoints, and/or apoptosis), this suggested that TLS also plays a role in these pathways. The standard method of identifying a novel protein involved in DNA repair is to assess whether the absence of the protein results in cellular sensitivity to DNA damaging agents. If a cell is defective in a certain repair pathway due to the absence of a key protein, it should be more sensitive to the affects of DNA damage repaired by that pathway, as determined by cytotoxicity assays.

3.1 Derivation of *TLS* $^{-/-}$ and *TLS* $^{+/+}$ Mouse Embryonic Fibroblast (MEF) Cultures

Because MEFs are easily generated from embryos, they are frequently used to investigate the phenotype of knock-out and transgenic mice at a cellular level, especially if the mouse exhibits perinatal lethality. Another advantage is that MEFs are primary cells, making it less likely that additional mutations acquired through cell culture are affecting the phenotype of the cells. *TLS* $^{+/-}$ C57Bl/6NCrl mice were previously derived in the Hicks laboratory[111]. A timed mating of heterozygous mice was used to generate a day 14.5 pregnant mouse, and the MEF cultures were generated from these day E14.5 embryos. Embryo genotypes (*TLS* $^{-/-}$, *TLS* $^{+/-}$, and *TLS* $^{+/+}$) were verified using both PCR- and Southern-based techniques (Figure 3.1). No phenotype has ever been observed in

heterozygous animals or in the heterozygous cells; therefore, the experiments presented in this thesis only show data for *TLS* $^{-/-}$ and *TLS* $^{+/+}$ cells. All MEF experiments in this thesis were carried out with passage 1-6 MEFs, with most carried out using passage 2-4 MEFs. Of note, experiments on MEFs derived from C57[319], Balb/c[319] and Swiss[320] mice have demonstrated that primary MEFs typically begin to temporarily senesce at around passage ten. After a period of time in senescence, the cells will spontaneously immortalize. Therefore, the MEFs used in this thesis have not yet entered the initial senescence crisis stage.

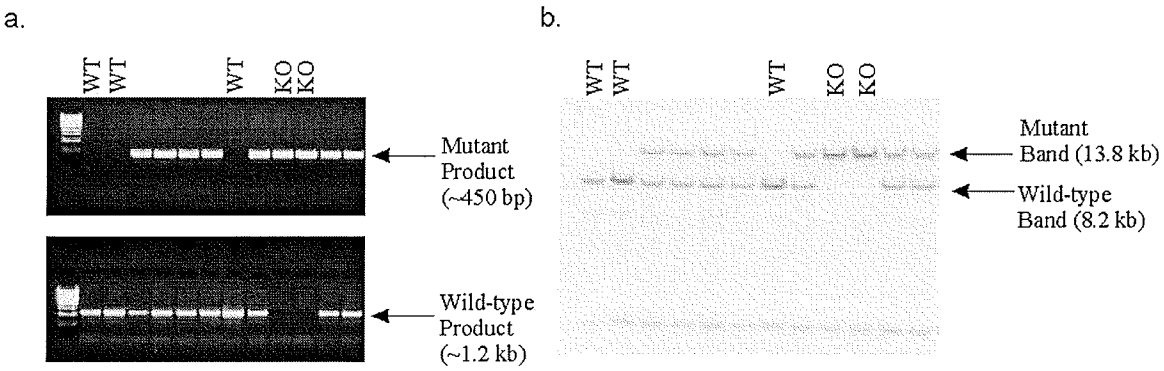

Figure 3.1: Genotyping for *TLS* $^{-/-}$, *TLS* $^{+/-}$, and *TLS* $^{+/+}$ status. Examples of genotyping results generated by (**a**) PCR and (**b**) Southern analysis for MEF 350, and MEF 354-364 cell preparations. WT indicates wild-type (*TLS* $^{+/+}$) MEFs and KO indicates knockout (*TLS* $^{-/-}$) MEFs.

3.2 Evaluation of the proliferation characteristics of *TLS*$^{-/-}$ primary mouse embryonic fibroblasts (MEFs)

More than 67% of *TLS*$^{-/-}$ P0 (passage zero) MEFs exhibit aneuploidy or other chromosomal aberrations, including breaks and fusions[111]. This severity of damage would be expected to affect the proliferation potential of these cells; therefore, doubling times were measured for low passage number *TLS*$^{+/+}$ and *TLS*$^{-/-}$ MEFs (Figure 3.2). (Doubling times for each cell type were also needed for the subsequent cytotoxicity assays.) Briefly, 10^5 passage 3 primary MEFs were plated in triplicate on 10 cm dishes. On days 1, 3, 5, 7, 9, and 11, three plates of each genotype were harvested and counted. The data represent the average of two experiments done in triplicate, with each experiment carried out with MEFs from different embryonic origins. Doubling times were then calculated using the linear portion of the growth curves. The doubling time of *TLS*$^{+/+}$ MEFs was 33 hours, while the doubling time of *TLS*$^{-/-}$ MEFs was 49 hours. While there is a growth disadvantage associated with the *TLS*$^{-/-}$ genotype, it is clear that *TLS*$^{-/-}$ MEFs are still able to undergo cell division despite their genomic instability. The saturation density (where the cell number per plate starts to plateau) of *TLS*$^{-/-}$ MEFs was lower than that of *TLS*$^{+/+}$ MEFs (Figure 3.2). We have also observed that *TLS*$^{-/-}$ MEFs are qualitatively larger in size than *TLS*$^{+/+}$ MEFs, suggesting a reason why the saturation density was lower in the *TLS*$^{-/-}$ MEFs than in the wild-type MEFs, and also agreeing with a previous observation that TLS is involved in regulating cell spreading[94].

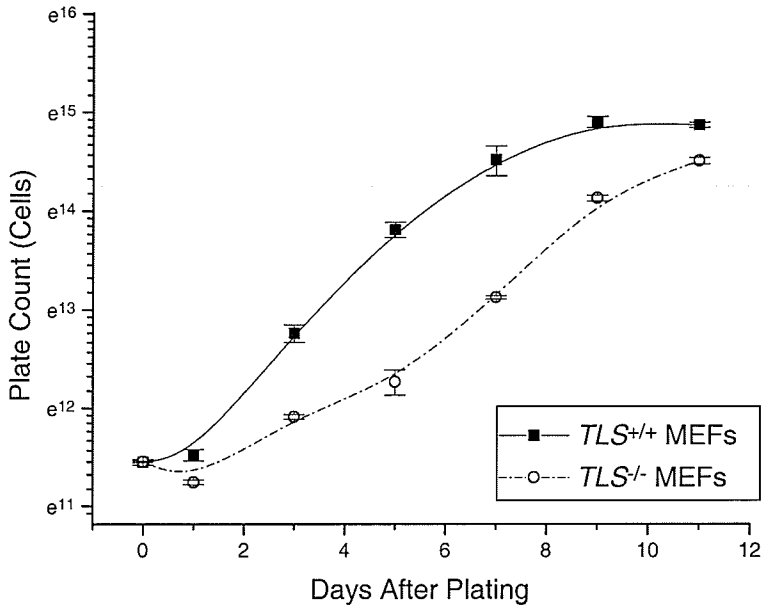

Figure 3.2: *TLS* $^{-/-}$ MEFs do not undergo growth arrest despite their inherent genomic instability. Low passage (P3) primary MEFs were plated in triplicate on 10 cm dishes for each of day 1, 3, 5, 7, 9, and 11. Three plates were harvested and counted per assessment day. The data represent two embryonic origins for each genotype done in triplicate. Error bars represent standard error of the mean.

3.3 Evaluation of the sensitivity of *TLS* $^{-/-}$ MEFs to different DNA damaging agents.

There are two standard assays for cell sensitivity following exposure to a DNA-damaging agent: the MTT (3-[4,5-dimethylthiazol-2-yl]-2,5-diphenyl-tetra-zolium bromide) assay, and the clonogenic assay[321-323]. Primary MEFs do not grow well after plating at a low density, and they also have a finite life span, so using the clonogenic assay would be inherently problematic. Therefore, we chose to use the MTT assay, a standard assay used in pharmacology to assess the sensitivity of cells to specific chemicals. Dehydrogenase enzymes in live cells convert MTT into a blue formazan product, and the amount of dye produced correlates to the number of cells present[321-324].

In the protocol we used, the cells are grown for four doubling times after exposure to the DNA damaging agents, allowing detection of downstream proliferation effects.

We chose to evaluate three different types of DNA damaging agents: γ-irradiation, mitomycin C, and UV-irradiation. γ-irradiation, mitomycin C, and UV-irradiation produce different kinds of DNA damage (DSBs, interstrand cross-links, and intrastrand cross-links, respectively), and the damage is repaired by different pathways (these pathways were reviewed in sections **1.7** and **1.8**).

3.3.1 *TLS* $^{-/-}$ MEFs are sensitive to γ-irradiation

TLS $^{-/-}$ and *TLS* $^{+/+}$ MEFs were γ-irradiated at room temperature with increasing doses (0, 0.5, 1.0, 1.5, 2.0, and 2.5 Gy). The cells were then incubated at 37°C for a further 1 h, at which time serial dilutions of the cells were seeded into 96-well plates and allowed to grow for four doubling times. The MTT assay was then carried out, and the absorbance of each well at 540 nm was measured. The slope of increasing cell number versus absorbance for each dose was calculated, and the surviving cell fraction is the ratio of the dose slope to the control slope. For each experiment, a resulting slope of dose versus log surviving cell fraction was calculated. A t-test between the slopes of *TLS* $^{+/+}$ MEFs and *TLS* $^{-/-}$ MEFs was carried out. At least three experiments, with fibroblasts derived from at least two different embryonic origins, were carried out for each cell type.

Our results show that *TLS* $^{-/-}$ MEFs are more sensitive than *TLS* $^{+/+}$ MEFs to γ-irradiation ($p=0.029$, t-test, $df=7$) (Figure 3.3). This finding is supported by a previous study that showed sensitivity of *TLS* $^{-/-}$ mice to ionizing radiation[116]. The IC_{50}, the concentration/dose at which there is a 50% inhibition of growth, for *TLS* $^{+/+}$ MEFs was

2.5 Gy, while the IC_{50} for *TLS* $^{-/-}$ MEFs was 1.7 Gy. (IC_{50} values were calculated using the slope of dose versus log surviving cell fraction.)

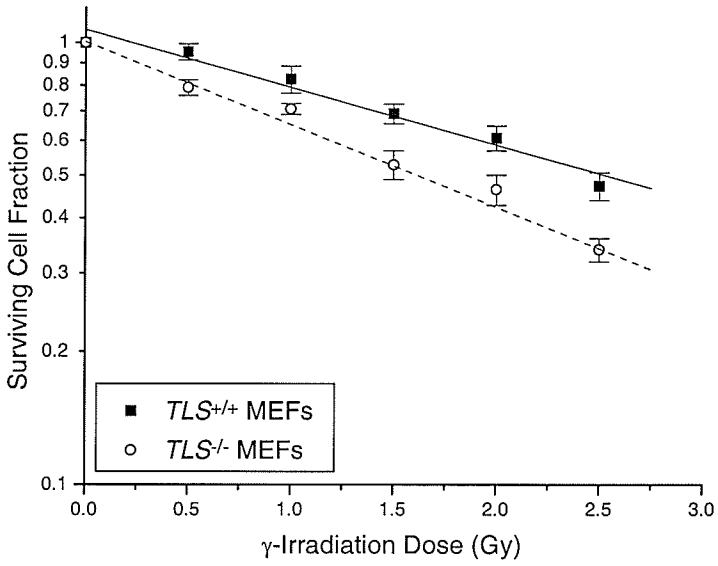

Figure 3.3: *TLS* $^{-/-}$ MEFs are more sensitive to γ-irradiation than *TLS* $^{+/+}$ MEFs. *TLS* $^{+/+}$ and *TLS* $^{-/-}$ MEFs were treated for 1 h with increasing doses of γ-irradiation (0, 0.5, 1.0, 1.5, 2.0, and 2.5 Gy). They were then grown for four doubling times, at which time the MTT assay was done. The data represent the average of at least three independent experiments, and represents at least two different embryonic origins per genotype. Error bars represent standard error of the mean.

3.3.2 *TLS* $^{-/-}$ MEFs are sensitive to mitomycin C

TLS $^{+/+}$ and *TLS* $^{-/-}$ MEFs were exposed to increasing concentrations of mitomycin C (0, 0.5, 1.0, 1.5, 2.0, and 2.5 μM) for 1 h, at which point serial dilutions of the cells were plated in 96-well plates and allowed to grow for four doubling times before the MTT assay was done. Statistical analysis and IC_{50} value determination were carried out as for γ-irradiation.

Our results show that *TLS* $^{-/-}$ MEFs are significantly more sensitive to mitomycin C ($p=0.012$, t-test, $df=6$) than *TLS* $^{+/+}$ MEFs (Figure 3.4). The IC_{50} for *TLS* $^{+/+}$ MEFs was 1.8 μM, while the IC_{50} for *TLS* $^{-/-}$ MEFs was 1.0 μM. The data represent the average of at least three independent experiments representing at least two different embryonic origins per genotype.

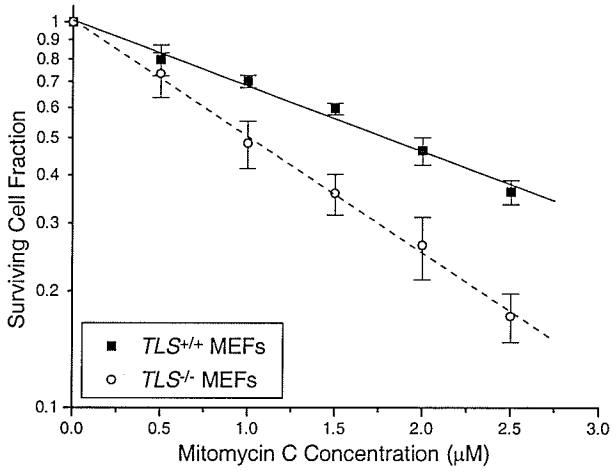

Figure 3.4: *TLS* $^{-/-}$ MEFs are more sensitive to mitomycin C than *TLS* $^{+/+}$ MEFs. *TLS* $^{+/+}$ and *TLS* $^{-/-}$ MEFs were treated for 1 h with increasing concentrations of mitomycin C (0, 0.5, 1.0, 1.5, 2.0, and 2.5 μM). They were then grown for four doubling times, at which time the MTT assay was done. The data represent the average of at least three independent experiments, and represent at least two different embryonic origins per genotype. Error bars represent standard error of the mean.

3.3.3 *TLS* $^{-/-}$ MEFs are not sensitive to ultraviolet-irradiation

TLS $^{-/-}$ and *TLS* $^{+/+}$ MEFs were exposed to increasing doses (0, 2, 4, 6, 8, 10 J/m^2) of the UV-irradiation (254 nm, a short UV wavelength in the UVC range). One hour post exposure, serial dilutions of the cells were plated in 96-well plates and allowed to grow for four doubling times before the MTT assay was done. *TLS* $^{-/-}$ MEFs did not exhibit sensitivity to UV-irradiation, and at higher doses were generally less sensitive to UV-irradiation than wild-type MEFs. At 10 J/m^2, the difference in surviving cell fractions between *TLS* $^{-/-}$ and *TLS* $^{+/+}$ MEFs is not statistically significant ($p=0.132$, t-test, $df=4$). The MTT assay is affected by cellular proliferation differences, so the slight resistance to UV-irradiation observed in the *TLS* $^{-/-}$ MEFs could simply reflect the slightly slower doubling time observed in the *TLS* $^{-/-}$ MEFs. In fact, this result would be expected if the only difference is in the proliferation rates and not sensitivity to UV-irradiation. This observation does not bring into question the MTT assays for γ-irradiation and mitomycin C, because such a proliferation difference would only result in an over-estimation of the surviving cell fraction and, despite this, we observed a cellular sensitivity in the *TLS* $^{-/-}$ MEFs to both of these agents.

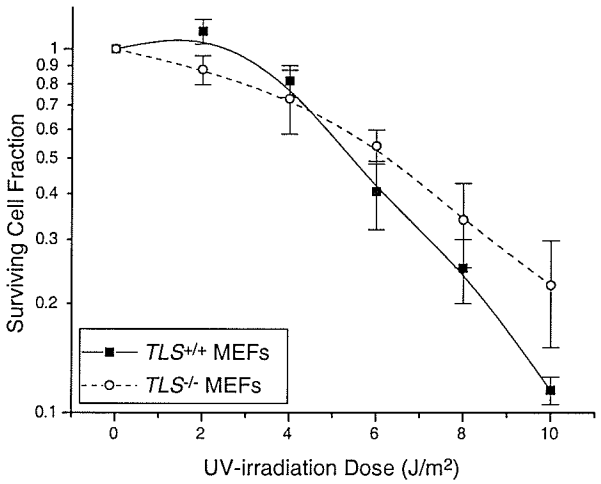

Figure 3.5: *TLS* $^{-/-}$ MEFs are not sensitive to UV-irradiation. *TLS* $^{+/+}$ and *TLS* $^{-/-}$ MEFs were treated for 1 h with increasing doses of UV-irradiation (0, 2, 4, 6, 8, and 10 J/m^2). They were then grown for four doubling times, at which time the MTT assay was done. The data represent the average of at least three independent experiments representing at least two different embryonic origins per genotype. Error bars represent standard error of the mean.

3.4 Evaluation of the DNA damage-induced apoptotic response in *TLS* $^{-/-}$ pre-B cells

We were able to establish that *TLS* $^{-/-}$ MEFs are sensitive to both γ-irradiation and mitomycin C, suggesting that TLS has a functional role in specific DNA damage response pathways. If this hypothesis is correct, we would also expect functional defects in the biological responses initiated by these pathways, specifically growth arrest and apoptosis following DNA damage. Because lymphocytes undergo apoptosis following DNA damage[292], pre-B cells provide a great cell model to analyze apoptosis, and to examine the robustness of the *TLS* $^{-/-}$ phenotype. Therefore, to investigate the role of TLS in DNA damage-induced apoptosis, we analyzed the sensitivity of *TLS* $^{-/-}$ pre-B

cells to apoptosis induced by the same agents that were analyzed in the MEF cells by the MTT assay (this work was done in collaboration with Dr. Ludger Klewes).

Healthy cells can be distinguished from apoptotic and dead cells using live-cell flow cytometry. In this protocol, Annexin V-FITC and 7AAD (7-aminoactinomycin D) are used to stain the cell population. Annexin V binds to phosphatidylserine, a phospholipid that is normally found on the inner leaflet of the plasma membrane, but during early apoptosis flips to the outer leaflet. Only cells with phosphatidylserine on the cell surface will be stained with Annexin V, allowing healthy cells and apoptotic cells to be distinguished using flow cytometry[308-310]. 7AAD is a vital DNA intercalater, only entering and staining dead cells, and can therefore be used to distinguish live and dead cells[325] (see Figure 3.6).

3.4.1 *TLS*$^{-/-}$ pre-B cells are resistant to γ-irradiation-induced apoptosis

TLS$^{-/-}$ and *TLS*$^{+/+}$ pre-B cells were exposed to increasing doses of γ-irradiation (0, 2.5, 5, 7.5, 10, and 12.5 Gy) and incubated for 6 h at 37°C. The cells were then stained with 7AAD and Annexin V, and analyzed using flow cytometry. Healthy cells (surviving cells) are cells that are negative for both 7AAD and Annexin V. Our results show that the *TLS*$^{-/-}$ pre-B cells are resistant to apoptosis induced by γ-irradiation (Figure 3.6 and Figure 3.7). At a dose of 2.5 Gy, the *TLS*$^{-/-}$ pre-B cells were 3.1 times as resistant to apoptosis as wild-type pre-B cells ($p<0.001$, t-test, df=8). The data suggest that *TLS*$^{-/-}$ pre-B cells are defective in the DNA damage-induced apoptotic pathway. While resistance to IR-induced apoptosis might seem counter-intuitive when compared to the IR sensitivity observed in the *TLS*$^{-/-}$ MEFs, it is consistent with the response of *ATM*$^{-/-}$ cells to IR-induced DNA damage. *ATM*$^{-/-}$ cells are generally associated with

radiation hypersensitivity[112, 296], but $ATM^{-/-}$ thymocytes are actually resistant to radiation-induced apoptosis[296, 297]. These contradictory observations are due to the dual roles ATM plays in initiating both cell-cycle arrest and apoptosis[122, 124-127, 176].

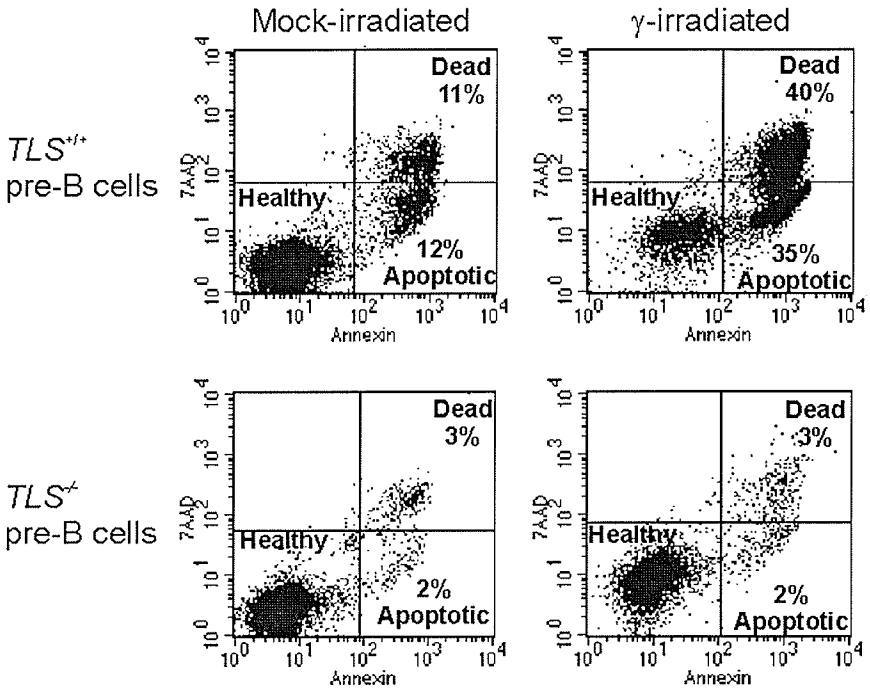

Figure 3.6: Representative flow cytometric data for determining the percentage of surviving cells. $TLS^{+/+}$ and $TLS^{-/-}$ pre-B cells were mock-irradiated or γ-irradiated, and incubated for six hours at 37°C. The cells were then stained with 7AAD and Annexin V-FITC, and analyzed using flow cytometry. (L. Klewes)

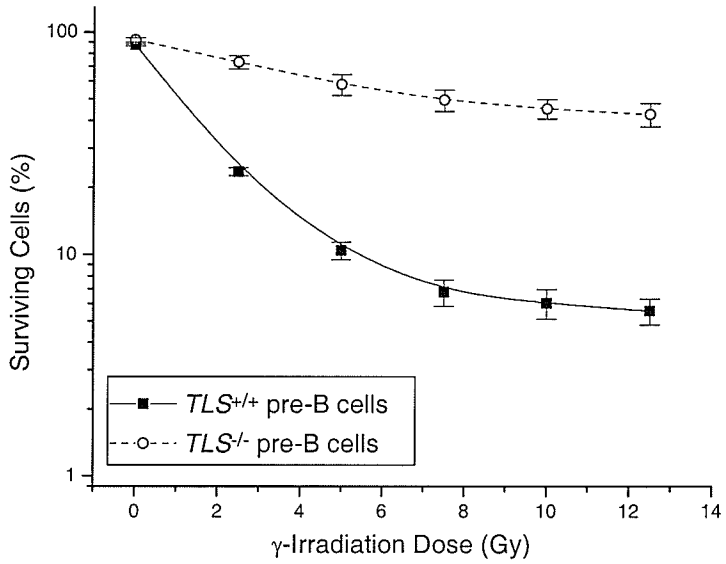

Figure 3.7: *TLS* $^{-/-}$ pre-B cells are resistant to apoptosis induced by γ-irradiation. *TLS* $^{+/+}$ and *TLS* $^{-/-}$ pre-B cells were exposed to increasing doses of γ-irradiation (0-12.5 Gy), and incubated at 37°C for 6 h. The cells were then stained with 7AAD and Annexin V-FITC, and analyzed using flow cytometry. Surviving cells are those negative for both 7AAD and Annexin-V. Error bars represent standard error of the mean, and the experiment was repeated five times. (L. Klewes)

3.4.2 *TLS* $^{-/-}$ pre-B cells are resistant to mitomycin C-induced apoptosis

TLS $^{-/-}$ and *TLS* $^{+/+}$ pre-B cells were exposed to increasing concentrations of mitomycin C (0, 1, 2, 3, 4, and 5 μM) and incubated for 6 h at 37°C. The cells were then stained as described above and analyzed by flow cytometry. Our results show that the *TLS* $^{-/-}$ pre-B cells are resistant to apoptosis induced by mitomycin C (Figure 3.8). At a concentration of 1 μM, the *TLS* $^{-/-}$ pre-B cells were 3.6 times more resistant to apoptosis than the wild-type pre-B cells were ($p<0.001$, t-test, df=8).

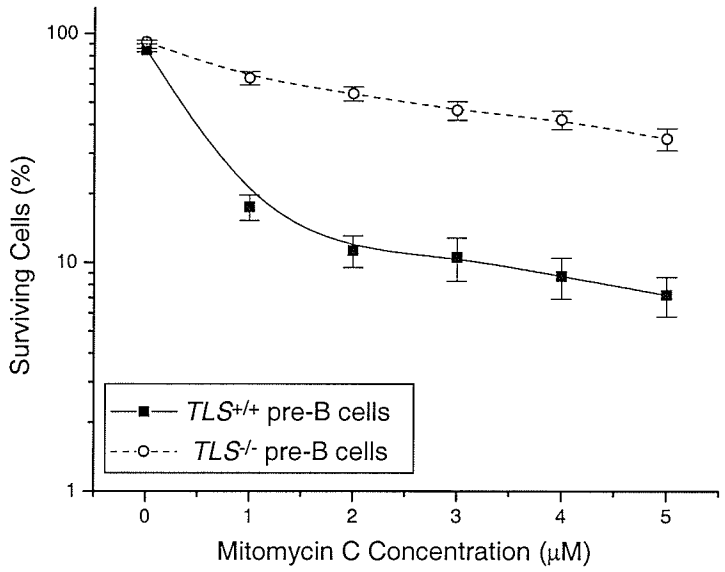

Figure 3.8: *TLS*$^{-/-}$ pre-B cells are resistant to apoptosis induced by mitomycin C. *TLS*$^{+/+}$ and *TLS*$^{-/-}$ pre-B cells were exposed to increasing concentrations of mitomycin C (0, 1, 2, 3, 4, and 5 μM), and incubated at 37°C for 6 h. The cells were then stained with 7AAD and Annexin V-FITC, and analyzed using flow cytometry. Surviving cells are those negative for both 7AAD and Annexin-V. Error bars represent standard error of the mean, and the experiment was repeated five times. (L. Klewes)

3.4.3 *TLS*$^{-/-}$ pre-B cells are resistant to UV-irradiation-induced apoptosis

TLS$^{-/-}$ and *TLS*$^{+/+}$ pre-B cells were exposed to increasing doses of UV-irradiation (0, 15, 30, 60, 90, and 120 J/m^2) and incubated for 6 h at 37°C. The cells were then stained as described above and analyzed by flow cytometry. Our results show that the *TLS*$^{-/-}$ pre-B cells are resistant to apoptosis induced by UV-irradiation, although at higher doses there is an induction of apoptosis in the *TLS*$^{-/-}$ pre-B cells (Figure 3.9). At a dose of 60 J/m^2, the *TLS*$^{-/-}$ pre-B cells were 2.3 times more resistant to apoptosis than the wild-type pre-B cells were ($p=0.006$, t-test, df=8). It is important to note that while a

dose of 10 J/m^2 had significant growth repercussions for the MEFs, a dose of 15 J/m^2 did not induce apoptosis in either the *TLS* $^{+/+}$ or the *TLS* $^{-/-}$ pre-B cells. Why excessive doses of UV-irradiation were required to induce apoptosis in the pre-B cells is unknown at this time, but it could be due to the nature of the DNA damage induced.

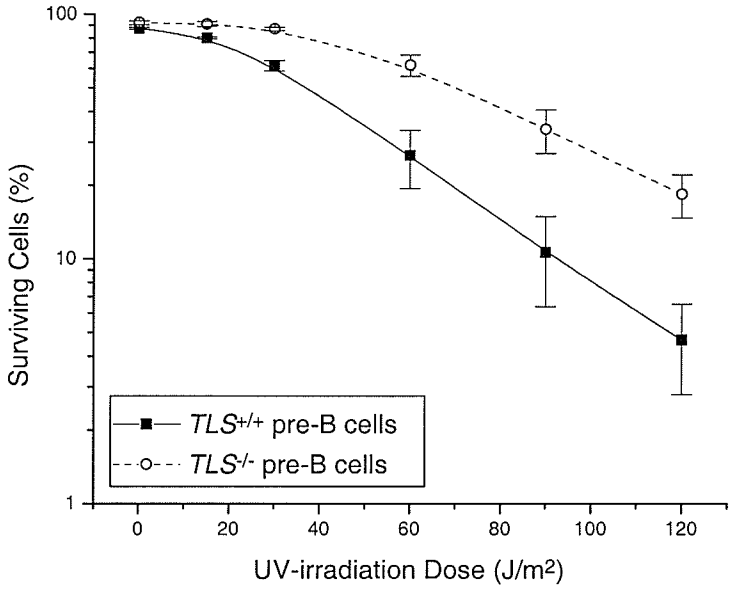

Figure 3.9: *TLS* $^{-/-}$ pre-B cells are resistant to apoptosis induced by UV-irradiation. *TLS* $^{+/+}$ and *TLS* $^{-/-}$ pre-B cells were exposed to increasing doses of UV-irradiation (0, 15, 30, 60, 90, 120 J/m^2), and incubated at 37°C for 6 h. The cells were then stained with 7AAD and Annexin V-FITC, and analyzed using flow cytometry. Surviving cells are those negative for both 7AAD and Annexin-V. Error bars represent standard error of the mean, and the experiment was repeated five times. (L. Klewes)

3.4.4 *TLS* $^{-/-}$ pre-B cells undergo apoptosis following staurosporine treatment

Staurosporine, an inhibitor of protein kinases, induces apoptosis exclusive of the DNA damage-response pathways[326]. Therefore, by analyzing the apoptotic response of the *TLS* $^{-/-}$ pre-B cells in response to staurosporine, we could determine whether the

apoptotic defect observed in these cells was specific for the damage-induced apoptotic pathways, or was a general apoptotic defect. *TLS*$^{-/-}$ and *TLS*$^{+/+}$ pre-B cells were exposed to increasing concentrations of staurosporine (0, 5, 10, 25, and 50 nM) and incubated for 6 h at 37°C. The cells were then stained as described above and analyzed by flow cytometry. Our results show that *TLS*$^{-/-}$ pre-B cells induce apoptosis following staurosporine treatment, indicating that the apoptotic defect is specific for DNA damage-induced apoptosis. At 50 nm staurosporine, the difference in the percentage of surviving cells between *TLS*$^{-/-}$ and *TLS*$^{+/+}$ pre-B cells was not statistically significant (p=0.078, t-test, df=8).

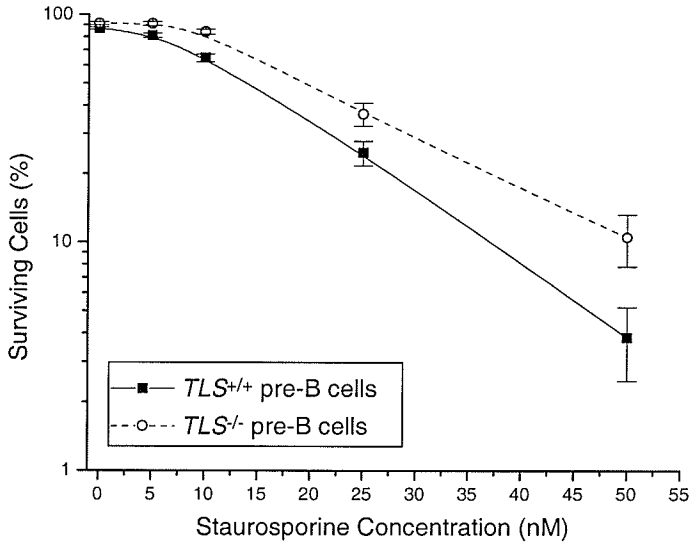

Figure 3.10: *TLS*$^{-/-}$ pre-B cells are able to undergo apoptosis in response to staurosporine. *TLS*$^{+/+}$ and *TLS*$^{-/-}$ pre-B cells were exposed to increasing concentrations of staurosporine (0, 5, 10, 25, and 50 nM), and incubated at 37°C for 6 h. The cells were then stained with 7AAD and Annexin V-FITC, and analyzed using flow cytometry. Surviving cells are those negative for both 7AAD and Annexin-V. Error bars represent standard error of the mean, and the experiment was repeated five times. (L. Klewes)

3.5 Chapter Summary: TLS is a DNA-damage response protein

- *TLS*$^{-/-}$ MEFs proliferate with only a slightly slower doubling time than *TLS*$^{+/+}$ MEFs (49 hours and 33 hours respectively). Because *TLS*$^{-/-}$ MEFs have widespread genomic instability[111], the *TLS*$^{-/-}$ MEFs are in fact proliferating with DNA damage, indicating that they may not be activating or responding to the cell cycle checkpoints regulated by gatekeepers such as p53 and Chk1.
- *TLS*$^{-/-}$ MEFs are more sensitive to both γ-irradiation and mitomycin C, which induce two different forms of DNA damage (DNA double-strand breaks, and interstrand cross-links, respectively). *TLS*$^{-/-}$ MEFs did not exhibit an increased sensitivity to UV-irradiation. The finding that the *TLS*$^{-/-}$ MEFs are more sensitive to γ-irradiation is consistent with what has been shown in the literature[116]. Because we have implicated TLS in the response to both DNA double-strand breaks (DSBs) and interstrand cross-links (ICLs), we have identified TLS as a novel member of the class of proteins that respond to both types of lesions.
- *TLS*$^{-/-}$ pre-B cells are resistant to apoptosis induced by γ-irradiation, mitomycin C, and UV-irradiation. This apoptotic defect is specific for apoptosis induced by DNA damaging agents, because *TLS*$^{-/-}$ pre-B cells are able to undergo apoptosis following staurosporine treatment. While these results may appear contradictory when considered in the context of the MEF data, they are consistent with data from *ATM*$^{-/-}$ cells. *ATM*$^{-/-}$ cells are generally associated with radiation hypersensitivity[112, 296], but *ATM*$^{-/-}$ thymocytes are actually resistant to radiation-induced apoptosis[296, 297]. These observations reflect to the dual roles ATM plays in initiating both cell-cycle arrest and apoptosis[122, 124-127, 176].

Conclusion: *TLS*$^{-/-}$ mice exhibit characteristics consistently found in mouse models of the human genomic instability syndromes AT[112-114] and NBS[115], specifically genomic instability[111], immune system defects[111], and sensitivity to ionizing irradiation[116]. Because the causative genes of these syndromes are involved in the DNA damage response pathways, we hypothesized that TLS also functions in these pathways. We have now established that TLS is a DNA damage-response protein, as it is involved in the response to at least two different forms of DNA damage: DNA double-strand breaks and interstrand cross-links, caused by γ-irradiation and mitomycin C, respectively. Furthermore, defects in the DNA damage response were observed in multiple types of *TLS*$^{-/-}$ cells, underscoring a clear functional role for TLS in the DNA damage response pathways. The *TLS*$^{-/-}$ pre-B cells were defective in the DNA damage-induced apoptotic pathway, and the *TLS*$^{-/-}$ MEFs were sensitive to both γ-irradiation and mitomycin C. The DNA damage-sensitivity observed in the *TLS*$^{-/-}$ MEFs suggests that cells deficient for TLS are defective in the ability to repair and/or cell cycle arrest following DNA damage, and these possibilities will be addressed in Chapter 5.

Chapter 4

Characterization of the dynamic localization of TLS in response to DNA damage and transcriptional inhibition.

Rationale: We established TLS as a DNA damage response protein functioning in the cellular responses to both DNA double-strand breaks and interstrand cross-links in the preceding chapter. However, the molecular function(s) of TLS within these pathways still remains unknown. Because many known DNA damage-response proteins form ionizing radiation-induced foci (IRIF)[203, 204, 212, 213, 327-329], we chose to investigate the function of TLS by characterizing its subcellular relocalization following γ-irradiation, mitomycin C exposure, and other cellular stresses. Furthermore, TLS is known to dynamically relocalize following exposure to the DNA-damaging agent and transcriptional inhibitor actinomycin D, providing an assay that can be used to identify key regulatory domains within TLS[91, 95, 96].

4.1 EGFP (enhanced green fluorescent protein)-FLAG-TLS dynamically relocalizes to the nucleoli following transcriptional inhibition, validating its use in investigating DNA-damage induced relocalization of TLS.

To investigate the dynamic localization of TLS following DNA damage, we chose to use enhanced green fluorescent protein-tagged TLS, as it has several advantages over immunocytochemistry. For example, changes in subnuclear localization can be difficult to detect using immunocytochemistry if the protein is highly expressed and found throughout the nucleoplasm like TLS. The EGFP tag also allowed us to analyze the localization of mutation and deletion constructs, a property that is important for identifying the domains within TLS that are controlling its localization. Finally, it also left open the opportunity to analyze live cells in future experiments.

4.1.1 Cloning and expression of human *TLS*

Human *TLS* was cloned from a human fetal liver cDNA library, and inserted in-frame with and downstream of the FLAG epitope in the pCMV-Tag1 vector, generating a pCMV-FLAG-TLS plasmid. A FLAG-TLS cDNA from this vector was then subcloned in-frame with and downstream of the gene for the enhanced green fluorescent protein (EGFP) in the pEGFP-C1 vector, generating a pEGFP-FLAG-TLS plasmid. When expressed, this plasmid results in an EGFP-FLAG-TLS fusion protein. The TLS cDNA in both of these expressions vectors were sequenced using vector-specific and gene-specific primers, and the sequence of the cDNA was compared with Genbank sequence NM_004960 (the verified *TLS* cDNA sequence is provided in Appendix 1).

To verify that expression of the pEGFP-FLAG-TLS and pCMV-FLAG-TLS plasmids generated in-frame fusion proteins, an α-TLS (monoclonal 10F7) was used to detect the proteins generated from exogenous expression of these plasmids. pEGFP-FLAG-TLS and pCMV-FLAG-TLS were transiently transfected into 293T cells, and whole-cell lysates were prepared from the cells. The western blots were probed with α-TLS (10F7) antibody or with α-FLAG antibody (Figure 4.1). The α-FLAG antibody recognized both EGFP-FLAG-TLS and FLAG-TLS. The α-TLS (10F7) antibody recognized endogenous TLS, and both EGFP-FLAG-TLS and FLAG-TLS, indicating that the tagged TLS expression vectors were being expressed, and that TLS was in-frame in both plasmid constructs. The exogenous TLS was typically expressed at levels comparable to that of endogenous TLS, as shown by the levels of EGFP-FLAG-TLS and endogenous TLS in the third lane of the left-hand blot in Figure 4.1. The doublet band

observed for EGFP-FLAG-TLS may represent TLS modified by phosphorylation and/or methylation, but it could also represent a degradation product of EGFP-FLAG-TLS.

4.1.2 EGFP-FLAG-TLS recapitulates the localization of endogenous TLS.

To verify that EGFP-FLAG-TLS was localizing like endogenous TLS, the subcellular distribution of EGFP-FLAG-TLS was analyzed. pEGFP-FLAG-TLS was transiently transfected into MEF cells. The following day, the cells were fixed in 4% paraformaldehyde, and then processed for immunocytochemistry. α-TLS(10F7) was used to detect TLS (endogenous and EGFP-FLAG-TLS). The fluorescence of the EGFP protein was used to detect the localization of only the EGFP-FLAG-TLS protein. Fluorescence microscopy showed that EGFP-FLAG-TLS is restricted to the nucleus, and is generally excluded from the nucleoli (Figure 4.2). This localization is consistent with what has been shown for endogenous TLS, both in our own data (see Figure 4.2) and in the literature [91, 95, 96]. The sensitivity of the EGFP-FLAG-TLS approach also allowed us to more reproducibly observe other TLS-containing structures, as the EGFP-FLAG-TLS localized in approximately 2-5 perinucleolar foci. These foci are not an artifactual trait of EGFP overexpression, as EGFP itself does not form these structures (data not shown). The 10F7 antibody by comparison was not sensitive enough to distinguish these structures amidst the relatively high Texas Red signal level of TLS found throughout the nucleoplasm, indicating that the use of EGFP-FLAG-TLS could provide us with a very sensitive indicator of any changes in the subcellular localization of TLS.

4.1.3 EGFP-FLAG-TLS relocalizes to the nucleoli following actinomycin D treatment.

Endogenous TLS has been shown in the literature to relocalize to the nucleoli following treatment with the transcriptional inhibitor actinomycin D[91, 95, 96]. To validate

that EGFP-FLAG-TLS was functionally behaving in the same manner as endogenous TLS, we analyzed the relocalization of EGFP-FLAG-TLS following actinomycin D treatment. pEGFP-FLAG-TLS was transiently transfected in MEFs, and the following day, the cells were treated with actinomycin D (0.5 μg/mL) for various times (0, 10, 20, 30, 45, and 60 min). The cells were then fixed with 4% paraformaldehyde, and analyzed using fluorescence microscopy. Relocalization of EGFP-FLAG-TLS to the nucleoli was visible within 10 min with this concentration of actinomycin D (Figure 4.3a). As the exposure time of the cells to actinomycin D increased, the distribution of TLS changed from a ringing around the nucleoli to semicircular caps (Figure 4.3a). These TLS-containing semicircular caps have been identified as dark nucleolar caps (DNCs)[95]. actinomycin D causes the nucleoli to separate[95], and the changing localization of EGFP-FLAG-TLS in response to increased drug exposure is dynamically demonstrating this separation of nucleolar structure. When a higher concentration of actinomycin D (2 μg/mL) was used over a longer exposure period (3 h), the localization of EGFP-FLAG-TLS changed to large foci (Figure 4.3b), consistent with what has been shown for endogenous TLS in the literature and indicative of nucleolar disintegration[96]. Therefore, EGFP-FLAG-TLS is functioning in the same manner as endogenous TLS with respect to its dynamic localization.

4.2 The association of TLS with the nucleoli is specifically associated with transcriptional inhibitors, and is not a general response to DNA damage or cellular stress.

The aim of this chapter was to determine whether TLS relocalizes following DNA damage, or forms DNA damage-induced foci similar to the ionizing radiation-induced foci (IRIF) observed for other DNA damage response proteins[202, 207, 208, 212, 213]. As

described in the above section, TLS is already known to dynamically respond to actinomycin D treatment[91, 95, 96]. Because actinomycin D intercalates into DNA[97], it also damages DNA. We hypothesized that the relocalization of TLS to the nucleolus following actinomycin D treatment might be a stress response to DNA damage. To distinguish the relative contributions of the DNA damaging and transcriptional inhibition effects of actinomycin D to the nucleolar relocalization of TLS, we evaluated the localization of EGFP-FLAG-TLS to a panel of transcriptional inhibitors and DNA-damaging agents. The additional transcriptional inhibitor we chose to evaluate was DRB (5,6-dichlorobenzimidazole riboside), a purine analogue that results in the premature termination of RNA transcripts[330]. We also chose to evaluate the DNA-damaging agents camptothecin, UV-irradiation, mitomycin C, and γ-irradiation.

pEGFP-FLAG-TLS was transiently transfected into MEFs. The following day, the cells were treated with 40 μM DRB for 1 h, 10 μM camptothecin for 1h, or 2.5 μM mitomycin C for 1.5 h, or exposed to 20 J/m^2 of UV-irradiation or 5 Gy of γ-irradiation and then incubated for 1 h. EGFP-FLAG-TLS relocalized to the nucleoli following transcriptional inhibition with DRB (Figure 4.4), which is consistent with what has been shown in the literature for endogenous TLS[53, 96]. However, the pattern of relocalization is distinct from that induced following actinomycin D treatment. Unlike actinomycin D which permanently halts transcription, DRB is a reversible inhibitor[330]. The DRB-induced EGFP-FLAG-TLS relocalization is to intact nucleoli, with the cells exhibiting none of the nucleolar caps indicative of nucleolar segregation.

We also observed relocalization of EGFP-FLAG-TLS to the nucleoli following treatment with the DNA damaging agent camptothecin (Figure 4.4). Camptothecin is an

inhibitor of topoisomerase I[331], an enzyme that makes and repairs single-strand breaks (SSBs) to relieve torsional strain in the DNA[332]. By inhibiting topoisomerase I, camptothecin will stabilize these SSBs, which may then be converted to DSBs during S phase[172]. However, camptothecin is also associated with a rapid inhibition of transcriptional activity through its inhibition of topoisomerase I[331]. EGFP-FLAG-TLS also relocalized to the nucleoli following UV-irradiation. UV-irradiation induces intrastrand cross-links in the form of cyclobutane pyrimidine dimers and pyrimidine (6-4) pyrimidone photoproducts, but like camptothecin, it has also been linked to transcriptional inhibition[333-335].

Unexpectedly, our results showed that EGFP-FLAG-TLS does not relocalize to the nucleoli following either γ-irradiation or mitomycin C treatment (Figure 4.4). No association between γ-irradiation and a general inhibition of transcription has been reported in the literature. Mitomycin C could potentially inhibit transcription, but the dose we used, while toxic to the cells, may not induce enough interstrand cross-links to generate a general repression of transcription. While TLS does not relocalize to the nucleoli following treatment with either γ-irradiation or mitomycin C, our initial observations did suggest that the number of EGFP-FLAG-TLS foci increased following exposure to either γ-irradiation and mitomycin C, potentially indicating that TLS does localize to sites of DNA damage exclusive of its dynamic association with the nucleoli.

In summary, the dynamic relocalization of EGFP-FLAG-TLS to the nucleoli is only associated with agents that are known to cause a general inhibition of transcription, including actinomycin D, DRB, camptothecin, and UV-irradiation.

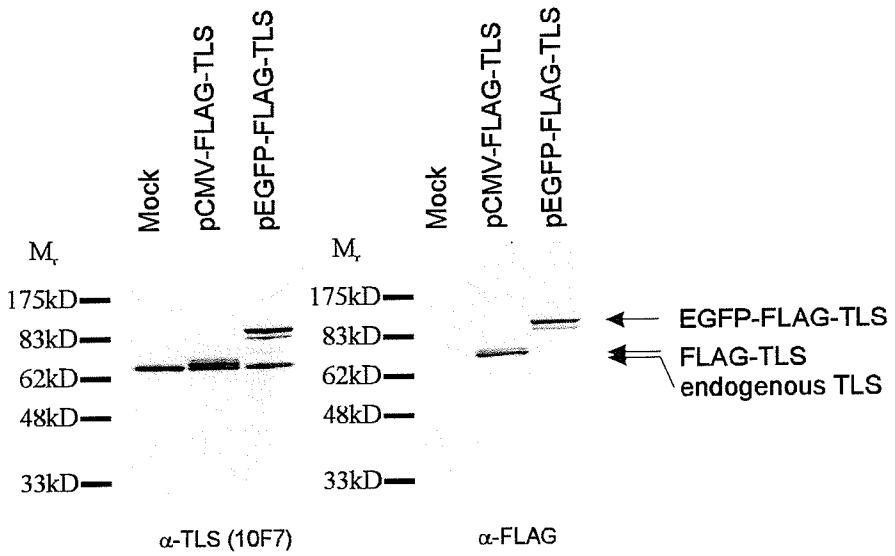

Figure 4.1: Tagged TLS is expressed from both pEGFP-FLAG-TLS and pCMV-FLAG-TLS expression vectors. Whole-cell lysates were prepared from pCMV-FLAG-TLS and pEGFP-FLAG-TLS transiently transfected 293T cells. Blots were probed with α-TLS (10F7) or α-FLAG.

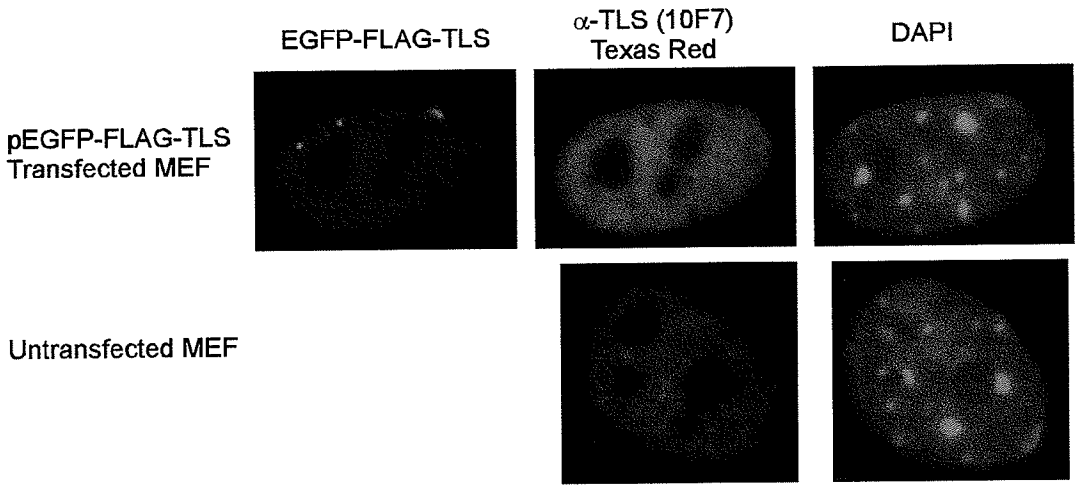

Figure 4.2: Endogenous TLS and EGFP-FLAG-TLS are restricted to the nucleus, and are generally excluded from the nucleoli. EGFP-FLAG-TLS also localizes in perinucleolar foci. pEGFP-FLAG-TLS was transiently transfected into wild-type MEFs. The cells were fixed in 4% paraformaldehyde. α-TLS (10F7) was used to detect endogenous TLS and EGFP-FLAG-TLS. Images were captured using a 60x oil immersion objective. The EGFP, Texas Red (10F7), and their corresponding DAPI images are shown.

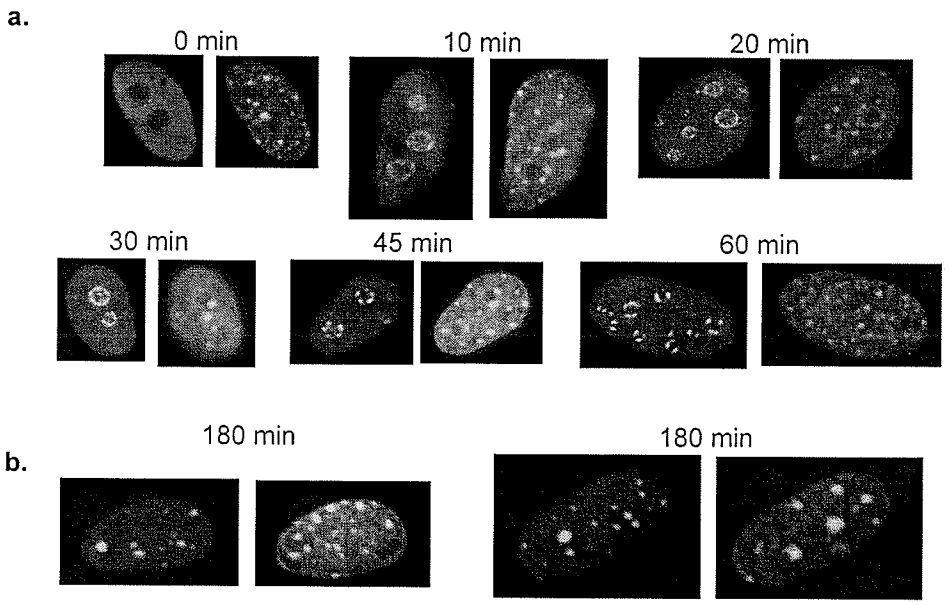

Figure 4.3: EGFP-FLAG-TLS rapidly relocalizes to the nucleoli following Actinomycin D treatment. pEGFP-FLAG-TLS was transiently transfected into MEFs. **a.** The cells were treated with 0.5 μg/mL Actinomycin D for the indicated times. **b.** The cells were treated with 2 μg/mL for 3 h. Two examples are shown. The cells were then fixed with 4% paraformaldehyde. Images were captured with a 60x oil immersion objective.

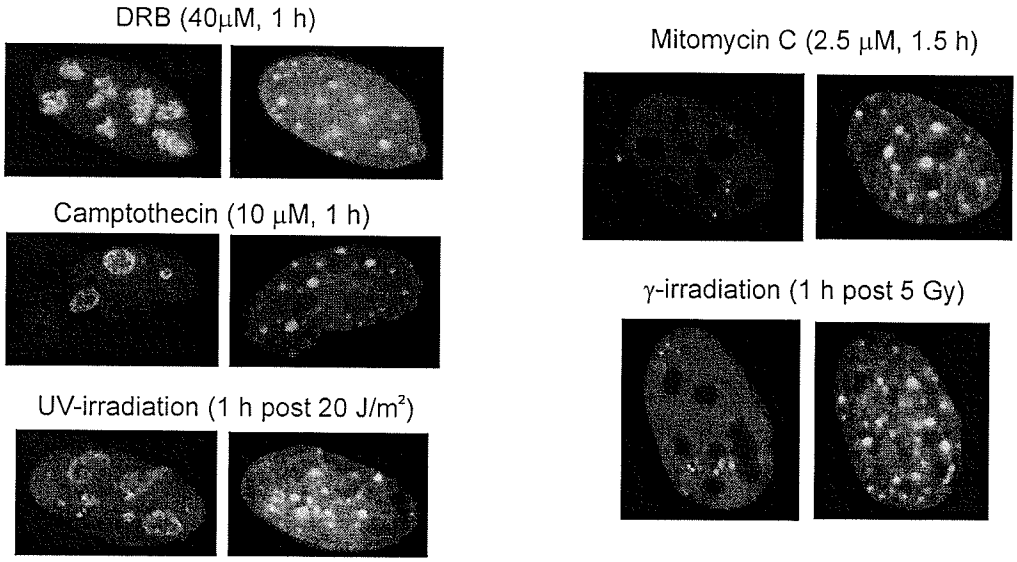

Figure 4.4: EGFP-FLAG-TLS relocalizes to the nucleoli following exposure to other agents known to inhibit transcription. pEGFP-FLAG-TLS was transiently transfected into MEFs. The transfected cells were treated with 40μM DRB for 1 h, or 10 μM camptothecin for 1 h, exposed 20 J/m^2 of UV-irradiation and incubated for 1 h, treated with 2.5 μM Mitomycin C for 1.5 h, or exposed to 5 Gy of γ-irradiation . The cells were then fixed in 4% paraformaldehyde. Images were captured using a 60x oil immersion objective.

4.3 TLS does not localize to additional foci following γ-irradiation or mitomycin C treatment.

Many DNA damage-response proteins relocalize to ionizing radiation-induced foci (IRIF) following DNA double-strand breaks (DSBs), including γH2AX, ATM, the MRN complex, Rad51, BRCA1, and Rad52[202, 207, 208, 212, 213]. Based on our qualitative observations in the previous section, we believed that the number of EGFP-FLAG-TLS foci was increasing following treatment with both γ-irradiation and mitomycin C, which induce DSBs and interstrand cross-links, respectively. Furthermore, in some cases the EGFP-FLAG-TLS foci localized to micronuclei, structures that have a known association with DNA damage[336]. It is important to note that the TLS foci distribution is different from the foci pattern observed for proteins such as Rad51 and the MRN complex[212, 213, 327], indicating that the TLS foci represent sites distinct from those identified previously. To establish whether these foci might represent sites of DNA damage, we quantified the number of cells with large and small numbers of EGFP-FLAG-TLS foci before and after DNA damage.

pEGFP-FLAG-TLS was transiently transfected into MEFs. The following day, the cells were exposed to γ-irradiation (5 Gy) and allowed to recover for 1 h, or were treated with mitomycin C (5 μM) for 3 h. The cells were then fixed in 4% paraformaldehyde, mounted onto slides, and analyzed by fluorescence microscopy. Example images are shown in Figure 4.4. The MEFs contain either a few TLS foci, or dozens of foci. Therefore, we categorized cells as either having four or less foci, or greater than four foci. When quantified however, our results showed that there was no significant difference between treated and untreated cells with respect to foci number following either γ-irradiation or mitomycin C (Table 4.1). Therefore, the number of

EGFP-FLAG-TLS foci does not increase after either DNA double-strand breaks or interstrand cross-links, indicating that the foci probably do not represent sites of DNA damage.

Table 4.1: Analysis of EGFP-TLS foci following DNA damage in MEFs

		Cells with ≤ 4 Foci	Cells with >4 Foci
γ-Irradiation	1 h post mock-irradiation 1 h post γ-irradiation (5 Gy)	11 (20%) 15 (24%)	45 (80%) 47 (76%)
Mitomycin C	Untreated 5 μM mitomycin C (3 h)	39 (55%) 39 (51%)	32 (45%) 37 (49%)

4.4 Investigation into the identity of the TLS perinucleolar foci

The EGFP-FLAG-TLS foci were not found to increase in number following cellular exposure to γ-irradiation and mitomycin C, indicating that they are probably not sites of DNA damage. Another possibility is that these foci represent nuclear suborganelles containing TLS, the identification of which could help elucidate the function of TLS. The perinucleolar location of the majority of the EGFP-FLAG-TLS foci suggested that they may correspond to Cajal bodies[98] or SMN-containing gems[105, 107], both of which are nuclear suborganelles that localize near the nucleoli. TLS has been previously shown to localize to Cajal bodies[108], and also has an association with SMN, because both it and SMN associate with NFAR-2 (nuclear factor associated with dsRNA-)2[103].

To determine whether the TLS perinucleolar foci corresponded to Cajal bodies, an antibody to p80 coilin, the definitive marker protein for Cajal bodies[98], was used. pEGFP-FLAG-TLS was transiently transfected into HeLa cells. The next day, the cells were fixed with paraformaldehyde, processed for immunocytochemistry with the anti-p80

coilin antibody, and analyzed using fluorescence microscopy. Unexpectedly, we found that the EGFP-FLAG-TLS perinucleolar foci did not correspond to Cajal bodies in all cells analyzed (N=13) (Figure 4.5a).

To determine whether the TLS perinucleolar foci corresponded to SMN-containing gems, red fluorescent protein (RFP)-tagged SMN was used. *SMN* was cloned from a mouse fetal cDNA library, and then ligated into the pDsRED-C1. When expressed, the SMN protein is fused C-terminal to the RFP protein. pEGFP-FLAG-TLS and pDsRED-SMN were transiently cotransfected into HeLa cells. The following day, the cells were fixed, and analyzed by fluorescence microscopy. The EGFP-FLAG-TLS perinucleolar foci did not correspond to SMN-containing gems in all cells analyzed (N=5) (Figure 4.5b). As of now, the identity and the significance of the EGFP-FLAG-TLS perinucleolar foci remain to be established.

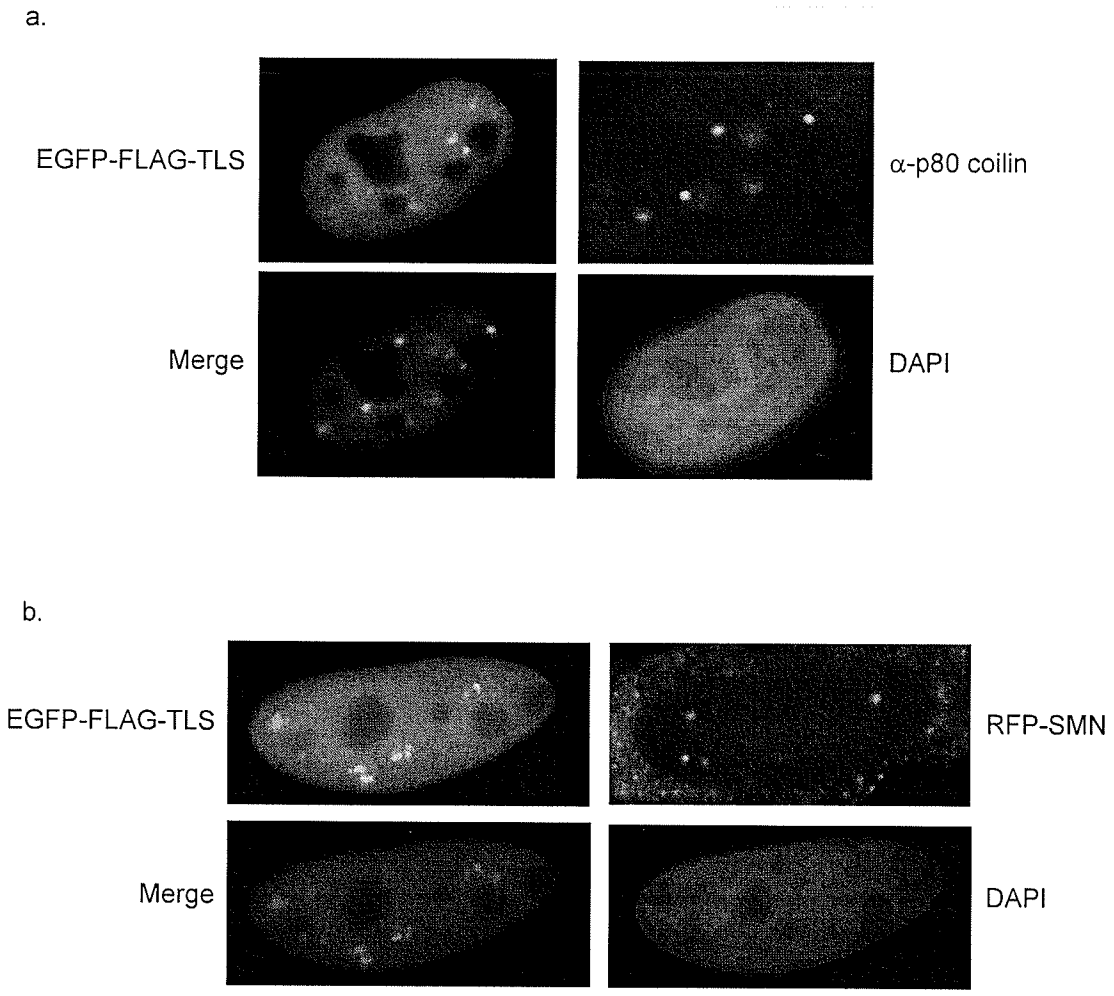

Figure 4.5: EGFP-FLAG-TLS perinucleolar foci do not correspond to either Cajal bodies or SMN-containing bodies. a. pEGFP-FLAG-TLS was transiently transfected into HeLa cells. The cells were fixed with 4% paraformaldehyde and detected with α-p80 coilin. **b.** pEGFP-FLAG-TLS and pDsRED-SMN were transiently cotransfected into MEFs. The cells were fixed as above. All images were captured with a 60x oil immersion objective. A merged image and the corresponding DAPI image for each example cell are also shown.

4.5 Identification of the nucleolar localization domain(s) of TLS

The dynamic relocalization of TLS following transcriptional inhibition provides a functional assay that can be used to identify critical regulatory domains and/or molecular interaction sites within TLS. Identifying these regulatory and interaction sites will help elucidate the role of TLS in not only gene expression, but probably also in the DNA damage response pathways, as TLS may be functioning in the DNA damage response pathways through its ability to regulate gene expression. To identify the critical domain(s) mediating the relocalization to the nucleoli following transcriptional inhibition, we analyzed the localization of deletion constructs of TLS.

4.5.1 The N-terminus of TLS mediates its relocalization to the nucleoli

The N-terminus of TLS has been shown previously to be responsible for its relocalization to the nucleoli following transcriptional inhibition[96]. To confirm this observation in our system, we investigated the relocalization of two N-terminal fragments of TLS (TLS[1-265] and TLS[1-216]), and a C-terminal fragment of TLS [292-526] following actinomycin D treatment (Figure 4.6a). pEGFP vectors of these constructs were transiently transfected into MEF cells. Two days later, the cells were treated with 10 μg/mL of actinomycin D for 1 h. The experiment was then scored using the following criteria: no relocalization, weak relocalization (weak ringing of the nucleolus) or strong relocalization (clear ringing of the nucleolus). The cells were scored using these criteria to control for cell variability, as not all cells exhibited the same extent of TLS relocalization. EGFP-FLAG-TLS strongly relocalized to the nucleoli following transcriptional inhibition in 100% of the cells (Table 4.2). The two N-terminal fragments of TLS (EGFP-TLS[1-216] and EGFP-TLS[1-265]) were present in both the cytoplasm

and the nucleus, and were excluded from the nucleoli in untreated cells. Because these N-terminal constructs localize to both the nucleus and the cytoplasm, this region must be lacking a nuclear restriction domain. Following transcriptional inhibition by actinomycin D, both EGFP-TLS[1-216] (Figure 4.6c) and EGFP-TLS[1-265] (Figure 4.6d) strongly relocalized to the nucleoli in 100% of cells, as expected (Table 4.2).

The C-terminal fragment of TLS (EGFP-TLS[292-526]) was restricted to the nucleus and excluded from the nucleoli in untreated cells, indicating that the domain responsible for the nuclear restriction of TLS is within the C-terminal RNA/DNA binding region of TLS. Following actinomycin D treatment, 49% of the cells did not exhibit any relocalization to the nucleoli. A weak relocalization was observed in 48% of cells, and a strong relocalization, such as that observed for full-length TLS or the N-terminal fragments, was observed in only 4.3% of cells (Figure 4.6e and Table 4.2). Therefore, the C-terminus of TLS cannot mediate a strong association with the nucleolus following transcriptional inhibition.

Our results have shown that the N-terminal 216 amino acids of TLS contain the domain(s) mediating the relocalization of TLS to the nucleoli following actinomycin D treatment. This is the region that is maintained within the fusion oncoproteins, and it contains the SYGQQS repeat region. It has been shown previously that TLS is not maintained in these structures via DNA or RNA[96]. It therefore may not be surprising that a fragment of TLS lacking the RNA- and DNA-binding domains (the RRM motif, the zinc finger, and most of the RGG repeats) can still strongly relocalize to the nucleoli following transcriptional inhibition. These observations suggest that TLS is targeted and maintained at the nucleolar border through protein-protein interactions.

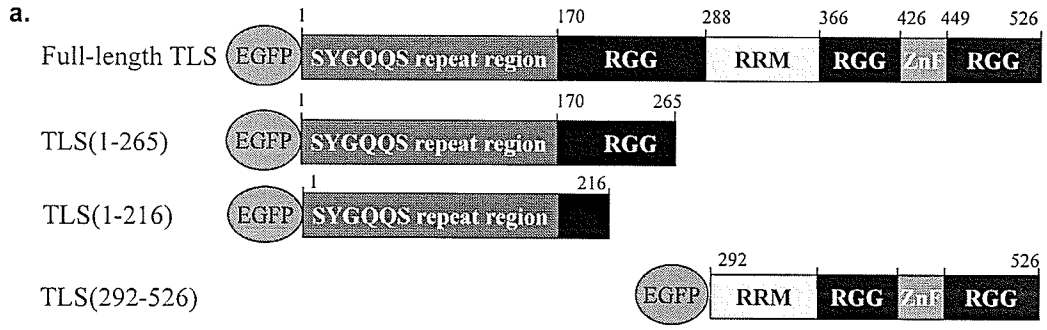
a.
Full-length TLS
EGFP
SYGQQS repeat region
RGG
RRM
RGG
ZnF
RGG
1
170
288
366
426
449
526
TLS(1-265)
265
TLS(1-216)
216
TLS(292-526)
292

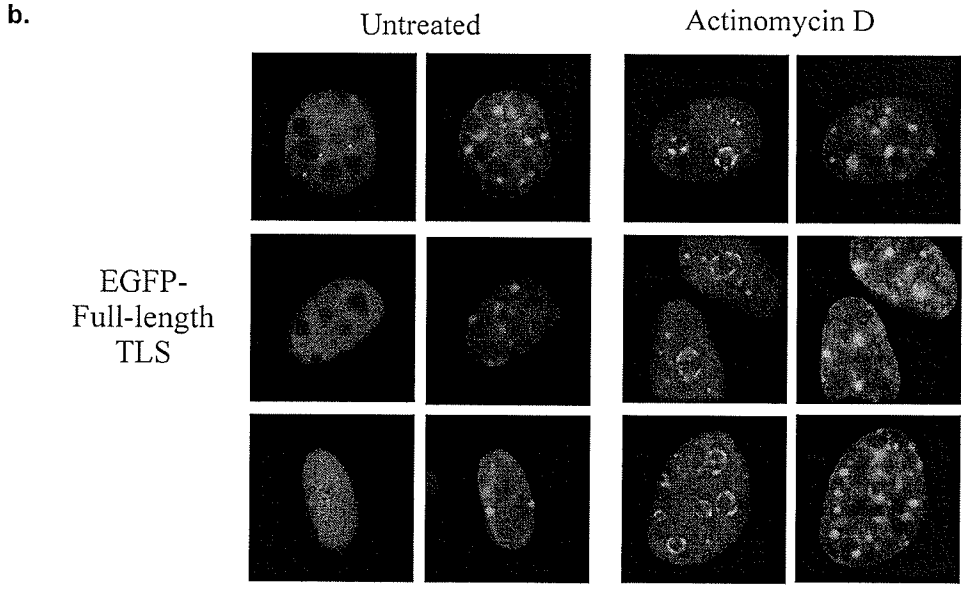
b.
Untreated
Actinomycin D
EGFP-
Full-length
TLS

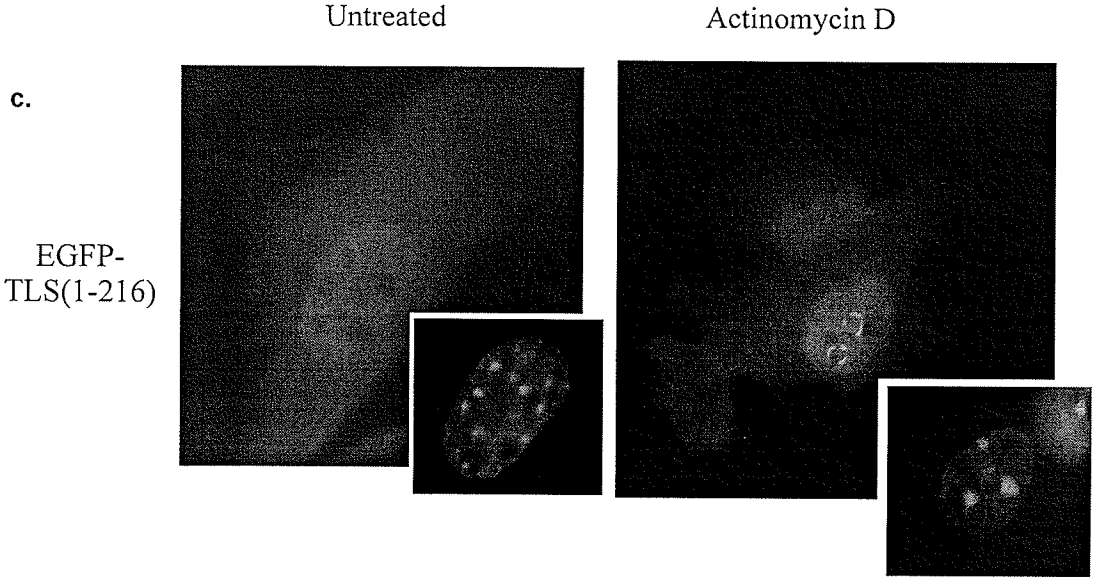
Untreated
Actinomycin D
c.
EGFP-
TLS(1-216)

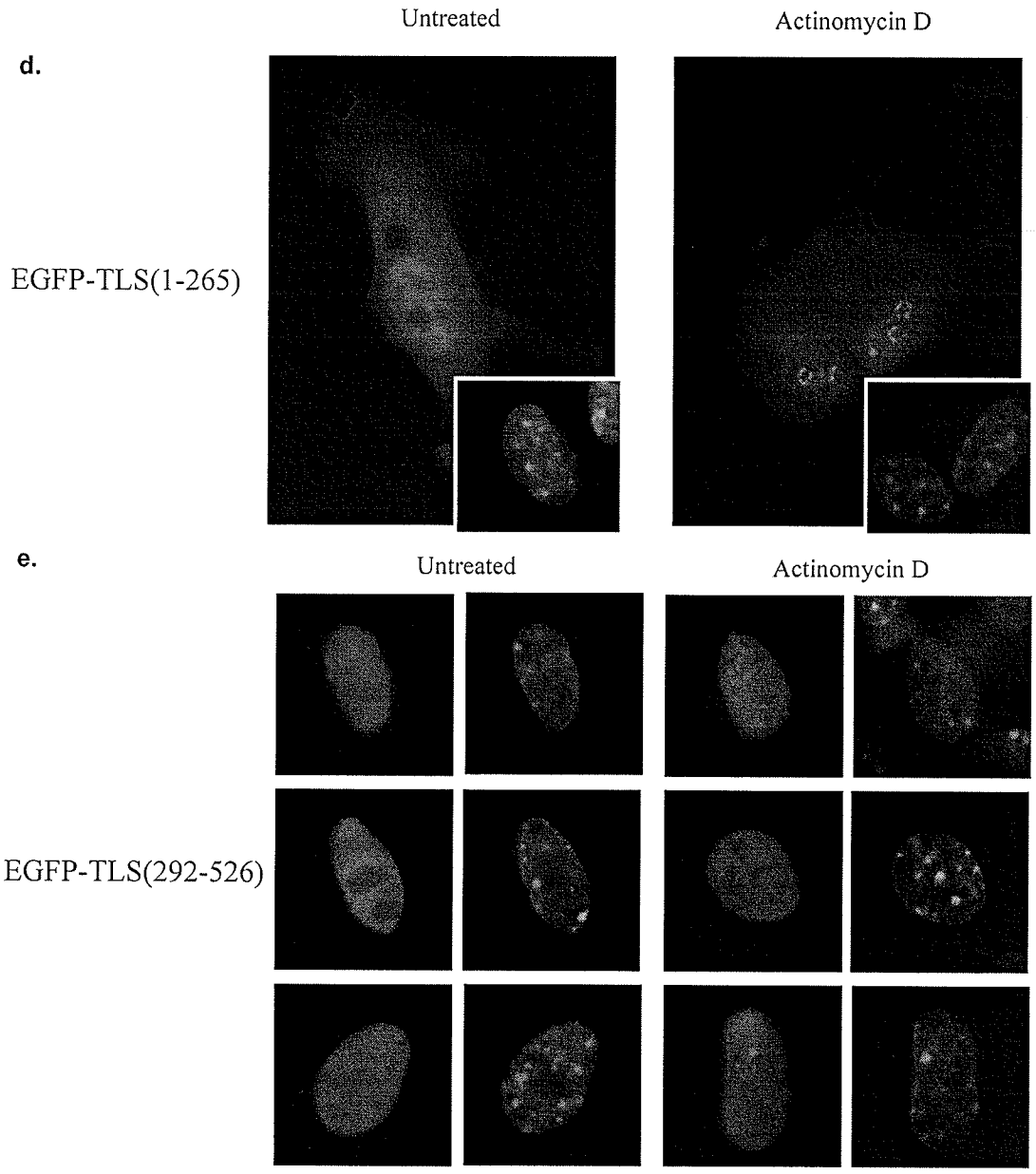

Figure 4.6: The domain regulating the relocalization of TLS to the nucleoli is in the N-terminal region of TLS, specifically amino acids 1-216. **a.** Diagram of the deletion constructs of TLS in reference to full-length TLS. The SYGQQS repeat region, the RGG repeat regions, the RNA recognition motif (RRM) and the zinc finger (ZnF) are indicated. EGFP is represented as a small green circle. pEGFP-TLS (**b**), pEGFP-TLS(1-216) (**c**), pEGFP-TLS(1-265) (**d**), and pEGFP-TLS(292-526) (**e**) expression vectors were transiently transfected into MEFs. The cells were either mock-treated or treated with 10 μg/mLActinomycin D for 1 h. The cells were then fixed in 4% paraformaldehyde. All images were captured using a 100x oil immersion objective.

4.5.2 Identification of a relocalization domain between amino acids 93 and 138 of TLS.

The N-terminus of TLS is unstructured[68] and contains multiple SYGQQS repeats. This region contains many serines, tyrosines and threonines, all of which are amino acids that can be phosphorylated. Analysis of this region with NetPhos 2.0[337] identified specific putative phosphorylation sites (Figure 4.7a). There are also numerous SQ and TQ sites, and both of these motifs are targets for the phosphatidylinositol 3-kinase-like family of serine/threonine protein kinases, including ATR, ATM, and DNA-PK[127] (Figure 4.7a). Therefore, this region is also potentially an important regulatory domain for the function of TLS within the DNA damage response pathways.

To identify the domain within the N-terminus of TLS responsible for its relocalization, sequential deletions of this region were made (TLS[δ1-21], TLS[δ1-34], TLS[δ1-51], TLS[δ1-73], TLS[δ1-92], TLS[δ 1-138], and TLS[δ 1-193]) (Figure 4.7). Each deletion also removes several potential phosphorylation sites (Figure 4.7a). Therefore, if a phosphorylation event is regulating its relocalization, we anticipated that we would be able to identify putative sites using this method.

pEGFP vectors of the deletion constructs (pEGFP-TLS[δ1-21], pEGFP-TLS[δ1-34], pEGFP-TLS[δ1-51], pEGFP-TLS[δ1-73], pEGFP-TLS[δ1-92], pEGFP-TLS[δ1-138], and pEGFP-TLS[δ1-193]) were transiently transfected into MEFs. Two days later the cells were treated with 10 μg/mL of actinomycin D for 1 h. The cells were then fixed in 4% paraformaldehyde, and analyzed using fluorescence microscopy. Our results show that, in untreated cells, all of these constructs were restricted to the nucleus and excluded from the nucleoli (Figure 4.8). Following actinomycin D treatment, constructs with deletions up to amino acid 92 all relocalized strongly to the nucleoli in 100% of cells

(Figure 4.8 and Table 4.2). Therefore, amino acids 1-92 are not required for the relocalization of TLS to the nucleoli.

However, we observed that the removal of the first 138 amino acids of TLS severely reduced its association with the nucleoli following actinomycin D treatment. EGFP-TLS(δ1-138) did not relocalize at all in 31% of cells, showed only weak association with the nucleoli in 52% of cells, and had a strong association with the nucleoli in only 17% of cells. Deleting the first 193 amino acids of TLS reduced its association with the nucleoli following actinomycin D treatment even further. EGFP-TLS(δ1-193) did not relocalize at all in 59% of cells, showed only weak association with the nucleoli in 48% of cells, and never exhibited strong a strong association with the nucleoli. Therefore, we have identified a critical relocalization domain between amino acids 93 and 138, with potentially part of the domain extending into the region between amino acids 138-193. Amino acids 93-193 of TLS contain two potential ATM target sites as well as other putative phosphorylation sites.

a.

```
                                21                  33                          51
  1 masndytqqa tqsygayptq pgqgysqqss qpygqqsysg ysqstdtsgy gqssyssygq
                              ▶ δ1–21             ▶ δ1–34                   ▶ δ1–51
                    73                  92
 61 sqntgygtqs tpqgygstgg ygssqssqss ygqqssypgy gqqpapssts gsygsssqss
                  ▶ δ1–73             ▶ δ1–92
                        138
121 sygqpqsgsy sqqpsyggqq qsygqqqsyn ppqgygqqnq ynsssggggg gggggnygqd
                          ▶ δ1–138
                   193
181 qssmssgggs gggygnqdqs ggggsggygq qdrggrgrgg sggggggggg ...    526
                  ▶ δ1–193
```

b.

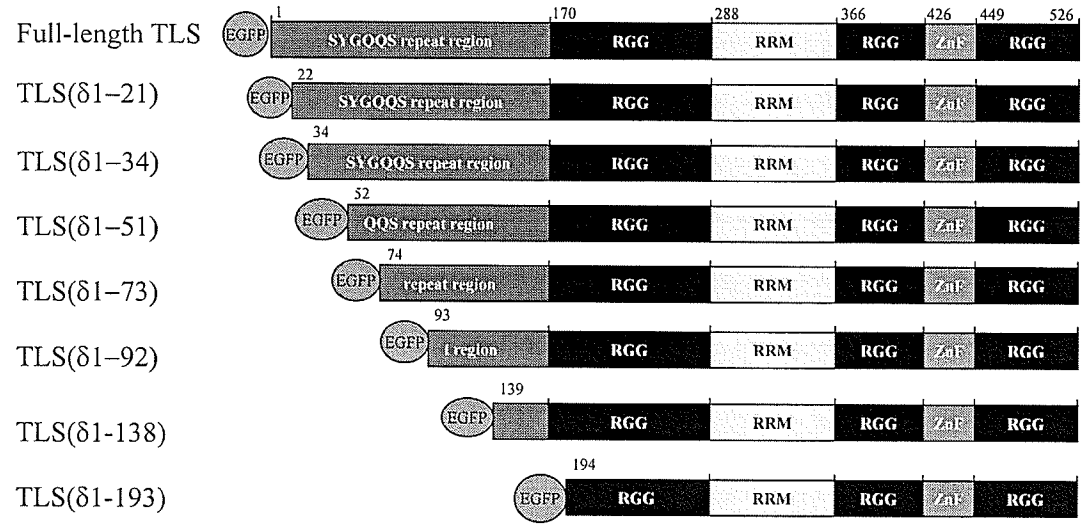

Figure 4.7: Sequential N-terminal deletion of TLS. a. The N-terminus of TLS contains an unstructured SYGQQS-repeat region. Phosphorylation sites predicted by NetPhos 2.0 are shown in red. Potential ATM phosphorylation sites are shown in green. Sites predicted by both methods are shown in purple and underlined. Start sites of the deletions shown in b are indicated. **b.** Sequential deletions of TLS were cloned into the pEGFP-C1 vector. The SYGQQS repeat region, the RGG repeat regions, the RNA recognition motif (RRM), and the zinc finger (ZnF) are indicated. EGFP is represented as a small green circle.

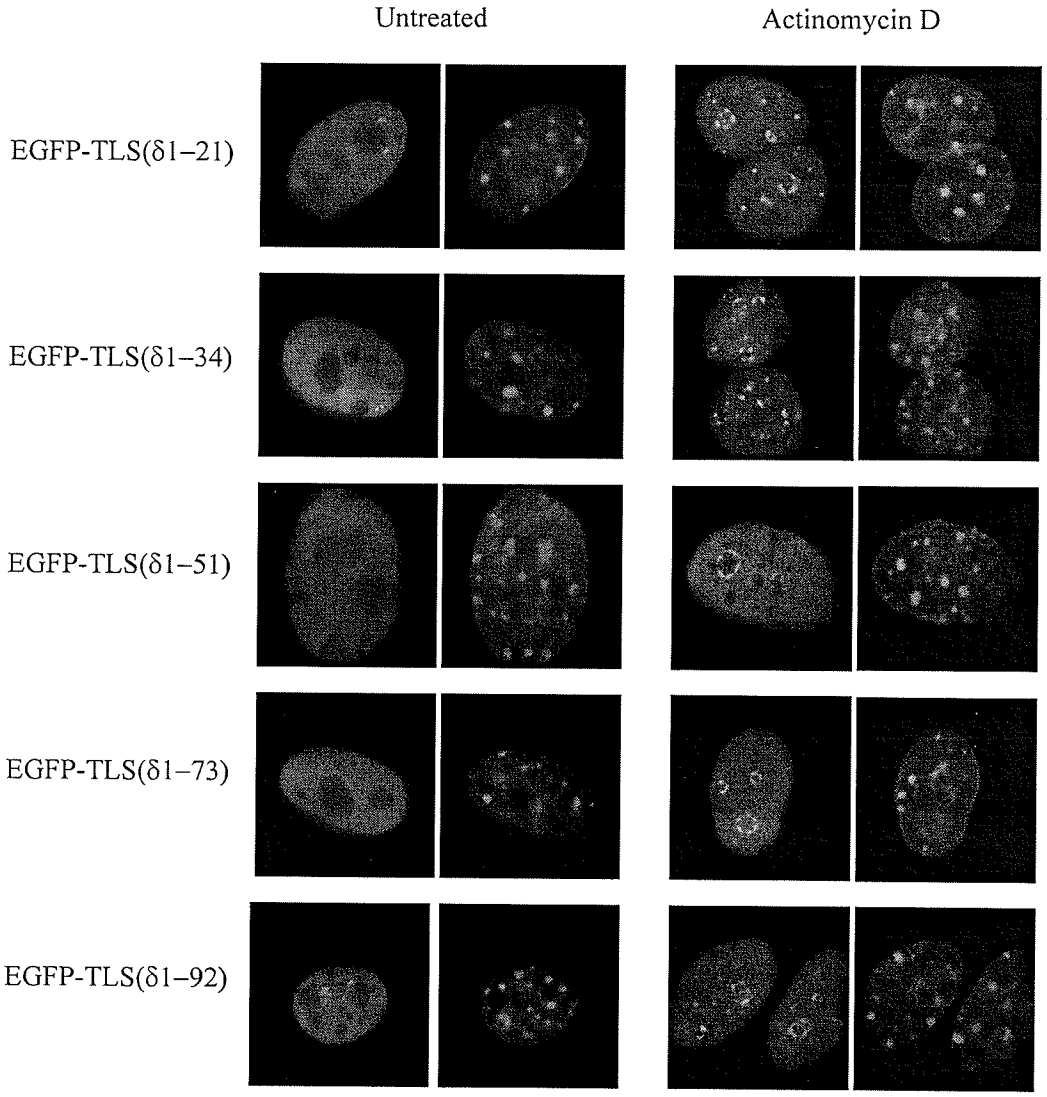

Figure 4.8: Amino acids 1-92 are not required for the relocalization of TLS to the nucleolus in response to transcriptional inhibition. The N-terminal deletion constructs (pEGFP-TLS[δ1-21], pEGFP-TLS[δ1-34], pEGFP-TLS[δ1-51], pEGFP-TLS[δ1-73], and pEGFP-TLS[δ1-92]) were transiently transfected into MEFs. The cells were mock-treated or treated with Actinomycin D (10 μg/mL) for 1 h and then fixed in paraformaldehyde. Images were acquired with a 100x oil immersion objective.

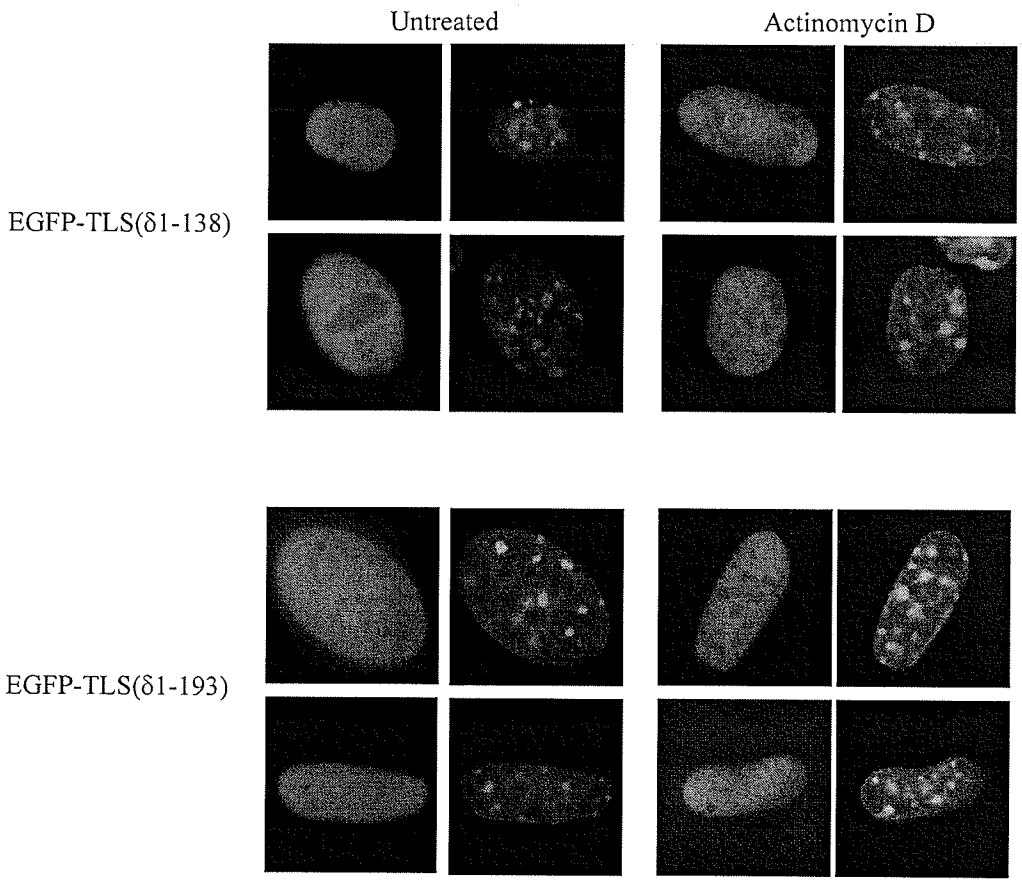

Figure 4.9: EGFP-TLS(δ1-138) has a weak association with the nucleolus following transcriptional inhibition, and the majority of cells transfected with EGFP-TLS(δ1-193) showed no relocalization to the nucleolus following transcriptional inhibition. pEGFP-TLS(δ1-138) and pEGFP-TLS(δ1-193) were transiently transfected into MEFs. The cells were mock-treated or treated with Actinomycin D (10 μg/mL) for 1 h and then fixed in paraformaldehyde. Images were acquired with a 100x oil immersion objective.

4.5.3 Amino acids 1-73 can rescue the actinomycin D-induced nucleolar relocalization of a TLS construct missing amino acids 74 to 193.

We identified a minimum required region between amino acids 93-138 that can mediate a strong relocalization to the nucleolus following transcriptional inhibition. However, the δ(1-138) and δ(1-193) deletions resulted in the removal of the majority of the N-terminus. To establish that the critical region identified in the previous section (amino acids 93-138) is the domain regulating the relocalization, internal deletions of TLS were constructed, specifically a δ(74-93) construct, a δ(74-138) construct, and a δ(74-193) construct (Figure 4.10a) using overlap extension PCR. Our rationale for choosing these deletions is as follows. A TLS construct with an internal deletion of amino acids 74-93 should still relocalize strongly following actinomycin D treatment, as amino acids 1-93 are not required for the relocalization. A construct with an internal deletion of amino acids 74-138 should not relocalize if the only domain capable of mediating a strong relocalization is between amino acids 93-138. However, the deletion of the first 138 amino acids of TLS did not abolish the strong relocalization of TLS to the nucleoli in all cells, whereas a deletion of amino acids 1-193 did. Therefore, the third internal deletion spans this entire region (amino acids 74-193).

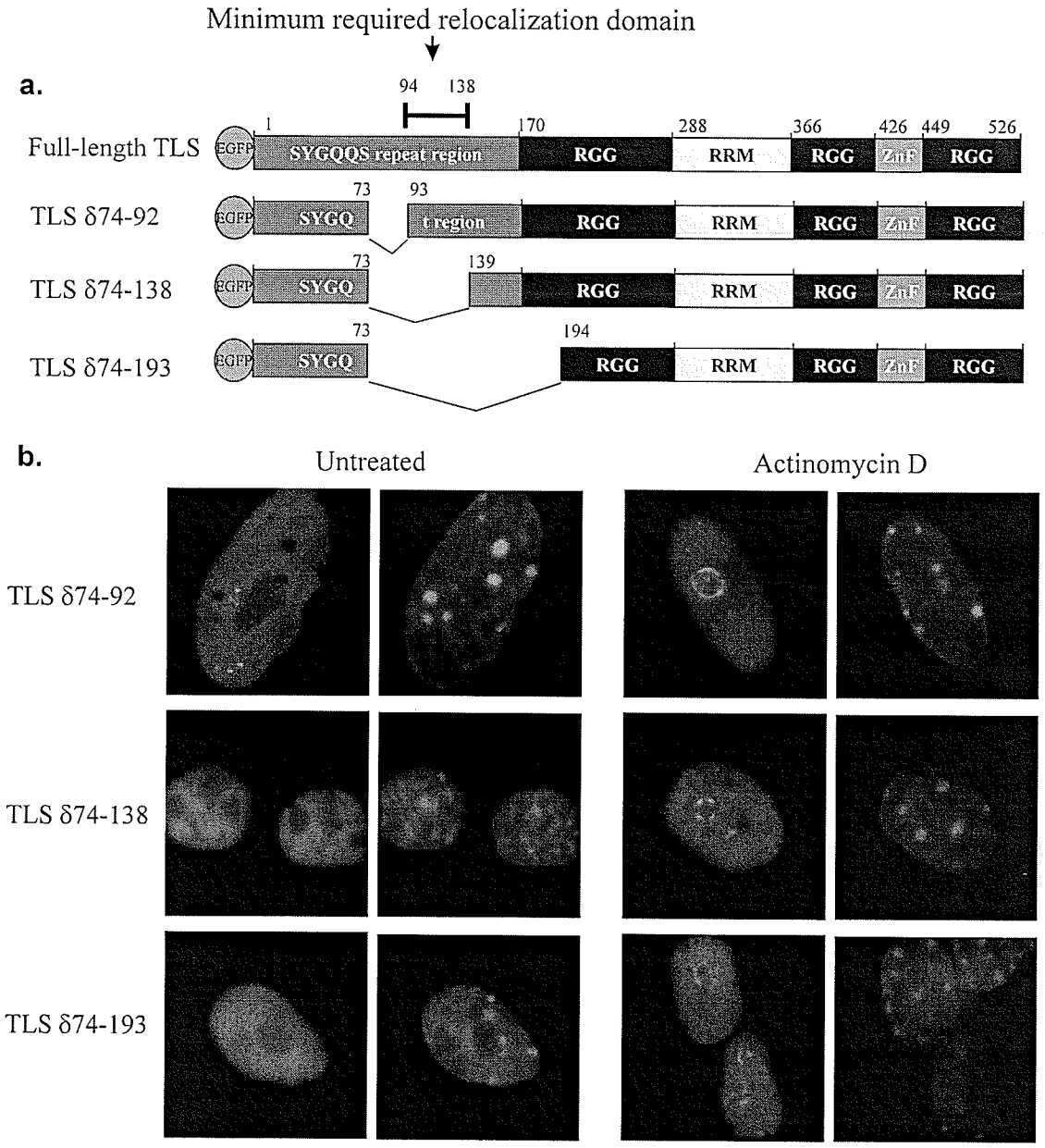

Figure 4.10: Amino acids 1-73 are capable of rescuing the nucleolar association defect observed in the TLS deletions δ1-138 and δ1-193, indicating that there are at least two domains in the N-terminus that are capable of mediating the relocalization of TLS to the nucleolus following transcriptional inhibition. a. A diagram showing the internal deletions of TLS (δ74-92, δ74-138, and δ74-193) that were cloned into the pEGFP vector. The minimum required relocalization domain identified using progressive N-terminal deletions (aa 94-138) is identified. **b.** The internal deletions of TLS were transiently transfected into MEFs. The cells were then treated with Actinomycin D (10 μg/mL) for 1 h and then fixed in paraformaldehyde. Images were acquired with a 100x oil immersion objective.

pEGFP-TLS(δ74-93), pEGFP-TLS(δ74-138), and pEGFP-TLS(δ74-193) were transiently transfected into MEFs. Two days later, the cells were treated with 10 μg/mL of actinomycin D for 1 h. The cells were then fixed in 4% paraformaldehyde, and analyzed using fluorescence microscopy. In untreated cells, all three constructs were restricted to the nucleus, and excluded from the nucleoli. Unexpectedly, all three deletions relocalized strongly to the nucleoli following actinomycin D treatment (EGFP-TLS[δ74-93], EGFP-TLS[δ74-138], and EGFP-TLS[δ74-193] relocalized in 100%, 98.5%, and 100% of cells, respectively) (Figure 4.10b and Table 4.2). Therefore, amino acids 1-73 are able to rescue the nucleolar relocalization defect observed when the minimal required domain (aa 93-138) was removed by sequential N-terminal deletion, indicating that there are at least two relocalization domains in the N-terminus of TLS that can mediate its relocalization to the nucleoli following transcriptional inhibition.

To identify a specific residue sequence that might be mediating the localization of TLS to the nucleoli, I used MultiAlign[338] (default alignment parameters) to align amino acids 1-73 and amino acids 93-193 of TLS (Figure 4.11). A motif of YGQQ (Figure 4.11) is found in both sequences. Amino acids 93-193 contain three of these YGQQ motifs, with two in close proximity starting at amino acid 142, potentially explaining why the deletion of amino acids 1-138 still allowed a strong localization in 17% of cells. Further studies will be required to investigate whether this motif, alone or in conjunction with the other conserved amino acids found N-terminal to this motif, are mediating the localization of TLS to the nucleoli. Of note, this motif does not represent a known kinase site or a known protein-protein interaction motif.

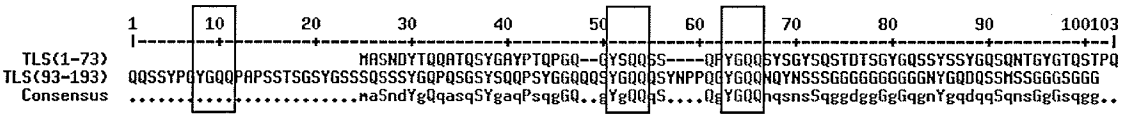

Figure 4.11: Alignment of TLS amino acids 1-73 and TLS amino acids 93-193. Alignment was done using MultiAlign[338] with its default alignment parameters for protein sequences (Blosum62-12-2). Amino acids in red indicate matching residues. YGQQ motifs are boxed.

Table 4.2: Summary of relocalization data of the TLS deletion constructs to the nucleoli following actinomycin D treatment.

EGFP Construct	*Number of cells with no relocalization*	*Number of cells with weak relocalization*	*Number of cells with strong relocalization*	*Percentage of cells with strong relocalization*
Full-length TLS	0	0	214	100%
TLS(1-216)	0	0	43	100%
TLS(1-265)	0	0	117	100%
TLS(292-526)	**23**	**22**	**2**	**4.3%**
TLS(δ1–21)	0	0	51	100%
TLS(δ1–34)	0	0	91	100%
TLS(δ1–51)	0	0	53	100%
TLS(δ1–73)	0	0	38	100%
TLS(δ1–92)	0	0	62	100%
TLS(δ1-138)	**18**	**31**	**10**	**17%**
TLS(δ1-193)	**40**	**28**	**0**	**0%**
TLS δ74-92	0	0	49	100%
TLS δ74-138	1	0	67	98.5%
TLS δ74-193	0	0	49	100%

4.6 TLS-ERG does not relocalize to the nucleoli following transcriptional inhibition, indicating that the ability to relocalize has been lost in the fusion oncoprotein.

The formation of the *TLS-ERG* and *TLS-CHOP* fusion genes are thought to be the primary causes of their associated cancers (myeloid leukemia and myxoid liposarcoma, respectively). However the exact mechanisms of oncogenesis remain ill-defined. In the previous section, we were able to identify regulatory domains within the N-terminus of TLS that can induce its relocalization to the nucleolus following transcriptional inhibition. It is the N-terminus of TLS that is retained in the fusion oncoproteins; therefore, these key regulatory domains are also retained. To explore how these regulatory domains may be functioning in the fusion proteins and oncogenesis, we evaluated the ability of the TLS-ERG fusion to relocalize to the nucleolus following actinomycin D treatment.

pEGFP-TLS-ERG, pEGFP-ERG, and pEGFP-FLAG-TLS were transiently transfected into MEFs. The following day, the cells were treated with 1 μg/mL actinomycin D for 3 h. The cells were then fixed with 4% paraformaldehyde, and analyzed using fluorescence microscopy. Our results show that EGFP-TLS-ERG is restricted to the nucleus, and excluded from the nucleoli in untreated cells. Following actinomycin D treatment, this localization pattern did not change (N=10) (Figure 4.12). Therefore, despite the presence of domains of TLS regulating relocalization, the oncoprotein does not relocalize to the nucleoli following transcriptional inhibition, indicating that the ETS DNA binding domain or the proline-rich activation domain of ERG is able to interfere with or override the domains of TLS responsible for its relocalization to the nucleolus following transcriptional inhibition.

In contrast to our finding for TLS-ERG, TLS-CHOP has been shown to relocalize to the nucleoli following transcriptional inhibition[96], indicating that the amino terminus of TLS can affect the localization of the oncogenic fusion proteins, at least for TLS-CHOP. These data suggest that TLS may be functioning within the two oncoproteins in different capacities, and therefore functioning in the oncogenesis of myeloid leukemia and myxoid liposarcoma in different ways.

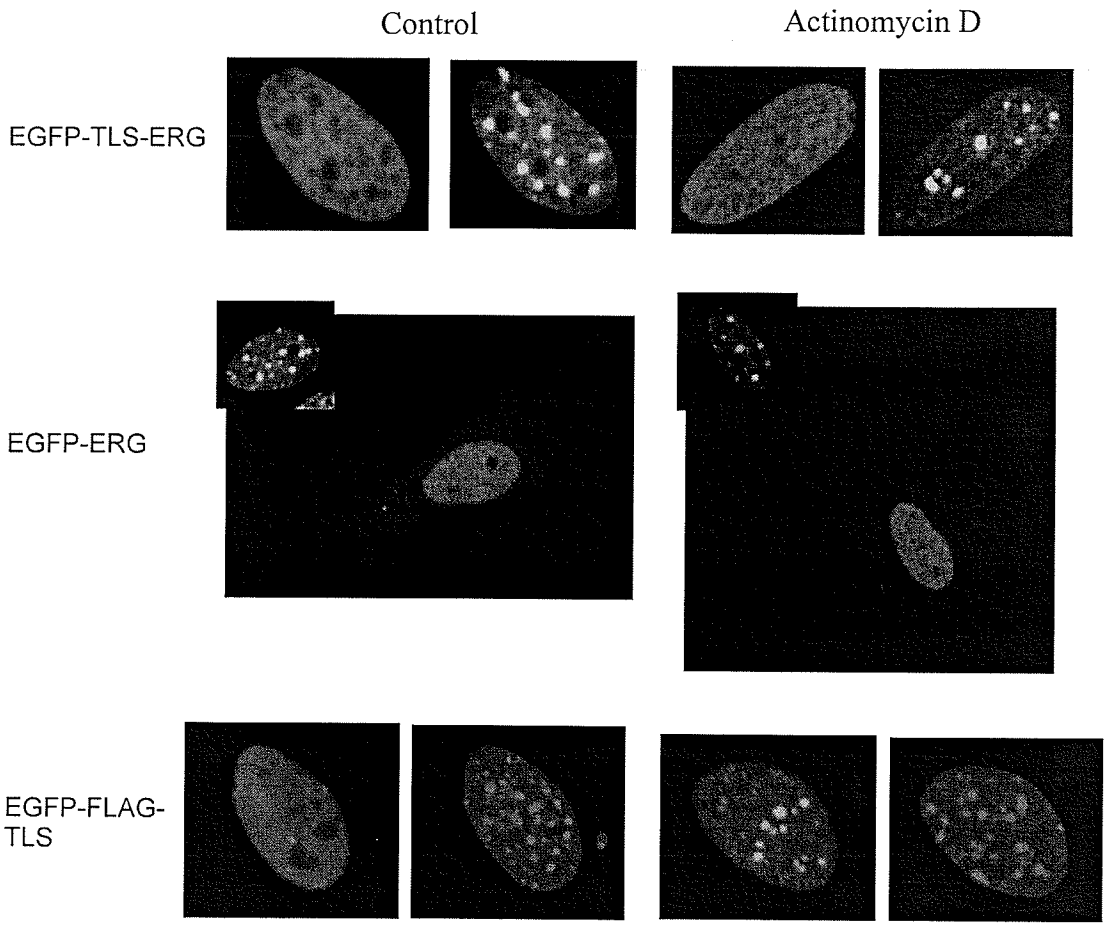

Figure 4.12: The oncoprotein TLS-ERG does not relocalizes to the nucleoli following Actinomycin D treatment. pEGFP-TLS-ERG, pEGFP-ERG, and pEGFP-FLAG-TLS were transiently transfected in MEFs. The cells were treated with 1 μg/mL Actinomycin D for 3 h, after which they were fixed in 4% paraformaldehyde. All images were acquired using a 40x objective.

4.7 Nucleolar localization of TLS occurs in 4% of untreated MEFs.

The relocalization of TLS to nucleoli that occurs following transcriptional inhibition is a dynamic response to a metabolic change within the cell, and is assumed to be representative of a normal function of TLS within the cell. We observed that EGFP-FLAG-TLS localized to the nucleoli in a subpopulation of untreated cells (Figure 4.13), indicating that this association may occur under normal metabolic changes within the cell as well as under induced transcriptional inhibition. To establish what percentage of the population exhibits this phenotype, we quantified the number of cells that had nucleolar localization in two separate experiments.

pEGFP-FLAG-TLS was transiently transfected into MEFs. Two days later, the cells were fixed in 4% paraformaldehyde, mounted onto slides, and analyzed by fluorescence microscopy. In the first experiment, 198 cells were scored, and 8 showed nucleolar TLS localization, or 4.2% of the cells. In the second experiment, 27 cells were scored, and 1 exhibited nucleolar TLS localization, or 3.8% of cells. Therefore, approximately 4% of untreated MEFs exhibit nucleolar localization of TLS.

In a cell population in culture, one of the ways cells can vary with respect to their metabolic status is by what stage of the cell cycle they are currently in, as a cell population will have cells progressing through G1, S phase, G2 and mitosis. The nucleolus itself is cell cycle regulated, as Cdk1-cyclin B represses RNA polymerase I function from the beginning of prophase to the end of anaphase, causing the nucleoli to disintegrate[100]. Therefore, the subpopulation of untreated cells exhibiting nucleolar TLS could potentially represent late-G2 cells just before the chromosomes start condensing and when the nucleoli are being decommissioned for mitosis, or after mitosis when the

nucleoli are being re-established in early G1. Another possibility is that this subpopulation of cells exhibiting nucleolar TLS represents a population of cells that are stressed because of the culture conditions. Whether either of these two hypotheses is correct remains to be investigated.

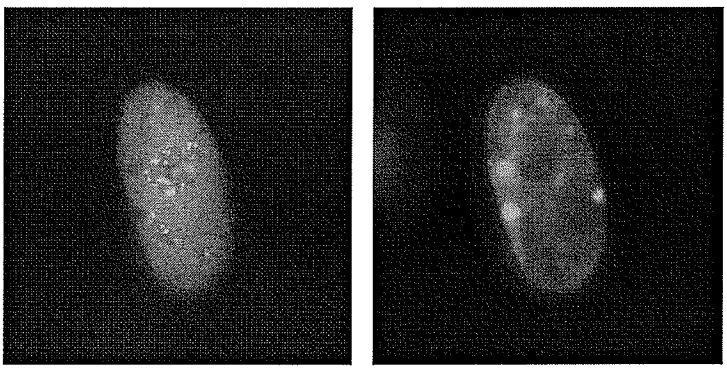

Figure 4.13: An untreated MEF exhibiting nucleolar localization of TLS. EGFP-FLAG-TLS was transiently transfected into MEFs, and fixed in 4% paraformaldehyde. Images were acquired using a 100x objective.

4.8 Chapter Summary: Identification of two regulatory regions within TLS: amino acids 1-73 and amino acids 93-138

- EGFP-FLAG-TLS is restricted to the nucleus, and is generally excluded from the nucleoli, a localization pattern consistent with what has been shown for endogenous TLS, both in our own data and in the literature [91, 95, 96]. Furthermore, EGFP-FLAG-TLS relocalized to the nucleoli within minutes following exposure to actinomycin D, an inhibitor of transcription, consistent with what has been shown previously for TLS[91, 95, 96], validating the use of EGFP-FLAG-TLS in the relocalization experiments.
- EGFP-FLAG-TLS does not form additional foci following γ-irradiation or mitomycin C treatment, indicating that TLS may not be recruited or maintained at sites of DNA damage or repair.
- EGFP-FLAG-TLS does not relocalize to the nucleoli following treatment with either γ-irradiation or mitomycin C treatment. The association of TLS with the nucleolus specifically occurs following exposure to agents known to cause transcriptional inhibition, including the purine analogue DRB, and the DNA damaging agents actinomycin D, camptothecin and UV-irradiation.
- The use of EGFP-FLAG-TLS allowed us to visualize additional TLS-containing structures in the form of perinucleolar foci. These foci do not correspond to the nuclear suborganelles Cajal bodies or SMN-containing gems. As of now, the identity of these foci and their significance remain to be determined.
- Because TLS may be functioning in the DNA repair pathways through its ability to regulate gene expression, identifying the key domain(s) within TLS that mediate its dynamic relocalization to the nucleoli following transcriptional inhibition may help pinpoint the molecular mechanisms of TLS regulation within the DNA damage

response pathways. We have identified two domains within TLS that can mediate its relocalization following actinomycin D treatment: amino acids 1-73 and amino acids 93-193 (with important elements potentially present within a smaller region between amino acids 93 and 138). Alignment of TLS amino acids 1-73 and 93-193 using MultiAlign[338] identified YGQQ motifs in both regions, identifying a target sequence for future experiments.

- Despite the presence of the two key regulatory regions of TLS (amino acids 1-73, and amino acids 93-193), EGFP-TLS-ERG does not relocalize to the nucleolus following actinomycin D treatment. Therefore, within the context of this fusion oncoprotein, these regions no longer mediate an association with the nucleoli following transcriptional inhibition, indicating that the ETS DNA-binding domain or proline-rich activation domain of ERG may be functioning dominantly over TLS to dictate localization. This finding is contrary to what has been shown for TLS-CHOP[96], indicating that TLS may function in the two fusion oncoproteins in distinct ways.
- Approximately 4% of untreated cells exhibit a nucleolar localization of TLS. This subpopulation could represent cells in which transcription has been inhibited and the nucleoli decommissioned for mitosis (either shortly before or after mitosis, as these cells are not mitotic), or this subpopulation could also represent cells that are under stress while in culture.

Conclusion: Because many DNA double-strand break (DSB) response proteins dynamically relocalize following DSBs, we chose to investigate the molecular function of TLS by investigating its localization in response to DSBs, interstrand cross-links (ICLs), and other cellular stresses. Unlike other damage response proteins, TLS does not relocalize to foci following either DSBs or ICLs, indicating it may not be recruited to or maintained at sites of DNA damage or repair. However, TLS does relocalize to the nucleolus following exposure to agents that are known to repress transcription[91, 95, 96], providing an assay that could be used to identify critical regulatory regions within TLS. Because TLS may be functioning in the DNA damage response pathways through its ability to regulate gene expression, identifying these key regulatory elements may lead to a better understanding of the molecular function of TLS within the DNA damage response. We were able to identify two regions (amino acids 1-73 and amino acids 93-193) that can mediate this association with the nucleolus. Alignment of these two sequences identified YGQQ motifs in both regions, providing a target sequence for future experiments.

Chapter 5

Characterization of the ability of *TLS* $^{-/-}$ MEFs to recognize DNA double-strand breaks, and to subsequently activate the cell cycle checkpoints that provide time for DNA repair.

Rationale: *TLS* $^{-/-}$ mice exhibit characteristics consistently found in mouse models of the human genomic instability syndromes AT[112-114] and NBS[115], specifically genomic instability[111], immune system defects[111], and sensitivity to ionizing irradiation[116]. The causative genes of these syndromes are involved in the DNA damage response pathways, suggesting that TLS also functions in these pathways. We have established that TLS is in fact an integral protein in the DSB response, because *TLS* $^{-/-}$ MEFs are sensitive to γ-irradiation. As such, we can hypothesize that TLS functions in the ATM-activated DSB-signalling cascades initiating DNA repair, cell cycle arrest and apoptosis. We have already established that TLS is required for DSB-induced apoptotic induction, because *TLS* $^{-/-}$ pre-B cells are resistant to apoptosis induced by γ-irradiation. Therefore, we next wanted to investigate the ATM-regulated pathways of DNA repair and cell cycle arrest, and the MEFs provide an ideal model cell type for analyzing these pathways. Because *TLS* $^{-/-}$ MEFs are sensitive to γ-irradiation, we can speculate that DNA repair and/or the DNA damage-induced cell cycle checkpoints are defective in these cells. To test these pathways, we chose to evaluate H2AX phosphorylation, one of the earliest responses to DSBs[204], the dephosphorylation kinetics of H2AX, an indicator of DNA repair[215], and the induction of the G1/S and G2/M cell cycle checkpoints following γ-irradiation in the *TLS* $^{-/-}$ MEFs.

5.1 Evaluation of H2AX phosphorylation in *TLS* $^{-/-}$ MEFs following γ-irradiation

5.1.1 H2AX is phosphorylated in a dose-dependent manner in *TLS* $^{-/-}$ MEFs following γ-irradiation.

ATM is the pinnacle kinase of the DSB signalling cascade[122, 124-127, 176], and one of the initial events in this signalling cascade is the phosphorylation of H2AX on serine 139 by ATM[202-204]. Therefore, analyzing H2AX phosphorylation post γ-irradiation would tell us if DSBs are being recognized, and whether ATM is being activated in the *TLS* $^{-/-}$ MEFs. Furthermore, TLS could be functioning either upstream or downstream of ATM in the DSB signalling cascade. If TLS is functioning upstream of ATM and required for proper ATM activation, H2AX should not be phosphorylated in the *TLS* $^{-/-}$ MEFs.

Subconfluent *TLS* $^{-/-}$ and *TLS* $^{+/+}$ MEFs were exposed to 0, 0.5, 1.0, 2.5, or 5 Gy at room temperature and incubated for 1 h at 37°C. The cells were then processed for γH2AX immunocytochemistry (Figure 5.1a) or immunoblotting (Figure 5.1b). In untreated *TLS* $^{+/+}$ MEFs, 15% of cells stained positive for H2AX phosphorylation (N=152). In untreated *TLS* $^{-/-}$ MEFs, 30% of cells stained positive for H2AX phosphorylation (N=82). The higher percentage of *TLS* $^{-/-}$ MEFs that exhibit H2AX phosphorylation suggests that these cells have a higher level of endogenous damage, a finding that is consistent with the genomic instability observed previously in these cells[111]. For example, the chromosomal breaks observed in some of the metaphases from the *TLS* $^{-/-}$ cells[111] would be expected to induce H2AX phosphorylation at those sites.

γH2AX foci were induced in 100% of both *TLS* $^{-/-}$ MEFs and *TLS* $^{+/+}$ MEFs in response to DNA double-strand breaks induced by γ-irradiation. The intensity of staining for H2AX phosphorylation increased with increasing dose of γ-irradiation, and was

visible even at the low dose of 0.5 Gy (Figure 5.1a). Immunoblot analysis of total histone preparations supported the immunocytochemistry data (Figure 5.1b). Induced H2AX phosphorylation was visible in histone preparations from both *TLS*$^{+/+}$ and *TLS*$^{-/-}$ MEFs following 0.5 Gy of γ-irradiation, and the level of H2AX phosphorylation increased with increasing dose. Therefore, ATM activation is intact in the *TLS*$^{-/-}$ MEFs and H2AX phosphorylation following DSBs occurs independently of TLS, placing TLS downstream of ATM in the DSB-signalling cascade.

We did observe a difference in the γH2AX immunoblots from the *TLS*$^{-/-}$ MEFs and *TLS*$^{+/+}$ MEFs. An additional, higher molecular weight protein was observed at a higher intensity in histone preparations from *TLS*$^{-/-}$ MEFs than from preparations from *TLS*$^{+/+}$ MEFs in two separate experiments. Of note, this protein was also phosphorylated in a dose-dependent manner following γ-irradiation. This protein probably corresponds to a monoubiquitinated form of H2AX, as the observed molecular weight is approximately 25 kDa, consistent with monoubiquitinated H2A^{339}. However, the antibodies to phosphorylated H2AX are not suitable for immunoprecipitation experiments, so we were unable to prove conclusively through the use of an anti-ubiquitin antibody that this band corresponded to monoubiquitinated H2AX.

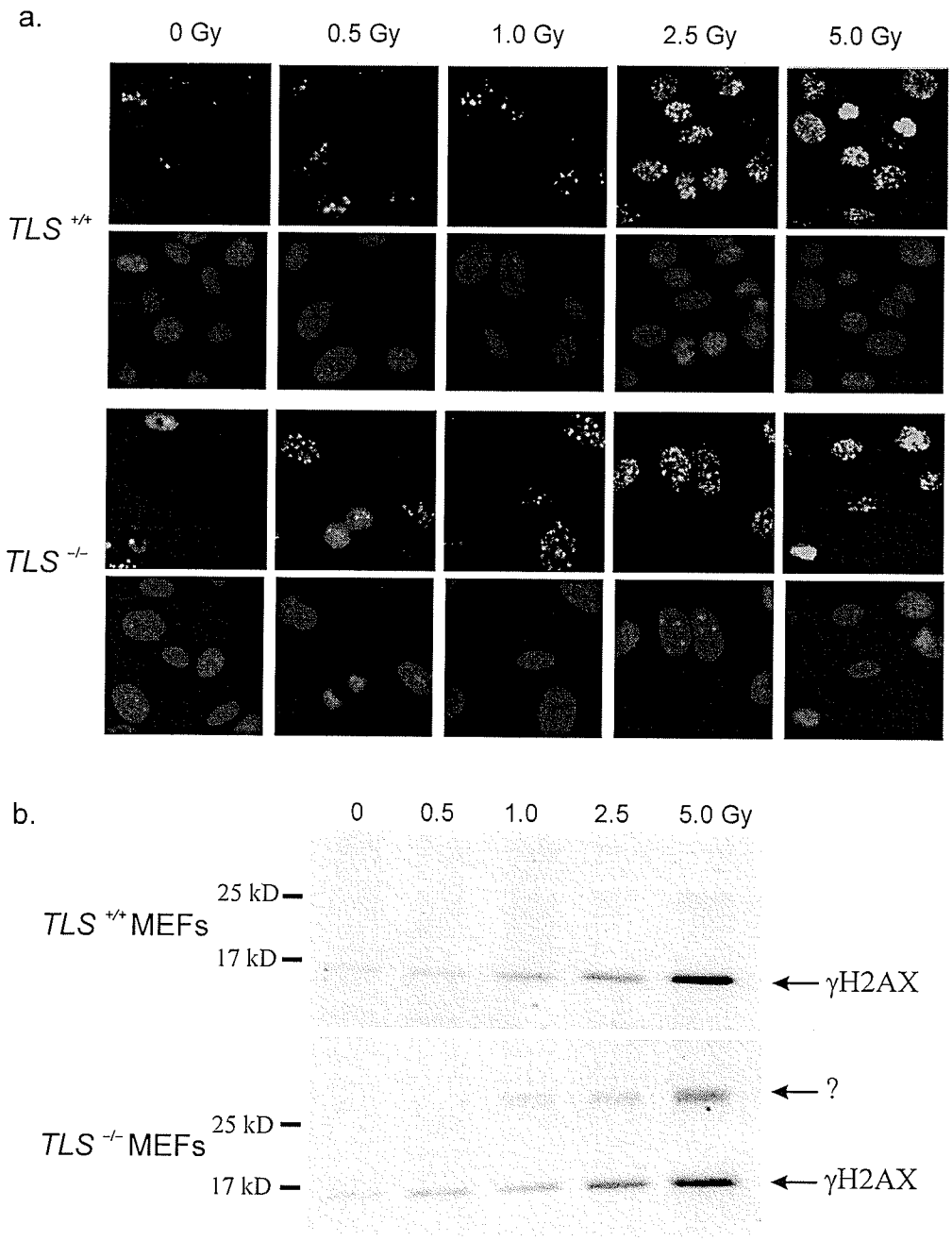

Figure 5.1: H2AX is phosphorylated in *TLS* $^{-/-}$ MEFs at low doses of γ-irradiation. *TLS* $^{+/+}$ and *TLS* $^{-/-}$ MEFs were exposed to increasing doses of γ-irradiation. One hour post-irradiation, the cells were processed for γH2AX immunocytochemistry (***a***) or immunoblot analysis (***b***). Images were acquired using a 40x objective.

5.1.2 γH2AX is dephosphorylated in *TLS*$^{-/-}$ MEFs with qualitatively the same kinetics as in *TLS*$^{+/+}$ MEFs.

H2AX phosphorylation can be used as an indicator of the presence of DSBs, and as these breaks are repaired, H2AX is dephosphorylated by protein phosphatase 2A[215]. Therefore, by evaluating the kinetics of H2AX dephosphorylation, we could qualitatively assess the repair of DSBs in *TLS*$^{-/-}$ MEFs.

TLS$^{-/-}$ and *TLS*$^{+/+}$ MEFs were γ-irradiated with 2.5 Gy and incubated at 37°C for various times post-exposure (1, 6, and 24 h), at which point they were processed for γH2AX immunocytochemistry. As before, high levels of γH2AX were evident in both *TLS*$^{-/-}$ and *TLS*$^{+/+}$ MEFs within 1 h following γ-irradiation. By 6 h following exposure, both *TLS*$^{-/-}$ and *TLS*$^{+/+}$ MEFs exhibited a qualitative reduction in γH2AX levels, and by 24 h both cell types exhibited only small numbers of residual γH2AX foci per cell (Figure 5.2). Therefore, *TLS*$^{-/-}$ MEFs appear to be repairing DSBs with the same qualitative efficiency as wild-type cells. However, this method would not detect small changes in repair efficiency, or whether the DSBs were repaired correctly.

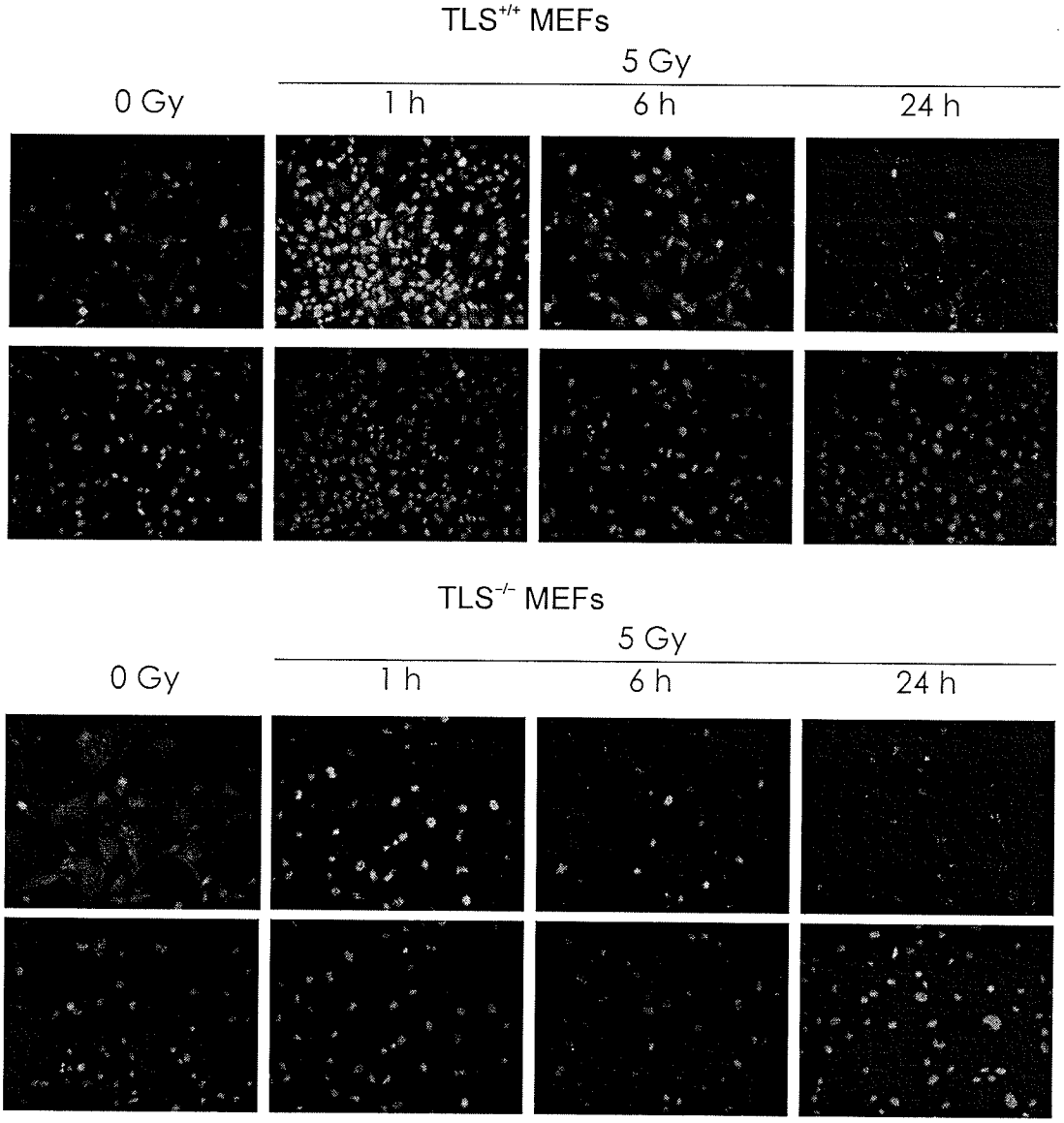

Figure 5.2: H2AX phosphorylation and dephosphorylation occur with qualitatively the same kinetics in *TLS* $^{-/-}$ and TLS $^{+/+}$ MEFs following γ-irradiation. *TLS* $^{+/+}$ and *TLS* $^{-/-}$ MEFs were exposed to a dose of 2.5 Gy γ-irradiation and incubated for various times post-irradiation (1, 6, and 24 h). The cells were then processed for γH2AX immunocytochemistry. Images were acquired using a 20x objective.

5.2 Evaluation of the G2/M checkpoint in *TLS*$^{-/-}$ MEFs following γ-irradiation.

There are three main cell cycle checkpoints following DNA damage: the G1/S, the intra-S-phase, and the G2/M checkpoints. The ionizing irradiation (IR)-induced G2/M checkpoint is initiated by ATM- and p53-dependent pathways (described in detail in section **1.9c**), and manifests as a rapid reduction in the percentage of mitotic cells. Histone H3 phosphorylation can be used as a mitotic marker for flow cytometric analysis, and, using this technique, the G2/M checkpoint can be analyzed within one hour post IR[214]. Histone H3 is phosphorylated on both serine 10 and serine 28 during mitosis[340], and I chose to use an antibody to phosphorylated serine 28 (Sigma, clone HTA28) after having analyzed the mitotic specificity of commercial antibodies to both phosphorylation sites (data not shown). Figure 5.3 shows examples of the staining of the antibody to phosphorylated serine 28 on histone H3 for both immunocytochemistry and flow cytometric analysis.

5.2.1 The G2/M checkpoint is intact in *TLS*$^{-/-}$ MEFs

Subconfluent *TLS*$^{-/-}$ and *TLS*$^{+/+}$ MEFs were exposed to increasing doses (0, 0.5, 1, 2.5, 5, and 10 Gy) of γ-irradiation, and incubated for 1 h at 37°C. The cells were then fixed and processed for flow cytometry with the antibody to phosphorylated serine 28 on H3. The fraction of mitotic cells after each dose was normalized to that of the average mitotic fraction of the mock-irradiated control. Both *TLS*$^{-/-}$ and *TLS*$^{+/+}$ MEFs exhibited a dose-dependent induction of the G2/M checkpoint. However, a smaller normalized fraction of *TLS*$^{-/-}$ MEFs than of wild-type MEFs were undergoing mitosis following 0.5, 1.0, and 2.5 Gy (Figure 5.4a), indicating that more *TLS*$^{-/-}$ MEFs than *TLS*$^{+/+}$ MEFs were being arrested by the G2/M checkpoint. For example, one hour after a dose of 2.5 Gy,

TLS $^{+/+}$ MEFs had a normalized mitotic fraction of 0.23, while *TLS* $^{-/-}$ MEFs had a normalized mitotic fraction of 0.16. While this is not a statistically significant difference based on a required $p<0.05$, it did have a p-value of 0.099 (t-test, df=48). (The data for the 2.5 Gy dose point represent at least six independent experiments carried out in triplicate. Other dose points represent data from one experiment carried out in triplicate.)

5.2.2 *TLS* $^{-/-}$ MEFs do not recover pre-irradiation mitotic levels as effectively as *TLS* $^{+/+}$ MEFs

Once DNA damage is repaired, the cells that were being held in G2 by the G2/M checkpoint are then allowed to progress into mitosis. Therefore, release from the G2/M checkpoint can also potentially be used as a measure of repair[269]. Subconfluent *TLS* $^{-/-}$ and *TLS* $^{+/+}$ MEFs were γ-irradiated with a dose of 2.5 Gy, and incubated for various times (1 h, 6 h, 24 h) at 37°C. The cells were then fixed and processed for flow cytometry with the antibody to phosphorylated serine 28 on H3. The mitotic fraction at each time point was normalized to that of the average mitotic fraction of the mock-irradiated control at 1 h. The data represent at least four independent experiments carried out in triplicate for each genotype. Again, in both *TLS* $^{-/-}$ and *TLS* $^{+/+}$ MEFs, a G2/M checkpoint was observed within 1 h post γ-irradiation (Figure 5.4b). By 6 h, a release of cells into mitosis was evident in both *TLS* $^{-/-}$ and *TLS* $^{+/+}$ MEFs, but the levels of mitotic cells did not recover to those of the mock-irradiated cells. By 24 h, the levels of mitotic cells in both *TLS* $^{-/-}$ and *TLS* $^{+/+}$ MEFs decreased from those of the 6 h time point (Figure 5.4b).

As in the previous section, more *TLS* $^{-/-}$ MEFs than *TLS* $^{+/+}$ MEFs were affected by the G2/M checkpoint following γ-irradiation. Furthermore, the TLS $^{-/-}$ MEFs had a

smaller normalized fraction of mitotic cells at both 6 h and 24 h following γ-irradiation than the wild-type MEFs. This indicates that fewer *TLS*$^{-/-}$ MEFs are able to progress through the cell cycle following γ-irradiation, providing early evidence of their sensitivity to γ-irradiation as measured by the MTT assay four doubling times post-exposure (Figure 3.3). One potential reason for this would be a defect in repairing the DNA damage. We did not observe a defect in γH2AX (an indicator of DSBs) dephosphorylation in the *TLS*$^{-/-}$ MEFs (section **5.1.2**). However, using γH2AX dephosphorylation as an indicator of DSB repair does not allow for any assessment as to whether the repair occurred without any errors (such as mutations, or translocations). Furthermore, small differences in repair efficiency would not necessarily be identified using this technique. Our observation that *TLS*$^{-/-}$ MEFs are more severely affected by the G2/M checkpoint, at 1 h post-γ-irradiation, and at later time points, does suggest that the *TLS*$^{-/-}$ MEFs are being more severely affected by a given dose of γ-irradiation than wild-type MEFs.

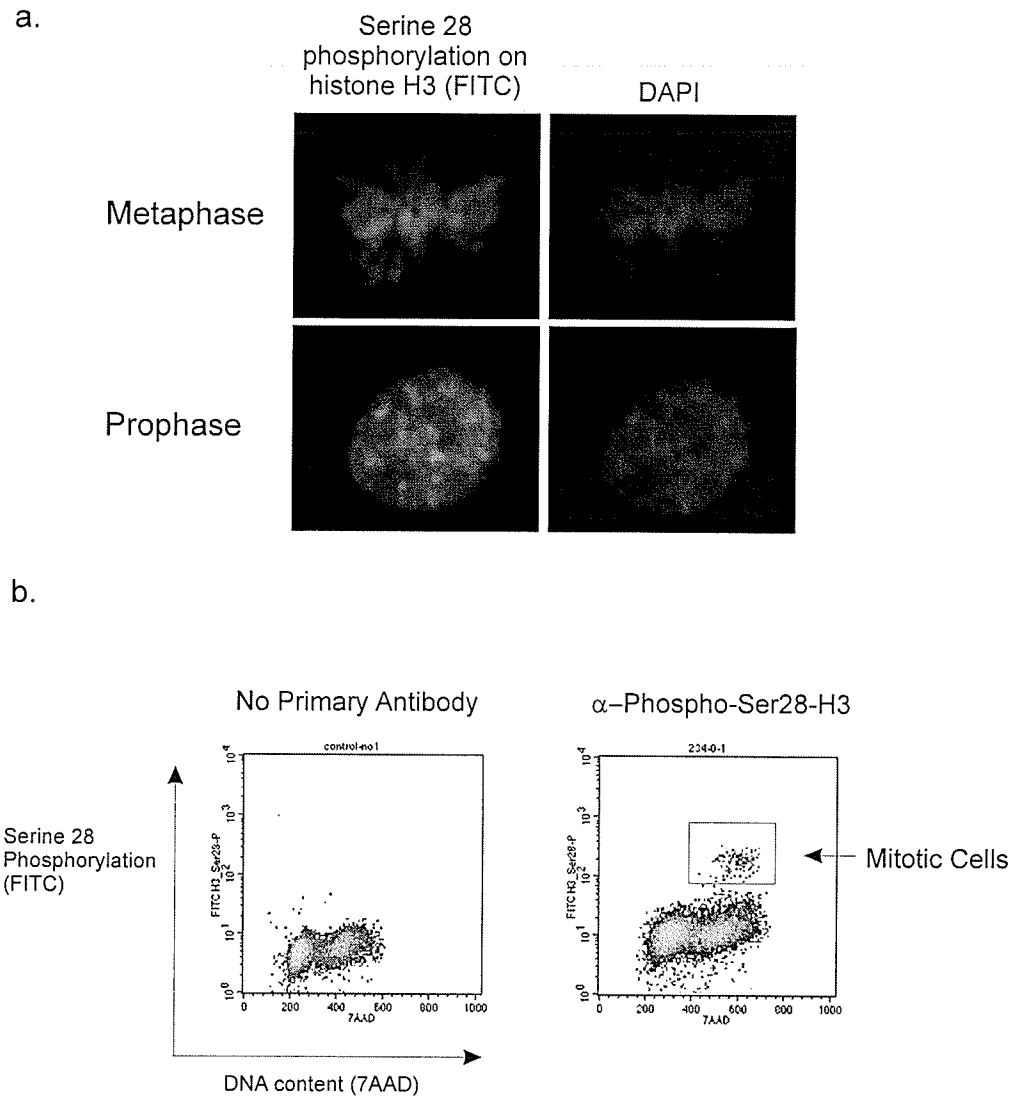

Figure 5.3: Phospho-histone H3 method for analyzing the G2/M checkpoint. Phosphorylation of serine 28 on histone H3 can be used as a mitotic marker allowing rapid determination of the mitotic index of a cell population using flow cytometry. **a.** Examples of metaphase and prophase cells displaying serine 28 phosphorylation. **b.** Flow cytometric data showing the specificity of the antibody for quantifying mitotic cells. A population of mitotic cells with 4 N DNA content becomes visible when an antibody to phosphorylated serine 28 is used.

a.

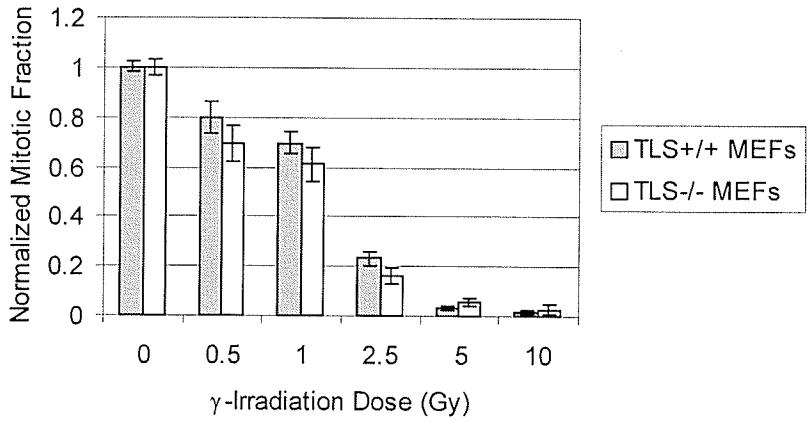

b.

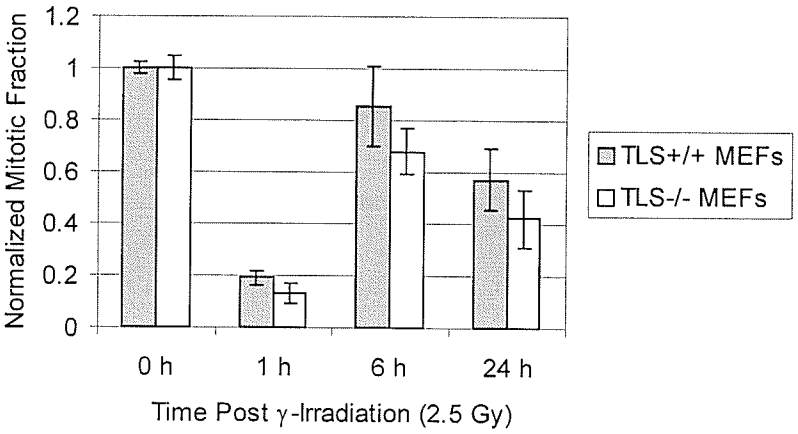

Figure 5.4: The G2/M checkpoint is intact in *TLS* $^{-/-}$ MEFs. a. A greater fraction of G2 *TLS* $^{-/-}$ MEFs are affected by a G2/M checkpoint than *TLS* $^{+/+}$ MEFs at low doses of γ-irradiation. The cells were exposed to increasing doses of γ-irradiation (0, 0.5, 1, 2.5, 5,and 10 Gy) and allowed to recover at 37°C for 1 h. The cells were then processed for flow cytometric analysis using an antibody to phosphorylated serine 28 on histone H3. The 2.5 Gy dose point was repeated at least six times in triplicate. The other dose points represent one experiment carried out in triplicate. **b.** *TLS* $^{-/-}$ MEFs are not released from a G2/M checkpoint as effectively as wild-type cells. The cells were exposed to 2.5 Gy and allowed to recover for various amounts of time (1 h, 6 h, and 24 h), at which time they were processed for flow cytometric analysis. The mitotic recovery experiment was repeated at least four times in triplicate. Mitotic fractions were normalized to the average mitotic fraction of the mock-irradiated control harvested at 1 h post γ-irradiation. The mitotic recovery experiment was repeated at least four times in triplicate for each genotype. All error bars represent standard error of the mean.

5.3 The delayed G1/S checkpoint following γ-irradiation is intact in *TLS*$^{-/-}$ MEFs

The delayed G1/S checkpoint is regulated by an ATM-p53-p21-Cdk2 pathway[237], and manifests itself as an overall decrease in S-phase cells observable 13-24 h post-ionizing-irradiation[245, 246] (described in detail in section **1.9a**). The standard technique for labelling S-phase cells uses 5-bromo-2'-deoxyuridine (BrdU), a thymidine analogue that will be incorporated into DNA being actively synthesized[255] (Figure 5.5).

Subconfluent *TLS*$^{-/-}$ and *TLS*$^{+/+}$ MEFs were γ-irradiated with a dose of 5 Gy, and incubated for various times (1 h, 6 h, and 24 h) at 37°C. The cells were further incubated for 1 h with BrdU in the medium, and then fixed and processed for flow cytometric analysis using a FITC-conjugated antibody to BrdU. S-phase fractions at each time point were normalized to that of the average mock-irradiated S-phase fraction for that time point. This experiment was repeated three times in triplicate, with MEFs of different embryonic origins used in each experiment. Our results show that at 1 h following γ-irradiation, there was no change in the fraction of S-phase cells in either the *TLS*$^{-/-}$ or *TLS*$^{+/+}$ MEFs when compared with mock-irradiated cells (Figure 5.6a). Figure 5.7 shows representative 7AAD versus BrdU-FITC plots and their corresponding DNA histograms.

At 24 h post γ-irradiation, both *TLS*$^{-/-}$ and *TLS*$^{+/+}$ MEFs exhibited a similar delayed G1/S checkpoint, as their normalized S-phase fraction decreased to 0.26 and 0.21, respectively (Figure 5.6a). The difference between the normalized S-phase fractions of the *TLS*$^{-/-}$ and *TLS*$^{+/+}$ MEFs was not statistically significant ($p=0.338$, t-test, $df=16$).

The time point at 6 h proved to be the most informative with respect to the affects on the cell cycle by γ-irradiation. At this time point, both *TLS*$^{-/-}$ and *TLS*$^{+/+}$ MEFs

exhibited a decrease in the total S-phase fraction when compared to the mock-irradiated cells for this time point (Figure 5.6a). However, the *TLS*$^{-/-}$ MEFs exhibited a more pronounced reduction in the fraction of S-phase cells, as they had a normalized S-phase fraction of 0.67, while *TLS*$^{+/+}$ MEFs had a normalized S-phase fraction of 0.83 (t-test, p=0.044, df=16). The more severe reduction in S-phase cells observed in *TLS*$^{-/-}$ MEFs could have been due to either an increased fraction of cells affected by the G1/S checkpoint or a failure to induce an intra-S-phase checkpoint, effects which cannot be directly distinguished using this assay. The *TLS*$^{-/-}$ MEFs had a significantly higher normalized G1 fraction than *TLS*$^{+/+}$ MEFs (t-test, p=0.002, df=16) (Figure 5.6b), indirectly suggesting that the *TLS*$^{-/-}$ MEFs are in fact more sensitive to the G1/S checkpoint. (This issue will be addressed in more depth in the next section). The *TLS*$^{+/+}$ MEFs exhibited a larger normalized G2 fraction than *TLS*$^{-/-}$ MEFs (Figure 5.6c), although this was not a statistically significant difference (p=0.064, Mann-Whitney Rank Sum test). (The data at this time point failed an equal variance test, which is why the Mann-Whitney Rank Sum test was used instead of a t-test.) The difference in the normalized G2 fraction between the two cell-types could have been due to a failure of *TLS*$^{-/-}$ MEFs to arrest in G2 or to a more severe intra-S-phase arrest; however, we have established that the *TLS*$^{-/-}$ MEFs do arrest at the G2/M checkpoint (see section **5.2**). Furthermore, the relative build-up of cells in the G2 fraction seen in the *TLS*$^{+/+}$ MEFs can be explained by the observation that wild-type MEFs generally have a higher mitotic index than *TLS*$^{-/-}$ MEFs. Therefore, even though *TLS*$^{-/-}$ MEFs are more sensitive to the G2/M checkpoint than wild-type cells, the actual percentage of cells within the whole population affected by the G2/M checkpoint would be higher in the *TLS*$^{+/+}$ MEFs

resulting in the observed build-up. Finally, cells of both genotypes exhibit a build-up of S-phase cells with a G2 DNA content, and a depletion of cells with a G1 DNA content (Figure 5.7). This build-up of S-phase cells with G2 content was probably due to the activation of both the delayed G1/S checkpoint, and the intra-S-phase checkpoint. The activation of the delayed G1/S checkpoint prevents cells from entering S phase, causing depletion in S-phase cells with a G1 DNA content, while the activation of the intra-S-phase checkpoint prevents cells from exiting S phase, causing an accumulation of cells with a G2 DNA content.

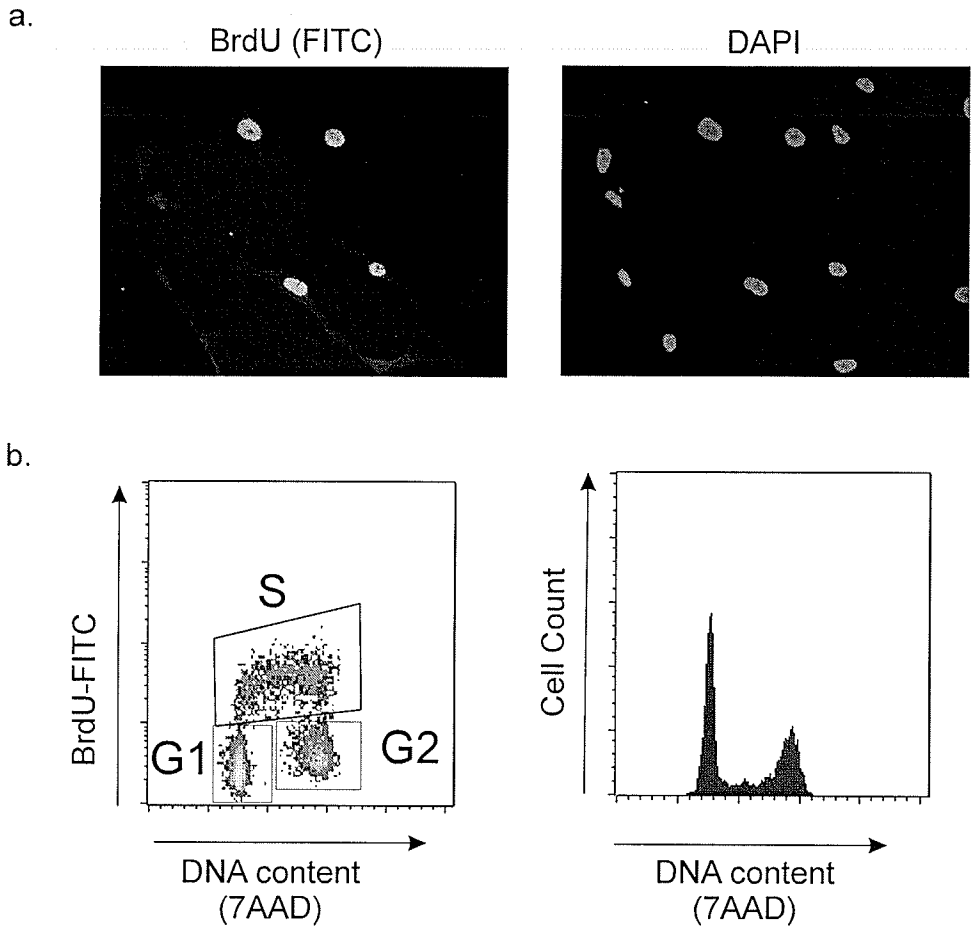

Figure 5.5: BrdU-incorporation method for analyzing S-phase cells. BrdU (5-bromo-2'-deoxyuridine) is incorporated into DNA being actively synthesized, and can be used to identify and quantify S-phase cells. **a.** Examples of cells in S phase as detected by immunocytochemistry. The left-hand panel is the BrdU-FITC image and the right-hand panel is the corresponding DAPI image. **b.** Flow cytometric data showing a cell population labelled with BrdU, stained with anti-BrdU-FITC antibody, and counterstained with 7AAD. A 7AAD versus BrdU-FITC plot is shown on the left. G1, S phase, and G2 cells are indicated. The corresponding DNA histogram is shown on the right.

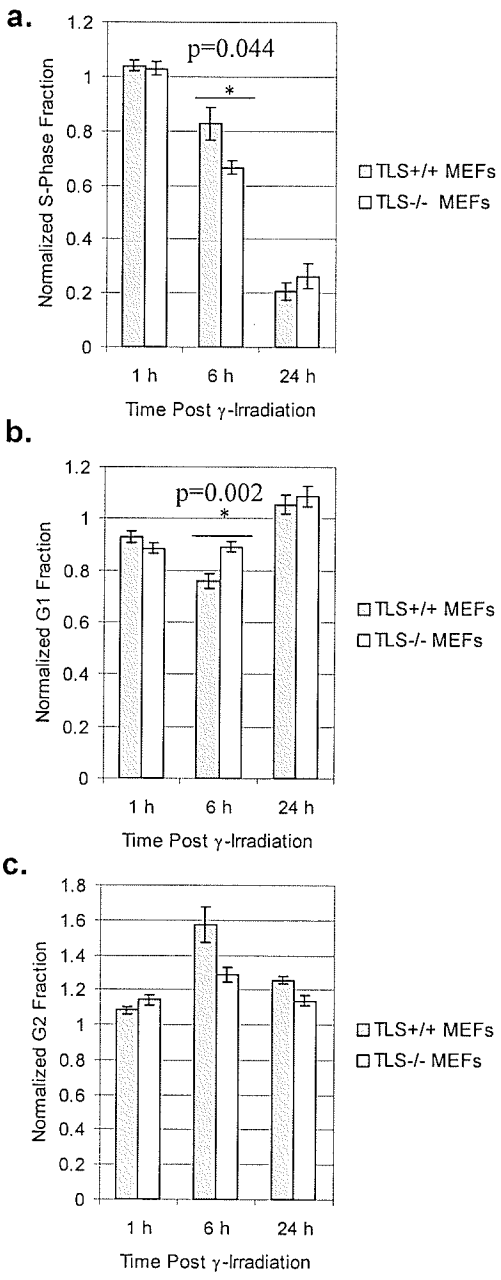

Figure 5.6: The delayed G1/S checkpoint following γ-irradiation is intact in *TLS* $^{-/-}$ MEFs. *TLS* $^{-/-}$ and *TLS* $^{+/+}$ MEFs were exposed to 5 Gy γ-irradiation. At the times indicated (1 h, 6 h, or 24 h), the cells were further incubated for 1 h with BrdU, at which time they were fixed and processed for flow cytometric analysis using a FITC-conjugated anti-BrdU antibody. **a.** Normalized cells in S phase. At 6 h post γ-irradiation, *TLS* $^{-/-}$ MEFs had fewer cells in S phase than wild-type MEFs. **b.** Normalized cells in G1. At 6 h, *TLS* $^{-/-}$ MEFs had more cells in G1 than the wild-type MEFs. **c.** Normalized cells in G2. At 6 h, TLS$^{+/+}$ MEFs had more cells in G2 than *TLS* $^{-/-}$ MEFs. The data represent three experiments done in triplicate. Each independent experiment was done using MEFs of different embryonic origins. Error bars represent standard error of the mean.

a.

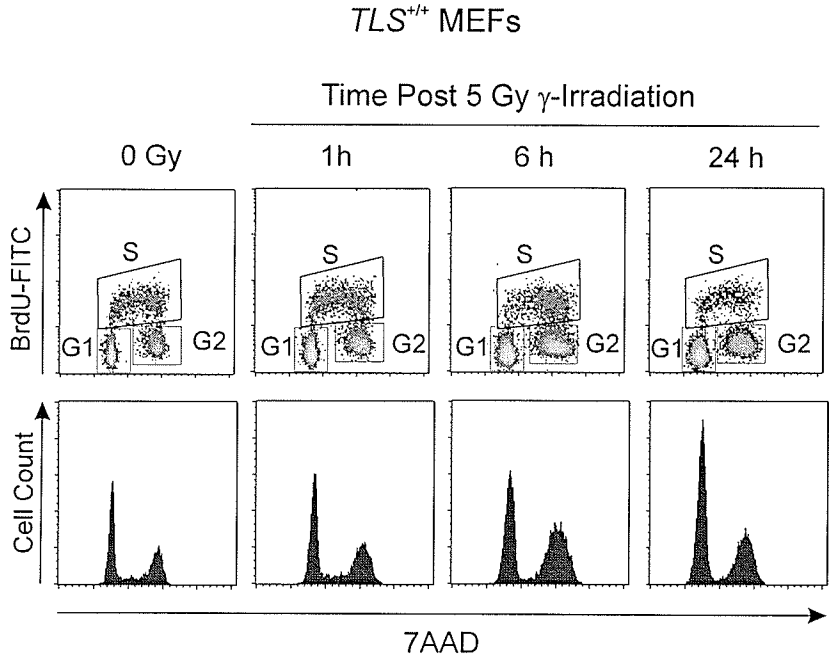

b.

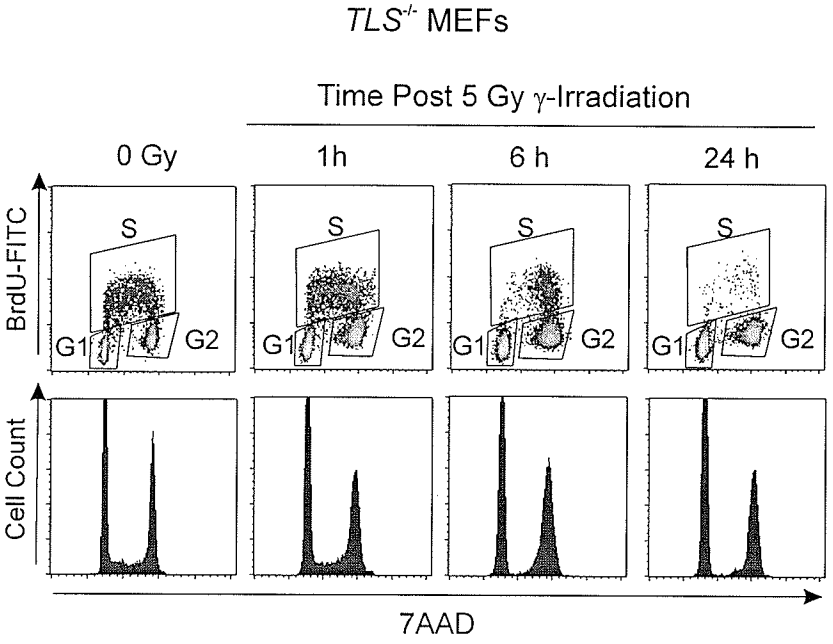

Figure 5.7: Both *TLS* $^{+/+}$ MEFs and *TLS* $^{-/-}$ MEFs exhibit an accumulation of S-phase cells with G2 content of DNA and a depletion of S-phase cells with a G1 content of DNA at 6 h post γ-irradiation. Representative 7AAD versus FITC-BrdU plots, and their corresponding 7AAD DNA histograms are shown for both *TLS* $^{+/+}$ (**a**) and *TLS* $^{-/-}$ (**b**) MEFs. Complete data analysis is shown in Figure 5.6.

5.4 More *TLS*$^{-/-}$ MEFs induce a G1/S checkpoint following γ-irradiation that than *TLS*$^{+/+}$ MEFs.

Labelling cells with 5-bromo-2'-deoxyuridine (BrdU) allows for the total fraction of S-phase cells in a population to be measured at any given time point, and can only infer, but not directly measure, the G1/S checkpoint. To directly analyze the G1/S checkpoint, I developed a novel strategy that quantifies the G1/S and S/G2 transition percentages within a 3 h time period following γ-irradiation using a staggered CldU (5-chloro-2'-deoxyuridine) and IdU (5-iodo-2'-deoxyuridine) labelling protocol. The strategy and the unexpected implications for cell cycle regulation are described in the next chapter and are now published[306].

TLS$^{-/-}$ and *TLS*$^{+/+}$ MEFs were mock-irradiated and γ-irradiated (5 or 10 Gy) at the beginning of a 1-h CldU-labelling period. The CldU was then washed out, and replaced with fresh medium for 1 h. The cells were incubated with IdU for the final hour of the experiment. The cells were then fixed, and processed for immunocytochemistry with antibodies to CldU and IdU. G1/S transition, S/G2 transition, and total S-phase percentages were normalized to that of the mock-irradiated control.

The *TLS*$^{-/-}$ MEFs exhibited a signficantly more severe reduction in the G1/S transition percentage after a dose of 5-Gy γ-irradiation than wild-type MEFs (Figure 5.8a), with the *TLS*$^{-/-}$ and wild-type MEFs having normalized G1/S transition percentages of 50% and 65%, respectively ($p=0.004$, t-test, $df=23$). After a high dose of 10 Gy, the *TLS*$^{-/-}$ MEFs had a normalized G1/S transition percentage of 39%, while wild-type MEFs had a normalized G1/S transition percentage of 46%; however, this was not a statistically significant difference ($p=0.52$, t-test, $df=10$). My CldU/IdU double-labelling strategy has allowed a direct measurement of the regulation of the G1/S

transition following γ-irradiation. In the previous section, BrdU-labelling showed that at 6 h post-γ-irradiation, *TLS*$^{-/-}$ MEFs had a significantly smaller normalized S-phase fraction than *TLS*$^{+/+}$ MEFs and a significantly larger normalized G1 fraction, indirectly suggesting that more *TLS*$^{-/-}$ MEFs than *TLS*$^{+/+}$ MEFs are affected by a G1/S checkpoint. By directly measuring the change in the G1/S transition percentage in these cells following γ-irradiation, we have now been able to unequivocally establish that more *TLS*$^{-/-}$ MEFs than *TLS*$^{+/+}$ MEFs are activating a G1/S checkpoint after a dose of 5 Gy.

Our results also demonstrated that following γ-irradiation, both *TLS*$^{-/-}$ MEFs and *TLS*$^{+/+}$ MEFs exhibited a decrease in the S/G2 transition percentage. The S/G2 transition percentage can be used to assess the intra-S-phase checkpoint, because induction of this checkpoint will slow cellular progression through and out of S phase. Therefore, our data indicates that both cell types are activating the intra-S-phase checkpoint (Figure 5.8b). The reduction in the S/G2 transition percentage was slightly larger in the *TLS*$^{-/-}$ MEFs than in the *TLS*$^{+/+}$ MEFs after both 5 Gy and 10 Gy γ-irradiation; however, the difference between genotypes was not statistically significant for either dose (5 Gy: p=0.484, Mann-Whitney Rank Sum test [data failed normality test]; 10 Gy: p=0.721, t-test, df=9). Therefore, our results show that more *TLS*$^{-/-}$ MEFs than *TLS*$^{+/+}$ MEFs are being affected by the G1/S checkpoint, but almost the same number of *TLS*$^{-/-}$ MEFs as *TLS*$^{+/+}$ MEFs are inducing an intra-S-phase checkpoint following γ-irradiation.

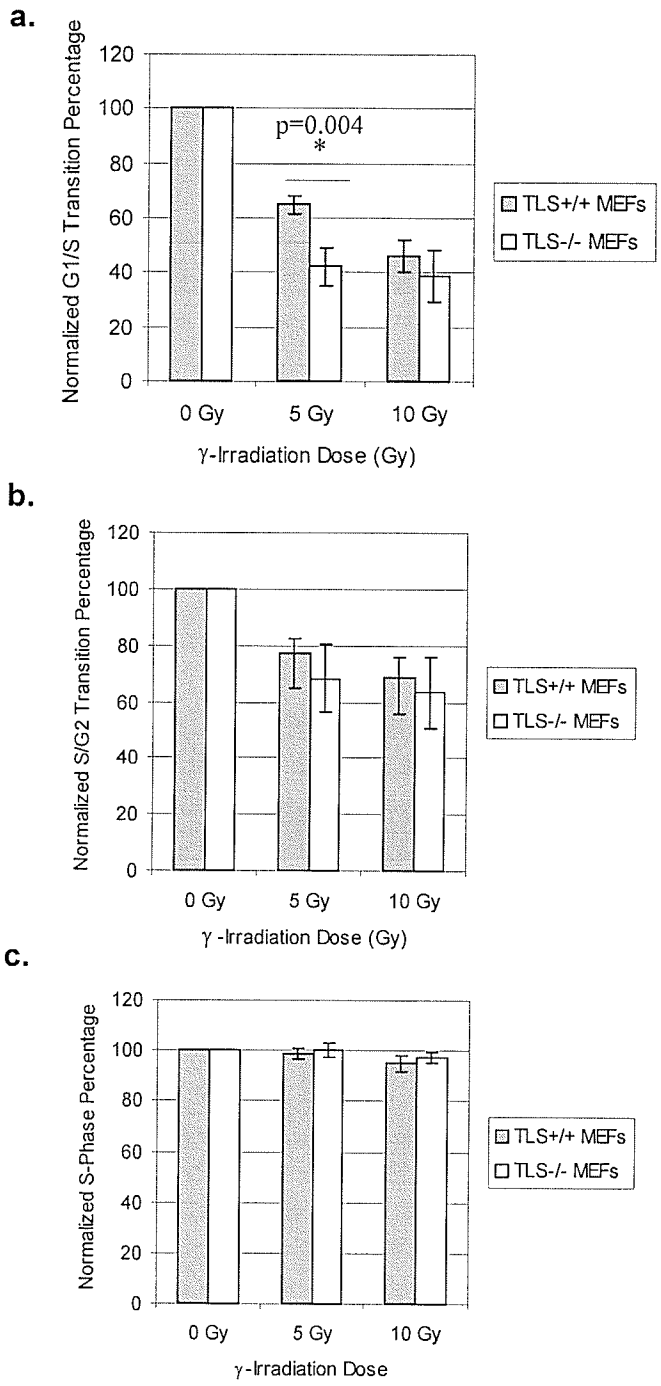

Figure 5.8: More *TLS* $^{-/-}$ than *TLS* $^{+/+}$ MEFs initiate a G1/S checkpoint following γ-irradiation. G1/S (**a**) and S/G2 (**b**) transitions, and total S-phase percentages (**c**) in *TLS* $^{-/-}$ and *TLS* $^{+/+}$ MEFs were compared during a 3-h period following γ-irradiation. The percentages of cells that had transitioned from G1 to S and S to G2, and the total S-phase percentage were normalized to those of the mock-irradiated control for each experiment. * p=0.004. Error bars represent standard error of the mean.

5.5 Chapter Summary: *TLS* $^{-/-}$ MEFs are more sensitive to γ-irradiation-induced cell cycle checkpoints than wild-type MEFs.

- H2AX is phosphorylated in a dose-dependent manner following γ-irradiation in *TLS* $^{-/-}$ MEFs, indicating that TLS is not required for DSB recognition or ATM activation. Furthermore, because ATM is activated in *TLS* $^{-/-}$ MEFs, we can conclude that TLS is not upstream of ATM in the DSB-signalling cascades.
- DSB repair occurs with qualitatively the same kinetics in both *TLS* $^{-/-}$ MEFs and *TLS* $^{+/+}$ MEFs, as determined by the dephosphorylation of H2AX. However, this assay will not necessarily be able to detect small differences in repair efficiency, and will not indicate whether the repair was error-prone.
- TLS is not required for activation of the G2/M checkpoint following γ-irradiation. However, more *TLS* $^{-/-}$ MEFs than wild-type MEFs are affected by the G2/M checkpoint, and the *TLS* $^{-/-}$ MEFs do not recover the pre-irradiation mitotic levels as effectively as wild-type MEFs.
- TLS is not required for the induction of the delayed G1/S checkpoint following γ-irradiation, but *TLS* $^{-/-}$ MEFs do exhibit a more severe depletion of S-phase cells at 6 h post γ-irradiation, suggesting that more *TLS* $^{-/-}$ MEFs than *TLS* $^{+/+}$ MEFs induce a G1/S checkpoint following γ-irradiation.
- Analysis of the change in the G1/S transition percentage following γ-irradiation directly demonstrated that more *TLS* $^{-/-}$ MEFs than *TLS* $^{+/+}$ MEFs induce a G1/S checkpoint following γ-irradiation. Analysis of the S/G2 transition percentage following γ-irradiation demonstrated that the same number of *TLS* $^{-/-}$ MEFs and *TLS* $^{+/+}$ MEFs induce an intra-S-phase checkpoint following γ-irradiation.

Conclusion:

To help identify the function of TLS in the DNA damage response, we assessed the integrity of the downstream pathways initiated by ATM. Our results show that TLS is not required for recognition of DNA DSBs, or the activation of the ATM-dependent G1/S and G2/M checkpoints. However, more $TLS^{-/-}$ MEFs than $TLS^{+/+}$ MEFs activated the G1/S, and the G2/M checkpoints following DSBs, indicating that the $TLS^{-/-}$ MEFs are being more severely affected by the γ-irradiation than $TLS^{+/+}$ MEFs. One potential explanation for this observed checkpoint sensitivity is that the $TLS^{-/-}$ MEFs are not repairing the DSBs as effectively as wild-type MEFs. $TLS^{-/-}$ MEFs did repair DSBs with qualitatively the same kinetics as $TLS^{+/+}$ MEFs, as measured by the phosphorylation status of H2AX, but this analysis does not detect whether repair occurs without error and is not sensitive enough to detect small differences in repair efficiency. These results show that the sensitivity of the $TLS^{-/-}$ MEFs to γ-irradiation is not due to a failure to recognize DSBs, activate ATM, or initiate the cell cycle checkpoints, perhaps indicating that TLS has a role in DNA repair.

Chapter 6

Absence of an immediate G1/S checkpoint in primary MEFs following γ-irradiation identifies a novel checkpoint switch

Rationale: There are three main cell cycle checkpoints responding to DNA double-strand breaks (DSBs): the G1/S, the intra-S-phase, and the G2/M checkpoints[153]. The immediate induction of these checkpoints after DNA damage provides time for repair before the damage is exacerbated through DNA replication or mitosis. The current model of the G1/S checkpoint is that of a two-wave response: p53-independent pathways initiating an immediate G1 block, and a delayed, p53-dependent arrest[237, 248]. The classical p53-dependent G1/S checkpoint manifests itself as an overall decrease in S-phase cells observable 13-24 h post ionizing radiation (IR)[245, 246], and is analyzed by BrdU-labelling. This approach to analyzing the G1/S checkpoint has its advantages. However, it does not distinguish cells that were already replicating DNA at the time of damage from cells that entered S phase following the DNA damage. Therefore, it cannot be used to assess the immediate G1/S checkpoint following DNA damage. To further our understanding of the biology of this checkpoint, I developed a novel strategy for assessing the initiation of the G1/S checkpoint within asynchronous cell cultures using a staggered CldU/IdU double-labelling approach. Unexpectedly, we found that the majority of late-G1, low-passage, primary MEFs do not initiate an immediate G1/S block following γ-irradiation, suggesting that the general model of the G1/S checkpoint needs to be re-evaluated. The results presented in this chapter and the implications to our understanding of cell cycle regulation have recently been published[306].

6.1 Novel strategy for analyzing the immediate G1/S checkpoint following γ-irradiation.

Analysis of the immediate G1/S checkpoint requires the ability to measure the percentage of cells that have progressed from G1 into S phase following DNA damage, or the G1/S transition percentage. To measure this G1/S transition percentage, I have developed a novel strategy using a CldU (5-chloro-2'-deoxyuridine) and IdU (5-iodo-2'-deoxyuridine) staggered double-labelling approach. One major advantage of this assay is that it does not require that cells be synchronized, so the cells should be progressing through G1 with no alteration to normal replication origin licensing. Many studies on cell cycle regulation have used cell synchronization techniques that damage DNA or stress cells prior to the actual experiment[341]. Therefore, my method avoids any artefacts generated through these synchronization techniques.

The labelling strategy is shown in Figure 6.1 and the experimental methods are described in detail in section **2.19**. Briefly, the cells are mock-irradiated or γ-irradiated at the beginning of a one-hour incubation with CldU. Next, the cells are incubated sequentially with no replication label, and then IdU. Following the staggered CldU/IdU-labelling, the cells are fixed, processed for immunocytochemistry, and analyzed using fluorescence microscopy. A method to distinguish CldU and IdU incorporated into cellular DNA has been described previously by Bakker et al[307], and has been mainly used to analyze origin firing[342-344]. My novel strategy for analyzing the G1/S checkpoint identifies cells in four stages of the cell cycle. Cells labelled with both CldU and IdU must have been in S phase during at least part of both labelling periods. Cells labelled with only CldU must have left S phase prior to the second labelling period (or between 0 and 2 h of the experiment). Most importantly, cells labelled with only IdU must have

entered S phase after the first labelling period (or between 1-3 h of the experiment). These cells represent cells that have progressed from G1 into S phase during the experiment, and it is this G1/S transition percentage that can be used to analyze the immediate initiation of the G1/S checkpoint following DNA damage. Finally, cells labelled with neither CldU nor IdU were not in S phase during either labelling period. Examples of images displaying single-labelled CldU cells, single-labelled IdU cells, double-labelled cells, and cells exhibiting no replication label are shown in Figure 6.2 and Figure 6.3. Taken together, our strategy has allowed us to quantify G1/S and S/G2 transitions during a three-hour time period following γ-irradiation.

One important aspect of our labelling strategy is that γ-irradiating cells at the beginning of the CldU-labelling period allows the cells one hour to initiate the checkpoint pathways. Alternatively, the cells could have been γ-irradiated at the end of the CldU-labelling period, providing no time period for checkpoint initiation. However, using this approach, the assay would be less stringent, as some cells that had actually entered S phase prior to γ-irradiation might not have incorporated enough CldU to be detected and identified as such.

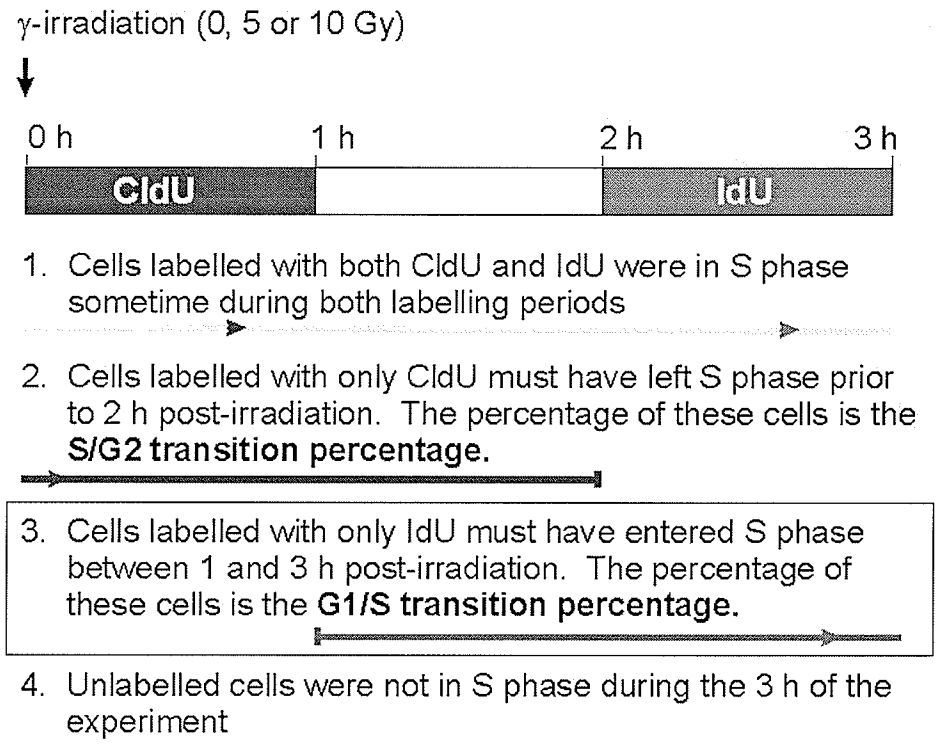

Figure 6.1: Novel CldU/IdU labelling strategy for determining the G1/S transition percentages and S/G2 transition percentages following γ-irradiation. Cells were mock-irradiated or γ-irradiated (5 or 10 Gy) at the beginning of a 1 h CldU labelling period. The CldU was then washed out, and replaced with fresh medium. A 1 h IdU labelling period followed. The cells were then fixed and processed for immunocytochemistry.

6.2 Absence of an immediate G1/S checkpoint in primary MEFs following γ-irradiation.

To analyze the immediate G1/S checkpoint, we chose low-passage, primary MEFs as our model cell type. Because MEFs are easily generated from embryos, they are frequently used to analyze the phenotype of knock-out mice at a cellular level. The MEFs were mock-irradiated or γ-irradiated with a dose of 5 or 10 Gy at the beginning of the staggered CldU/IdU labelling strategy described in the previous section. Contrary to the current model of the G1/S checkpoint, we found that 65% of late-G1 primary MEFs

continued to progress into S phase after a γ-irradiation dose of 5 Gy (Figure 6.4). This experiment was carried out 18 times (N=18), and MEFs of 10 different embryonic origins are represented. At least 1000 cells were analyzed for each dose in every experiment. MEFs treated with a high dose of 10 Gy also failed to arrest in G1, as 46% of late-G1 primary MEFs still progressed into S phase (N=6 with four different embryonic origins represented). Examples of image fields used for analysis are shown for primary MEFs both mock-irradiated (Figure 6.2a) and γ-irradiated with 5 Gy (Figure 6.2b). Higher magnification images are also shown for MEFs mock-irradiated (Figure 6.3a) and γ-irradiated with 5 Gy (Figure 6.3b). Therefore, the majority of late-G1 primary MEFs do not initiate an immediate G1/S checkpoint following γ-irradiation.

Using this assay, an S/G2 transition percentage can also be measured. A cell γ-irradiated while in S phase does not permanently halt progression through S phase, but instead, down-regulates unfired origins until the DNA damage has been repaired[256] (described in detail in section **1.9b**). The change in the S/G2 transition percentage following γ-irradiation can assess the integrity of this intra-S-phase checkpoint, as it reflects progression through and out of S phase. In primary MEFs, the S/G2 transition percentage decreased by 23% following 5 Gy, and by 31% following 10 Gy (Figure 6.4), indicating that replication has been slowed due to the intra-S-phase checkpoint.

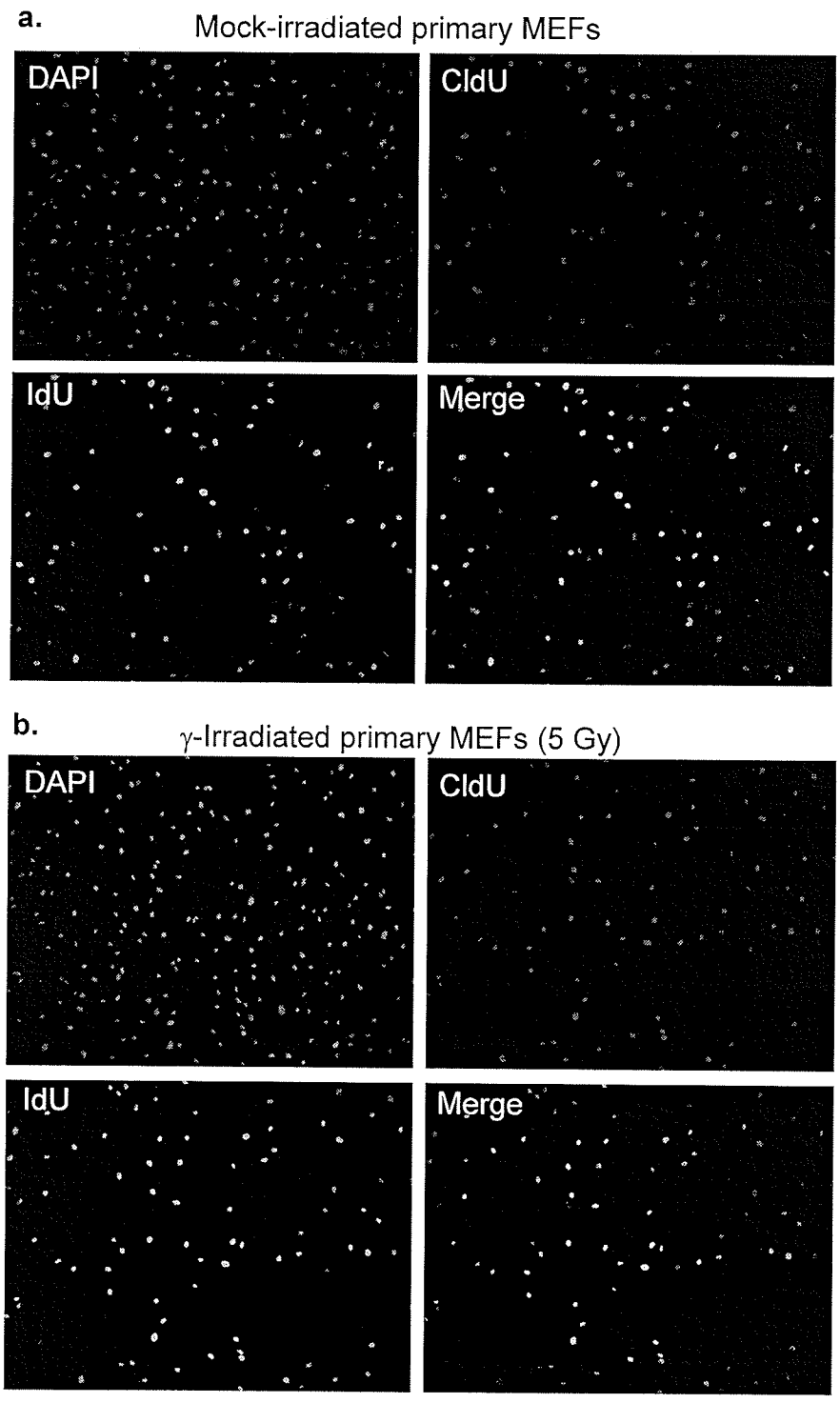

Figure 6.2: Primary Mouse Embryonic Fibroblasts (MEFs) do not initiate an immediate G1/S checkpoint following γ-irradiation. Example images of MEFs that were mock-irradiated (**a**) or γ-irradiated (5 Gy) (**b**) at the beginning of the staggered labelling protocol (Figure 6.1). DAPI, IdU, CldU, and the merged CldU/IdU images are shown. The images were acquired using a 10x objective, and are respresentative of those used for quantitative analysis.

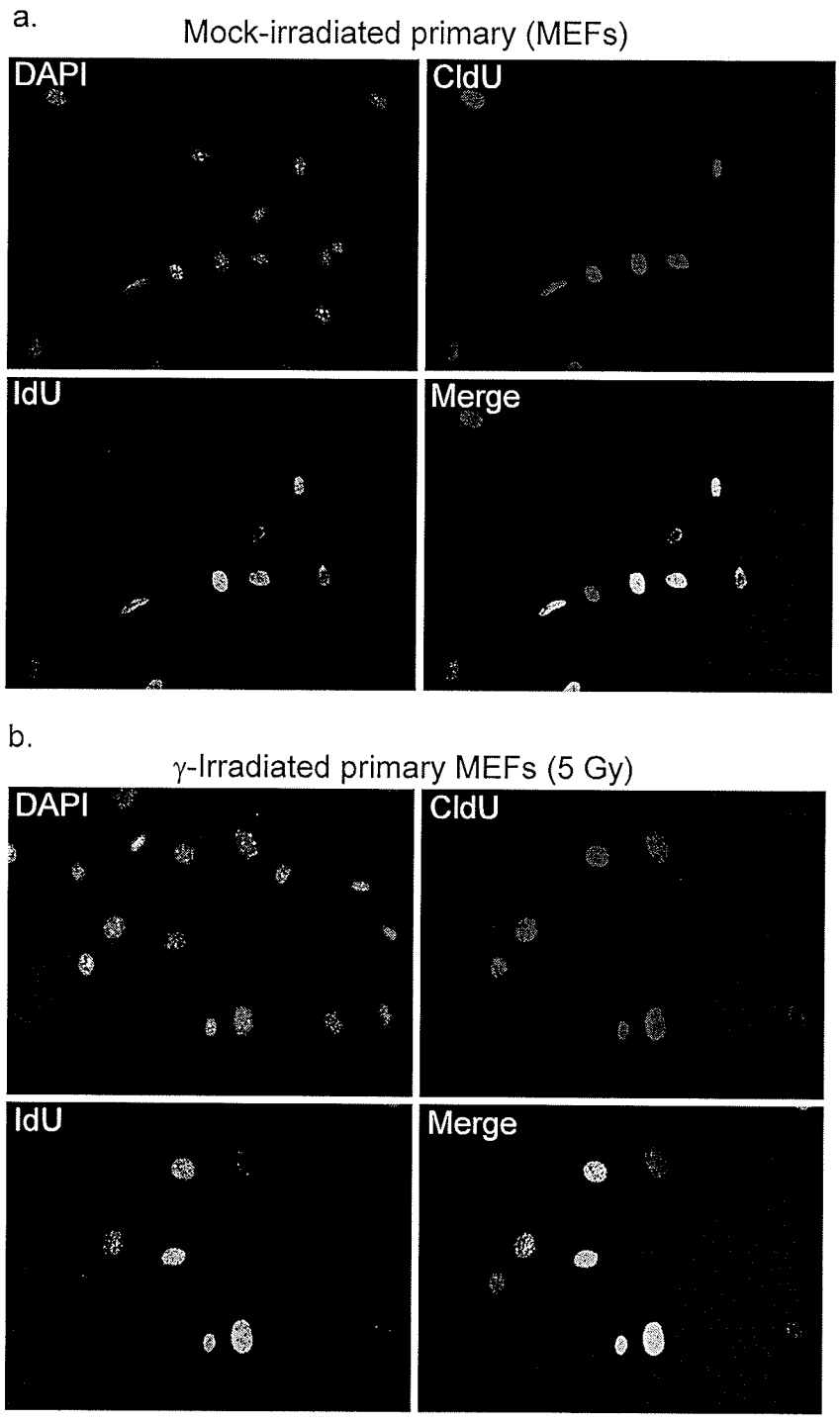

Figure 6.3: Higher magnification images showing MEFs with only IdU-labelling, only CldU-labelling, both replication labels, or neither replication label. Example images of MEFs that were mock-irradiated (**a**) or γ-irradiated (5 Gy) (**b**) at the beginning of the staggered labelling protocol (Figure 6.1). DAPI, CldU, IdU, and CldU/IdU merged images are shown. The images were acquired using a 40x objective.

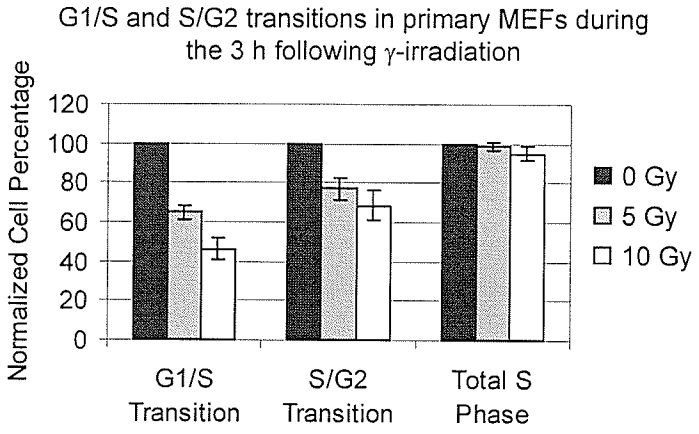

Figure 6.4: The majority of late-G1 low passage, primary MEFs fail to induce an immediate G1/S checkpoint following γ-irradiation. Analysis of the G1/S and the S/G2 transitions in primary MEFs during a period of 3 h following γ-irradiation. The percentage of cells that had transitioned from G1 to S, or S to G2 was normalized to that of the mock-irradiated control for each experiment. Error bars represent standard error of the mean.

6.3 The delayed G1/S checkpoint following γ-irradiation is intact in primary MEFs.

Because the majority of late-G1 primary MEFs did not induce an immediate G1/S checkpoint after γ-irradiation, we wanted to determine whether the delayed, p53-dependent G1/S checkpoint was intact in these cells. MEFs were mock-irradiated or γ-irradiated with 5 Gy. At 1, 6, and 24 h post-γ-irradiation, the cells were labelled for 1 h with BrdU, and then fixed and processed for flow cytometry. The experiment was repeated three times in triplicate. The percentages of S-phase, G1, and G2 cells were all normalized to the average corresponding percentage of the mock-irradiated control for each time point. At 24 h post-5 Gy, the number of primary MEFs in S phase was 20.6% of that observed in mock-irradiated MEFs (Figure 6.5a), indicating that the delayed G1/S checkpoint is intact, as expected.

At 6 h post-5 Gy, the BrdU-labelling pattern observed by flow cytometry exhibited a depletion of BrdU-positive cells with G1 DNA content and a build-up of BrdU-positive cells with G2 DNA content (Figure 6.5b). This lopsided distribution of BrdU-positive cells likely reflects both the induction of the delayed G1/S checkpoint and the intra-S-phase checkpoint. Measurement of the S/G2 transition percentage following γ-irradiation showed that the primary MEFs slowed exit from S phase (Figure 6.4 and section **6.2**), indicating that an intra-S-phase checkpoint was induced. At 6 h post-5 Gy, the γ-irradiated MEFs also exhibited a G1 percentage that was 76% of the mock-irradiated control (Figure 6.5c), indicating that more cells had left than entered G1 during this time period, and supporting our initial direct observation that primary MEFs do not induce an immediate G1/S checkpoint.

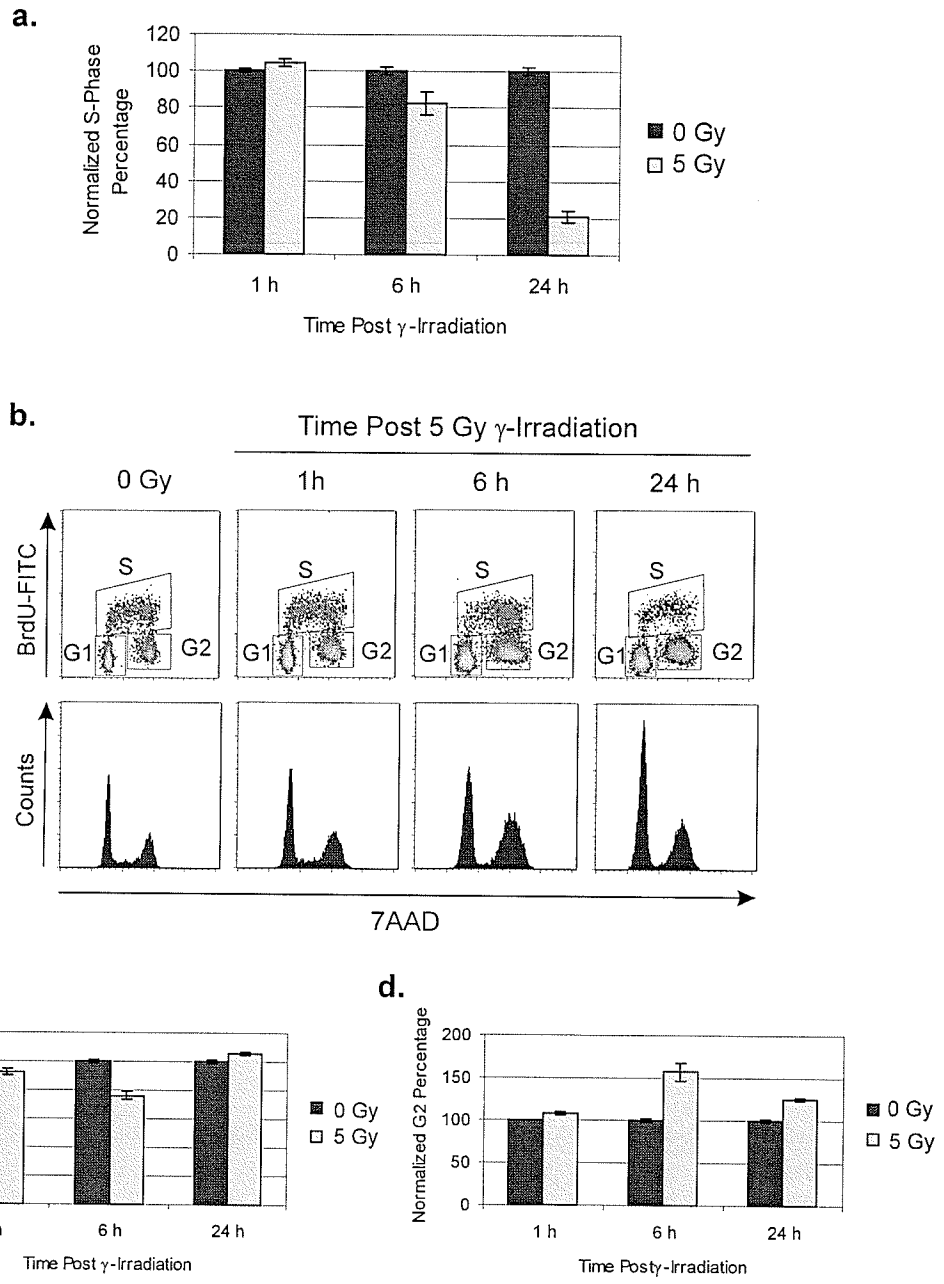

Figure 6.5: The delayed, p53-dependent G1/S checkpoint is intact in primary MEFs following 5 Gy γ-irradiation. **a**. Cells were mock-irradiated or γ-irradiated with 5 Gy. At the times indicated, BrdU was added for 1 h, and the cells were then fixed and processed for flow cytometry. The S-phase percentages were normalized to that of the average S-phase percentage of the mock-irradiated samples for each time point. The data represent the average of three independent experiments done in triplicate. Representative 7AAD versus BrdU-FITC plots, and the corresponding 7AAD DNA histograms, are shown in **b**. Gates for region statistics (G1, S, and G2) are shown. Changes in G1 percentage (**c**) and G2 percentage (**d**) following 5-Gy γ-irradiation are also shown. All error bars represent standard error of the mean.

6.4 p53 protein is transiently stabilized, and p21 is induced following γ-irradiation in primary MEFs

p53 is a major regulator of the delayed G1/S checkpoint in response to γ-irradiation. Once stabilized by ATM, p53 induces the expression of the Cdk2-inhibitor p21[125] (described in detail in section **1.9a**). To validate that p53 was being activated and stabilized, and that p21 was being induced, we next examined the stabilization of p53 protein, the upregulation of p21 mRNA expression, and the upregulation of p21 protein levels in the MEF cells following γ-irradiation.

For p21 mRNA level analysis, MEF cells were mock-irradiated or γ-irradiated with 5 Gy. At 2 h and 6 h post-irradiation, total RNA was extracted from the cells. Semi-quantitative reverse-transcription PCR (RT-PCR) was then used to determine p21 transcript levels. A representative experiment is shown in Figure 6.6a. p21 band intensities were first normalized to the corresponding Actin B band intensity for each time point, and then normalized against the relative p21 band intensity of the mock-irradiated control. Our results show that there was a 1.6 fold induction of p21 within 2 h following a γ-irradiation dose of 5 Gy, and that the p21 mRNA levels remained elevated at 6 h post-γ-irradiation (Figure 6.6b). The data represent results from three independent experiments.

For p53 and p21 protein level analysis, MEFs were mock-irradiated or γ-irradiated with 5 Gy. At 1 h, 3 h, 6 h, and 16 h post-irradiation, whole cell lysates were prepared. 100 μg of whole cell lysate for each time point was used for immunoblot analysis. An upregulated p53 protein level is observable by 1 h post-γ-irradiation, indicating that p53 was activated and stabilized in the MEFs (Figure 6.6c). By 3 h

following γ-irradiation, the level of p53 protein has almost returned to that observed in the mock-irradiated samples. The rapid, but transitory, stabilization observed for p53 is typical of the response of mammalian cells to ionizing radiation[345]. Upregulated p21 protein is also observable by 1 h post-γ-irradiation, and remained elevated through 16 h following γ-irradiation (Figure 6.6d). These data are consistent with a p53-mediated induction of p21 that initiates the delayed G1/S checkpoint shown in Figure 6.5. However, given that upregulated p21 protein levels were observable within 1 h following γ-irradiation, these observations also provide further evidence that cells in late G1 are not receptive to signals that halt progression into S phase following DNA damage.

6.5 The G2/M checkpoint is induced within 1 h, and maintained through 6 h in primary MEFs following a γ-irradiation dose of 5 Gy.

The G2/M checkpoint is induced very rapidly in cells following ionizing radiation[214, 230]. Therefore, we next chose to investigate the initiation and duration of G2/M checkpoint in the primary MEFs. If the absence of an immediate G1/S checkpoint in primary MEFs is caused by a generally slow response to DNA damage in primary MEFs, the induction of the G2/M checkpoint should be delayed as well.

Primary MEFs were mock-irradiated or γ-irradiated with a dose of 5 Gy, and incubated for 1, 3, 6, or 24 h, at which time the cells were fixed and processed for flow cytometry using phosphorylated histone H3 as a mitotic marker[340]. The mitotic percentages were normalized to that of the average mitotic percentage of the mock-irradiated control for each time point. The data represent two independent experiments done in triplicate. Representative 7AAD versus phosphorylated serine 28-FITC with their corresponding DNA histograms are shown in Figure 6.7a.

Within 1 h following a dose of 5 Gy, the mitotic index of primary MEFs decreased to less than 5% of that of mock-irradiated MEFs (Figure 6.7b). This checkpoint was maintained until at least 3 h post-irradiation, and at 6 h the mitotic index was less than 10% of that of the mock-irradiated MEFs (Figure 6.7b). While the mitotic index of γ-irradiated MEFs at 24 h was still low when compared to mock-irradiated cells (Figure 6.7b), a large number of G2 cells had progressed back into G1 between the 6 h and 24 h time points, as shown by a decrease in the normalized G2 percentage (Figure 6.5d) and a concomitant increase in the normalized G1 percentage (Figure 6.5c). Therefore, over 90% of late-G2 primary MEFs rapidly induce a G2/M checkpoint that is maintained through at least 6 h following a γ-irradiation dose of 5 Gy, indicating that primary MEFs can initiate a rapid and sustained response to DSBs.

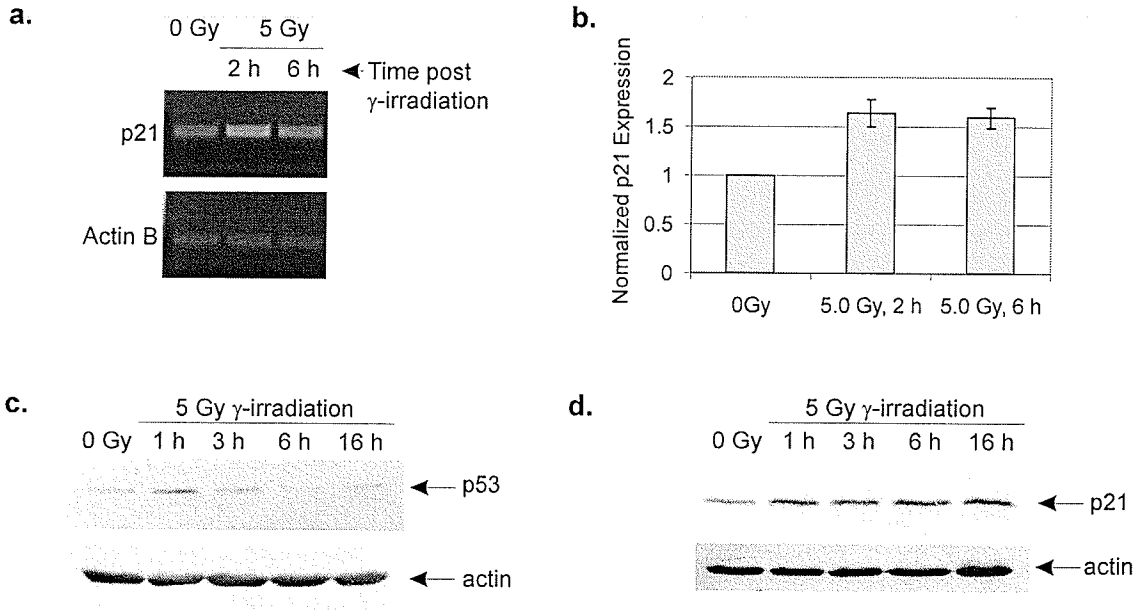

Figure 6.6: p21 mRNA levels increase, p53 protein is transiently stabilized, and p21 protein levels increase in primary MEFs following γ-irradiation. Primary MEFs were mock-irradiated or γ-irradiated (5 Gy), and at the time indicated RNA or whole cell lysates were prepared from the cells. Reverse transcription-PCR of p21 and actin B were carried out (**a**), and the resulting band intensities were measured. The p21 levels were first normalized to the corresponding actin B levels, and then to the mock-irradiated p21 levels The data shown in **b** represent the average of three independent experiments. All error bars represent standard error of the mean. Representative p53 (**c**) and p21(**d**) protein blots are shown with their corresponding Actin blots.

a.

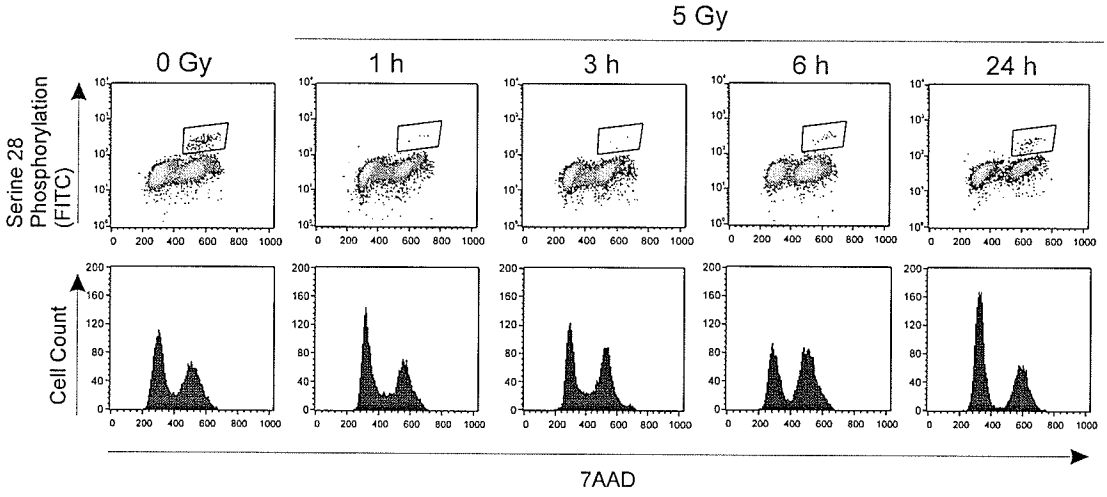

b.

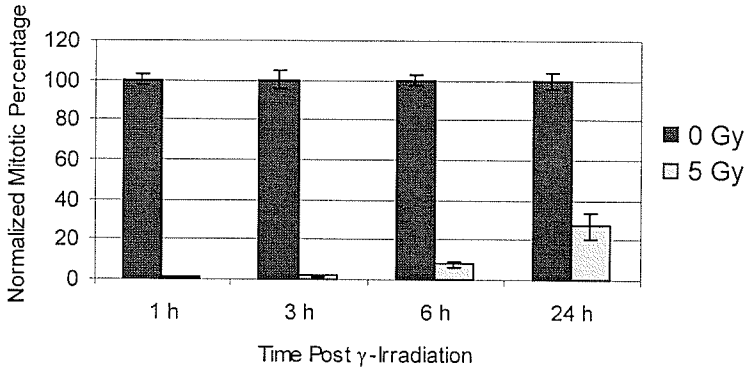

Figure 6.7: The G2/M checkpoint is activated within 1 h following γ-irradiation (5 Gy), and maintained through 6 h post-γ-irradiation in primary MEFs. Primary MEFs were mock-irradiated or γ-irradiated (5 Gy). At the times indicated, the cells were fixed processed for flow cytometry with anti-phospho-histone H3 ($pSer^{28}$). Representative 7AAD versus FITC-H3-$pSer^{28}$ plots, and their corresponding 7AAD DNA histograms, are shown in **a**. The gates for mitotic index region statistics are indicated. The data from two independent experiments done in triplicate are summarized in **b**. The mitotic percentages were normalized to that of the average mitotic percentage of the mock-irradiated samples for each time point. All error bars represent standard error of the mean.

6.6 H2AX phosphorylation occurs within 1 h and is maintained through 3 h in primary MEFs following a γ-irradiation dose of 5 Gy.

H2AX phosphorylation is an indicator of the presence of DNA double-strand breaks (DSBs)[202-204]. Cells are expected to initiate the cell cycle checkpoints immediately following DSBs, and maintain these checkpoints until the DSBs have been repaired[153]. To investigate the relationship between the presence of DSBs and the initiation and maintenance of the cell cycle checkpoints, we next analyzed the phosphorylation status of H2AX following γ-irradiation with a dose of 5 Gy.

Primary MEFs were mock-irradiated or γ-irradiated with a dose of 5 Gy. At 1, 3, 6, and 24 h post-irradiation, the cells were fixed in 4% paraformaldehyde and processed for γH2AX immunocytochemistry. H2AX phosphorylation was observable within 1 h, as expected (Figure 6.8). High levels were still observable at 3 h, but by 6 h post-exposure, we observed a qualitative reduction in overall H2AX phosphorylation levels, with H2AX phosphorylation being concentrated into punctate foci. By 24 h, H2AX phosphorylation was reduced to almost background levels (Figure 6.8). Therefore, unlike the G1/S checkpoint, the G2/M checkpoint was initiated rapidly following the generation of DSBs, and maintained until many DSBs had been repaired.

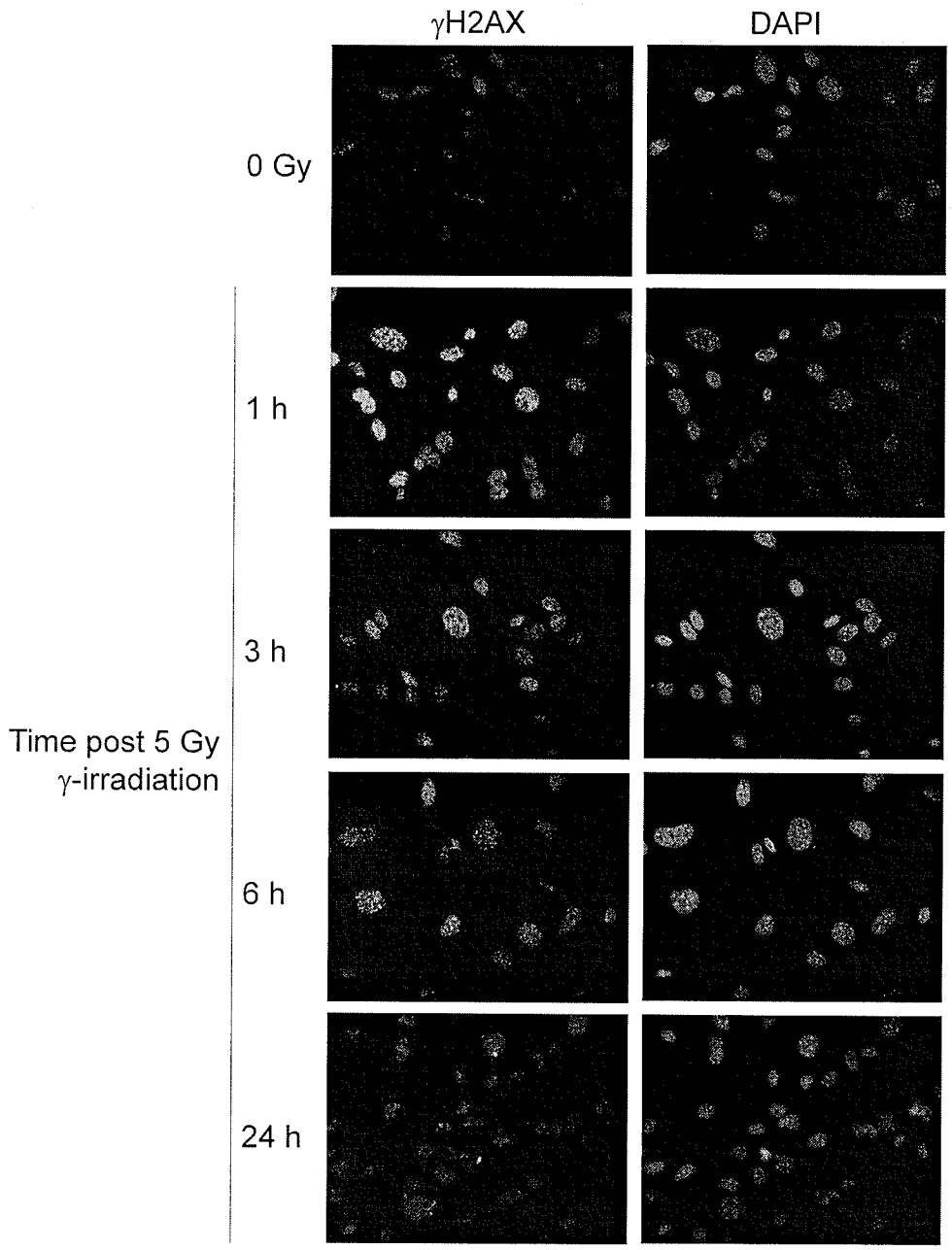

Figure 6.8: H2AX is phosphorylated in MEFs within 1 h following following 5-Gy γ-irradiation, with a high level of phosphorylation being maintained through 3 h post-irradiation. Primary MEFs were mock-irradiated or γ-irradiated. At the times indicated, the cells were fixed with 4% paraformaldehyde and processed for immunocytochemistry using an antibody to γH2AX. Images were acquired using a 40x objective.

6.7 The G2/M checkpoint is not indirectly affecting the delayed G1/S checkpoint through G1 depletion in primary MEFs following γ-irradiation.

Our results show that the majority of late-G1 primary MEFs do not induce an immediate G1/S checkpoint after γ-irradiation (Figure 6.4), and a delayed G1/S checkpoint is not observable in the MEFs until approximately 6 h following γ-irradiation (Figure 6.5a). The G2/M checkpoint is initiated much faster than this. Over 90% of late-G2 primary MEFs induce a G2/M checkpoint within 1 h and maintain it through 6 h following a γ-irradiation dose of 5 Gy (Figure 6.7), resulting in G1 depletion (Figure 6.5c). Therefore, we wanted to verify that the G2/M checkpoint was not indirectly inducing or exacerbating the delayed G1/S checkpoint through this G1 depletion. To address this question, entry into mitosis was blocked in both mock-irradiated and γ-irradiated MEFs using nocodazole. Nocodazole disrupts microtubules by binding to β-tubulin, preventing proper mitotic spindle formation, and arresting cells at the G2/M border[346]. A nocodazole concentration of 1 μg/mL is sufficient to block cells in mitosis[347].

Nocodazole was added to the primary MEFs to a concentration of 1 μg/mL at the time of γ-irradiation (5 Gy) or mock-irradiation. At 1 h and 24 h post-irradiation, the cells were labelled for 1 h with BrdU, after which they were fixed and processed for flow cytometry. S-phase percentages were normalized to that of the average S-phase percentage of the mock-treated cells for each time point. This experiment was carried out twice in triplicate.

At 24 h, there was a statistical difference between the G2 percentages of the different treatment groups (one way ANOVA: $F=21.771$; 2, 15 df, $p<0.001$). Nocodazole

was able to block the primary MEFs at mitosis, as we observed a build-up of G2 cells at 24 h post-treatment (Figure 6.9c), and the normalized G2 percentages of both nocodazole-treated/mock-irradiated and nocodazole-treated/γ-irradiated MEFs were significantly larger than that of the untreated MEFs (Holm-Sidak unadjusted p=0.0000601 with a critical p of 0.025, and unadjusted p= 0.0000292 with a critical p of 0.017, respectively). The normalized G2 percentages of the two nocodazole-treated groups were not significantly different (Holm-Sidak unadjusted p= 0.701 with a critical p of 0.05).

At 24 h post-irradiation, there was a significant difference between the normalized S-phase percentages of the different treatment groups (one way ANOVA: F=48.926; 2, 15 df, p<0.001). Our results show that blocking cells from progressing back into G1 did not rescue the delayed G1/S checkpoint (Figure 6.9a) observed in the MEFs, because the normalized S-phase percentage of the nocodazole-treated/γ-irradiated MEFs at 24 h (32%) was statistically smaller than that of the nocodazole-treated/mock-irradiated MEFs (81%) (Holm-Sidak unadjusted p= 0.00000472 with a critical p of 0.025). These data indicate that the delayed G1/S checkpoint was not due to G1 depletion and is an independent response to DSBs. However, with a normalized S-phase percentage of 81% when compared to untreated MEFs, the nocodazole-treated/mock-irradiated MEFs did exhibit a statistically significant reduction in the S-phase percentage at 24 h (Holm-Sidak unadjusted p= 0.0188 with a critical p of 0.050). Therefore, G1 depletion did cause a small reduction in S phase entry. (The difference between the normalized S-phase percentages of untreated and nocodazole-treated/γ-irradiated MEFs was also significant as expected [Holm-Sidak unadjusted p= 0.0000000883 with a critical p of 0.017].)

Furthermore, at 24 h, there was also a statistical difference in the normalized G1 percentage between treatment groups (one way ANOVA: $F=49.213$; 2, 15 df, $p<0.001$). Blocking cells in G2 led to a depletion of G1 cells, as the normalized G1 percentages of both nocodazole-treated/mock-irradiated and nocodazole-treated/γ-irradiated MEFs were significantly smaller than that of the untreated MEFs (Holm-Sidak unadjusted p= 0.0000000850 with a critical p of 0.017, and unadjusted p= 0.00000457 with a critical p of 0.025, respectively). γ-irradiation did not substantially rescue the depletion of G1 cells caused by nocodazole treatment (Figure 6.9b), although there was a statistical difference (Holm-Sidak unadjusted p= 0.0185 with a critical p of 0.050). These data suggest that γ-irradiation does not immediately block primary MEFs from entering S phase, supporting the data obtained from directly assessing the G1/S transition percentage following γ-irradiation.

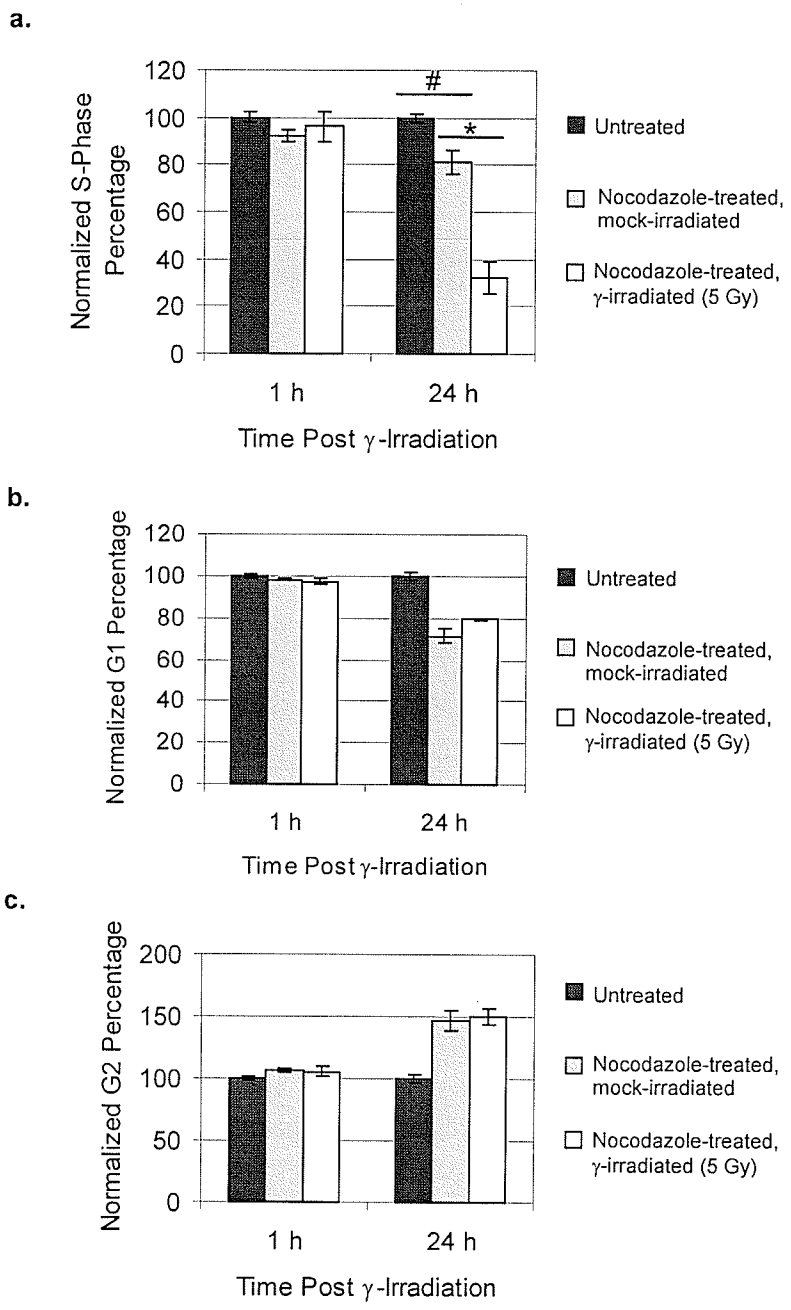

Figure 6.9: Blocking primary MEFs at G2/M does not rescue the delayed G1/S checkpoint observed in primary MEFs. For primary MEFs treated with nocodazole, nocodazole was added at the time of mock-irradiation or γ-irradiation (5 Gy) to a final concentration of 1 μg/mL. At the times indicated, the cells were incubated for 1h with BrdU and processed for flow cytometry. Normalized S-phase percentages (**a**), normalized G1 percentages (**b**), and normalized G2 percentages (**c**) are shown. The data represent two independent experiments done in triplicate. All error bars represent standard error of the mean. *$p<0.001$, #=0.0188

6.8 A γ-irradiation dose of 5 Gy severely affects the downstream proliferation of primary MEFs.

To investigate how a γ-irradiation dose of 5 Gy affects the ability of the primary MEFs to proceed through several cell divisions, the MTT assay[315] was used to quantify the surviving cell fraction of the primary MEFs four doubling times after exposure to increasing doses of γ-irradiation. Our results show that the surviving cell fraction of primary MEFs exposed to a dose of 5 Gy was only 0.12 of mock-irradiated cells four doubling times after exposure (Figure 6.10). A surviving cell fraction of approximately 0.12 is generated when γ-irradiated cells only undergo one cell doubling for every four cell doublings that mock-irradiated cells undergo. This result demonstrates that a dose of 5 Gy generates enough DNA damage to severely affect downstream cell proliferation, providing further evidence that the inability of the MEFs to initiate an immediate G1/S arrest is not due to an absence of DNA damage.

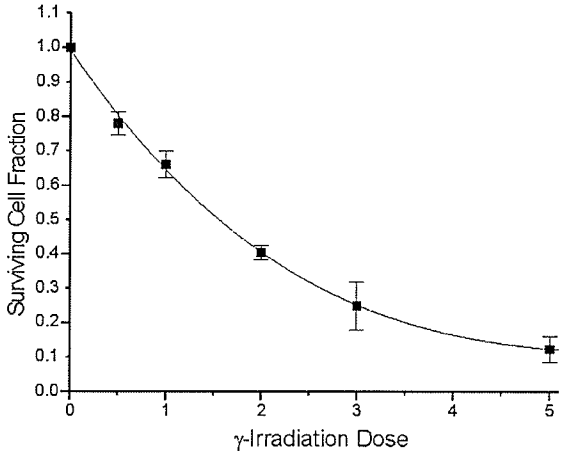

Figure 6.10: A γ-irradiation dose of 5 Gy severely affects the downstream proliferation of primary MEFs. Primary MEFs at 50-70% confluency were treated with increasing doses of γ-irradiation. After 1 h, serial dilutions of each dose, based on the cell count from the untreated, control plate, were made. The cells were then grown for 4 doubling times, at which point the MTT assay was done. The data represent the average of three independent experiments. Error bars represent standard error of the mean.

6.9 Primary MEFs do not globally degrade either Cdc25a or cyclin D1.

Two pathways with the potential to initiate an immediate G1/S checkpoint have been identified, and both function to inhibit Cdk2. The first pathway targets Cdc25a, the phosphatase responsible for removing inhibitory phosphates on Cdk2. Following IR, Cdc25a is targeted for degradation through an ATM-Chk2 pathway[240]. The second pathway targets cyclin D1 for degradation, freeing any p21 that was bound to the Cdk4(6)/cyclin D1 complexes to inhibit Cdk2/cyclin E complexes[241]. To investigate what effect these two pathways were having in our primary MEFs, we investigated the levels of both Cdc25a and cyclin D1 following γ-irradiation.

Primary MEFs were mock-irradiated or γ-irradiated (5 Gy), and at 1, 3, and 6 h post-irradiation, whole-cell lysates were prepared. 100 μg of whole-cell lysate for each time point was used for immunoblot analysis. Equal loading was verified by Ponceau S staining prior to immunoblot analysis for Cdc25a or Cyclin D1. To generate a positive control for the Cdc25a immunoblots, mouse Cdc25a was cloned and inserted into the pCMV-Tag1 vector. This construct was transiently transfected into 293T cells, and a whole-cell lysate of these cells was used as the positive control for Cdc25a.

Our results show that there was no qualitative reduction in Cdc25a protein levels at 1, 3, or 6 h post-5 Gy in the primary MEFs (Figure 6.11a). There was also no observable degradation of Cyclin D1 at 1, 3, or 6 h post-γ-irradiation in the primary MEFs (Figure 6.11b). However, this lack of global degradation of Cdc25a and cyclin D1 does not preclude there being localized destruction or inactivation of these two proteins.

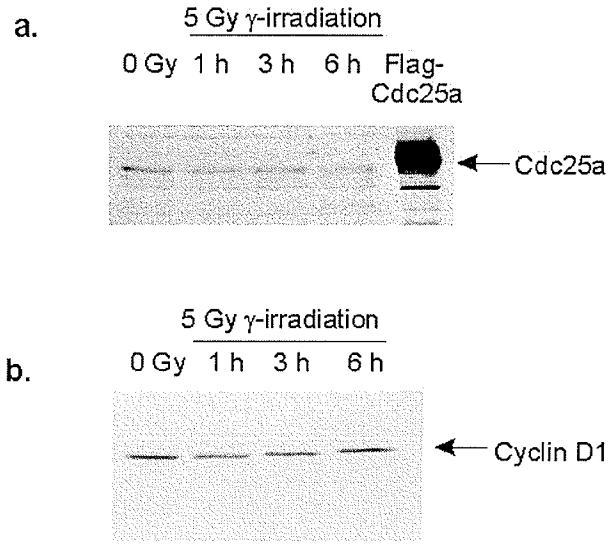

Figure 6.11: Global levels of Cdc25a and cyclin D1 do not decrease in the primary MEFs following γ-irradiation. Primary MEFs were mock-irradiated or γ-irradiated (5 Gy). At the times indicated, whole cell lysates were prepared. Representative blots of Cdc25a (**a**), with exogenously expressed mouse Cdc25a as a positive control, and cyclin D1 (**b**) are shown.

6.10 HeLa cells initially promote entry in S phase following γ-irradiation, but then induce a delayed G1/S checkpoint.

Our results show that primary MEFs do not induce an immediate G1/S checkpoint following γ-irradiation, yet all of the other checkpoints are functioning as expected. To further validate this finding, we next chose to investigate the immediate G1/S checkpoint in the commonly used cancer cell line HeLa, which is positive for human papillomavirus 18. HeLa cells were mock-irradiated or γ-irradiated with a dose of 5 or 10 Gy at the beginning of the staggered CldU/IdU labelling strategy described in detail in section **6.1**. The delayed G1/S and the G2/M checkpoints were also analyzed in the HeLa cells as described for the primary MEFs in sections **6.3** and **6.5**, respectively.

Like the primary MEFs, HeLa cells did not induce an immediate G1/S checkpoint. In fact, they promoted S-phase entry after doses of both 5 Gy and 10 Gy (Figure 6.12a), with these doses generating normalized G1/S transition percentages of 152% and 148%, respectively (N=4). This induced S-phase entry can also be seen as an increased normalized S-phase percentage measured at 1 h and 6 h post-γ-irradiation (Figure 6.12b). The HeLa cells were capable of inducing the delayed G1/S checkpoint, as shown by the decreased S-phase percentage observed at 24 h post-irradiation (Figure 6.12b). In agreement with our data, Murata et al. have also shown that following IR HeLa cells initially promote entry into S phase, but then proceed to induce a delayed G1 block[348]. At 6 h post-irradiation, γ-irradiated HeLa cells had a G1 percentage that was 51% of the observed in the mock-irradiated HeLa cells (Figure 6.1c), indicating that more cells have left G1 than have entered G1 in HeLa cells during the 6 h following a dose of 5 Gy, providing indirect evidence for the absence of the immediate G1/S checkpoint.

The HeLa cells exhibited a strong intra-S-phase checkpoint, as γ-irradiated HeLa cells had a S/G2 transition percentage that was only 38% (5 Gy) or 34% (10 Gy) of that of the mock-irradiated control (Figure 6.12a). After a dose of 5 Gy, HeLa cells were also capable of rapidly inducing a G2/M checkpoint within 1 h, and they maintained this checkpoint through 6 h (Figure 6.12d). By 24 h, the G2/M checkpoint had been relaxed, and a large release of mitotic cells was observable. Therefore, the HeLa cells exhibit the same general pattern of checkpoint control as primary MEFs, specifically they do not activate an immediate G1/S checkpoint, but they do induce a delayed G1/S checkpoint, an intra-S-phase checkpoint, and a rapid and sustained G2/M checkpoint.

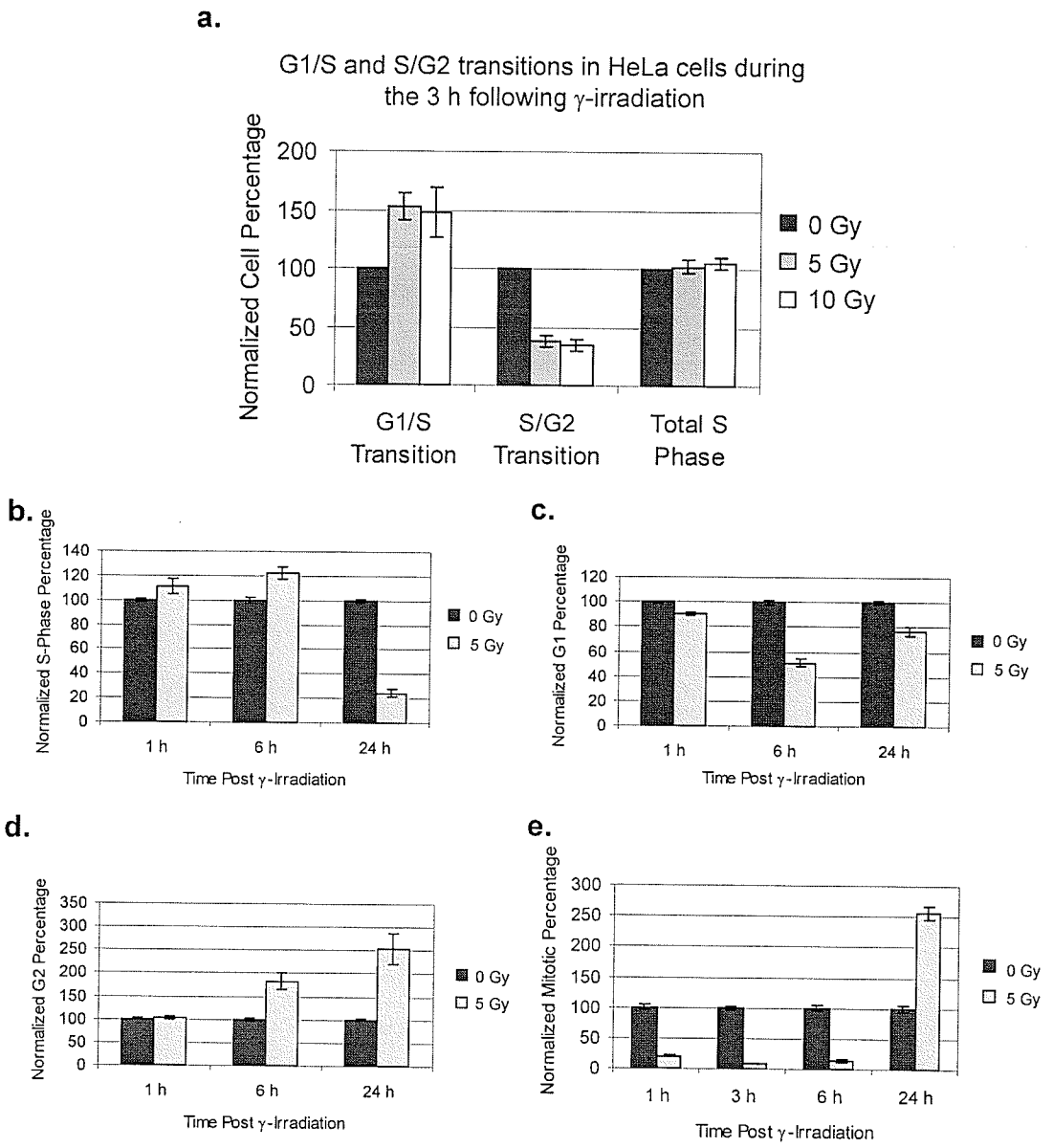

Figure 6.12: HeLa cells initially promote S-phase entry following γ-irradiation. **a.** HeLa cells were mock-irradiated or γ-irradiated (5 or 10 Gy) at the beginning of the staggered CldU/IdU labelling strategy. Data represent the average of four independent experiments. **HeLa cells induce the delayed G1/S checkpoint.** HeLa cells were mock-irradiate or γ-irradiated (5 Gy). At the times indicated, the cells were incubated with BrdU for 1 h, fixed and processed for flow cytometry. The data represent the average of three independent experiments done in triplicate. S-phase, G1, and G2 percentages were normalized to the corresponding percentage of the mock-irradiated samples for each time point. Changes in S-phase (**b**), G1 (**c**), and G2 (**d**) are shown. **e. The G2/M checkpoint is intact in HeLa cells.** HeLa cells were mock-irradiate or γ-irradiated (5 Gy). At the indicated times, the cells were fixed and processed for flow cytometry. The data represent the average of two independent experiments done in triplicate. All error bars represent standard error of the mean.

6.11 Chapter Summary: Absence of an immediate G1/S checkpoint in primary MEFs following γ-irradiation identifies a novel checkpoint switch

- The classic method of analyzing the G1/S checkpoint (BrdU-labelling) does not assess changes in the G1/S transition immediately following DNA damage, as it only measures the total S-phase percentage. Therefore, this method cannot be used to directly analyze the immediate G1/S checkpoint. To address the biology of the immediate G1/S checkpoint, I have developed a novel strategy for analyzing the G1/S and S/G2 transition percentages following γ-irradiation using a staggered CldU/IdU double-labelling approach.
- Our results show that contrary to the current model of the G1/S checkpoint, 65% of late-G1 primary MEFs continued to progress into S phase after a γ-irradiation dose of 5 Gy, indicating that the majority of late-G1 cells are no longer responsive to signals that induce a G1/S checkpoint. After a high dose of 10 Gy, 46% of late-G1 primary MEFs still progressed into S-phase.
- Primary MEFs are able to induce a delayed G1/S checkpoint, as γ-irradiated MEFs (5 Gy) had an S-phase percentage that was 20.6% of that of the mock-irradiated control at 24 h post-irradiation. Furthermore, p53 protein was stabilized within 1h following γ-irradiation. There was also an upregulation of both p21 mRNA and protein levels, with upregulated p21 protein also observable by 1 h and stabilized through 16 h post γ-irradiation. However, given that upregulated p21 protein levels were observable within 1 h following γ-irradiation, these observations also provide further evidence that cells in late G1 are not receptive to signals that halt progression into S phase following DNA damage.

- The primary MEFs induced an intra-S-phase checkpoint, because the S/G2 transition percentage decreased by 23% following 5 Gy, and by 31% following 10 Gy, indicating that replication had been slowed.
- Primary MEFs induced a G2/M checkpoint that was over 90% effective within 1 h post-γ-irradiation (5 Gy), and this checkpoint was maintained through at least 6 h. The induction of the G2/M checkpoint coincided with H2AX phosphorylation, and this checkpoint was maintained until γH2AX, and the presence of DSBs that it indicates, had begun to be dephosphorylated/repaired. Therefore, primary MEFs are capable of activating a rapid and sustained response to DSBs.
- The absence of an immediate G1/S checkpoint after γ-irradiation in the primary MEFs is not due to an absence of DNA damage, because the surviving cell fraction four doubling times after a γ-irradiation dose of 5 Gy was only 0.12 of mock-irradiated cells. This demonstrated that a dose of 5 Gy dose has severe downstream repercussions for cell proliferation.
- Two pathways for the immediate G1/S checkpoint have been proposed: one targeting Cdc25a for degradation[240], and the other targeting cyclin D1 for degradation[241]. Neither Cdc25a nor cyclin D1 degradation was observed in the primary MEFs following γ-irradiation, but this does not preclude localized degradation or inactivation of these two proteins.
- Like the primary MEFs, HeLa cells did not induce an immediate G1/S checkpoint. In fact, HeLa cells actually promoted entry into S phase following a γ-irradiation dose of 5 or 10 Gy. However, HeLa cells did induce a delayed G1/S checkpoint, and a strong intra-S-phase checkpoint. Furthermore, HeLa cells induced

a G2/M checkpoint within 1 h, and maintained this checkpoint through 6 h following γ-irradiation. Therefore, HeLa cells exhibit the same general pattern of checkpoint control as primary MEFs, specifically they do not activate an immediate G1/S checkpoint, but they do induce a delayed G1/S checkpoint, an intra-S-phase checkpoint, and a rapid and sustained G2/M checkpoint.

Conclusions: Analysis of the immediate induction of the G1/S checkpoint at a cellular level has been hampered by the inability to distinguish cells that were already replicating DNA at the time of damage from cells that entered S phase following the DNA damage. We have developed a novel strategy for assessing the initiation of the G1/S checkpoint following γ-irradiation within asynchronous, low passage, primary mouse embryonic fibroblast cultures (MEFs) using a staggered CldU/IdU double-labelling protocol. Our results show that the majority (65%) of late-G1 primary MEFs still progress into S phase following a γ-irradiation dose of 5 Gy. Primary MEFs are capable of inducing a delayed G1/S checkpoint, an intra-S-phase checkpoint, and a rapid and sustained G2/M checkpoint. Furthermore, a dose of 5 Gy has severe downstream repercussions for cellular proliferation. Therefore, the inability of the late-G1 primary MEFs to initiate an immediate G1/S checkpoint is not due an insufficient amount of DNA damage for checkpoint initiation, and instead suggests that late-G1 cells are no longer responsive to the signals that induce the G1/S checkpoint. This result is contrary to what would be expected based on the current model of the G1/S checkpoint, and suggests that we need to re-evaluate how cells regulate progression from G1 to S phase in the presence of DNA damage. The model of G1/S checkpoint that we have developed based on these results is that cells in late G1 may predominantly respond to DNA damage at the level of

individual replication origins, like cells already in S phase, rather than by inducing a complete block to S-phase entry. This switch in checkpoint use from a global G1/S checkpoint to origin-specific regulation in late G1 identifies a novel regulatory point within the cell cycle. (This model will be described in more detail in the Discussion.)

Chapter 7

Discussion

7.1 A role for TLS in the DNA damage response pathways

TLS/FUS was initially identified as the fusion partner of *CHOP* in a translocation found in human myxoid liposarcoma[1-3], and of *ERG* in a translocation found in human myeloid leukemia[4, 5]. The formation of these fusion genes is believed to be the primary cause of these cancers when they occur; however, the exact mechanisms of TLS-associated oncogenesis are unknown. One proposed mechanism of oncogenesis is that these fusion oncoproteins function as aberrant transcription factors, interfering with the normal transcriptional regulation of the target genes of the fusion partner and/or recognizing new transcriptional targets[26, 27]. However, there is also evidence that these fusion oncoproteins may function in a dominant-positive manner as a dysregulated version of TLS, or in a dominant-negative manner to inhibit the function of wild-type TLS[59], providing other potential mechanisms of oncogenesis. Therefore, elucidating the wild-type function of TLS will provide a greater understanding of the mechanisms initiating oncogenesis. To that end, the Hicks lab has been investigating the normal, wild-type function of TLS through the use of *TLS*$^{-/-}$ mice and cells.

TLS$^{-/-}$ mice exhibit characteristics consistently found in mouse models of the human genomic instability syndromes AT[112-114] and NBS[115], specifically genomic instability[111], immune system defects[111], and sensitivity to ionizing irradiation[116]. The causative genes of these syndromes are involved in the DNA damage response pathways (repair, cell cycle checkpoints, and/or apoptosis), and this suggested that TLS also plays a role in these pathways. Therefore, the hypothesis of this thesis was that TLS maintains

genome stability through a role in DNA repair. The aims of this thesis were to identify a role for TLS in the cellular response to DNA damage, and to evaluate its function within the ATM-activated signalling pathways responding to DNA double-strand breaks.

We rationalized that if TLS is a DNA damage response protein, cells deficient for TLS should be defective in their ability to respond to DNA damage. To test this directly, we analyzed the sensitivity of *TLS*$^{-/-}$ MEFs to different DNA damaging agents. We have demonstrated that *TLS*$^{-/-}$ MEFs are more sensitive than *TLS*$^{+/+}$ MEFs to both γ-irradiation and mitomycin C, but not to UV-irradiation. Mitomycin C and γ-irradiation induce interstrand cross-links (ICLs) and DSBs, respectively, as their most severe forms of DNA damage. These two types of DNA lesions are repaired by different, but overlapping repair pathways (described in detail in sections **1.7f** and **1.8**). Therefore, we have established TLS as a novel member of the group of proteins required for the response to both DSBs and ICLs, genetically linking TLS to a select group of proteins that includes FANCD2[146], NBS1[138, 139, 142], ATR[164, 165, 262], BRCA1[119, 132], and BRCA2[121, 131, 132]. These proteins are all critical for both DNA repair and the induction of the cell cycle checkpoints.

The mouse embryonic fibroblasts provide a cellular model for the pathways that initiate growth arrest and repair following DNA damage[292]. Lymphocytes, on the other hand, provide a cellular model for the pathways that initiate apoptosis (programmed cell death)[292]. Therefore, to assess whether TLS is also required for the induction of apoptosis following DNA damage, we examined the apoptotic response of *TLS*$^{-/-}$ pre-B cells to DNA damage. Our results show that *TLS*$^{-/-}$ pre-B cells are resistant to apoptosis induced by γ-irradiation, mitomycin C, and, to a lesser extent, UV-irradiation. In

contrast, *TLS*$^{-/-}$ pre-B cells do induce apoptosis following exposure to staurosporine, which induces apoptosis exclusive of the DNA damage response pathways. These data indicate that the apoptotic defect observed in the *TLS*$^{-/-}$ pre-B cells does not represent a general apoptotic defect, but one specific for signals generated by DNA damage. (These experiments were conducted in collaboration with Ludger Klewes.)

One of the ways to help validate the phenotype of a knock-out cell line is to exogenously express the gene in these cells, as this may be able to rescue the wild-type phenotype. Therefore, we attempted to rescue the apoptotic defect observed in the *TLS*$^{-/-}$ pre-B cell line by exogenously expressing *TLS*, but we were unable to reproducibly rescue the defect. Because TLS has known roles in transcription, mRNA splicing, and mRNA transport, TLS may function in the apoptotic pathway at the level of gene regulation. If this is the case, exogenously expressing TLS may not be able to correct the dysregulated gene regulation present in the *TLS*$^{-/-}$ pre-B cells within the time frame of the experiment. Another explanation is that the apoptotic defect is due to a subsequent change in the cell line, potentially a mutation required for pre-B cell survival in a *TLS*$^{-/-}$ genetic background.

Taken together, the MEF and pre-B cell data indicate that TLS is required for the DNA damage response to DSBs and ICLs induced by γ-irradiation and mitomycin C, respectively. Furthermore, the presence of TLS is required for an efficient response to DNA damage in both MEFs, a model cell type for cell cycle arrest and DNA repair, and pre-B cells, a model cell type for DNA damage-induced apoptosis. Therefore, TLS affects multiple DNA damage responses, and is reminiscent of ATM, which initiates the DSB signalling cascades, directly activating proteins required for repair, cell cycle

checkpoints (G1/S, intra-S-phase, and G2/M) and apoptosis[122, 124-127, 176]. ATM is placed at the apex of the mutually exclusive pathways of apoptosis and cell cycle checkpoints/DNA repair, because while *ATM* $^{-/-}$ cells generally exhibit radiation hypersensitivity[112, 296], *ATM* $^{-/-}$ thymocytes are actually resistant to radiation-induced apoptosis[296, 297]. We would expect this phenotype for proteins involved in both types of responses to DNA damage. As such, it is not surprising that this duality of function is not exclusive to ATM and TLS, and is also seen for p53[302-305] and DNA-PKcs[303]. These seemingly contradictory phenotypes of radiation sensitivity and apoptotic resistance also emphasize the need to understand the biology of the cell type under study. Because *TLS* $^{-/-}$ cells were defective in their responses to multiple types of DNA damage, we could then predict that TLS functions in the signalling pathways initiated following DNA damage, including the ATM-mediated DSB-signalling cascade.

7.2 TLS and ATM-regulated DSB-response

Following DNA damage, fibroblasts typically arrest the cell cycle and repair the DNA damage[292]. Defects in either the ability to repair DNA damage or the ability to induce the cell cycle checkpoints that allow for repair could be responsible for the observed sensitivity of the *TLS* $^{-/-}$ MEFs to DSBs and ICLs. We already had preliminary evidence for a defect in the cell cycle checkpoints/growth arrest pathways in the *TLS* $^{-/-}$ MEFs, because they continued to proliferate despite the fact that the majority of *TLS* $^{-/-}$ MEFs have inherent genomic damage. Over 67% of *TLS* $^{-/-}$ MEFs exhibit abnormal karyotypes, including aneuploidy, extrachromosomal elements, chromosome breakage, centromere loss, and chromosome fusion[111], and this level of damage would be expected to cause cells to undergo growth arrest. Therefore, to pinpoint the defect in the

DNA damage response of the *TLS*$^{-/-}$ cells, we chose to systematically assess the ATM-mediated DSB-signalling pathways in the *TLS*$^{-/-}$ MEFs, including the cell cycle checkpoints.

The multi-system defects observed in the *TLS*$^{-/-}$ cells indicated that TLS could either be functioning upstream or downstream of ATM within these pathways. To assess DSB recognition and ATM activation, we analyzed one of the first events that occurs following DSBs, the phosphorylation of histone H2AX on serine 139 by ATM[202-204]. In untreated cells, more *TLS*$^{-/-}$ MEFs than *TLS*$^{+/+}$ MEFs exhibited staining for H2AX phosphorylation. This result suggests that the *TLS*$^{-/-}$ MEFs have a higher level of endogenous damage that wild-type cells, a finding that is consistent with the genomic instability observed previously in these cells[111]. For example, the chromosomal breaks observed in some of the metaphases from the *TLS*$^{-/-}$ cells[111] would be expected to induce H2AX phosphorylation at those sites.

H2AX was phosphorylated in the *TLS*$^{-/-}$ MEFs in a dose-dependent manner following γ-irradiation, indicating that the DSBs are recognized and that ATM is activated in *TLS*$^{-/-}$ MEFs, placing TLS downstream of ATM in the DSB-signalling cascade. However, in two separate experiments, we observed that *TLS*$^{-/-}$ MEFs also induced phosphorylation of what was possibly a monoubiquitinated form of H2AX. (This higher molecular mass H2AX was also visible in wild-type cells, but was more prevalent in *TLS*$^{-/-}$ MEFs.) Monoubiquitination of histones does not result in their degradation, instead it appears to act as a signal for trans-acting factors, and functions in combination with other histone modifications to affect chromatin structure[349-352]. Further experiments would be required to verify that this upper band was a monoubiquitinated

version of H2AX, and whether this represents a general ubiquitination of histones, or is specific for H2AX. This observation is also interesting given that EWS has been found to interact with BARD1 (BRCA1 associated RING domain protein)[118], as the BRCA1/BARD1 complex is an E3 ubiquitin ligase[353, 354]. If TLS interacts with BARD1 in a similar manner to EWS, and if the BRCA1/BARD1 complex can ubiquitinate H2AX, then TLS could be affecting H2AX ubiquitination through an association with this ubiquitin ligase complex.

Because γH2AX levels are an indicator of the presence of DSBs, γH2AX dephosphorylation can be used as a qualitative measure of DNA repair. *TLS*$^{-/-}$ MEFs dephosphorylated γH2AX with approximately the same kinetics as wild-type cells, indicating that DSBs are being repaired in *TLS*$^{-/-}$ MEFs. However, this analysis would not necessarily be able to distinguish minor differences in repair efficiencies and would not assess the frequency of repair errors, including deletions (small and large), translocations, or inversions, all of which could potentially cause serious downstream repercussions as to the genomic integrity of the cells. In fact, there are data in the literature to support a role for TLS in homologous recombination (HR), as TLS has homologous pairing activity[64] and can promote D-loop formation[117]. The association of TLS with HR is also intriguing given that HR can be used to repair both DSBs and ICLs. If TLS did specifically function in repair by HR, its absence would lead to the use of NHEJ repair in instances when HR could have been used. Because NHEJ is error-prone[126, 176, 232-234], this could result in deletions, translocations, and inversions being introduced during repair. In fact, many of the aberrations observed in the *TLS*$^{-/-}$ cells,

such as the fusions, chromosomal breakage, and amplifications[111], can be explained by these types of repair errors, and this relationship will be discussed in more detail later.

Our observations show that the *TLS*$^{-/-}$ MEFs continue to proliferate despite their inherent genomic damage. Therefore, we next chose to investigate the DSB-induced cell cycle checkpoints. The *TLS*$^{-/-}$ MEFs induced a dose-dependent G2/M checkpoint within 1 h of γ-irradiation, indicating that the *TLS*$^{-/-}$ MEFs are not defective in their ability to induce the G2/M checkpoint. However, more *TLS*$^{-/-}$ MEFs than *TLS*$^{+/+}$ MEFs are affected by the G2/M checkpoint following low doses of γ-irradiation (0.5, 1.0, or 2.5 Gy), and the *TLS*$^{-/-}$ MEFs also did not recover pre-irradiation mitotic levels as effectively as wild-type cells. While the differences between the *TLS*$^{-/-}$ MEFs and *TLS*$^{+/+}$ MEFs were not significant at individual doses or time points, when the data are taken together, they do suggest that *TLS*$^{-/-}$ MEFs cannot recover from DSBs as effectively as wild-type MEFs.

Our results also demonstrated that *TLS*$^{-/-}$ MEFs induce a delayed G1/S checkpoint following γ-irradiation, which was observable as a decrease in the percentage of S-phase cells at 24 h post-irradiation. At 6 h post-γ-irradiation, the *TLS*$^{-/-}$ MEFs exhibited a significantly lower percentage of S-phase cells than wild-type MEFs, and also a significantly higher percentage of G1 cells than wild-type MEFs, both of which indicate that more *TLS*$^{-/-}$ MEFs initiate a G1/S checkpoint following γ-irradiation than wild-type cells. However, by 24 h the two cell types did not display any significant difference. Using a staggered CldU/IdU labelling strategy, we were also able to directly measure the G1/S and S/G2 transition percentage within a 3 h time period following γ-irradiation in *TLS*$^{-/-}$ and *TLS*$^{+/+}$ MEFs. The percentage of cells that continued to progress into S phase

following γ-irradiation was statistically lower in the *TLS*$^{-/-}$ MEFs than in the wild-type MEFs, directly demonstrating that more *TLS*$^{-/-}$ MEFs than *TLS*$^{+/+}$ MEFs are affected by a G1/S checkpoint. Both cell types exhibited a decrease in the percentage of cells progressing from S phase to G2 follwing γ-irradiation. These results demonstrate that the DSB-induced G1/S, the intra-S-phase, and the G2/M checkpoints are intact in *TLS*$^{-/-}$ MEFs, indicating that these branches of the ATM-mediated DSB-signalling cascades are independent of TLS. The observation that more *TLS*$^{-/-}$ MEFs than *TLS*$^{+/+}$ MEFs initiate G1/S, and G2/M checkpoints suggests that *TLS*$^{-/-}$ MEFs are more adversely affected by a given dose of γ-irradiation than wild-type MEFs. The severity of the cell cycle checkpoints (the percentage of cells affected within a population) is indicative of the amount of DNA damage, as the cell cycle checkpoints are induced in a dose-dependent manner. With lower amounts of DNA damage, more cells are able to repair the lesions and proceed through the cell cycle without a noticeable checkpoint. Therefore, the observation that *TLS*$^{-/-}$ MEFs induce more severe cell cycle checkpoints than wild-type MEFs indicates that the *TLS*$^{-/-}$ MEFs may be unable to repair the DNA damage as effectively and/or as quickly as wild-type cells, potentially identifying a repair defect that could not be detected using the H2AX dephosphorylation assay. In summary, DNA double-strand break recognition, ATM activation, and the initiation of the G1/S, intra-S-phase, and G2/M cell cycle checkpoints are independent of TLS. While *TLS*$^{-/-}$ MEFs removed DNA double-strand breaks with qualitatively the same kinetics as wild-type MEFs, the increased severity of the cell cycle checkpoints observed in the *TLS*$^{-/-}$ MEFs indicates that these cells may not repair the DSBs as effectively or as quickly as *TLS*$^{+/+}$ MEFs.

We established that *TLS*$^{-/-}$ MEFs are more sensitive to both mitomycin C and γ-irradiation, but we chose to specifically evaluate the DSB-response pathways for several reasons. γ-irradiation induces DSBs at a very well defined time point, whereas mitomycin C exposure requires an incubation period, during which cells have already begun repairing the DNA damage. Most ICLs are also detected and repaired in S phase with a DSB-repair intermediate[162]. Furthermore, because DSBs are produced endogenously in cells[120, 126], they can be contributing to the genomic instability observed in the *TLS*$^{-/-}$ cells. Therefore, γ-irradiation provides a simpler and more relevant model for investigating TLS function. However, there are several caveats to using the ATM-regulated DSB-signalling cascades to pinpoint the function of TLS in the DNA damage response. While it is convenient to discuss the cellular DSB response in the context of the ATM-dependent signalling cascade, there are AT patients with null mutations in ATM, and ATM knock-out mice are viable[112-114, 121]. On the other hand, knocking-out Nbs1[143], Mre11[196], Rad50[197], ATR[198, 199], the recombinase Rad51[200, 201], or TLS[111] results in embryonic or perinatal lethality in the mouse models. These observations suggest that the MRN complex, Rad51, and TLS have additional functions exclusive of the ATM pathway and/or can function to some extent without the presence of ATM. Furthermore, we found that *TLS*$^{-/-}$ MEFs are sensitive to mitomycin C, while *ATM*$^{-/-}$ cells are not[146]. These data indicate that TLS function in the DNA damage response is not limited to the ATM-signalling cascades.

7.3 Cellular localization of TLS and its association with the nucleolus

Another method by which we are trying to identify the molecular mechanism of TLS function in the DNA damage response is by analyzing its subcellular localization.

Many known DNA damage-response proteins form ionizing radiation-induced foci (IRIF), including ATM, phosphorylated H2AX, the MRN complex, Rad51, BRCA1, and Rad52 [203, 204, 212, 213, 327-329]. Therefore, we chose to investigate TLS function by characterizing its localization following both DNA double-strand breaks and interstrand cross-links. TLS is known to relocalize to the nucleoli following treatment with the transcriptional inhibitor and DNA-damaging agent actinomycin D[53, 91, 95, 96], providing an assay for identifying key regulatory domains within TLS that control its localization and function. TLS may be functioning in DNA damage response pathways through its ability to regulate gene expression. Therefore, the regulatory domains controlling its association with the nucleolus may also be critical for its function in the DNA damage response.

7.3.1 TLS and sites of DNA damage and repair

To dynamically study the localization of TLS in the cell following DNA damage, an EGFP (enhanced green fluorescent protein)-FLAG-TLS construct was used. EGFP-FLAG-TLS is restricted to the nucleus and generally excluded from the nucleoli, consistent with what has been shown for endogenous TLS (our data and [91, 95, 96]). Furthermore, this construct rapidly relocalized to the nucleoli following transcriptional inhibition by actinomycin D, consistent with what has been shown previously for TLS[53, 91, 95, 96], and validating its use in assessing TLS localization following DNA damage.

The use of EGFP-FLAG-TLS allowed us to visualize additional TLS-containing structures in the form of perinucleolar foci, structures the antibody to TLS was unable to resolve because of the high endogenous levels of TLS found throughout the nucleoplasm. Preliminary evidence suggested that the number of these foci was increasing following γ-irradiation or mitomycin C treatment. Furthermore, in some cells, these TLS foci were

also present in micronuclei, structures that are associated with DNA damage[336]. Therefore, we wanted to determine whether these foci were actually sites of DNA damage/repair. Because the MEFs typically exhibited either zero to four foci, or many more than four foci, we quantified the number of cells with four or less foci and the number of cells with over four foci in untreated cells and cells exposed to γ-irradiation or treated with mitomycin C. The relative distribution of cells into these two groups did not change following treatment with γ-irradiation or mitomycin C, suggesting that these foci are not sites of DNA damage or repair. This finding does not preclude TLS being associated with sites of DNA damage/repair, because some proteins are only associated with sites of DNA damage in a modified form, phosphorylated H2AX[202, 203] for example. Furthermore, the critical repair protein DNA-PK is not retained at sites of DNA double-strand breaks[355], suggesting that observable relocalization to sites of DNA damage is not a prerequisite for involvement in DNA repair. However, given the association TLS has with gene expression, TLS may be functioning in the DNA repair pathways in this capacity, and if so it would not necessarily be expected to be maintained at sites of DNA damage or repair.

7.3.2 Perinucleolar foci containing TLS

The EGFP-FLAG-TLS foci were not found to increase in number following cellular exposure to γ-irradiation and mitomycin C, indicating that these foci probably do not represent sites of DNA damage. Another possibility is that these foci represent nuclear suborganelles containing TLS, the identification of which could help elucidate the function of TLS. The perinucleolar location of the majority of these suggested that they may correspond to Cajal bodies[98] or SMN-containing gems[105, 107], both of which are

nuclear suborganelles that localize near the nucleoli. Furthermore, TLS has been previously found to localize to Cajal bodies[108]. TLS also has an association with SMN, because both it and SMN associate with NFAR-2 (nuclear factor associated with dsRNA-)2[103]. However, the EGFP-FLAG-TLS foci did not correspond to either Cajal bodies or SMN-containing gems. It is possible that these structures are due to the expression of EGFP-FLAG-TLS; however, these structures were usually localized adjacent to nucleoli, and they disappeared following actinomycin D treatment, indicating that the TLS had been redistributed out of these structures into the nucleoplasm and/or the DNCs. Furthermore, many subnuclear structures are known to form through self-organization, with the presence of certain proteins seeding the formation of the structure[356]. Therefore, structures formed because of the presence of additional protein may still be functional. The identity of these structures and the other proteins they contain remain to be determined. Two other potential structures that the TLS foci could represent are the perinucleolar compartment (PNC) and Sam68 nuclear body[357]; however, both of these structures are more commonly found in transformed cells[357].

7.3.3 TLS and the nucleolus

TLS relocalizes to the nucleolus following treatment with actinomycin D[53, 91, 95, 96]. However, because actinomycin D is a DNA intercalator, it induces DNA damage as well as inhibits transcription[358-360]. To distinguish between a relocalization due to transcriptional inhibition or cellular stress caused by the DNA damage, we analyzed the nucleolar relocalization of TLS following exposure to the reversible transcriptional inhibitor DRB, and the DNA-damaging agents camptothecin, mitomycin C, γ-irradiation, and UV-irradiation. TLS nucleolar localization was observed following treatment with

the reversible transcriptional inhibitor DRB, which is consistent with what has been shown for TLS in the literature[53, 96]. TLS also relocalized to the nucleoli following exposure to the DNA damaging agents camptothecin and UV-irradiation, but not mitomycin C or γ-irradiation. Camptothecin is an inhibitor of topoisomerase I[331], an enzyme that makes and repairs single-strand breaks (SSBs) to relieve torsional strain in the DNA induced during processes such as transcription and DNA replication[332]. By inhibiting topoisomerase I, camptothecin will stabilize these SSBs, which could then be converted to DSBs during S phase[172]. However, because topoisomerase I function is required for transcription, camptothecin has also been associated with a rapid inhibition of transcriptional activity[331]. UV-irradiation, which induces cyclobutane pyrimidine dimers and pyrimidine (6-4) pyrimidone photoproducts, has also been associated with transcriptional inhibition[333-335]. On the other hand, no association of γ-irradiation with transcriptional inhibition has been reported in the literature. Mitomycin C does have the potential to inhibit transcription because of the interstrand cross-links it induces. However, the concentration we used to analyze the relocalization, while having significant down-stream repercussions as to proliferation potential, may not have induced enough ICLs to cause widespread transcriptional inhibition. The concentrations of actinomycin D used in this thesis to inhibit transcription are 8 times to 160 times those required to cause cell lethality[361], indicating that inducing general transcriptional inhibition does require a higher dose of actinomycin D than inducing toxic DNA damage. Overall, these results suggest that the relocalization of TLS to the nucleolus is due to transcriptional inhibition, and not because of cellular stress induced by DNA damage per se.

Currently, the function of this relocalization of TLS is unknown, but it is intriguing given the multifunctional nature of the nucleolus. Besides being the site of RNA polymerase I transcription of pre-rRNAs, pre-rRNA processing, and assembly of pre-ribosomes[98], the nucleolus is also the site of formation for some ribonucleoprotein complexes, including telomerase[99], and also functions in p53 activation and cell cycle regulation through MDM2 sequestration by ARF[101]. As I described in section **1.4**, the specific structures TLS relocalizes to following actinomycin D treatment have been identified as dark nucleolar caps (DNCs)[95]. Besides TLS, these structures also contain PSF, EWS, Cdk2, p54^{nrb}, the p68 helicase, hnRNP F, and U1-70K[95]. TLS, PSF, p54^{nrb} and U1-70K were previously found together, in addition to RNA polymerase II, TFIIF, and TFIIH, in joint transcription and splicing machinery complexes[88]. This suggests that most of the proteins in the DNCs had a relationship prior to their association in the DNCs, and that the DNCs may represent storage repositories of transcription/splicing factors during metabolic periods when transcription is shutdown. However, this localization is not a general trait of all RNA transcription and processing machinery, because RNA polymerase II, TFIIF, and TFIIH were not found in the DNCs[95].

There are periods in the cell cycle when transcription is shutdown. Specifically, transcription in the nucleolus is inhibited from the beginning of prophase to the end of anaphase, causing the nucleolus to disintegrate[100]. Therefore, it may not be completely unexpected that we observed nucleolar localization of EGFP-FLAG-TLS in 4% of untreated cells. This subpopulation of cells could represent late-G2 cells when the nucleoli are being decommissioned for mitosis, or early G1 cells when the nucleoli are being re-established in early G1. This subpopulation of cells exhibiting nucleolar TLS

could also represent cells that are stressed because of the culture conditions, but the nucleolar relocalization of TLS was not a general response to stress caused by DNA damage. Further experiments would be required to identify the reason for this nucleolar localization of TLS in untreated cells.

Finally, while pre-rRNAs were also found to colocalize with the DNCs[95] following transcriptional inhibition, TLS is not bound to these structure via DNA or RNA[96], and the RNA- and DNA-binding domains of TLS (the RRM, the RGG repeats, and the zinc finger) are not required for localization of TLS to these structures (our data and [96]). These data strongly suggest that the localization of TLS to these structures is through a protein-protein interaction.

7.3.4 Regulation of TLS localization to the nucleoli following transcriptional inhibition.

The dynamic relocalization of TLS to the nucleoli following transcriptional inhibition provides an assay that can be used to identify critical regulatory domains within TLS, potentially including those involved in its function within the DNA damage response pathways. To identify the sequence in TLS that regulates this relocalization to the DNCs following transcriptional inhibition, we made N-terminal deletion constructs of TLS. The N-terminus of TLS is an unstructured region[68] of SYGQQS-repeats. Therefore, sequential deletion of this region should not destroy any secondary or tertiary protein structure. We found that removing amino acids 1-138, but not amino acids 1-92, substantially reduced the association of TLS with the nucleolus following transcriptional inhibition. Removing amino acids 1-193 reduced this association even further. These results indicate that there is a minimal required sequence between amino acids 93-138 that can mediate the localization of TLS to the nucleolus.

The deletion of the first 138 (or 193) amino acids of TLS removes much of the N-terminus of TLS. To establish that the region between amino acids 93-138, or between amino acids 93-193 contains the domain regulating the relocalization, we analyzed the relocalization of internal deletions, specifically TLS(δ74-93), TLS(δ74-138), and TLS(δ74-193). Unexpectedly, even the largest internal deletion (TLS[δ74-193]) still strongly relocalized to the nucleoli following actinomycin D treatment, indicating that amino acids 1-74 can rescue the relocalization phenotype of TLS. Therefore, we have identified two sequences that can mediate the relocalization of TLS to the nucleoli: amino acids 1-73 and amino acids 93-193. Furthermore, even the C-terminal fragment of TLS (292-526) displayed a slight association with the nucleolus following actinomycin D treatment, albeit a far weaker association than that displayed by the N-terminal fragments (1-216 or 1-265). These data indicate that multiple regions of TLS can mediate an association with the nucleolus and the protein partner(s) that instigate and maintain this localization pattern.

Because two regions within the repetitive region of TLS (1-73 and 93-138) can mediate its association with the nucleoli, we rationalized that a domain that is repeated between these two regions regulates the relocalization. To identify a specific residue sequence that might be mediating the localization of TLS to the nucleoli, I used MultiAlign[338] to align amino acids 1-73 and the larger region of amino acids 93-193 of TLS. A motif of YGQQ is found in both sequences. A YGQQ motif does not correspond to any known functional or kinase-recognition motif, and may therefore represent a novel type of regulatory sequence. Amino acids 93-193 contain three of these YGQQ motifs. Further studies will be required to investigate whether this motif, alone or

in conjunction with the other conserved amino acids are mediating the localization of TLS to the nucleoli.

We initially speculated that phosphorylation events could be inducing the relocalization of TLS to the nucleoli, because of the prevalence of amino acids with the potential to be phosphorylated within the N-terminus of TLS. Our results also support this possibility, because the regions contained within amino acids 1-73 and amino acids 93-138 both include many phosphorylation sites, including SQ sites, which are potential targets of kinases such as ATM (Figure 4.8a). Furthermore, deleting amino acids 1-138 of TLS removes all of the SQ and TQ motifs, and most of the other potential phosphorylation sites, and we saw the most pronounced change in the ability to strongly relocalize between TLS(δ1-92) and TLS(δ1-138). Therefore, we are currently analyzing both the YGQQ motifs and the SQ motifs to investigate the regulation of TLS. For example, if phosphorylation of the SQ motifs regulates the association of TLS with the nucleoli, and if ATM is the kinase responsible, we will have directly placed TLS in the ATM-regulated DSB-signalling cascades.

7.3.5 TLS-ERG and TLS-CHOP and nucleolar localization

We have identified two key regulatory domains within TLS, amino acids 1-73 and amino acids 93-138, because both of these regions can mediate an association with the nucleoli following transcriptional inhibition. These domains are retained in the TLS-ERG and TLS-CHOP fusion oncoproteins. The formation of these oncogenic fusions is thought to be the primary causes of their associated cancers (myeloid leukemia and myxoid liposarcoma, respectively). However the exact mechanisms of oncogenesis remain ill-defined. To explore how these regulatory domains may be functioning in the

fusion proteins and oncogenesis, we evaluated the ability of the TLS-ERG fusion to relocalize to the nucleolus following actinomycin D treatment. We observed that EGFP-TLS-ERG does not relocalize to the nucleoli following transcriptional inhibition, suggesting that the ability to relocalize has been lost in the TLS-ERG fusion oncoprotein. In this fusion, the ETS DNA-binding domain or the proline-rich activation domain of ERG rather than the TLS N-terminus may be controlling the localization. Contrary to our observations of TLS-ERG, the TLS-CHOP fusion has been shown to relocalize to the nucleoli following actinomycin D treatment[96]. These data suggest that TLS may be functioning within TLS-CHOP and TLS-ERG, and the oncogenic pathways they initiate, in distinct ways.

7.4 Models for TLS function in the response to DNA damage

We have established that TLS is a novel DNA damage response protein, responding to both DNA double-strand breaks and interstrand cross-links. This finding has allowed us to begin studying the molecular mechanisms of TLS function, both in the MEFs and in the pre-B cells. The sensitivity of *TLS*$^{-/-}$ MEFs to DNA damage, observed in both the MTT assays and the checkpoint analysis, could be due to several reasons. First, TLS might function directly or indirectly in DNA repair. As discussed, there is evidence that TLS may function directly in repair via a role homologous recombination activity[64, 117]. However, we did not observe a global recruitment of TLS to sites of DNA damage and repair, indicating that TLS may not be specifically present at sites of repair. Furthermore, the DNA damage-induced apoptotic defect in the *TLS*$^{-/-}$ pre-B cells cannot be due to TLS exclusively functioning in DNA repair. TLS also dynamically relocalizes to the nucleoli following exposure to agents known to inhibit transcription (our data and

[91, 95, 96]). Finally, the majority of evidence in the literature suggests the TLS primarily functions through a role in transcription, mRNA splicing, and/or mRNA transport. Therefore, our observations and the data from the literature support a model in which TLS functions indirectly in repair, and in the DNA damage response in general, by the regulation of genes whose protein products are required in the DNA damage response (Figure 7.1). This gene regulation could be in a housekeeping capacity, or inducible following DNA damage. A role for TLS indirectly (or directly) in DNA repair might explain why TLS is highly expressed in proliferating cells, as most endogenous DNA damage occurs during S phase[173]. Therefore, potential transcriptional targets of TLS have been and are currently being investigated in the Hicks laboratory.

Warren Law utilized microarray technology to identify genes differentially expressed in $TLS^{-/-}$ and $TLS^{+/+}$ pre-B cells prior and post γ-irradiation, and found that $TLS^{-/-}$ pre-B cells upregulate Bfl-1 (Bcl2a1a; B-cell leukemia/lymphoma 2 related protein A1a) gene expression following γ-irradiation (Law and Hicks, unpublished results). The Bfl-1 protein has an anti-apoptotic function[362-364], providing one potential explanation why the $TLS^{-/-}$ pre-B cells were resistant to DNA damage-induced apoptosis. He also found that there was dysregulation of some p53 target genes, including p21, MDM2, NOXA and PUMA in the $TLS^{-/-}$ pre-B cells following γ-irradiation (Law and Hicks, unpublished results). NOXA and PUMA are both important pro-apoptotic p53-targets[298], providing additional explanations as to why $TLS^{-/-}$ pre-B cells were resistant to DNA damage-induced apoptosis. A similar microarray study with the $TLS^{-/-}$ MEFs has yet to be undertaken, but the Hicks laboratory is currently investigating whether genes found to be dysregulated in the $TLS^{-/-}$ pre-B cells are also

being dysregulated in the *TLS*$^{-/-}$ MEFs. Of note, the transcription factor and integral cell cycle checkpoint and apoptosis protein p53 is stabilized in both untreated *TLS*$^{-/-}$ MEFs and untreated *TLS*$^{-/-}$ pre-B cells (Klewes and Hicks, unpublished results), indicating that p53 might not be able to regulate its transcriptional targets properly in a *TLS*$^{-/-}$ background. Another heteronuclear ribonucleoprotein, hnRNP K, has been found to be a transcriptional coactivator of p53 following DNA damage[365], and TLS may function in a similar manner. TLS is a heteronuclear ribonucleoprotein, but it is not known whether TLS is complexed with specific RNAs in the cell, and this question provides one avenue of future research. Messenger RNAs complexed to RNA-binding proteins have been successfully identified using microarray technology[366]. A similar study with TLS before and after DNA damage would identify direct targets of TLS function.

Another potential reason for the sensitivity of *TLS*$^{-/-}$ MEFs to DNA damage is that these cells have an inherent susceptibility to DNA lesions that causes a given dose of γ-irradiation to induce more DSBs in *TLS*$^{-/-}$ MEFs than in wild-type MEFs. One possible way this could occur is through chromatin structure. A relatively relaxed chromatin structure would provide a larger surface area, and therefore larger target, for the γ-irradiation, potentially resulting in more strand-breaks. In a similar manner, relatively relaxed chromatin structure could also provide greater access to mitomycin C, causing more ICLs. We did observe that a higher molecular mass form of H2AX, possibly a monoubiquitinated form of H2AX, was more prevalent in *TLS*$^{-/-}$ MEFs than in *TLS*$^{+/+}$ MEFs, providing preliminary evidence that the chromatin structure in *TLS*$^{-/-}$ MEFs is in fact different from that in wild-type MEFs. TLS could be regulating a ubiquitin ligase, such as the BRCA1/BARD1 complex with which EWS is associated[118].

However, because *TLS*$^{-/-}$ MEFs only exhibited sensitivity to γ-irradiation and mitomycin C, and not UV-irradiation, the sensitivity is restricted to specific forms of DNA damage. Therefore, it does not represent a general sensitivity to all DNA damage through increased accessibility.

A third possibility is that the additional genomic damage already present in the *TLS*$^{-/-}$ MEFs complicates repair. For example, a joint research project between the Hicks and Mai laboratories is investigating whether TLS has a role in telomere maintenance, and preliminary evidence suggests that this is indeed the case. A role in telomere maintenance is completely consistent with a function in the DNA damage response, because these two cellular systems are intimately linked. Many DNA repair proteins, including pinnacle kinase ATM[367], have dual roles in telomere maintenance and the DNA damage response. Repair machinery must be able to distinguish between true DSBs and the actual ends of chromosomes when repairing damage, and the telomeres play an important role in maintaining and identifying the ends of chromosomes[368]. Therefore, if TLS does function in telomere maintenance, this function further links TLS to ATM and the DSB-signalling cascades. Finally, any telomeric abnormalities that were present in the *TLS*$^{-/-}$ MEFs could cause the chromosome ends to be identified as DSBs, providing additional unattached chromosome ends to a cell already overwhelmed by the DSBs induced by the γ-irradiation. However, this function would not explain the DNA damage-induced apoptotic resistance observed in the *TLS*$^{-/-}$ pre-B cells. Therefore, I believe that the defective cellular responses to DNA damage observed in both the *TLS*$^{-/-}$ MEFs and the *TLS*$^{-/-}$ pre-B cells are due to the dysregulation of TLS target genes (discussed above and shown in Figure 7.1).

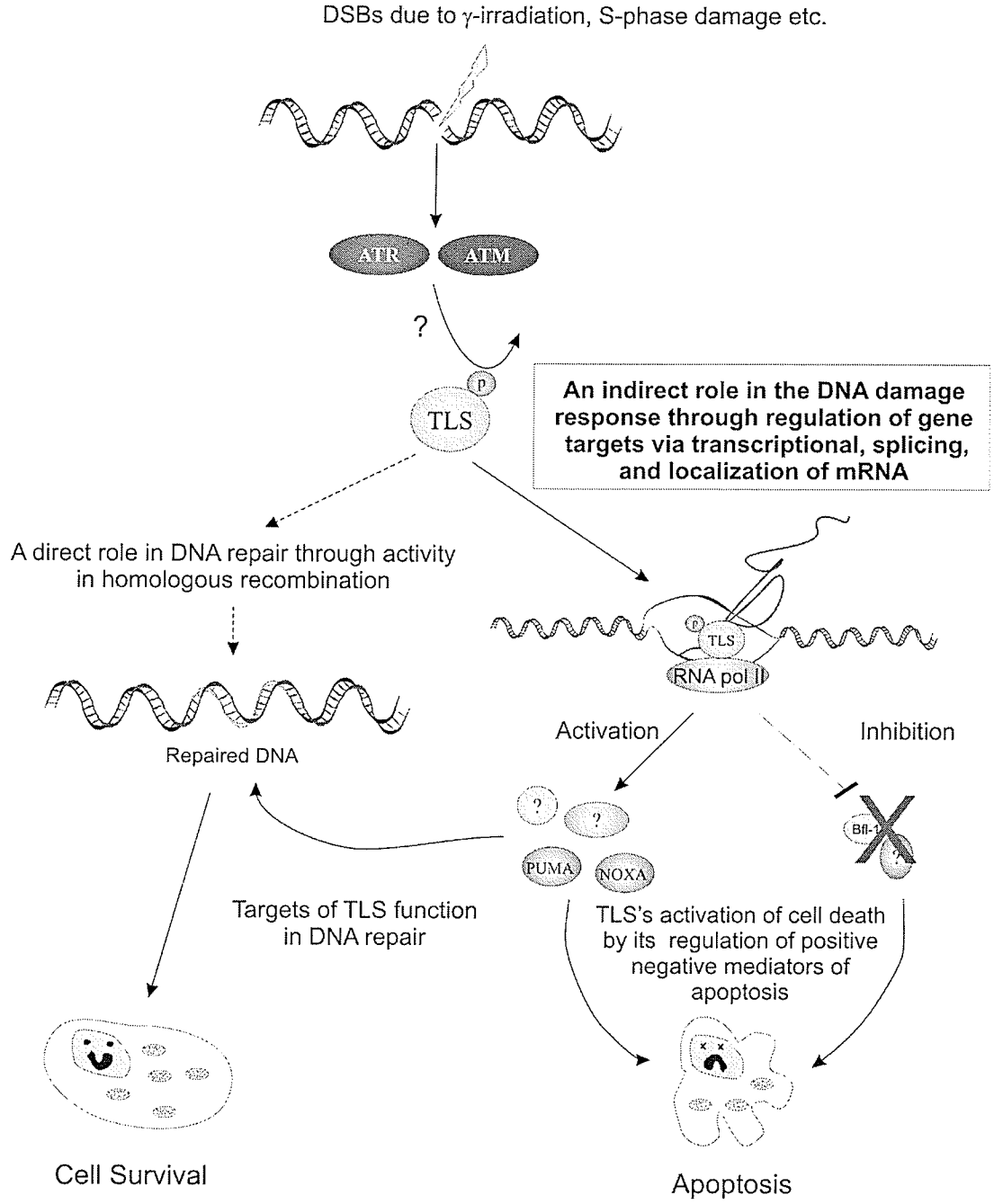

Figure 7.1: Models for TLS function in the DNA damage response. TLS may function in the DNA damage response pathways both directly, through a role in repair by homologous recombination, and indirectly through the regulation of DNA damage-induced gene expression. However, TLS function cannot be limited to a direct role in DNA repair, as this would not explain the apoptotic resistance observed in the *TLS* $^{-/-}$ pre-B cells. Furthermore, we did not observe recruitment of TLS to sites of DNA damage. Therefore, TLS probably functions predominantly through the regulation of gene expression.

7.5 TLS, DNA repair, and genomic stability

The hypothesis of this thesis was that TLS maintains genome stability through a role in DNA repair. The results presented in this thesis demonstrate that the function of TLS within the DNA damage response pathways goes beyond what we initially speculated. The data from the *TLS* $^{-/-}$ MEFs in which they exhibited sensitivity to DNA damaging agents in the MTT cytotoxicity assays and the checkpoint assays suggests that these cells may have error-prone repair, identifying an indirect or direct role for TLS in DNA repair. However, *TLS* $^{-/-}$ pre-B cells are defective in their ability to undergo DNA damage-induced apoptosis, a defect that cannot be due to TLS exclusively functioning in DNA repair. As I have discussed, the most likely model for TLS function within the DNA damage response is through the regulation of gene expression, which would suggest that TLS functions indirectly in DNA repair. Therefore, we can speculate that TLS regulates the expression of DNA repair genes.

Error-prone repair resulting from defects in the expression of DNA repair genes would result in genomic instability, and many of the chromosomal abnormalities observed in *TLS* $^{-/-}$ cells can be explained by error-prone repair, including aneuploidy, extrachromosomal elements, deletions, centromere loss, and chromosome fusion. Terminal chromosomal deletions, including centromere loss, can occur when a cell fails to repair a DSB[369-371]. Internal deletions and chromosome fusions can occur when mismatched broken chromosome ends are ligated together[369-371]. Gene amplification, which can lead to extrachromsomal elements, can also occur at sites of DNA repair through uncontrolled replication[372]. Finally, centromere loss could result in chromosome loss during the subquent mitosis, resulting in aneuploidy. In fact, defects in homologous

recombination have been shown to cause aneuploidy[373, 374]. Therefore, the results presented in this thesis are beginning to explain the genomic instability observed in the *TLS* $^{-/-}$ mice.

7.6 Insights into the role of TLS in the development of its associated cancers

The formation of a TLS-containing fusion oncoprotein, such as TLS-CHOP or TLS-ERG, is thought to be the primary cause of their associated cancers when it occurs; however, the exact mechanisms of TLS-associated oncogenesis are unknown. One proposed mechanism of oncogenesis is that these fusion oncoproteins function as aberrant transcription factors, interfering with the normal transcriptional regulation of the target genes of the fusion partner and/or recognizing new transcriptional targets[26, 27]. However, the N-terminus of TLS can still promote liposarcoma development in mice when it and CHOP are overexpressed as physically separate domains[59], suggesting that the N-terminus of TLS has a function separate from that of the fusion protein, and that it may function in a dominant-negative manner against the wild-type function of TLS or in a dominant-positive manner as a dysregulated version of TLS. (It is important to note that the presence of the N-terminus of TLS is required for oncogenesis, as mice only overexpressing CHOP do not develop liposarcoma[58].)

In the first scenario, the N-terminus of TLS would function in a dominant-negative manner to inhibit the wild-type function of TLS, initiating oncogenesis. If this is true, wild-type TLS would be a tumour suppressor, as its function would be required to prevent cancer development. One of the ways cells prevent cancer development is by maintaining genomic stability, thereby preventing mutagenesis[375, 376]. In fact, disruption of the prototypical tumour suppressor p53 leads to genomic instability in mouse

models[134, 135]. The Hicks TLS knock-out mouse model has shown that TLS is critical for the maintenance of genomic stability[111]. Therefore, TLS shares this attribute with p53. Another mouse model has also shown that the absence of TLS leads to IR sensitivity in both the whole mouse and MEFs, and chromosomal mispairing in premeiotic spermatocytes[116]. The results presented in this thesis have now shown that TLS is required for the proper biological response to both DSBs and ICLs in MEFs and pre-B cells, establishing a more specific role for TLS in DNA repair and genome maintenance. These data support a hypothesis in which the formation of the fusion proteins results in the disruption of the normal function of TLS in genome maintenance, promoting mutagenesis and cell transformation. If this scenario is correct, we can speculate on the steps involved in oncogenesis following the formation of the TLS fusion protein based on the model of TLS function in the DNA damage response proposed in Figure 7.1. First, TLS fusion-containing cells would be further stressed by the presence of DNA damage, such as that occurring every S phase. The TLS fusion (such as TLS-CHOP) would then function in a dominant-negative manner to prevent the activation of TLS-regulated genes required for both DNA repair and apoptosis. In such a scenario, the cells would not be able to properly repair the damage, or undergo apoptosis, leading to mutagenesis, and eventually oncogenesis by double-hit when cells with additional mutations driving cell proliferation are generated. In support of this hypothesis, TLS-ERG-driven leukemic transformation of normal human hematopoietic cells includes the accumulation of additional spontaneous mutations[52, 377], potentially identifying a mutator phenotype. While myxoid liposarcoma cells are not associated with gross chromosomal changes, with the obvious exception of the t(12;16)(q13;p11) translocation that generates the TLS-

CHOP fusion[7], this does not exclude the possibility that the expression of TLS-CHOP has accelerated other mutations that promote oncogenesis.

If TLS is functioning as a classical tumour suppressor, we can make several predictions. We would expect that loss-of-heterozygosity at the TLS loci would be observed in cancer cells with TLS-fusions, that there would be *TLS* $^{-/-}$ tumours, and that carriers of *TLS* mutations would exhibit cancer predisposition. However, no loss-of-heterozygosity has been reported for any TLS-associated cancer, although if the TLS fusions are functioning dominantly over wild-type TLS, mutation of the other copy of TLS may not be required for oncogenesis. Furthermore, we have not observed that heterozygous mice (*TLS* $^{+/-}$) exhibit cancer predisposition (data not shown). Therefore, a simple knock-out of TLS function may not initiate oncogenesis, or some function of TLS may be required for continued proliferation. For example, as *TLS* $^{-/-}$ mice are not viable[111], the *TLS* $^{-/-}$ genotype may also eventually be lethal to cancer cells as well.

The question of whether TLS can function as tumour suppressor has yet to be addressed directly. To test this hypothesis, the system developed in John Dick's laboratory to study the human leukemic program induced by TLS-ERG[52, 377] could be used to assess whether the absence of TLS induces leukemia, in either human hematopoietic cells by using small interference RNA to TLS, or in mouse hematopoietic cells of *TLS* $^{+/+}$, *TLS* $^{+/-}$, and *TLS* $^{-/-}$ genotypes. If TLS is functioning as a classical tumour suppressor, we would expect to see leukemia develop in TLS-deficient hematopoietic stem cells. In heterozygotes, we would expect to see a loss-of-heterozygosity at the TLS loci, which would then lead to an increased number of mutations, and the earlier-onset development of leukemia.

Ultimately, we would also need to investigate whether the TLS-fusions can interefere with wild-type TLS function. One simple assay to address this issue would be to analyze whether TLS-ERG can prevent endogenous TLS from relocalizing to the nucleolus following transcriptional inhibition, as we have observed that TLS-ERG itself does not relocalize to the nucleoli. If TLS-ERG can prevent TLS from dynamically relocalizing to the nucleoli, we could speculate that it is also interfering with the wild-type function of TLS in DNA repair and genome maintenance. Furthermore, once TLS gene targets in the DNA damage response pathways have been identified, the regulation and expression of these targets in TLS-associated cancers could be analyzed to better identify how the TLS fusions are affecting TLS function within these pathways.

The alternative hypothesis of TLS-associated oncogenesis is that the N-terminus of TLS functions as a dominant-positive, either having acquired novel functions or behaving as a dysregulated TLS. In support of this hypothesis, increased expression of TLS is associated with both proliferation and an undifferentiated state[60-64]. Therefore, a dominant-positive TLS may promote proliferation through uncontrolled upregulation of genes required during the cell cycle. In fact, the RGG repeats of EWS have been shown to have an inhibitory effect on the transcriptional activity of EWS[76]. If TLS were regulated in a similar manner, the lack of all or most of the RGG repeats in the fusions oncoproteins would potentially result in dysregulated expression of TLS target genes, or the recognition of novel genes. We would not expect that dysregulation in a dominant-positive manner of the function of TLS in the DNA damage response would promote oncogensis, as increased DNA repair or apoptosis following DNA damage would not initiate mutagenesis. However, there could be a function of TLS associated with its role

in DNA repair, such as a putative role in telomere maintenance, that when dysregulated in a positive manner allows cells to immortalize.

It is important to note that dominant-negative and dominant-positive functions of the N-terminus of TLS are not necessarily mutually exclusive. In fact, the N-terminus of TLS may function both as a dominant-negative against TLS's function in genome maintenance and as a dominant-positive with respect to its role in promoting proliferation and preventing differentiation. Therefore, TLS may be both a proto-oncogene and a tumour suppressor. In support of this hypothesis, the Ku heterodimer has been shown to be both an oncogene, as overexpression leads to hyperproliferation and apoptotic resistance, and a tumour suppressor, as underexpression leads to genomic instability[378], indicating that proteins can be an oncogene or a tumour suppressor depending on expression and/or regulation.

Finally, while the data indicates that the N-terminus of TLS has a function independent of its fusion partner in promoting oncogenesis[59], it is important to note that the abnormal expression of the TET fusion partner is also required for the development of the TLS-associated cancers. In fact, it is the TET fusion partner that seems to dictate the cell-specificity of the cancers; for example, CHOP in myxoid liposarcoma and ATF-1 in angiomatoid fibrous hystiocytoma (see Table 1.1). Furthermore, mice ubiquitously expressing a TLS-CHOP construct specifically develop myxoid liposaroma, but do not exhibit susceptibility to other cancers[57, 58]. Therefore, when considering the oncogenic properties of the N-terminus of TLS, we must also consider the contribution of its fusion partner.

7.7 Absence of an immediate G1/S checkpoint in primary MEFs following γ-irradiation identifies a novel checkpoint switch.

Cancer is prevented by both genomic caretakers, proteins that help repair or prevent DNA damage, and cell gatekeepers, proteins that regulate progression through the cell cycle or the induction of apoptosis[149]. Regulation of the cell cycle following DNA damage is controlled by the cell cycle checkpoints, specifically the G1/S, the intra-S-phase, and the G2/M checkpoints. Therefore, in order to understand how cells prevent cancer, we need to understand the regulation of these checkpoints. The G1/S checkpoint prevents cells from entering into S phase with DNA damage, and the current model of the G1/S checkpoint is that of a two-wave response: p53-independent pathways initiating an immediate G1 block, and a delayed p53-dependent arrest[237]. The classic p53-dependent G1/S checkpoint manifests itself as an overall decrease in S-phase cells observable 13-24 h post-ionizing-irradiation (IR) using BrdU labelling[245, 246], and is regulated by an ATM-p53-p21-Cdk2 pathway[125] that can prevent both origin licensing[242, 243] and firing[244]. Because this pathway requires both the transcription and translation of p21, it is not believed to induce an immediate block to S phase entry[237]. Following IR, immediate G1/S checkpoint pathways are thought to block progression into S phase even if the cell has passed the restriction point, the point at which a cell no longer requires growth factors to enter S phase and complete the cell cycle[237]. However, analysis of the immediate G1/S checkpoint at the cellular level has been hampered by an inability to distinguish cells that had been replicating DNA at the time of γ-irradiation from cells that had entered S phase following γ-irradiation. The classic method of analyzing the G1/S checkpoint uses BrdU labelling, which only analyzes the total percentage of S-phase cells[255]. While this method has its advantages, it cannot be used to measure the immediate G1/S checkpoint.

Analysis of the immediate G1/S checkpoint requires the ability to measure the percentage of cells that have progressed from G1 into S phase following DNA damage, or the G1/S transition percentage. To measure this G1/S transition percentage, I have developed a novel strategy using a CldU (5-chloro-2'-deoxyuridine) and IdU (5-iodo-2'-deoxyuridine) staggered double-labelling approach (described in detail in section **6.1**). This strategy has allowed us to assess the G1/S and S/G2 transitions within a 3 h time period following γ-irradiation. The assay does not require that cells be synchronized, so the cells should be progressing through G1 with no alteration to normal replication origin licensing.

Contrary to the current model of the G1/S checkpoint, we have demonstrated that 65% of late-G1 primary MEFs continued to progress into S phase after a dose of 5 Gy, indicating that the majority of late-G1 MEFs do not initiate an immediate G1/S checkpoint. MEFs treated with a high dose of 10 Gy also failed to arrest in G1, as 46% of late-G1 primary MEFs still progressed into S-phase. This absence of an immediate checkpoint was not due to an overall failure of the G1/S checkpoint, as the delayed G1/S checkpoint was induced in these cells, and upregulation of p53 and p21 protein levels were observed within 1 h following a dose of 5 Gy. Furthermore, a G2/M checkpoint was induced in over 90% of the MEFs that would have gone into mitosis within 1 h following a dose of 5 Gy. This checkpoint was maintained until at least 6 h post-exposure, a time point by which there was a visible decrease in H2AX phosphorylation levels. In addition, the MEFs did exhibit an intra-S-phase replication slow-down, as the S/G2 transition percentage decreased by 23% following 5 Gy, and by 31% following 10 Gy. Finally, at 6 h, the γ-irradiated MEFs exhibited a G1 percentage that was 76% of the

mock-irradiated control, indicating that more cells had left than entered G1 during this time period, and supporting our initial observation that primary MEFs do not induce an immediate G1/S checkpoint. A dose of 5 Gy does have significant downstream repercussions to the proliferation potential of MEFs, as the surviving cell fraction of γ-irradiated MEFs is only 0.12 of mock-irradiated cells. Therefore, the inability of the majority of late-G1, low-passage, primary MEFs to prevent entry into S phase suggests that they are no longer responsive to the signals that induce the G1/S checkpoint, despite there being sufficient damage.

Like the primary MEFs, the commonly-cultured, immortalized cell line HeLa did not induce an immediate G1/S checkpoint, validating the observations in the primary MEFs. In fact, the HeLa cells promoted S-phase entry after doses of both 5 Gy and 10 Gy. This induced G1/S transition was also seen as an increased normalized S-phase percentage measured at 1 h and 6 h post-γ-irradiation. The HeLa cells were capable of inducing the delayed G1/S checkpoint. In agreement with our data, Murata et al. have also shown that following γ-irradiation HeLa cells initially promote entry into S phase, but then proceed to induce a delayed G1 block[348]. The HeLa cells exhibited a strong intra-S-phase checkpoint, and were capable of inducing a G2/M checkpoint within 1 h, and maintaining it through 6 h. Therefore, the primary MEFs and the HeLa cell line exhibit the same general pattern of checkpoint control, specifically they do not activate an immediate G1/S checkpoint, but they do induce a delayed G1/S checkpoint, an intra-S-phase checkpoint, and a rapid and sustained G2/M checkpoint.

A possible reason for this inability of late-G1 cells to halt progression into S phase following DNA damage can be found in our understanding of replication origin

licensing, maturation, and firing. As a cell progresses through G1, origins are licensed for replication through the formation of pre-replicative complexes (pre-RCs)[281]. The transition from G1 to S phase can be defined by the activation of the first replication origin, but it is necessarily separate from the activation of other origins, as origin firing is staggered throughout S phase[276]. How late-G1 replication origins differ from unfired S-phase origins is unknown, but because of the asynchronous nature of origin firing, we can assume that (1) at some stage of origin maturation regulation becomes origin-specific, and (2) this transition must occur prior to S phase entry. The definitive event that activates individual replication origins has not been identified, but two kinases, Cdk2 and Cdc7, are considered the S-phase-promoting kinases, and at least one other protein, Cdc45, is involved in post-licensing origin maturation and activation[281].

In a similar fashion, checkpoint regulation is thought to switch from global regulation in G1 to origin-specific regulation in S phase. Once a cell begins S phase, it must complete replication, otherwise a partially replicated genome that is incapable of undergoing an error-free mitosis would result. Furthermore, S-phase cells must have some degree of tolerance for DSBs, because up to fifty of these lesions occur during a normal S phase[172]. If a cell stopped S phase after a DSB, it would never be able to complete replication, so cells must balance a timely completion of S phase with the need to prevent origin firing near detected damage. The DNA damage-response kinases ATM and/or ATR are active throughout S phase[258, 259], and control both the timing and spacing of origin firing via feedback from active replicons even in the absence of DNA damage[260, 261]. Therefore, ATM and ATR are poised to quickly down-regulate unfired origins in the event of DNA damage. After IR, the intra-S-phase checkpoint manifests

itself as an ATM-dependent down-regulation of DNA synthesis[257] that is at least partially mediated through an inhibition of origin firing[256].

The model that can be developed from our data is that the switch between using a G1/S checkpoint and using origin-specific regulation actually occurs during late G1. This checkpoint switch probably occurs concomitantly with the normal transition from global control of origin maturation to origin-specific regulation that occurs prior to S phase entry, and even potentially with the restriction point. Further studies will be required to identify the level of origin maturation and the specific origin components required for this switch in checkpoint usage. However, we can speculate that the global control of origins is effected through overexpression of licensing factors, and the switch to origin specific regulation occurs when origin-limiting factors are expressed. For example, global licensing factors such as Cdc6 and Cdt1 may be overexpressed within the cell. As the replication origins are saturated, and the levels of free Cdc6 and Cdt1 rise, the expression of an origin-limiting factor may be triggered, initiating the checkpoint switch. Origin-limiting factors would regulate the rate of replication, preventing cells from exhausting nucleotide pools and energy before they can be replenished, and allowing cells to regulate origins near DNA damage.

The lag time between this checkpoint switch and the entry into S phase may be variable between cell types. Cells that induce this switch close to the time of S phase entry would be expected to have a more severe reduction in the G1/S transition following IR than cells with a longer lag time before S phase entry. In HeLa cells, the promotion of S-phase entry after γ-irradiation may have been due to both a larger population of cells that had already switched to using origin-specific regulation, and early, abnormal origin

firing in this population. HeLa cells express the viral oncoproteins E6 and E7, which inhibit p53[379] and pRB[380] function, respectively. While the delayed, p53-dependent G1/S checkpoint was induced in HeLa cells, further experiments would be required to investigate whether the E6 or E7 protein was contributing to this premature S phase entry.

Our labelling strategy has allowed us to quantify G1/S and S/G2 transitions following γ-irradiation in asynchronous, low passage, primary MEF cultures. The observed absence of an immediate G1/S checkpoint in the primary MEFs suggests a model in which cells switch to using origin-specific regulation in late G1 (Figure 7.2). If a cell did not switch its use of checkpoints at the same time as replication origins become individually regulated, it would run the risk of having unintended DNA synthesis at a time when the cell can no longer complete S phase. If even one origin erroneously fires after a signal for a complete G1/S block is initiated, damage in the form of an amplified segment of DNA may result. By switching the checkpoint control in late-G1 from the G1/S block to using origin-specific regulation, the cell would be able to minimize any permanent damage by repairing DSBs at the same time as it progresses into S phase. A more permanent arrest could then be initiated in G2, if necessary. (This thesis work and model has recently been published[306].)

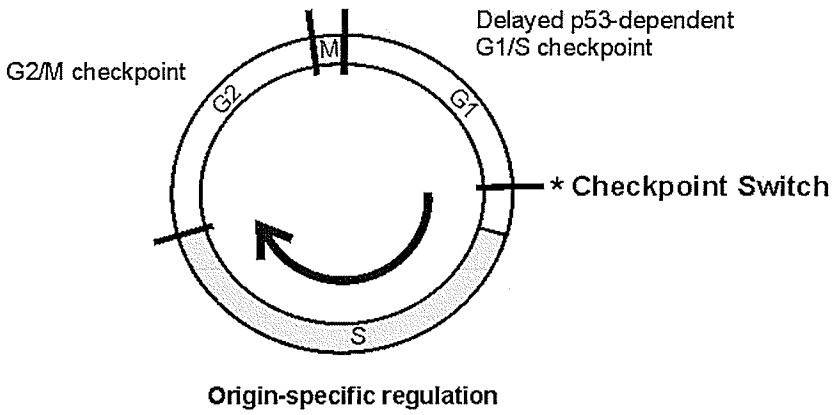

Figure 7.2: The proposed model of checkpoint regulation in mammalian cells. As G1 cells progress towards S phase, they pass a point where they can no longer initiate a global shutdown of S phase entry when confronted with DNA double-strand breaks. Instead, they may predominantly respond to DNA damage, like cells already in S phase, at the level of individual replication origins.

7.9 Conclusions and Significance

The hypothesis of this thesis was that TLS helps maintain genomic stability through a role in DNA repair. The work presented in this thesis has shown that TLS is a multifunctional protein required for an effective biological response to both DNA double-strand breaks and interstrand cross-links in MEFs. Therefore, we have identified TLS as a novel member of a group of proteins required for the repair of both DSBs and ICLs, including FANCD2[146], NBS1[138, 139, 142], ATR[164, 165, 262], BRCA1[119, 132], and BRCA2[121, 131, 132]. The sensitivity of *TLS* $^{-/-}$ MEFs to DSBs is not due checkpoint failure, and instead probably represents an inherent susceptibility to DNA damage and/or an error-prone repair. Error-prone repair would explain most of the abnormal karyotypes observed in the *TLS* $^{-/-}$ MEFs, including aneuploidy, extrachromosomal elements, chromosome breakage, centromere loss, and chromosome fusion. Futhermore, TLS exhibits a duality of function reminiscent of ATM, as it is also required for induction of apoptosis following DNA damage in the form of DSBs, ICLs, and cyclobutane pyrimidine dimers

and pyrimidine (6-4) pyrimidone photoproducts in pre-B cells. The most likely model for TLS function in the DNA damage response is through the regulation of genes whose protein products function directly in these pathways (Figure 7.1). The work presented in this thesis has also resulted in the identification of two regulatory regions in TLS (amino acids 1-73 and 93-193) that can mediate its association with the nucleolus, a nuclear suborganelle associated with cell cycle regulation and the maturation of ribonucleoprotein complexes.

These observations are providing novel insights into how the wild-type function of TLS may be contributing to the oncogenesis of its associated cancers. The roles of hnRNPs in regulating cellular processes are not as well-defined as those of canonical transcription factors, and further investigation of how TLS functions will lead to a better understanding of how cells maintain genomic stability, repair DNA, and prevent cell transformation.

Perhaps the most significant finding presented in this thesis is that the majority of late-G1, low-passage, primary wild-type MEFs cannot induce an immediate G1/S checkpoint following γ-irradiation, a finding that contradicts the current model of the G1/S checkpoint. The observed absence of an immediate G1/S checkpoint in these primary cells identifies a novel control point in late-G1 at which cells switch from using a global G1/S checkpoint to using origin-specific regulation in response to DNA damage (Figure 7.2). This model provides a significant contribution to our general understanding of the mammalian cell cycle, and how it is regulated following DNA damage. Furthermore, cell cycle dysregulation is a common characteristic of cancer cells;

therefore, this model, and also the G1/S checkpoint assay that I have developed, will ultimately provide further insights into oncogenesis.

7.9 Future Directions

7.9.1 Analysis of TLS function

TLS$^{-/-}$ mice exhibit characteristics consistently found in mouse models of the human genomic instability syndromes AT[112-114] and NBS[115], specifically genomic instability[111], immune system defects[111], and sensitivity to ionizing irradiation[116]. The causative genes of these syndromes are involved in the DNA damage response pathways (repair, cell cycle checkpoints, and/or apoptosis. We have now shown that TLS is also a DNA damage response protein, required for the induction of apoptosis following DNA damage, and potentially preventing an inherent susceptibility to DNA damage and/or error prone repair. These findings are allowing us to now investigate TLS at a molecular level, specifically its regulation and functions within the DNA damage response pathways.

The data presented in this thesis have identified several putative points of regulation for TLS. We were able to identify two minimum localization domains within TLS that can mediate its relocalization to the nucleolus following transcriptional inhibition, including candidate sequences within these regions and potential post-translational modifications. Comparison of the amino acid sequences between these two regions found a common YGQQ sequence. This sequence may represent a novel regulatory motif, and mutation analysis of this motif would identify whether it is critical for relocalization. Another possibility is that the SQ motifs are functional ATM phosphorylation targets, and phosphorylation may be driving the relocalization of TLS.

If this is the case, we should be able to directly place TLS in the DNA damage response signalling pathways. Indeed, the Hicks laboratory is now investigating the possibility that TLS is a direct phosphorylation target of ATM, ATR, or DNA-PK as part of a recently funded NCIC grant. The repetitive nature of this region, and the presence of many other potential phosphorylation sites, has complicated this analysis, but the deletion constructs produced, and the regulatory regions identified during the course of this thesis work will aid in the identification of the critical phosphorylation sites.

Finally, another point of regulation for TLS that should be analyzed is the methylation of the RGG repeats. The RGG-repeat regions of both EWS[76] and TLS[77] can be extensively methylated. Furthermore, the RGG-repeats of EWS can also repress transcriptional activity[78]. Therefore, we can hypothesize that TLS would also share this characteristic, identifying another regulatory target for TLS. Arginine methylation in arginine and glycine-rich regions has been shown to be critical for the function of both 53BP1 and Mre11 in the DNA damage response pathways[381-384]. Further studies should be done to identify the significance of this methylation to TLS function and its interaction with other proteins.

Our strategy to identify a functional role of TLS in the DSB response was to interrogate the expected biological responses activated in the ATM-mediated DSB-signalling cascades. We observed that the sensitivity of the *TLS* $^{-/-}$ MEFs to DSBs is not due to checkpoint failure, and instead represents an inherent susceptibility to DNA damage and/or error-prone repair. The presence of potentially monoubiquitinated H2AX in *TLS* $^{-/-}$ MEFs provides a potential cause for an inherent susceptibility to DNA, as histone modifications such as this could fundamentally alter the chromatin structure

within these cells. Further investigation into the overall chromatin structure by examining the prevalence of histone modifications found in the *TLS*$^{-/-}$ MEFs could identify physical differences in the chromosomes of these cells when compared to those of wild-type cells. This investigation could identify specific epigenetic changes in chromatin structure that predispose to DNA damage, potentially identifying a novel mechanism by which cells maintain genomic stability. Preliminary discussions with the laboratory of Dr. J. Davie regarding the best approaches to address a chromatin hypothesis are underway.

Next, to investigate whether there is error-prone repair in *TLS*$^{-/-}$ MEFs, one potential avenue of research would be to assess the genomic aberrations induced in the *TLS*$^{-/-}$ MEFs following γ-irradiation as compared to those induced in wild-type cells. Spectral karyotyping analysis in the pre-B cells has been informative; however, given the inherent genomic damage found in these cells, this approach has been difficult to analyze. The Hicks laboratory is currently developing low passage, *TLS*$^{-/-}$ embryonic stem cells, and we expect that these cells will allow us to circumvent this problem in using E14.5 day MEFs or the pre-B cell lines.

Finally, the majority of evidence in the literature suggests that TLS primarily functions through a role in transcription, mRNA splicing, and/or mRNA transport. In this capacity, TLS might modulate expression of genes whose protein products are directly involved in the DNA damage response[385]. Therefore, identifying specific targets of TLS function would be pivotal to understanding its molecular function within the DNA damage response pathways. We already have preliminary evidence that the transcription factor and cell gatekeeper p53 is unable to function normally in both the *TLS*$^{-/-}$ pre-B

cells and MEFs (Klewes and Hicks). Furthermore, analysis of the gene expression profiles of the *TLS* $^{-/-}$ and wild-type cells has been used successfully in the Hicks laboratory to identify transcriptional targets of TLS, including p53 target genes (Law and Hicks).

However, differences in the regulation of mRNA splicing and translation would not necessarily be identified using mRNA expression profiles. Another avenue of investigation would be to analyze of the RNA-binding partners of TLS using a ribonomics approach, as it would identify direct targets of TLS function, inclusive and exclusive of its role in the cellular DNA damage response. Once these targets have been identified, the *TLS* $^{-/-}$ and *TLS* $^{+/+}$ MEFs would provide an excellent system for analyzing changes in the splicing and/or translation of these specific genes.

The results presented in this thesis are allowing us to begin analyzing the function of TLS in the DNA damage response pathways at a molecular level. Ultimately, this investigation will identify novel ways by which cells maintain genomic stability, repair DNA, and prevent cancer development.

7.9.2 Further analysis of the G1/S checkpoint

The novel G1/S checkpoint assay I developed has allowed us to directly analyze changes in the G1/S and S/G2 transitions immediately following DNA damage within asynchronous cell cultures. The classic method for analyzing the G1/S checkpoint used single BrdU-labelling, and could not directly measure these important changes to the cell cycle. Therefore, my novel assay provides a biologically relevant model of how actively cycling cells actually respond to DNA damage. In fact, this assay has already allowed us to make a significant contribution to our general understanding of the mammalian cell

cycle, and how it is regulated following DNA damage. Our finding that late-G1, primary MEFs are unable to stop progression into S phase following γ-irradiation identified a novel control point in late-G1 at which cells switch from using a global G1/S checkpoint to using origin-specific regulation in response to DNA damage. This assay has not only identified new questions with respect to the regulation of the cell cycle, such as which proteins are governing this checkpoint switch, but also provides a tool for answering questions already in the literature. For example, this assay could be used to tease out the relative contributions of proteins such as p53 and Cdc25a in regulating the G1/S and S/G2 transitions following DNA damage.

In the discussion, I described a model for the checkpoint switch in which high levels of free global licensing factors, occurring following origin saturation, trigger the expression/activation of origin-limiting factors, effectively switching checkpoint use from the G1/S checkpoint to origin-specific regulation. If this model is correct, we can make specific predictions. For example, free pools of global licensing factors, with Cdc6 and Cdt1 as potential condidates, should be detectable in late G1. Furthermore, free global licensing factors would act as coactivators for transcription factors, kinases, and/or replication factors. If the switch occurs by the relative expression levels of various origin licensing/maturation factors, we would not expect cells deficient in these proteins to be viable, as the cells would not be able to produce mature replication origins or replicate DNA, and temperature sensitive mutants would arrest in G1 under denaturing conditions. Therefore, the most informative avenue for investigating the proposed checkpoint switch would be to further elucidate the proteins involved in origin licensing, maturation and

firing, and their interactions with each other and components of the DNA damage checkpoint pathways.

Ultimately, these avenues of investigation will lead to a more profound understanding of the basic biological processes that regulate DNA repair, genome maintenance, and cell cycle checkpoints. All of these systems are critical for individual cells and for whole organisms, as they govern the fidelity of inheritance between mother and daughter cells, and also parent and offspring. These processes are critical for proper development, and also for the prevention of cancer. Because most therapies for treating cancers kill rapidly cycling cells by damaging DNA, and thereby inducing mitotic catastrophe or programmed cell death, these avenues of investigation may also lead to more effective treatments of these diseases.

Chapter 8: References

1. Calvio, C., Neubauer, G., Mann, M. & Lamond, A.I. Identification of hnRNP P2 as TLS/FUS using electrospray mass spectrometry. *Rna* **1**, 724-733 (1995).
2. Crozat, A., Aman, P., Mandahl, N. & Ron, D. Fusion of CHOP to a novel RNA-binding protein in human myxoid liposarcoma. *Nature* **363**, 640-644 (1993).
3. Rabbitts, T.H., Forster, A., Larson, R. & Nathan, P. Fusion of the dominant negative transcription regulator CHOP with a novel gene FUS by translocation t(12;16) in malignant liposarcoma. *Nat Genet* **4**, 175-180 (1993).
4. Ichikawa, H., Shimizu, K., Hayashi, Y. & Ohki, M. An RNA-binding protein gene, TLS/FUS, is fused to ERG in human myeloid leukemia with t(16;21) chromosomal translocation. *Cancer Res* **54**, 2865-2868 (1994).
5. Panagopoulos, I. *et al.* Fusion of the FUS gene with ERG in acute myeloid leukemia with t(16;21)(p11;q22). *Genes Chromosomes Cancer* **11**, 256-262 (1994).
6. Delattre, O. *et al.* Gene fusion with an ETS DNA-binding domain caused by chromosome translocation in human tumours. *Nature* **359**, 162-165 (1992).
7. Gibas, Z. *et al.* Cytogenetic and immunohistochemical profile of myxoid liposarcoma. *Am J Clin Pathol* **103**, 20-26 (1995).
8. Mertens, F. *et al.* Clinicopathologic and molecular genetic characterization of low-grade fibromyxoid sarcoma, and cloning of a novel FUS/CREB3L1 fusion gene. *Lab Invest* **85**, 408-415 (2005).
9. Zucman, J. *et al.* Combinatorial generation of variable fusion proteins in the Ewing family of tumours. *Embo J* **12**, 4481-4487 (1993).
10. Shimizu, Y. *et al.* Novel breakpoints of the EWS gene and the WT1 gene in a desmoplastic small round cell tumor. *Cancer Genet Cytogenet* **106**, 156-158 (1998).
11. Panagopoulos, I., Mandahl, N., Mitelman, F. & Aman, P. Two distinct FUS breakpoint clusters in myxoid liposarcoma and acute myeloid leukemia with the translocations t(12;16) and t(16;21). *Oncogene* **11**, 1133-1137 (1995).
12. Panagopoulos, I., Mertens, F., Isaksson, M. & Mandahl, N. A novel FUS/CHOP chimera in myxoid liposarcoma. *Biochem Biophys Res Commun* **279**, 838-845 (2000).
13. Gerald, W.L., Rosai, J. & Ladanyi, M. Characterization of the genomic breakpoint and chimeric transcripts in the EWS-WT1 gene fusion of desmoplastic small round cell tumor. *Proc Natl Acad Sci U S A* **92**, 1028-1032 (1995).
14. Panagopoulos, I. *et al.* Molecular genetic characterization of the EWS/ATF1 fusion gene in clear cell sarcoma of tendons and aponeuroses. *Int J Cancer* **99**, 560-567 (2002).
15. Waters, B.L., Panagopoulos, I. & Allen, E.F. Genetic characterization of angiomatoid fibrous histiocytoma identifies fusion of the FUS and ATF-1 genes induced by a chromosomal translocation involving bands 12q13 and 16p11. *Cancer Genet Cytogenet* **121**, 109-116 (2000).

16. Raddaoui, E., Donner, L.R. & Panagopoulos, I. Fusion of the FUS and ATF1 Genes in a Large, Deep-Seated Angiomatoid Fibrous Histiocytoma. *Diagn Mol Pathol* **11**, 157-162 (2002).
17. Storlazzi, C.T. *et al.* Fusion of the FUS and BBF2H7 genes in low grade fibromyxoid sarcoma. *Hum Mol Genet* **12**, 2349-2358 (2003).
18. Shing, D.C. *et al.* FUS/ERG gene fusions in Ewing's tumors. *Cancer Res* **63**, 4568-4576 (2003).
19. Kong, X.T. *et al.* Consistent detection of TLS/FUS-ERG chimeric transcripts in acute myeloid leukemia with t(16;21)(p11;q22) and identification of a novel transcript. *Blood* **90**, 1192-1199 (1997).
20. Antonescu, C.R. *et al.* Specificity of TLS-CHOP rearrangement for classic myxoid/round cell liposarcoma: absence in predominantly myxoid well-differentiated liposarcomas. *J Mol Diagn* **2**, 132-138 (2000).
21. Dei Tos, A.P. Liposarcoma: new entities and evolving concepts. *Ann Diagn Pathol* **4**, 252-266 (2000).
22. Sorensen, P.H. *et al.* A second Ewing's sarcoma translocation, t(21;22), fuses the EWS gene to another ETS-family transcription factor, ERG. *Nat Genet* **6**, 146-151 (1994).
23. Khoury, J.D. Ewing sarcoma family of tumors. *Adv Anat Pathol* **12**, 212-220 (2005).
24. Ferro, M.R. *et al.* t(16;21) in a Ph positive CML. *Cancer Genet Cytogenet* **60**, 210-211 (1992).
25. Kanazawa, T. *et al.* TLS/FUS-ERG fusion gene in acute lymphoblastic leukemia with t(16;21)(p11;q22) and monitoring of minimal residual disease. *Leuk Lymphoma* **46**, 1833-1835 (2005).
26. Ladanyi, M. The emerging molecular genetics of sarcoma translocations. *Diagn Mol Pathol* **4**, 162-173 (1995).
27. Ron, D. TLS-CHOP and the role of RNA-binding proteins in oncogenic transformation. *Curr Top Microbiol Immunol* **220**, 131-142 (1997).
28. Perez-Mancera, P.A. & Sanchez-Garcia, I. Understanding mesenchymal cancer: the liposarcoma-associated FUS-DDIT3 fusion gene as a model. *Semin Cancer Biol* **15**, 206-214 (2005).
29. Jeon, I.S. *et al.* A variant Ewing's sarcoma translocation (7;22) fuses the EWS gene to the ETS gene ETV1. *Oncogene* **10**, 1229-1234 (1995).
30. Kaneko, Y. *et al.* Fusion of an ETS-family gene, EIAF, to EWS by t(17;22)(q12;q12) chromosome translocation in an undifferentiated sarcoma of infancy. *Genes Chromosomes Cancer* **15**, 115-121 (1996).
31. Urano, F., Umezawa, A., Hong, W., Kikuchi, H. & Hata, J. A novel chimera gene between EWS and E1A-F, encoding the adenovirus E1A enhancer-binding protein, in extraosseous Ewing's sarcoma. *Biochem Biophys Res Commun* **219**, 608-612 (1996).
32. Peter, M. *et al.* A new member of the ETS family fused to EWS in Ewing tumors. *Oncogene* **14**, 1159-1164 (1997).
33. Panagopoulos, I. *et al.* Fusion of the EWS and CHOP genes in myxoid liposarcoma. *Oncogene* **12**, 489-494 (1996).

34. Zucman, J. *et al.* EWS and ATF-1 gene fusion induced by t(12;22) translocation in malignant melanoma of soft parts. *Nat Genet* **4**, 341-345 (1993).
35. Hallor, K.H. *et al.* Fusion of the EWSR1 and ATF1 genes without expression of the MITF-M transcript in angiomatoid fibrous histiocytoma. *Genes Chromosomes Cancer* **44**, 97-102 (2005).
36. Ladanyi, M. & Gerald, W. Fusion of the EWS and WT1 genes in the desmoplastic small round cell tumor. *Cancer Res* **54**, 2837-2840 (1994).
37. Rauscher, F.J., 3rd, Benjamin, L.E., Fredericks, W.J. & Morris, J.F. Novel oncogenic mutations in the WT1 Wilms' tumor suppressor gene: a t(11;22) fuses the Ewing's sarcoma gene, EWS1, to WT1 in desmoplastic small round cell tumor. *Cold Spring Harb Symp Quant Biol* **59**, 137-146 (1994).
38. Mastrangelo, T. *et al.* A novel zinc finger gene is fused to EWS in small round cell tumor. *Oncogene* **19**, 3799-3804 (2000).
39. Yamaguchi, S. *et al.* EWSR1 is fused to POU5F1 in a bone tumor with translocation t(6;22)(p21;q12). *Genes Chromosomes Cancer* **43**, 217-222 (2005).
40. Labelle, Y. *et al.* Oncogenic conversion of a novel orphan nuclear receptor by chromosome translocation. *Hum Mol Genet* **4**, 2219-2226 (1995).
41. Martini, A. *et al.* Recurrent rearrangement of the Ewing's sarcoma gene, EWSR1, or its homologue, TAF15, with the transcription factor CIZ/NMP4 in acute leukemia. *Cancer Res* **62**, 5408-5412 (2002).
42. Attwooll, C. *et al.* Identification of a novel fusion gene involving hTAFII68 and CHN from a t(9;17)(q22;q11.2) translocation in an extraskeletal myxoid chondrosarcoma. *Oncogene* **18**, 7599-7601 (1999).
43. Sjogren, H., Meis-Kindblom, J., Kindblom, L.G., Aman, P. & Stenman, G. Fusion of the EWS-related gene TAF2N to TEC in extraskeletal myxoid chondrosarcoma. *Cancer Res* **59**, 5064-5067 (1999).
44. Zagars, G.K., Goswitz, M.S. & Pollack, A. Liposarcoma: outcome and prognostic factors following conservation surgery and radiation therapy. *Int J Radiat Oncol Biol Phys* **36**, 311-319 (1996).
45. Kuby, J. *Immunology*, Edn. Third Edition. (W. H. Freeman and Company, New York; 1997).
46. Hayashi, Y. The molecular genetics of recurring chromosome abnormalities in acute myeloid leukemia. *Semin Hematol* **37**, 368-380 (2000).
47. *Canadian Cancer Statistics 2006*. (Canadian Cancer Society/National Cancer Institute of Canada, Toronto, Canada; 2006).
48. Ichikawa, H., Shimizu, K., Katsu, R. & Ohki, M. Dual transforming activities of the FUS (TLS)-ERG leukemia fusion protein conferred by two N-terminal domains of FUS (TLS). *Mol Cell Biol* **19**, 7639-7650 (1999).
49. Kanoe, H. *et al.* Characteristics of genomic breakpoints in TLS-CHOP translocations in liposarcomas suggest the involvement of Translin and topoisomerase II in the process of translocation. *Oncogene* **18**, 721-729 (1999).
50. Zoubek, A. *et al.* Variability of EWS chimaeric transcripts in Ewing tumours: a comparison of clinical and molecular data. *Br J Cancer* **70**, 908-913 (1994).
51. Kuroda, M. *et al.* Oncogenic transformation and inhibition of adipocytic conversion of preadipocytes by TLS/FUS-CHOP type II chimeric protein. *Am J Pathol* **151**, 735-744 (1997).

52. Pereira, D.S. *et al.* Retroviral transduction of TLS-ERG initiates a leukemogenic program in normal human hematopoietic cells. *Proc Natl Acad Sci U S A* **95**, 8239-8244 (1998).
53. Zinszner, H., Albalat, R. & Ron, D. A novel effector domain from the RNA-binding protein TLS or EWS is required for oncogenic transformation by CHOP. *Genes Dev* **8**, 2513-2526 (1994).
54. Goransson, M. *et al.* Myxoid liposarcoma FUS-DDIT3 fusion oncogene induces C/EBP beta-mediated interleukin 6 expression. *Int J Cancer* **115**, 556-560 (2005).
55. Engstrom, K. *et al.* The Myxoid/Round Cell Liposarcoma Fusion Oncogene *FUS-DDIT3* and the Normal *DDIT3* Induce Liposarcoma Phenotype in Transfected Human Fibrosarcoma Cells. *American Journal of Pathology* **168**, 1642-1653 (2006).
56. Zou, J. *et al.* The oncogenic TLS-ERG fusion protein exerts different effects in hematopoietic cells and fibroblasts. *Mol Cell Biol* **25**, 6235-6246 (2005).
57. Perez-Losada, J. *et al.* The chimeric FUS/TLS-CHOP fusion protein specifically induces liposarcomas in transgenic mice. *Oncogene* **19**, 2413-2422 (2000).
58. Perez-Losada, J. *et al.* Liposarcoma initiated by FUS/TLS-CHOP: the FUS/TLS domain plays a critical role in the pathogenesis of liposarcoma. *Oncogene* **19**, 6015-6022 (2000).
59. Perez-Mancera, P.A. *et al.* Expression of the FUS domain restores liposarcoma development in CHOP transgenic mice. *Oncogene* **21**, 1679-1684 (2002).
60. Perrotti, D. *et al.* TLS/FUS, a pro-oncogene involved in multiple chromosomal translocations, is a novel regulator of BCR/ABL-mediated leukemogenesis. *Embo J* **17**, 4442-4455 (1998).
61. Perrotti, D. *et al.* BCR-ABL prevents c-jun-mediated and proteasome-dependent FUS (TLS) proteolysis through a protein kinase CbetaII-dependent pathway. *Mol Cell Biol* **20**, 6159-6169 (2000).
62. Perrotti, D. & Calabretta, B. Post-transcriptional mechanisms in BCR/ABL leukemogenesis: role of shuttling RNA-binding proteins. *Oncogene* **21**, 8577-8583 (2002).
63. Alliegro, M.C. & Alliegro, M.A. A nuclear protein regulated during the transition from active to quiescent phenotype in cultured endothelial cells. *Dev Biol* **174**, 288-297 (1996).
64. Bertrand, P., Akhmedov, A.T., Delacote, F., Durrbach, A. & Lopez, B.S. Human POMp75 is identified as the pro-oncoprotein TLS/FUS: both POMp75 and POMp100 DNA homologous pairing activities are associated to cell proliferation. *Oncogene* **18**, 4515-4521 (1999).
65. Mills, K.I. *et al.* High FUS/TLS expression in acute myeloid leukaemia samples. *Br J Haematol* **108**, 316-321 (2000).
66. Morohoshi, F. *et al.* Genomic structure of the human RBP56/hTAFII68 and FUS/TLS genes. *Gene* **221**, 191-198 (1998).
67. Immanuel, D., Zinszner, H. & Ron, D. Association of SARFH (sarcoma-associated RNA-binding fly homolog) with regions of chromatin transcribed by RNA polymerase II. *Mol Cell Biol* **15**, 4562-4571 (1995).
68. Iko, Y. *et al.* Domain architectures and characterization of an RNA-binding protein, TLS. *J Biol Chem* **279**, 44834-44840 (2004).

69. Aman, P. *et al.* Expression patterns of the human sarcoma-associated genes FUS and EWS and the genomic structure of FUS. *Genomics* **37**, 1-8 (1996).
70. Prasad, D.D., Ouchida, M., Lee, L., Rao, V.N. & Reddy, E.S. TLS/FUS fusion domain of TLS/FUS-erg chimeric protein resulting from the t(16;21) chromosomal translocation in human myeloid leukemia functions as a transcriptional activation domain. *Oncogene* **9**, 3717-3729 (1994).
71. Sanchez-Garcia, I. & Rabbitts, T.H. Transcriptional activation by TAL1 and FUS-CHOP proteins expressed in acute malignancies as a result of chromosomal abnormalities. *Proc Natl Acad Sci U S A* **91**, 7869-7873 (1994).
72. Yang, L., Embree, L.J. & Hickstein, D.D. TLS-ERG leukemia fusion protein inhibits RNA splicing mediated by serine-arginine proteins. *Mol Cell Biol* **20**, 3345-3354 (2000).
73. Chansky, H.A., Hu, M., Hickstein, D.D. & Yang, L. Oncogenic TLS/ERG and EWS/Fli-1 fusion proteins inhibit RNA splicing mediated by YB-1 protein. *Cancer Res* **61**, 3586-3590 (2001).
74. Lerga, A. *et al.* Identification of an RNA binding specificity for the potential splicing factor TLS. *J Biol Chem* **276**, 6807-6816 (2001).
75. Birney, E., Kumar, S. & Krainer, A.R. Analysis of the RNA-recognition motif and RS and RGG domains: conservation in metazoan pre-mRNA splicing factors. *Nucleic Acids Res* **21**, 5803-5816 (1993).
76. Belyanskaya, L.L., Gehrig, P.M. & Gehring, H. Exposure on cell surface and extensive arginine methylation of ewing sarcoma (EWS) protein. *J Biol Chem* **276**, 18681-18687 (2001).
77. Rappsilber, J., Friesen, W.J., Paushkin, S., Dreyfuss, G. & Mann, M. Detection of arginine dimethylated peptides by parallel precursor ion scanning mass spectrometry in positive ion mode. *Analytical chemistry* **75**, 3107-3114 (2003).
78. Alex, D. & Lee, K.A. RGG-boxes of the EWS oncoprotein repress a range of transcriptional activation domains. *Nucleic Acids Res* **33**, 1323-1331 (2005).
79. Bertolotti, A., Lutz, Y., Heard, D.J., Chambon, P. & Tora, L. hTAF(II)68, a novel RNA/ssDNA-binding protein with homology to the pro-oncoproteins TLS/FUS and EWS is associated with both TFIID and RNA polymerase II. *Embo J* **15**, 5022-5031 (1996).
80. Uranishi, H. *et al.* Involvement of the pro-oncoprotein TLS (translocated in liposarcoma) in nuclear factor-kappa B p65-mediated transcription as a coactivator. *J Biol Chem* **276**, 13395-13401 (2001).
81. Powers, C.A., Mathur, M., Raaka, B.M., Ron, D. & Samuels, H.H. TLS (translocated-in-liposarcoma) is a high-affinity interactor for steroid, thyroid hormone, and retinoid receptors. *Mol Endocrinol* **12**, 4-18 (1998).
82. Kucharczak, J., Simmons, M.J., Fan, Y. & Gelinas, C. To be, or not to be: NF-kappaB is the answer--role of Rel/NF-kappaB in the regulation of apoptosis. *Oncogene* **22**, 8961-8982 (2003).
83. Janssens, S. & Tschopp, J. Signals from within: the DNA-damage-induced NF-kappaB response. *Cell Death Differ* (2006).
84. Hallier, M., Lerga, A., Barnache, S., Tavitian, A. & Moreau-Gachelin, F. The transcription factor Spi-1/PU.1 interacts with the potential splicing factor TLS. *J Biol Chem* **273**, 4838-4842 (1998).

85. Delva, L. *et al.* Multiple functional domains of the oncoproteins Spi-1/PU.1 and TLS are involved in their opposite splicing effects in erythroleukemic cells. *Oncogene* **23**, 4389-4399 (2004).
86. Sato, S. *et al.* beta-catenin interacts with the FUS proto-oncogene product and regulates pre-mRNA splicing. *Gastroenterology* **129**, 1225-1236 (2005).
87. Rapp, T.B., Yang, L., Conrad, E.U., 3rd, Mandahl, N. & Chansky, H.A. RNA splicing mediated by YB-1 is inhibited by TLS/CHOP in human myxoid liposarcoma cells. *J Orthop Res* **20**, 723-729 (2002).
88. Kameoka, S., Duque, P. & Konarska, M.M. p54(nrb) associates with the 5' splice site within large transcription/splicing complexes. *Embo J* **23**, 1782-1791 (2004).
89. Yang, L., Embree, L.J., Tsai, S. & Hickstein, D.D. Oncoprotein TLS interacts with serine-arginine proteins involved in RNA splicing. *J Biol Chem* **273**, 27761-27764 (1998).
90. Meissner, M., Lopato, S., Gotzmann, J., Sauermann, G. & Barta, A. Proto-oncoprotein TLS/FUS is associated to the nuclear matrix and complexed with splicing factors PTB, SRm160, and SR proteins. *Exp Cell Res* **283**, 184-195 (2003).
91. Zinszner, H., Sok, J., Immanuel, D., Yin, Y. & Ron, D. TLS (FUS) binds RNA in vivo and engages in nucleo-cytoplasmic shuttling. *J Cell Sci* **110 (Pt 15)**, 1741-1750 (1997).
92. Fujii, R. *et al.* The RNA binding protein TLS is translocated to dendritic spines by mGluR5 activation and regulates spine morphology. *Curr Biol* **15**, 587-593 (2005).
93. Belly, A., Moreau-Gachelin, F., Sadoul, R. & Goldberg, Y. Delocalization of the multifunctional RNA splicing factor TLS/FUS in hippocampal neurones: exclusion from the nucleus and accumulation in dendritic granules and spine heads. *Neurosci Lett* **379**, 152-157 (2005).
94. de Hoog, C.L., Foster, L.J. & Mann, M. RNA and RNA binding proteins participate in early stages of cell spreading through spreading initiation centers. *Cell* **117**, 649-662 (2004).
95. Shav-Tal, Y. *et al.* Dynamic sorting of nuclear components into distinct nucleolar caps during transcriptional inhibition. *Mol Biol Cell* **16**, 2395-2413 (2005).
96. Zinszner, H., Immanuel, D., Yin, Y., Liang, F.X. & Ron, D. A topogenic role for the oncogenic N-terminus of TLS: nucleolar localization when transcription is inhibited. *Oncogene* **14**, 451-461 (1997).
97. Sobell, H.M. Actinomycin and DNA transcription. *Proc Natl Acad Sci U S A* **82**, 5328-5331 (1985).
98. Dundr, M. & Misteli, T. Functional architecture in the cell nucleus. *Biochem J* **356**, 297-310 (2001).
99. Etheridge, K.T. *et al.* The nucleolar localization domain of the catalytic subunit of human telomerase. *J Biol Chem* **277**, 24764-24770 (2002).
100. Sirri, V., Hernandez-Verdun, D. & Roussel, P. Cyclin-dependent kinases govern formation and maintenance of the nucleolus. *J Cell Biol* **156**, 969-981 (2002).
101. Weber, J.D., Taylor, L.J., Roussel, M.F., Sherr, C.J. & Bar-Sagi, D. Nucleolar Arf sequesters Mdm2 and activates p53. *Nat Cell Biol* **1**, 20-26 (1999).

102. Andersen, J.S. *et al.* Directed proteomic analysis of the human nucleolus. *Curr Biol* **12**, 1-11 (2002).
103. Saunders, L.R. *et al.* Characterization of two evolutionarily conserved, alternatively spliced nuclear phosphoproteins, NFAR-1 and -2, that function in mRNA processing and interact with the double-stranded RNA-dependent protein kinase, PKR. *J Biol Chem* **276**, 32300-32312 (2001).
104. Gubitz, A.K., Feng, W. & Dreyfuss, G. The SMN complex. *Exp Cell Res* **296**, 51-56 (2004).
105. Young, P.J., Le, T.T., thi Man, N., Burghes, A.H. & Morris, G.E. The relationship between SMN, the spinal muscular atrophy protein, and nuclear coiled bodies in differentiated tissues and cultured cells. *Exp Cell Res* **256**, 365-374 (2000).
106. Hebert, M.D., Szymczyk, P.W., Shpargel, K.B. & Matera, A.G. Coilin forms the bridge between Cajal bodies and SMN, the spinal muscular atrophy protein. *Genes Dev* **15**, 2720-2729 (2001).
107. Carvalho, T. *et al.* The spinal muscular atrophy disease gene product, SMN: A link between snRNP biogenesis and the Cajal (coiled) body. *J Cell Biol* **147**, 715-728 (1999).
108. Alliegro, M.C. & Alliegro, M.A. Identification of a new coiled body component. *Exp Cell Res* **231**, 386-390 (1997).
109. Liu, J. *et al.* Cell cycle-dependent localization of the CDK2-cyclin E complex in Cajal (coiled) bodies. *J Cell Sci* **113 (Pt 9)**, 1543-1552 (2000).
110. Hicks, G.G. *et al.* Functional genomics in mice by tagged sequence mutagenesis. *Nat Genet* **16**, 338-344 (1997).
111. Hicks, G.G. *et al.* Fus deficiency in mice results in defective B-lymphocyte development and activation, high levels of chromosomal instability and perinatal death. *Nat Genet* **24**, 175-179 (2000).
112. Barlow, C. *et al.* Atm-deficient mice: a paradigm of ataxia telangiectasia. *Cell* **86**, 159-171 (1996).
113. Elson, A. *et al.* Pleiotropic defects in ataxia-telangiectasia protein-deficient mice. *Proc Natl Acad Sci U S A* **93**, 13084-13089 (1996).
114. Xu, Y. *et al.* Targeted disruption of ATM leads to growth retardation, chromosomal fragmentation during meiosis, immune defects, and thymic lymphoma. *Genes Dev* **10**, 2411-2422 (1996).
115. Kang, J., Bronson, R.T. & Xu, Y. Targeted disruption of NBS1 reveals its roles in mouse development and DNA repair. *Embo J* **21**, 1447-1455 (2002).
116. Kuroda, M. *et al.* Male sterility and enhanced radiation sensitivity in TLS(-/-) mice. *Embo J* **19**, 453-462 (2000).
117. Baechtold, H. *et al.* Human 75-kDa DNA-pairing protein is identical to the pro-oncoprotein TLS/FUS and is able to promote D-loop formation. *J Biol Chem* **274**, 34337-34342 (1999).
118. Spahn, L. *et al.* Interaction of the EWS NH2 terminus with BARD1 links the Ewing's sarcoma gene to a common tumor suppressor pathway. *Cancer Res* **62**, 4583-4587 (2002).
119. Yoshida, K. & Miki, Y. Role of BRCA1 and BRCA2 as regulators of DNA repair, transcription, and cell cycle in response to DNA damage. *Cancer Sci* **95**, 866-871 (2004).

120. Hoeijmakers, J.H. Genome maintenance mechanisms for preventing cancer. *Nature* **411**, 366-374 (2001).
121. O'Driscoll, M. & Jeggo, P.A. The role of double-strand break repair - insights from human genetics. *Nat Rev Genet* **7**, 45-54 (2006).
122. Shiloh, Y. ATM and related protein kinases: safeguarding genome integrity. *Nat Rev Cancer* **3**, 155-168 (2003).
123. Savitsky, K. *et al.* A single ataxia telangiectasia gene with a product similar to PI-3 kinase. *Science* **268**, 1749-1753 (1995).
124. Daboussi, F., Dumay, A., Delacote, F. & Lopez, B. DNA double-strand break repair signalling: The case of RAD51 post-translational regulation. *Cell Signal* **14**, 969 (2002).
125. Dasika, G.K. *et al.* DNA damage-induced cell cycle checkpoints and DNA strand break repair in development and tumorigenesis. *Oncogene* **18**, 7883-7899 (1999).
126. Khanna, K.K. & Jackson, S.P. DNA double-strand breaks: signaling, repair and the cancer connection. *Nat Genet* **27**, 247-254 (2001).
127. Kurz, E.U. & Lees-Miller, S.P. DNA damage-induced activation of ATM and ATM-dependent signaling pathways. *DNA Repair (Amst)* **3**, 889-900 (2004).
128. Shechter, D., Costanzo, V. & Gautier, J. Regulation of DNA replication by ATR: signaling in response to DNA intermediates. *DNA Repair (Amst)* **3**, 901-908 (2004).
129. O'Driscoll, M., Gennery, A.R., Seidel, J., Concannon, P. & Jeggo, P.A. An overview of three new disorders associated with genetic instability: LIG4 syndrome, RS-SCID and ATR-Seckel syndrome. *DNA Repair (Amst)* **3**, 1227-1235 (2004).
130. van den Bosch, M., Bree, R.T. & Lowndes, N.F. The MRN complex: coordinating and mediating the response to broken chromosomes. *EMBO Rep* **4**, 844-849 (2003).
131. D'Andrea, A.D. The Fanconi road to cancer. *Genes Dev* **17**, 1933-1936 (2003).
132. Kennedy, R.D. & D'Andrea, A.D. The Fanconi Anemia/BRCA pathway: new faces in the crowd. *Genes Dev* **19**, 2925-2940 (2005).
133. Varley, J. TP53, hChk2, and the Li-Fraumeni syndrome. *Methods Mol Biol* **222**, 117-129 (2003).
134. Donehower, L.A. *et al.* Mice deficient for p53 are developmentally normal but susceptible to spontaneous tumours. *Nature* **356**, 215-221 (1992).
135. Fukasawa, K., Wiener, F., Vande Woude, G.F. & Mai, S. Genomic instability and apoptosis are frequent in p53 deficient young mice. *Oncogene* **15**, 1295-1302 (1997).
136. Theunissen, J.W. *et al.* Checkpoint failure and chromosomal instability without lymphomagenesis in Mre11(ATLD1/ATLD1) mice. *Mol Cell* **12**, 1511-1523 (2003).
137. Williams, B.R. *et al.* A murine model of Nijmegen breakage syndrome. *Curr Biol* **12**, 648-653 (2002).
138. Nijmegen breakage syndrome. The International Nijmegen Breakage Syndrome Study Group. *Arch Dis Child* **82**, 400-406 (2000).
139. Petrini, J.H. The Mre11 complex and ATM: collaborating to navigate S phase. *Curr Opin Cell Biol* **12**, 293-296 (2000).

140. Stewart, G.S. *et al.* The DNA double-strand break repair gene hMRE11 is mutated in individuals with an ataxia-telangiectasia-like disorder. *Cell* **99**, 577-587 (1999).
141. Taylor, A.M., Groom, A. & Byrd, P.J. Ataxia-telangiectasia-like disorder (ATLD)-its clinical presentation and molecular basis. *DNA Repair (Amst)* **3**, 1219-1225 (2004).
142. Nakanishi, K. *et al.* Interaction of FANCD2 and NBS1 in the DNA damage response. *Nat Cell Biol* **4**, 913-920 (2002).
143. Zhu, J., Petersen, S., Tessarollo, L. & Nussenzweig, A. Targeted disruption of the Nijmegen breakage syndrome gene NBS1 leads to early embryonic lethality in mice. *Curr Biol* **11**, 105-109 (2001).
144. Reina-San-Martin, B., Nussenzweig, M.C., Nussenzweig, A. & Difilippantonio, S. Genomic instability, endoreduplication, and diminished Ig class-switch recombination in B cells lacking Nbs1. *Proc Natl Acad Sci U S A* **102**, 1590-1595 (2005).
145. Houghtaling, S. *et al.* Epithelial cancer in Fanconi anemia complementation group D2 (Fancd2) knockout mice. *Genes Dev* **17**, 2021-2035 (2003).
146. Taniguchi, T. *et al.* Convergence of the fanconi anemia and ataxia telangiectasia signaling pathways. *Cell* **109**, 459-472 (2002).
147. Lewin, B. *Genes VII.* (Oxford University Press, Oxford; 2000).
148. Lehninger, A., Nelson, D.L. & Cox, M.M. *Principles of Biochemistry*, Edn. Second Edition. (Worth Publishers, New York, NY; 1993).
149. Kinzler, K.W. & Vogelstein, B. Cancer-susceptibility genes. Gatekeepers and caretakers. *Nature* **386**, 761, 763 (1997).
150. Li, L. & Zou, L. Sensing, signaling, and responding to DNA damage: organization of the checkpoint pathways in mammalian cells. *J Cell Biochem* **94**, 298-306 (2005).
151. Zhou, B.B. & Elledge, S.J. The DNA damage response: putting checkpoints in perspective. *Nature* **408**, 433-439 (2000).
152. Niida, H. & Nakanishi, M. DNA damage checkpoints in mammals. *Mutagenesis* **21**, 3-9 (2006).
153. Sancar, A., Lindsey-Boltz, L.A., Unsal-Kacmaz, K. & Linn, S. Molecular mechanisms of mammalian DNA repair and the DNA damage checkpoints. *Annu Rev Biochem* **73**, 39-85 (2004).
154. Lukas, J., Lukas, C. & Bartek, J. Mammalian cell cycle checkpoints: signalling pathways and their organization in space and time. *DNA Repair (Amst)* **3**, 997-1007 (2004).
155. Wood, R.D. DNA repair in eukaryotes. *Annu Rev Biochem* **65**, 135-167 (1996).
156. Stojic, L., Brun, R. & Jiricny, J. Mismatch repair and DNA damage signalling. *DNA Repair (Amst)* **3**, 1091-1101 (2004).
157. Ura, K. & Hayes, J.J. Nucleotide excision repair and chromatin remodeling. *Eur J Biochem* **269**, 2288-2293 (2002).
158. Andreassen, P.R., Ho, G. & D'Andrea, A.D. DNA damage responses and their many interactions with the replication fork. *Carcinogenesis* (2006).
159. Dronkert, M.L. & Kanaar, R. Repair of DNA interstrand cross-links. *Mutat Res* **486**, 217-247 (2001).

160. Bizanek, R., McGuinness, B.F., Nakanishi, K. & Tomasz, M. Isolation and structure of an intrastrand cross-link adduct of mitomycin C and DNA. *Biochemistry* **31**, 3084-3091 (1992).
161. Bizanek, R. *et al.* Adducts of mitomycin C and DNA in EMT6 mouse mammary tumor cells: effects of hypoxia and dicumarol on adduct patterns. *Cancer Res* **53**, 5127-5134 (1993).
162. McHugh, P.J., Spanswick, V.J. & Hartley, J.A. Repair of DNA interstrand crosslinks: molecular mechanisms and clinical relevance. *Lancet Oncol* **2**, 483-490 (2001).
163. Rothfuss, A. & Grompe, M. Repair kinetics of genomic interstrand DNA cross-links: evidence for DNA double-strand break-dependent activation of the Fanconi anemia/BRCA pathway. *Mol Cell Biol* **24**, 123-134 (2004).
164. Bobabilla-Morales, L. *et al.* Chromosome instability induced in vitro with mitomycin C in five Seckel syndrome patients. *Am J Med Genet A* **123**, 148-152 (2003).
165. Andreassen, P.R., D'Andrea, A.D. & Taniguchi, T. ATR couples FANCD2 monoubiquitination to the DNA-damage response. *Genes Dev* **18**, 1958-1963 (2004).
166. Niedernhofer, L.J., Lalai, A.S. & Hoeijmakers, J.H. Fanconi anemia (cross)linked to DNA repair. *Cell* **123**, 1191-1198 (2005).
167. Montes de Oca, R. *et al.* Regulated interaction of the Fanconi anemia protein, FANCD2, with chromatin. *Blood* **105**, 1003-1009 (2005).
168. Taniguchi, T. *et al.* S-phase-specific interaction of the Fanconi anemia protein, FANCD2, with BRCA1 and RAD51. *Blood* **100**, 2414-2420 (2002).
169. Pichierri, P., Averbeck, D. & Rosselli, F. DNA cross-link-dependent RAD50/MRE11/NBS1 subnuclear assembly requires the Fanconi anemia C protein. *Hum Mol Genet* **11**, 2531-2546 (2002).
170. Wang, X. *et al.* Involvement of nucleotide excision repair in a recombination-independent and error-prone pathway of DNA interstrand cross-link repair. *Mol Cell Biol* **21**, 713-720 (2001).
171. Zheng, H. *et al.* Nucleotide excision repair- and polymerase eta-mediated error-prone removal of mitomycin C interstrand cross-links. *Mol Cell Biol* **23**, 754-761 (2003).
172. Vilenchik, M.M. & Knudson, A.G. Endogenous DNA double-strand breaks: production, fidelity of repair, and induction of cancer. *Proc Natl Acad Sci U S A* **100**, 12871-12876 (2003).
173. Rothkamm, K. & Lobrich, M. Evidence for a lack of DNA double-strand break repair in human cells exposed to very low x-ray doses. *Proc Natl Acad Sci U S A* **100**, 5057-5062 (2003).
174. Rothkamm, K., Kuhne, M., Jeggo, P.A. & Lobrich, M. Radiation-induced genomic rearrangements formed by nonhomologous end-joining of DNA double-strand breaks. *Cancer Res* **61**, 3886-3893 (2001).
175. Povirk, L.F. DNA damage and mutagenesis by radiomimetic DNA-cleaving agents: bleomycin, neocarzinostatin and other enediynes. *Mutat Res* **355**, 71-89 (1996).

176. Karagiannis, T.C. & El-Osta, A. Double-strand breaks: signaling pathways and repair mechanisms. *Cell Mol Life Sci* **61**, 2137-2147 (2004).
177. Roti Roti, J.L. & Wright, W.D. Visualization of DNA loops in nucleoids from HeLa cells: assays for DNA damage and repair. *Cytometry* **8**, 461-467 (1987).
178. Jaberaboansari, A., Nelson, G.B., Roti Roti, J.L. & Wheeler, K.T. Postirradiation alterations of neuronal chromatin structure. *Radiat Res* **114**, 94-104 (1988).
179. Malyapa, R.S., Wright, W.D., Taylor, Y.C. & Roti Roti, J.L. DNA supercoiling changes and nuclear matrix-associated proteins: possible role in oncogene-mediated radioresistance. *Int J Radiat Oncol Biol Phys* **35**, 963-973 (1996).
180. Bakkenist, C.J. & Kastan, M.B. DNA damage activates ATM through intermolecular autophosphorylation and dimer dissociation. *Nature* **421**, 499-506 (2003).
181. Lee, J.H. & Paull, T.T. ATM activation by DNA double-strand breaks through the Mre11-Rad50-Nbs1 complex. *Science* **308**, 551-554 (2005).
182. Lee, J.H. & Paull, T.T. Direct activation of the ATM protein kinase by the Mre11/Rad50/Nbs1 complex. *Science* **304**, 93-96 (2004).
183. Uziel, T. *et al.* Requirement of the MRN complex for ATM activation by DNA damage. *Embo J* **22**, 5612-5621 (2003).
184. Carson, C.T. *et al.* The Mre11 complex is required for ATM activation and the G2/M checkpoint. *Embo J* **22**, 6610-6620 (2003).
185. Girard, P.M., Riballo, E., Begg, A.C., Waugh, A. & Jeggo, P.A. Nbs1 promotes ATM dependent phosphorylation events including those required for G1/S arrest. *Oncogene* **21**, 4191-4199 (2002).
186. Paull, T.T. & Lee, J.H. The Mre11/Rad50/Nbs1 complex and its role as a DNA double-strand break sensor for ATM. *Cell Cycle* **4**, 737-740 (2005).
187. Kobayashi, J. Molecular mechanism of the recruitment of NBS1/hMRE11/hRAD50 complex to DNA double-strand breaks: NBS1 binds to gamma-H2AX through FHA/BRCT domain. *J Radiat Res (Tokyo)* **45**, 473-478 (2004).
188. D'Amours, D. & Jackson, S.P. The Mre11 complex: at the crossroads of dna repair and checkpoint signalling. *Nat Rev Mol Cell Biol* **3**, 317-327 (2002).
189. Gatei, M. *et al.* ATM-dependent phosphorylation of nibrin in response to radiation exposure. *Nat Genet* **25**, 115-119 (2000).
190. Lim, D.S. *et al.* ATM phosphorylates p95/nbs1 in an S-phase checkpoint pathway. *Nature* **404**, 613-617 (2000).
191. Manke, I.A., Lowery, D.M., Nguyen, A. & Yaffe, M.B. BRCT repeats as phosphopeptide-binding modules involved in protein targeting. *Science* **302**, 636-639 (2003).
192. Rodriguez, M., Yu, X., Chen, J. & Songyang, Z. Phosphopeptide binding specificities of BRCA1 COOH-terminal (BRCT) domains. *J Biol Chem* **278**, 52914-52918 (2003).
193. Williams, R.S. *et al.* Structural basis for phosphorylation-dependent signaling in the DNA-damage response. *Biochem Cell Biol* **83**, 721-727 (2005).
194. Glover, J.N., Williams, R.S. & Lee, M.S. Interactions between BRCT repeats and phosphoproteins: tangled up in two. *Trends Biochem Sci* **29**, 579-585 (2004).

195. Zhao, S., Renthal, W. & Lee, E.Y. Functional analysis of FHA and BRCT domains of NBS1 in chromatin association and DNA damage responses. *Nucleic Acids Res* **30**, 4815-4822 (2002).
196. Xiao, Y. & Weaver, D.T. Conditional gene targeted deletion by Cre recombinase demonstrates the requirement for the double-strand break repair Mre11 protein in murine embryonic stem cells. *Nucleic Acids Res* **25**, 2985-2991 (1997).
197. Luo, G. *et al.* Disruption of mRad50 causes embryonic stem cell lethality, abnormal embryonic development, and sensitivity to ionizing radiation. *Proc Natl Acad Sci U S A* **96**, 7376-7381 (1999).
198. Brown, E.J. & Baltimore, D. ATR disruption leads to chromosomal fragmentation and early embryonic lethality. *Genes Dev* **14**, 397-402 (2000).
199. de Klein, A. *et al.* Targeted disruption of the cell-cycle checkpoint gene ATR leads to early embryonic lethality in mice. *Curr Biol* **10**, 479-482 (2000).
200. Lim, D.S. & Hasty, P. A mutation in mouse rad51 results in an early embryonic lethal that is suppressed by a mutation in p53. *Mol Cell Biol* **16**, 7133-7143 (1996).
201. Tsuzuki, T. *et al.* Targeted disruption of the Rad51 gene leads to lethality in embryonic mice. *Proc Natl Acad Sci U S A* **93**, 6236-6240 (1996).
202. Rogakou, E.P., Pilch, D.R., Orr, A.H., Ivanova, V.S. & Bonner, W.M. DNA double-stranded breaks induce histone H2AX phosphorylation on serine 139. *J Biol Chem* **273**, 5858-5868 (1998).
203. Rogakou, E.P., Boon, C., Redon, C. & Bonner, W.M. Megabase chromatin domains involved in DNA double-strand breaks in vivo. *J Cell Biol* **146**, 905-916 (1999).
204. Burma, S., Chen, B.P., Murphy, M., Kurimasa, A. & Chen, D.J. ATM phosphorylates histone H2AX in response to DNA double-strand breaks. *J Biol Chem* **276**, 42462-42467 (2001).
205. Stiff, T. *et al.* ATM and DNA-PK function redundantly to phosphorylate H2AX after exposure to ionizing radiation. *Cancer Res* **64**, 2390-2396 (2004).
206. Ward, I.M. & Chen, J. Histone H2AX is phosphorylated in an ATR-dependent manner in response to replicational stress. *J Biol Chem* **276**, 47759-47762 (2001).
207. Celeste, A. *et al.* Genomic instability in mice lacking histone H2AX. *Science* **296**, 922-927 (2002).
208. Celeste, A. *et al.* Histone H2AX phosphorylation is dispensable for the initial recognition of DNA breaks. *Nat Cell Biol* **5**, 675-679 (2003).
209. Schultz, L.B., Chehab, N.H., Malikzay, A. & Halazonetis, T.D. p53 binding protein 1 (53BP1) is an early participant in the cellular response to DNA double-strand breaks. *J Cell Biol* **151**, 1381-1390 (2000).
210. Anderson, L., Henderson, C. & Adachi, Y. Phosphorylation and rapid relocalization of 53BP1 to nuclear foci upon DNA damage. *Mol Cell Biol* **21**, 1719-1729 (2001).
211. Stewart, G.S., Wang, B., Bignell, C.R., Taylor, A.M. & Elledge, S.J. MDC1 is a mediator of the mammalian DNA damage checkpoint. *Nature* **421**, 961-966 (2003).
212. Haaf, T., Golub, E.I., Reddy, G., Radding, C.M. & Ward, D.C. Nuclear foci of mammalian Rad51 recombination protein in somatic cells after DNA damage and

its localization in synaptonemal complexes. *Proc Natl Acad Sci U S A* **92**, 2298-2302 (1995).
213. Liu, Y., Li, M., Lee, E.Y. & Maizels, N. Localization and dynamic relocalization of mammalian Rad52 during the cell cycle and in response to DNA damage. *Curr Biol* **9**, 975-978 (1999).
214. Fernandez-Capetillo, O. *et al.* DNA damage-induced G2-M checkpoint activation by histone H2AX and 53BP1. *Nat Cell Biol* **4**, 993-997 (2002).
215. Chowdhury, D. *et al.* gamma-H2AX dephosphorylation by protein phosphatase 2A facilitates DNA double-strand break repair. *Mol Cell* **20**, 801-809 (2005).
216. Goldberg, M. *et al.* MDC1 is required for the intra-S-phase DNA damage checkpoint. *Nature* **421**, 952-956 (2003).
217. Xu, B., O'Donnell, A.H., Kim, S.T. & Kastan, M.B. Phosphorylation of serine 1387 in Brca1 is specifically required for the Atm-mediated S-phase checkpoint after ionizing irradiation. *Cancer Res* **62**, 4588-4591 (2002).
218. Xu, B., Kim, S. & Kastan, M.B. Involvement of Brca1 in S-phase and G(2)-phase checkpoints after ionizing irradiation. *Mol Cell Biol* **21**, 3445-3450 (2001).
219. Baskaran, R. *et al.* Ataxia telangiectasia mutant protein activates c-Abl tyrosine kinase in response to ionizing radiation. *Nature* **387**, 516-519 (1997).
220. Zhang, J. *et al.* Chk2 phosphorylation of BRCA1 regulates DNA double-strand break repair. *Mol Cell Biol* **24**, 708-718 (2004).
221. Chen, G. *et al.* Radiation-induced assembly of Rad51 and Rad52 recombination complex requires ATM and c-Abl. *J Biol Chem* **274**, 12748-12752 (1999).
222. Yuan, Z.M. *et al.* Regulation of Rad51 function by c-Abl in response to DNA damage. *J Biol Chem* **273**, 3799-3802 (1998).
223. Yuan, S.S., Chang, H.L. & Lee, E.Y. Ionizing radiation-induced Rad51 nuclear focus formation is cell cycle-regulated and defective in both ATM(-/-) and c-Abl(-/-) cells. *Mutat Res* **525**, 85-92 (2003).
224. Lou, Z. *et al.* MDC1 maintains genomic stability by participating in the amplification of ATM-dependent DNA damage signals. *Mol Cell* **21**, 187-200 (2006).
225. Zhang, J., Ma, Z., Treszezamsky, A. & Powell, S.N. MDC1 interacts with Rad51 and facilitates homologous recombination. *Nat Struct Mol Biol* **12**, 902-909 (2005).
226. Lou, Z., Chini, C.C., Minter-Dykhouse, K. & Chen, J. Mediator of DNA damage checkpoint protein 1 regulates BRCA1 localization and phosphorylation in DNA damage checkpoint control. *J Biol Chem* **278**, 13599-13602 (2003).
227. Lou, Z., Minter-Dykhouse, K., Wu, X. & Chen, J. MDC1 is coupled to activated CHK2 in mammalian DNA damage response pathways. *Nature* **421**, 957-961 (2003).
228. Cousineau, I., Abaji, C. & Belmaaza, A. BRCA1 regulates RAD51 function in response to DNA damage and suppresses spontaneous sister chromatid replication slippage: implications for sister chromatid cohesion, genome stability, and carcinogenesis. *Cancer Res* **65**, 11384-11391 (2005).
229. Foray, N. *et al.* A subset of ATM- and ATR-dependent phosphorylation events requires the BRCA1 protein. *Embo J* **22**, 2860-2871 (2003).

230. Xu, B., Kim, S.T., Lim, D.S. & Kastan, M.B. Two molecularly distinct G(2)/M checkpoints are induced by ionizing irradiation. *Mol Cell Biol* **22**, 1049-1059 (2002).
231. Mochan, T.A., Venere, M., DiTullio, R.A., Jr. & Halazonetis, T.D. 53BP1 and NFBD1/MDC1-Nbs1 function in parallel interacting pathways activating ataxia-telangiectasia mutated (ATM) in response to DNA damage. *Cancer Res* **63**, 8586-8591 (2003).
232. Kanaar, R., Hoeijmakers, J.H. & van Gent, D.C. Molecular mechanisms of DNA double strand break repair. *Trends Cell Biol* **8**, 483-489 (1998).
233. Jackson, S.P. Detecting, signalling and repairing DNA double-strand breaks. *Biochem Soc Trans* **29**, 655-661 (2001).
234. Jeggo, P.A. Identification of genes involved in repair of DNA double-strand breaks in mammalian cells. *Radiat Res* **150**, S80-91 (1998).
235. Hiom, K. Dna repair: Rad52 - the means to an end. *Curr Biol* **9**, R446-448 (1999).
236. Tan, T.L. *et al.* Mouse Rad54 affects DNA conformation and DNA-damage-induced Rad51 foci formation. *Curr Biol* **9**, 325-328 (1999).
237. Bartek, J. & Lukas, J. Mammalian G1- and S-phase checkpoints in response to DNA damage. *Curr Opin Cell Biol* **13**, 738-747 (2001).
238. Lee, H., Larner, J.M. & Hamlin, J.L. A p53-independent damage-sensing mechanism that functions as a checkpoint at the G1/S transition in Chinese hamster ovary cells. *Proc Natl Acad Sci U S A* **94**, 526-531 (1997).
239. Mailand, N. *et al.* Rapid destruction of human Cdc25A in response to DNA damage. *Science* **288**, 1425-1429 (2000).
240. Falck, J., Mailand, N., Syljuasen, R.G., Bartek, J. & Lukas, J. The ATM-Chk2-Cdc25A checkpoint pathway guards against radioresistant DNA synthesis. *Nature* **410**, 842-847 (2001).
241. Agami, R. & Bernards, R. Distinct initiation and maintenance mechanisms cooperate to induce G1 cell cycle arrest in response to DNA damage. *Cell* **102**, 55-66 (2000).
242. Mailand, N. & Diffley, J.F. CDKs promote DNA replication origin licensing in human cells by protecting Cdc6 from APC/C-dependent proteolysis. *Cell* **122**, 915-926 (2005).
243. Duursma, A. & Agami, R. p53-Dependent regulation of Cdc6 protein stability controls cellular proliferation. *Mol Cell Biol* **25**, 6937-6947 (2005).
244. Costanzo, V. *et al.* Reconstitution of an ATM-dependent checkpoint that inhibits chromosomal DNA replication following DNA damage. *Mol Cell* **6**, 649-659 (2000).
245. Kastan, M.B., Onyekwere, O., Sidransky, D., Vogelstein, B. & Craig, R.W. Participation of p53 protein in the cellular response to DNA damage. *Cancer Res* **51**, 6304-6311 (1991).
246. Kuerbitz, S.J., Plunkett, B.S., Walsh, W.V. & Kastan, M.B. Wild-type p53 is a cell cycle checkpoint determinant following irradiation. *Proc Natl Acad Sci U S A* **89**, 7491-7495 (1992).
247. Kastan, M.B. & Bartek, J. Cell-cycle checkpoints and cancer. *Nature* **432**, 316-323 (2004).

248. Bartek, J. & Lukas, J. Pathways governing G1/S transition and their response to DNA damage. *FEBS Lett* **490**, 117-122 (2001).
249. Khosravi, R. *et al.* Rapid ATM-dependent phosphorylation of MDM2 precedes p53 accumulation in response to DNA damage. *Proc Natl Acad Sci U S A* **96**, 14973-14977 (1999).
250. Maya, R. *et al.* ATM-dependent phosphorylation of Mdm2 on serine 395: role in p53 activation by DNA damage. *Genes Dev* **15**, 1067-1077 (2001).
251. DeGregori, J. The genetics of the E2F family of transcription factors: shared functions and unique roles. *Biochim Biophys Acta* **1602**, 131-150 (2002).
252. Flores-Rozas, H. *et al.* Cdk-interacting protein 1 directly binds with proliferating cell nuclear antigen and inhibits DNA replication catalyzed by the DNA polymerase delta holoenzyme. *Proc Natl Acad Sci U S A* **91**, 8655-8659 (1994).
253. Waga, S., Hannon, G.J., Beach, D. & Stillman, B. The p21 inhibitor of cyclin-dependent kinases controls DNA replication by interaction with PCNA. *Nature* **369**, 574-578 (1994).
254. Cazzalini, O. *et al.* p21CDKN1A does not interfere with loading of PCNA at DNA replication sites, but inhibits subsequent binding of DNA polymerase delta at the G1/S phase transition. *Cell Cycle* **2**, 596-603 (2003).
255. Xu, B. & Kastan, M.B. Analyzing cell cycle checkpoints after ionizing radiation. *Methods Mol Biol* **281**, 283-292 (2004).
256. Larner, J.M. *et al.* Radiation down-regulates replication origin activity throughout the S phase in mammalian cells. *Nucleic Acids Res* **27**, 803-809 (1999).
257. Painter, R.B. & Young, B.R. Radiosensitivity in ataxia-telangiectasia: a new explanation. *Proc Natl Acad Sci U S A* **77**, 7315-7317 (1980).
258. Miao, H., Seiler, J.A. & Burhans, W.C. Regulation of cellular and SV40 virus origins of replication by Chk1-dependent intrinsic and UVC radiation-induced checkpoints. *J Biol Chem* **278**, 4295-4304 (2003).
259. Sorensen, C.S., Syljuasen, R.G., Lukas, J. & Bartek, J. ATR, Claspin and the Rad9-Rad1-Hus1 complex regulate Chk1 and Cdc25A in the absence of DNA damage. *Cell Cycle* **3**, 941-945 (2004).
260. Marheineke, K. & Hyrien, O. Control of replication origin density and firing time in Xenopus egg extracts: role of a caffeine-sensitive, ATR-dependent checkpoint. *J Biol Chem* **279**, 28071-28081 (2004).
261. Shechter, D., Costanzo, V. & Gautier, J. ATR and ATM regulate the timing of DNA replication origin firing. *Nat Cell Biol* **6**, 648-655 (2004).
262. Jazayeri, A. *et al.* ATM- and cell cycle-dependent regulation of ATR in response to DNA double-strand breaks. *Nat Cell Biol* **8**, 37-45 (2006).
263. Zhao, H., Watkins, J.L. & Piwnica-Worms, H. Disruption of the checkpoint kinase 1/cell division cycle 25A pathway abrogates ionizing radiation-induced S and G2 checkpoints. *Proc Natl Acad Sci U S A* **99**, 14795-14800 (2002).
264. Molinari, M., Mercurio, C., Dominguez, J., Goubin, F. & Draetta, G.F. Human Cdc25 A inactivation in response to S phase inhibition and its role in preventing premature mitosis. *EMBO Rep* **1**, 71-79 (2000).
265. Costanzo, V. *et al.* An ATR- and Cdc7-dependent DNA damage checkpoint that inhibits initiation of DNA replication. *Mol Cell* **11**, 203-213 (2003).

266. Kim, S.T., Xu, B. & Kastan, M.B. Involvement of the cohesin protein, Smc1, in Atm-dependent and independent responses to DNA damage. *Genes Dev* **16**, 560-570 (2002).
267. Bartek, J., Lukas, C. & Lukas, J. Checking on DNA damage in S phase. *Nat Rev Mol Cell Biol* **5**, 792-804 (2004).
268. Falck, J., Petrini, J.H., Williams, B.R., Lukas, J. & Bartek, J. The DNA damage-dependent intra-S phase checkpoint is regulated by parallel pathways. *Nat Genet* **30**, 290-294 (2002).
269. Stark, G.R. & Taylor, W.R. Analyzing the G2/M checkpoint. *Methods Mol Biol* **280**, 51-82 (2004).
270. Chan, T.A., Hermeking, H., Lengauer, C., Kinzler, K.W. & Vogelstein, B. 14-3-3Sigma is required to prevent mitotic catastrophe after DNA damage. *Nature* **401**, 616-620 (1999).
271. Xiong, Y. *et al.* p21 is a universal inhibitor of cyclin kinases. *Nature* **366**, 701-704 (1993).
272. Obaya, A.J. & Sedivy, J.M. Regulation of cyclin-Cdk activity in mammalian cells. *Cell Mol Life Sci* **59**, 126-142 (2002).
273. Chen, M.S., Ryan, C.E. & Piwnica-Worms, H. Chk1 kinase negatively regulates mitotic function of Cdc25A phosphatase through 14-3-3 binding. *Mol Cell Biol* **23**, 7488-7497 (2003).
274. Takai, H. *et al.* Chk2-deficient mice exhibit radioresistance and defective p53-mediated transcription. *Embo J* **21**, 5195-5205 (2002).
275. Uto, K., Inoue, D., Shimuta, K., Nakajo, N. & Sagata, N. Chk1, but not Chk2, inhibits Cdc25 phosphatases by a novel common mechanism. *Embo J* **23**, 3386-3396 (2004).
276. O'Keefe, R.T., Henderson, S.C. & Spector, D.L. Dynamic organization of DNA replication in mammalian cell nuclei: spatially and temporally defined replication of chromosome-specific alpha-satellite DNA sequences. *J Cell Biol* **116**, 1095-1110 (1992).
277. Gilbert, D.M. Making sense of eukaryotic DNA replication origins. *Science* **294**, 96-100 (2001).
278. Antequera, F. Genomic specification and epigenetic regulation of eukaryotic DNA replication origins. *Embo J* **23**, 4365-4370 (2004).
279. Shechter, D. & Gautier, J. ATM and ATR check in on origins: a dynamic model for origin selection and activation. *Cell Cycle* **4**, 235-238 (2005).
280. Dimitrova, D.S. & Gilbert, D.M. The spatial position and replication timing of chromosomal domains are both established in early G1 phase. *Mol Cell* **4**, 983-993 (1999).
281. Nishitani, H. & Lygerou, Z. Control of DNA replication licensing in a cell cycle. *Genes Cells* **7**, 523-534 (2002).
282. Mendez, J. *et al.* Human origin recognition complex large subunit is degraded by ubiquitin-mediated proteolysis after initiation of DNA replication. *Mol Cell* **9**, 481-491 (2002).
283. Dimitrova, D.S., Prokhorova, T.A., Blow, J.J., Todorov, I.T. & Gilbert, D.M. Mammalian nuclei become licensed for DNA replication during late telophase. *J Cell Sci* **115**, 51-59 (2002).

284. Harper, J.W., Burton, J.L. & Solomon, M.J. The anaphase-promoting complex: it's not just for mitosis any more. *Genes Dev* **16**, 2179-2206 (2002).
285. Ayad, N.G. CDKs give Cdc6 a license to drive into S phase. *Cell* **122**, 825-827 (2005).
286. Pardee, A.B. A restriction point for control of normal animal cell proliferation. *Proc Natl Acad Sci U S A* **71**, 1286-1290 (1974).
287. Diffley, J.F. & Labib, K. The chromosome replication cycle. *J Cell Sci* **115**, 869-872 (2002).
288. Duursma, A.M. & Agami, R. CDK-dependent stabilization of Cdc6: linking growth and stress signals to activation of DNA replication. *Cell Cycle* **4**, 1725-1728 (2005).
289. Alexandrow, M.G. & Hamlin, J.L. Chromatin decondensation in S-phase involves recruitment of Cdk2 by Cdc45 and histone H1 phosphorylation. *J Cell Biol* **168**, 875-886 (2005).
290. Jiang, W., McDonald, D., Hope, T.J. & Hunter, T. Mammalian Cdc7-Dbf4 protein kinase complex is essential for initiation of DNA replication. *Embo J* **18**, 5703-5713 (1999).
291. Montagnoli, A. *et al.* Identification of Mcm2 phosphorylation sites by S-phase regulating kinases. *J Biol Chem* (2006).
292. Sionov, R.V. & Haupt, Y. The cellular response to p53: the decision between life and death. *Oncogene* **18**, 6145-6157 (1999).
293. Hong, Y. & Stambrook, P.J. Restoration of an absent G1 arrest and protection from apoptosis in embryonic stem cells after ionizing radiation. *Proc Natl Acad Sci U S A* **101**, 14443-14448 (2004).
294. Chaturvedi, P. *et al.* Mammalian Chk2 is a downstream effector of the ATM-dependent DNA damage checkpoint pathway. *Oncogene* **18**, 4047-4054 (1999).
295. Bree, R.T., Neary, C., Samali, A. & Lowndes, N.F. The switch from survival responses to apoptosis after chromosomal breaks. *DNA Repair (Amst)* **3**, 989-995 (2004).
296. Xu, Y. & Baltimore, D. Dual roles of ATM in the cellular response to radiation and in cell growth control. *Genes Dev* **10**, 2401-2410 (1996).
297. Westphal, C.H. *et al.* atm and p53 cooperate in apoptosis and suppression of tumorigenesis, but not in resistance to acute radiation toxicity. *Nat Genet* **16**, 397-401 (1997).
298. Schuler, M. & Green, D.R. Transcription, apoptosis and p53: catch-22. *Trends Genet* **21**, 182-187 (2005).
299. Borner, C. The Bcl-2 protein family: sensors and checkpoints for life-or-death decisions. *Mol Immunol* **39**, 615-647 (2003).
300. Chen, C., Shimizu, S., Tsujimoto, Y. & Motoyama, N. Chk2 regulates transcription-independent p53-mediated apoptosis in response to DNA damage. *Biochem Biophys Res Commun* **333**, 427-431 (2005).
301. Huang, Y. *et al.* Role for caspase-mediated cleavage of Rad51 in induction of apoptosis by DNA damage. *Mol Cell Biol* **19**, 2986-2997 (1999).
302. Matsui, Y., Tsuchida, Y. & Keng, P.C. Effects of p53 mutations on cellular sensitivity to ionizing radiation. *Am J Clin Oncol* **24**, 486-490 (2001).

303. Bernstein, C., Bernstein, H., Payne, C.M. & Garewal, H. DNA repair/pro-apoptotic dual-role proteins in five major DNA repair pathways: fail-safe protection against carcinogenesis. *Mutat Res* **511**, 145-178 (2002).
304. Clarke, A.R. *et al.* Thymocyte apoptosis induced by p53-dependent and independent pathways. *Nature* **362**, 849-852 (1993).
305. Lowe, S.W., Schmitt, E.M., Smith, S.W., Osborne, B.A. & Jacks, T. p53 is required for radiation-induced apoptosis in mouse thymocytes. *Nature* **362**, 847-849 (1993).
306. Cann, K.L. & Hicks, G.G. Absence of an Immediate G1/S Checkpoint in Primary MEFs Following gamma-Irradiation Identifies a Novel Checkpoint Switch. *Cell Cycle* **5**, 1823-1830 (2006).
307. Bakker, P.J. *et al.* An indirect immunofluorescence double staining procedure for the simultaneous flow cytometric measurement of iodo- and chlorodeoxyuridine incorporated into DNA. *Cytometry* **12**, 366-372 (1991).
308. Koopman, G. *et al.* Annexin V for flow cytometric detection of phosphatidylserine expression on B cells undergoing apoptosis. *Blood* **84**, 1415-1420 (1994).
309. Martin, S.J. *et al.* Early redistribution of plasma membrane phosphatidylserine is a general feature of apoptosis regardless of the initiating stimulus: inhibition by overexpression of Bcl-2 and Abl. *J Exp Med* **182**, 1545-1556 (1995).
310. Vermes, I., Haanen, C., Steffens-Nakken, H. & Reutelingsperger, C. A novel assay for apoptosis. Flow cytometric detection of phosphatidylserine expression on early apoptotic cells using fluorescein labelled Annexin V. *J Immunol Methods* **184**, 39-51 (1995).
311. Boss, M., Greaves, M. & Teich, N. Abelson virus-transformed haematopoietic cell lines with pre-B-cell characteristics. *Nature* **278**, 551-553 (1979).
312. Rosenberg, N., Baltimore, D. & Scher, C.D. In vitro transformation of lymphoid cells by Abelson murine leukemia virus. *Proc Natl Acad Sci U S A* **72**, 1932-1936 (1975).
313. Hicks, G.G. *et al.* Retrovirus gene traps. *Methods Enzymol* **254**, 263-275 (1995).
314. Laird, P.W. *et al.* Simplified mammalian DNA isolation procedure. *Nucleic Acids Res* **19**, 4293 (1991).
315. Mosmann, T. Rapid colorimetric assay for cellular growth and survival: application to proliferation and cytotoxicity assays. *J Immunol Methods* **65**, 55-63 (1983).
316. Graham, F.L. & van der Eb, A.J. A new technique for the assay of infectivity of human adenovirus 5 DNA. *Virology* **52**, 456-467 (1973).
317. Kwon, Y.H., Jovanovic, A., Serfas, M.S. & Tyner, A.L. The Cdk inhibitor p21 is required for necrosis, but it inhibits apoptosis following toxin-induced liver injury. *J Biol Chem* **278**, 30348-30355 (2003).
318. Imamura, Y., Katahira, T. & Kitamura, D. Identification and characterization of a novel BASH N terminus-associated protein, BNAS2. *J Biol Chem* **279**, 26425-26432 (2004).
319. Parrinello, S. *et al.* Oxygen sensitivity severely limits the replicative lifespan of murine fibroblasts. *Nat Cell Biol* **5**, 741-747 (2003).

320. Todaro, G.J. & Green, H. Quantitative studies of the growth of mouse embryo cells in culture and their development into established lines. *J Cell Biol* **17**, 299-313 (1963).
321. Perez, R.P., Godwin, A.K., Handel, L.M. & Hamilton, T.C. A comparison of clonogenic, microtetrazolium and sulforhodamine B assays for determination of cisplatin cytotoxicity in human ovarian carcinoma cell lines. *Eur J Cancer* **29A**, 395-399 (1993).
322. Chen, C.F., Hwang, J.M., Wu, C.H., Chen, C.S. & Chen, K.Y. Evaluation of a rapid tetrazolium-based colorimetric assay for selecting anticancer drugs. *Zhonghua Yi Xue Za Zhi (Taipei)* **46**, 7-16 (1990).
323. Denizot, F. & Lang, R. Rapid colorimetric assay for cell growth and survival. Modifications to the tetrazolium dye procedure giving improved sensitivity and reliability. *J Immunol Methods* **89**, 271-277 (1986).
324. Wilson, J.K., Sargent, J.M., Elgie, A.W., Hill, J.G. & Taylor, C.G. A feasibility study of the MTT assay for chemosensitivity testing in ovarian malignancy. *Br J Cancer* **62**, 189-194 (1990).
325. Schmid, I., Krall, W.J., Uittenbogaart, C.H., Braun, J. & Giorgi, J.V. Dead cell discrimination with 7-amino-actinomycin D in combination with dual color immunofluorescence in single laser flow cytometry. *Cytometry* **13**, 204-208 (1992).
326. Kruman, I., Guo, Q. & Mattson, M.P. Calcium and reactive oxygen species mediate staurosporine-induced mitochondrial dysfunction and apoptosis in PC12 cells. *J Neurosci Res* **51**, 293-308 (1998).
327. Maser, R.S., Monsen, K.J., Nelms, B.E. & Petrini, J.H. hMre11 and hRad50 nuclear foci are induced during the normal cellular response to DNA double-strand breaks. *Mol Cell Biol* **17**, 6087-6096 (1997).
328. Mirzoeva, O.K. & Petrini, J.H. DNA damage-dependent nuclear dynamics of the Mre11 complex. *Mol Cell Biol* **21**, 281-288 (2001).
329. Andegeko, Y. *et al.* Nuclear retention of ATM at sites of DNA double strand breaks. *J Biol Chem* **276**, 38224-38230 (2001).
330. Chodosh, L.A., Fire, A., Samuels, M. & Sharp, P.A. 5,6-Dichloro-1-beta-D-ribofuranosylbenzimidazole inhibits transcription elongation by RNA polymerase II in vitro. *J Biol Chem* **264**, 2250-2257 (1989).
331. Bendixen, C., Thomsen, B., Alsner, J. & Westergaard, O. Camptothecin-stabilized topoisomerase I-DNA adducts cause premature termination of transcription. *Biochemistry* **29**, 5613-5619 (1990).
332. D'Incalci, M. DNA-topoisomerase inhibitors. *Curr Opin Oncol* **5**, 1023-1028 (1993).
333. Luo, Z., Zheng, J., Lu, Y. & Bregman, D.B. Ultraviolet radiation alters the phosphorylation of RNA polymerase II large subunit and accelerates its proteasome-dependent degradation. *Mutat Res* **486**, 259-274 (2001).
334. McKay, B.C. & Ljungman, M. Role for p53 in the recovery of transcription and protection against apoptosis induced by ultraviolet light. *Neoplasia* **1**, 276-284 (1999).

335. McKay, B.C. *et al.* UV light-induced degradation of RNA polymerase II is dependent on the Cockayne's syndrome A and B proteins but not p53 or MLH1. *Mutat Res* **485**, 93-105 (2001).
336. Haaf, T. *et al.* Sequestration of mammalian Rad51-recombination protein into micronuclei. *J Cell Biol* **144**, 11-20 (1999).
337. Blom, N., Gammeltoft, S. & Brunak, S. Sequence and structure-based prediction of eukaryotic protein phosphorylation sites. *J Mol Biol* **294**, 1351-1362 (1999).
338. Corpet, F. Multiple sequence alignment with hierarchical clustering. *Nucleic Acids Res* **16**, 10881-10890 (1988).
339. Okawa, Y. *et al.* Purification of N-terminally truncated histone H2A-monoubiquitin conjugates from leukemic cell nuclei: probable proteolytic products of ubiquitinated H2A. *Int J Biochem Cell Biol* **35**, 1588-1600 (2003).
340. Goto, H. *et al.* Identification of a novel phosphorylation site on histone H3 coupled with mitotic chromosome condensation. *J Biol Chem* **274**, 25543-25549 (1999).
341. Kurose, A., Tanaka, T., Huang, X., Traganos, F. & Darzynkiewicz, Z. Synchronization in the cell cycle by inhibitors of DNA replication induces histone H2AX phosphorylation: an indication of DNA damage. *Cell Prolif* **39**, 231-240 (2006).
342. Shimura, T. *et al.* Suppression of replication fork progression in low-dose-specific p53-dependent S-phase DNA damage checkpoint. *Oncogene* **25**, 5921-5932 (2006).
343. Lau, E., Zhu, C., Abraham, R.T. & Jiang, W. The functional role of Cdc6 in S-G2/M in mammalian cells. *EMBO Rep* **7**, 425-430 (2006).
344. Dimitrova, D.S. & Gilbert, D.M. Temporally coordinated assembly and disassembly of replication factories in the absence of DNA synthesis. *Nat Cell Biol* **2**, 686-694 (2000).
345. Lu, X. & Lane, D.P. Differential induction of transcriptionally active p53 following UV or ionizing radiation: defects in chromosome instability syndromes? *Cell* **75**, 765-778 (1993).
346. Jordan, M.A., Thrower, D. & Wilson, L. Effects of vinblastine, podophyllotoxin and nocodazole on mitotic spindles. Implications for the role of microtubule dynamics in mitosis. *J Cell Sci* **102 (Pt 3)**, 401-416 (1992).
347. Daniel, R. *et al.* Caffeine inhibits human immunodeficiency virus type 1 transduction of nondividing cells. *J Virol* **79**, 2058-2065 (2005).
348. Murata, T., Akagi, K., Nasu, R., Kimura, H. & Tanaka, Y. Analysis of cell kinetics after gamma-ray irradiation using an anti-BrdU monoclonal antibody. *Int J Oncol* **12**, 345-349 (1998).
349. Dhananjayan, S.C., Ismail, A. & Nawaz, Z. Ubiquitin and control of transcription. *Essays Biochem* **41**, 69-80 (2005).
350. Gill, G. SUMO and ubiquitin in the nucleus: different functions, similar mechanisms? *Genes Dev* **18**, 2046-2059 (2004).
351. Jason, L.J., Moore, S.C., Lewis, J.D., Lindsey, G. & Ausio, J. Histone ubiquitination: a tagging tail unfolds? *Bioessays* **24**, 166-174 (2002).
352. Moore, S.C., Jason, L. & Ausio, J. The elusive structural role of ubiquitinated histones. *Biochem Cell Biol* **80**, 311-319 (2002).

353. Xia, Y., Pao, G.M., Chen, H.W., Verma, I.M. & Hunter, T. Enhancement of BRCA1 E3 ubiquitin ligase activity through direct interaction with the BARD1 protein. *J Biol Chem* **278**, 5255-5263 (2003).
354. Baer, R. & Ludwig, T. The BRCA1/BARD1 heterodimer, a tumor suppressor complex with ubiquitin E3 ligase activity. *Curr Opin Genet Dev* **12**, 86-91 (2002).
355. Bekker-Jensen, S. *et al.* Spatial organization of the mammalian genome surveillance machinery in response to DNA strand breaks. *The Journal of cell biology* **173**, 195-206 (2006).
356. Misteli, T. The concept of self-organization in cellular architecture. *J Cell Biol* **155**, 181-185 (2001).
357. Huang, S. Review: perinucleolar structures. *Journal of structural biology* **129**, 233-240 (2000).
358. Bachur, N.R. *et al.* Antihelicase action of DNA-binding anticancer agents: relationship to guanosine-cytidine intercalator binding. *Mol Pharmacol* **44**, 1064-1069 (1993).
359. Mischo, H.E., Hemmerich, P., Grosse, F. & Zhang, S. Actinomycin D induces histone gamma-H2AX foci and complex formation of gamma-H2AX with Ku70 and nuclear DNA helicase II. *J Biol Chem* **280**, 9586-9594 (2005).
360. Fox, J.M., Byrne, T.D. & Woods, W.G. Actinomycin D-associated lesions mimicking DNA-DNA interstrand crosslinks detected by alkaline elution in cultured mammalian cells. *Biochem Pharmacol* **34**, 2741-2747 (1985).
361. Salmon, A.B. *et al.* Fibroblast cell lines from young adult mice of long-lived mutant strains are resistant to multiple forms of stress. *Am J Physiol Endocrinol Metab* **289**, E23-29 (2005).
362. Chuang, P.I. *et al.* Perturbation of B-cell development in mice overexpressing the Bcl-2 homolog A1. *Blood* **99**, 3350-3359 (2002).
363. Craxton, A., Chuang, P.I., Shu, G., Harlan, J.M. & Clark, E.A. The CD40-inducible Bcl-2 family member A1 protects B cells from antigen receptor-mediated apoptosis. *Cell Immunol* **200**, 56-62 (2000).
364. Chuang, P.I., Yee, E., Karsan, A., Winn, R.K. & Harlan, J.M. A1 is a constitutive and inducible Bcl-2 homologue in mature human neutrophils. *Biochem Biophys Res Commun* **249**, 361-365 (1998).
365. Moumen, A., Masterson, P., O'Connor, M.J. & Jackson, S.P. hnRNP K: an HDM2 target and transcriptional coactivator of p53 in response to DNA damage. *Cell* **123**, 1065-1078 (2005).
366. Tenenbaum, S.A., Lager, P.J., Carson, C.C. & Keene, J.D. Ribonomics: identifying mRNA subsets in mRNP complexes using antibodies to RNA-binding proteins and genomic arrays. *Methods* **26**, 191-198 (2002).
367. Pandita, T.K. ATM function and telomere stability. *Oncogene* **21**, 611-618 (2002).
368. Viscardi, V., Clerici, M., Cartagena-Lirola, H. & Longhese, M.P. Telomeres and DNA damage checkpoints. *Biochimie* **87**, 613-624 (2005).
369. Jonnalagadda, V.S., Matsuguchi, T. & Engelward, B.P. Interstrand crosslink-induced homologous recombination carries an increased risk of deletions and insertions. *DNA Repair (Amst)* **4**, 594-605 (2005).

370. Karlsson, A. *et al.* Defective double-strand DNA break repair and chromosomal translocations by MYC overexpression. *Proc Natl Acad Sci U S A* **100**, 9974-9979 (2003).
371. Tsukamoto, Y. & Ikeda, H. Double-strand break repair mediated by DNA end-joining. *Genes Cells* **3**, 135-144 (1998).
372. Pipiras, E., Coquelle, A., Bieth, A. & Debatisse, M. Interstitial deletions and intrachromosomal amplification initiated from a double-strand break targeted to a mammalian chromosome. *Embo J* **17**, 325-333 (1998).
373. Thacker, J. & Zdzienicka, M.Z. The XRCC genes: expanding roles in DNA double-strand break repair. *DNA Repair (Amst)* **3**, 1081-1090 (2004).
374. Griffin, C.S. Aneuploidy, centrosome activity and chromosome instability in cells deficient in homologous recombination repair. *Mutat Res* **504**, 149-155 (2002).
375. Sieber, O., Heinimann, K. & Tomlinson, I. Genomic stability and tumorigenesis. *Semin Cancer Biol* **15**, 61-66 (2005).
376. Feinberg, A.P. The epigenetics of cancer etiology. *Semin Cancer Biol* **14**, 427-432 (2004).
377. Warner, J.K. *et al.* Direct evidence for cooperating genetic events in the leukemic transformation of normal human hematopoietic cells. *Leukemia* **19**, 1794-1805 (2005).
378. Gullo, C., Au, M., Feng, G. & Teoh, G. The biology of Ku and its potential oncogenic role in cancer. *Biochim Biophys Acta* **1765**, 223-234 (2006).
379. Huibregtse, J.M., Scheffner, M. & Howley, P.M. A cellular protein mediates association of p53 with the E6 oncoprotein of human papillomavirus types 16 or 18. *Embo J* **10**, 4129-4135 (1991).
380. Dyson, N., Howley, P.M., Munger, K. & Harlow, E. The human papilloma virus-16 E7 oncoprotein is able to bind to the retinoblastoma gene product. *Science* **243**, 934-937 (1989).
381. Boisvert, F.M., Rhie, A., Richard, S. & Doherty, A.J. The GAR motif of 53BP1 is arginine methylated by PRMT1 and is necessary for 53BP1 DNA binding activity. *Cell Cycle* **4**, 1834-1841 (2005).
382. Boisvert, F.M., Hendzel, M.J., Masson, J.Y. & Richard, S. Methylation of MRE11 regulates its nuclear compartmentalization. *Cell Cycle* **4**, 981-989 (2005).
383. Boisvert, F.M., Dery, U., Masson, J.Y. & Richard, S. Arginine methylation of MRE11 by PRMT1 is required for DNA damage checkpoint control. *Genes Dev* **19**, 671-676 (2005).
384. Adams, M.M. *et al.* 53BP1 oligomerization is independent of its methylation by PRMT1. *Cell Cycle* **4**, 1854-1861 (2005).
385. Law, W.J., Cann, K.L. & Hicks, G.G. TLS, EWS and TAF15: a model for transcriptional integration of gene expression. *Brief Funct Genomic Proteomic* **5**, 8-14 (2006).

Appendix 1: Sequence of the pEGFP-FLAG-TLS vector at the junctions of the pEGFP-C1 vector sequence, FLAG sequence, and TLS sequence

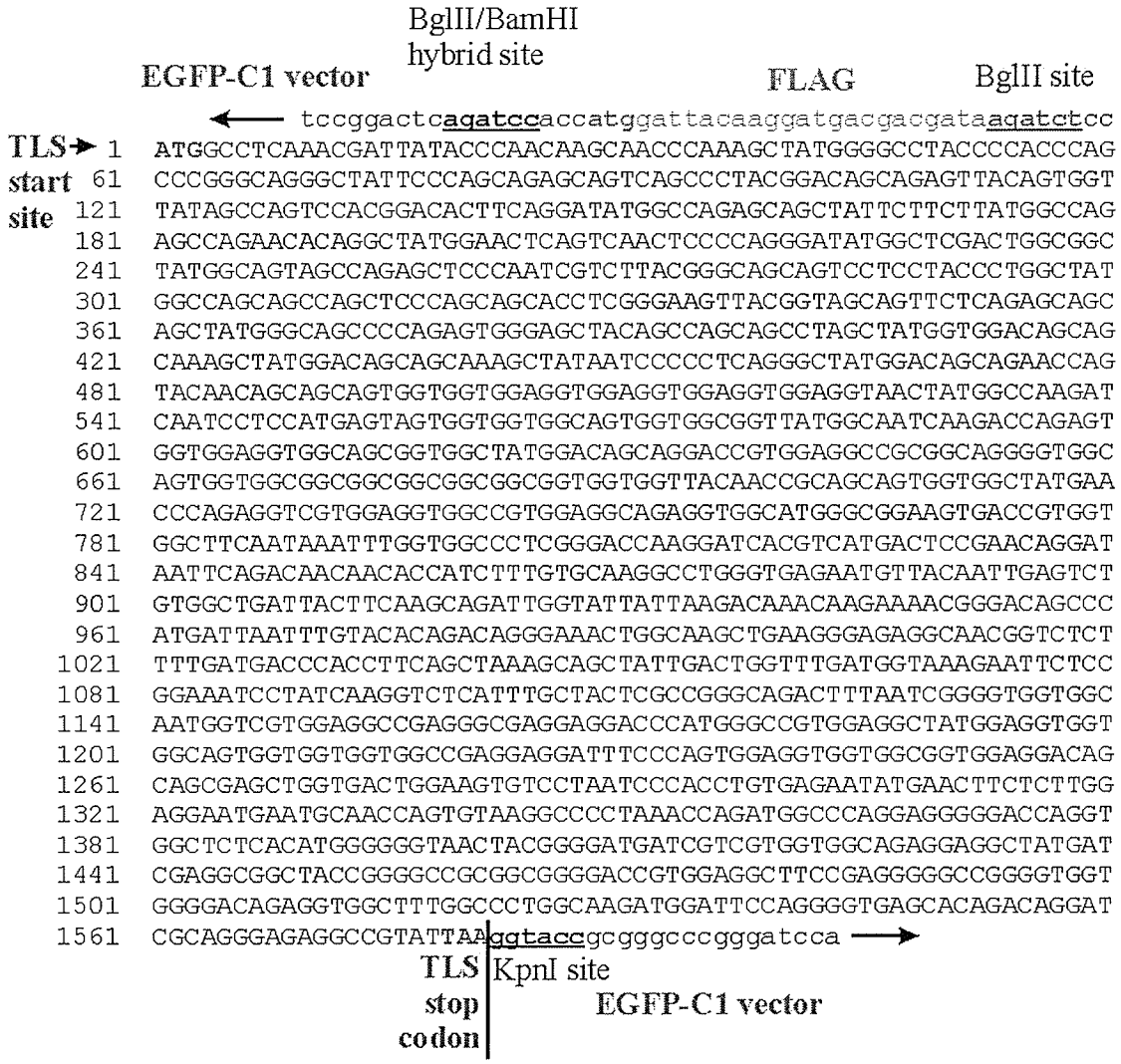

Appendix 2: Abbreviations

Abbreviations of nucleic acid bases

A	Adenine, Adenosine, Deoxyadenosine
BrdU	5-Bromo-2'-deoxyuridine
C	Cytosine, Cytidine, Deoxycytidine
CldU	5-Chloro-2'-deoxyuridine
G	Guanine, Guanosine, Deoxyguanosine
IdU	5-Iodo-2'-deoxyuridine
T	Thymine, Thymidine, Deoxythymidine
U	Uracil, Uridine

Abbreviations for amino acids

G	Glycine
Q	Glutamine
R	Arginine
S	Serine
T	Threonine
Y	Tyrosine

Other abbreviations

293T	A derivative of the 293 human renal epithelial cell line that also expresses SV40 large T antigen
53BP1	p53 binding protein 1
7AAD	7-aminoactinomycin D
A_{260}	Absorbance at 260 nanometres
aa	Amino acids
Abl	v-abl Abelson murine leukemia viral oncogene homolog 1
ALL	Acute lymphocytic leukemia
AML	Acute myeloid leukemia
AP	Apurinic or apyrimidinic sites
Apaf-1	Apoptotic protease activating factor 1
APC	Anaphase promoting complex
ARF	Alternate reading frame tumour-suppressor protein
ARS	Autonomously replicating sequences
AT	Ataxia Telangiectasia
ATF-1	Activating Transcription Factor 1
ATLD	AT-like disorder
ATM	Ataxia Telangiectasia Mutated
ATR	Ataxia Telangiectasia and Rad3 related
BARD1	BRCA1 associated RING domain protein
BCL	B-cell leukemia/lymphoma protein
BCR	Breakpoint cluster region
BCR-ABL	Fusion gene/protein resulting from a translocation between chromosomes 9 and 22 that generates the Philadelphia chromsome of CML
Bfl-1	Bcl2a1a, Bcl2 related protein A1a

BGS	Bovine growth serum
BH	Bcl homology domain
BLM	Bloom's syndrome helicase
bp	Base pair
BRCA	Breast cancer susceptibility
BRCT	BRCA1 carboxy-terminal domain
BSA	Bovine serum albumin
bZIP	Basic DNA binding and leucine zipper dimerization
c-Abl	Cellular Abl
Cdc	Cell division cycle
Cdk	Cyclin-dependent kinase
Cdt1	Cdc10-dependent transcript 1
C/EBP	CCAAT/Enhancer Binding Protein
Chk	Checkpoint
CIZ	Cas Interacting Zinc Finger Protein; NMP4 (Nuclear Matrix Protein 4); ZNF384 (Zinc Finger Protein 384)
CLL	Chronic lymphocytic leukemia
CML	Chronic myeloid leukemia
CHO	Chinese hamster ovary cell line
CHOP	C/EBP Homologous Protein; DDIT3 (DNA Damage Inducible Transcript 3); GADD153 (Growth Arrest- and DNA Damage-Inducible Gene 153)
CREB3L2	c-AMP Response Element-Binding Protein 3-Like 2; BBF2H7 (box B-binding factor-2 human homolog on chromosome 7)
DAPI	4',6'-diamidino-2-phenylindole
Dbf4	Double foot 4
ddH_2O	Deionizied, distilled water
df	Degrees of freedom
DFC	Dense fibrillar component
DMEM	Dulbecco's Modified Eagle Medium
DMSO	Dimethyl sulfoxide
DPC	Days post coitum
DNA	Deoxyribonucleic acid
DNA-PK	DNA-dependent protein kinase
DNA-PKcs	Catalytic subunit of DNA-PK
DNC	Dark nucleolar caps
dNTPs	Deoxynucleotides triphosphate
DRB	5,6-dichlorobenzimidazole riboside
DSB	Double-strand break
dsDNA	Double-stranded DNA
DTT	Dithiothreitol
E1A	Early region 1A Adenovirus oncogene
E2F	E2 (adenoviral protein) factor
EDTA	Ethylenediaminetetraacetic acid
EGFP	Enhanced green fluorescent protein
ERCC1	Excision repair cross-complementing rodent repair deficiency, complementation group 1

ERG	V-ets avian erythroblastosis virus E26 oncogene (ETS) related
ESFTs	Ewing's sarcoma family of tumors
ETS	V-ets avian erythroblastosis virus E26 oncogene
ETV1	ETS Variant Gene 1
ETV4	ETS Variant Gene4; E1A Enhancer Binding Protein (E1AF)
EWSR1	Ewing Sarcoma Breakpoint Region 1, EWS
FANC	Fanconi Anemia Subtype
FITC	Fluorescein isothiocyanate
FBS	Fetal bovine serum
FC	Fibrillar centre
FEV	Fifth Ewing Sarcoma Variant
FHA	Fork-head associated
FLI-1	Friend Leukemia Virus Integration 1
G1	Gap 1 phase
G2	Gap 2 phase
GC	Granular component
H2AX	H2A histone family, member X
H3-pSer^{28}	Histone H3 phosphorylated on serine 28
HEBS	HEPES buffered saline
HeLa	A human cervical cancer cell line.
HEPES	4-(2-Hydroxyethyl)piperazine-1-ethanesulfonic acid
hnRNP	heteronuclear ribonucleoprotein
IAPs	Inhibitor of apoptosis proteins
ICL	Interstrand cross-link
IR	Ionizing (Ir)radiation
IRIF	Ionizing radiation-induced foci
kb	Kilobase
kD(a)	Kilodalton
Ku	Ku thyroid autoantigen, regulatory subunit of DNA-PK
Lig4	Ligase IV
M	Mitosis
MCM	Minichromosome maintenance
MDC1	Mediator of mammalian DNA damage checkpoint 1
MDM2	transformed 3T3 cell double minute 2, p53 binding protein
MEF	Mouse embryonic fibroblast
MLH	MutL homolog 1
MMC	Mitomycin C
MMR	Mismatch repair
M_r	Relative molecular mass
Mre11	Meiotic recombination 11
MRN	Mre11, Rad50, Nbs1 complex
MSH	MutS homologue
MTT	3-[4,5-dimethylthiazol-2-yl]-2,5-diphenyl-tetra-zolium bromide
NBS	Nijmegen Breakage Syndrome
Nbs1	Gene mutated in NBS
NER	Nucleotide excision repair

NFAR	Nuclear factor associated with dsRNA
NF-κB	Nuclear factor of kappa light chain gene enhancer in B-cells 1
NHEJ	Non-homologous end-joining
NP-40	Nonidet P-40
NR4A3	Nuclear Receptor Subfamily 4, Group A, Member 3 (CHN/TEC)
NRB	54 kDa nuclear RNA- and DNA-binding protein
ODP	Origin decision point
ORC	Origin recognition complex
PAGE	Polyacrylamide gel electrophoresis
PBS	Phosphate buffered saline
PBS-B	PBS with BSA
PBST	PBS with Triton X-100
PBS-TB	PBS with BSA and Tween 20
PCR	Polymerase chain reaction
PKCβII	Protein kinase C, beta II; Prkcb1
PMS2	Postmeiotic segregation increased 2
PMSF	Phenylmethylsulfonyl fluoride
PNET	Primitive neuroectodermal tumour
Post-RC	Post-replicative complex
POU5F1	POU (Pit-1, Oct-1, Oct-2, Unc-86 DNA binding domain) domain, class 5, transcription factor 1; OCT3 (Octamer-binding transcription factor 3); OCT4
Pre-IC	Pre-initiation complex
Pre-RC	Pre-replicative complex
PSF	PTB-associated splicing factor
PTB	Polypyrimidine tract-binding protein
PUMA	BBC3; BCL2 binding component 3
RAD	RADiation sensitivity abnormal/yeast RAD-related
RB	pRB; Retinoblastoma protein
RDS	Radioresistant DNA synthesis
RECQL4	RecQ (recombinase Q) protein-like 4 helicase
RFP	Red fluorescent protein
RGG	Arginine-glycine-glycine
RING	Really Interesting New Gene Finger Domain
RIPA	Radioimmunoprecipitation assay buffer
RNA	Ribonucleic acid
RNP	Ribonucleoprotein
ROS	Reactive oxygen species
RPA	Replication protein A
RPMI	Roswell Park Memorial Institute medium
RRM	RNA-recognition motif
RS-SCID	Severe combined immunodeficiency with sensitivity to ionizing radiation
RT-PCR	Reverse transcription-polymerase chain reaction
S phase	Synthesis phase
SARFH	Sarcoma-associated RNA-binding fly homolog
SDS	Sodium dodecyl sulfate

SMAC	Second mitochondrial derived activator of caspases
SMC1	Structural maintenance of chromosomes 1
SMN	Survival motor neuron
Spi-1	Spleen focus forming virus (SFFV) proviral integration oncogene 1; PU.1
snoRNAs	Small nucleolar RNAs
snRNAs	Small nuclear RNAs
SSB	Single-strand break
ssDNA	Single-stranded DNA
SRm160	Serine/Arginine-related nuclear matrix protein
SSA	Single-strand annealing
SSC	Sodium chloride, sodium citrate buffer
SSCPE	Sodium chloride, sodium citrate, phosphate, EDTA buffer\
SWI2/SNF2	Switch 2/sucrose nonfermenting 2 nucleosome remodeling factor
SYGQQS	Serine-Tyrosine-Glycine-Glutamine-Glutamine-Serine
TAE	Tris acetic acid EDTA buffere
TAF15	TATA box binding protein (TBP)-associated factor 15; TAF[II]68
TASR	TLS-associated serine-arginine protein
TATA	TATA box consensus sequence (TATAAAA)
TBP	TATA box binding [protein
TBS	Tris buffered saline
TDP	Replication timing decision point
TE	Tris EDTA buffer
TEMED	N,N,N′,N′-Tetramethylethylenediamine
TET	*T*LS, *E*WS, *T*AF15 family
TFII	Transcription factor for RNA polymerase II
TLS	Translocated in LipoSarcoma; FUS; hnRNP P2
TP53	Tumor protein p53
tRNA	Transfer RNA
TTBS	Tris buffered saline with Tween 20
TTD	Trichothiodystrophy
U	Units
U1-70K	Spliceosomal protein U1A
U3NeoSV1	Retrovirus gene trap shuttle vector 1 carrying a promoterless neomycin resistance gene in the U3 region of the long terminal repeat
UV	Ultraviolet
WRN	Werner's syndrome helicase
WT1	Wilms Tumor 1
w/v	Weight per volume
XP	Xeroderma pigmentosum
XRCC	X-ray repair complementing defective repair in Chinese hamster cells
YB-1	Y-box DNA/RNA-binding factor-1
ZnF	Zinc finger motif
ZSG	Zinc Finger Sarcoma Gene; ZNF278 (Zinc Finger Protein 278)